LNG Interchangeability/Gas Quality: Results of the National Energy Technology Laboratory's Research for the FERC on Natural Gas Quality and Interchangeability

DOE/NETL-2007/1290

Prepared by
U.S. Department of Energy
National Energy Technology Laboratory

June 2007

Disclaimer

This report was prepared as an account of work sponsored by an agency of the United States Government. Neither the United States Government nor any agency thereof, nor any of their employees, makes any warranty, express or implied, or assumes any legal liability or responsibility for the accuracy, completeness, or usefulness of any information, apparatus, product, or process disclosed, or represents that its use would not infringe privately owned rights. Reference therein to any specific commercial product, process, or service by trade name, trademark, manufacturer, or otherwise does not necessarily constitute or imply its endorsement, recommendation, or favoring by the United States Government or any agency thereof. The views and opinions of authors expressed therein do not necessarily state or reflect those of the United States Government or any agency thereof.

LNG Interchangeability/Gas Quality: Results of the National Energy Technology Laboratory's Research for the FERC on Natural Gas Quality and Interchangeability

NETL Points of Contact:

Daniel Driscoll
Senior Project Manager - Gasification and Fuels Division
Strategic Center for Coal
National Energy Technology Laboratory
Morgantown, WV 26507-0880
Phone: (304) 285-4717
Fax: (304) 285-4403
Email: Daniel.Driscoll@netl.doe.gov

George Richards
Energy Systems Dynamics - Focus Area Leader
Office of Research and Development
National Energy Technology Laboratory
Morgantown, WV 26507-0880
Phone: (304) 285-4458
Fax: (304) 285-4403
Email: George.Richards@netl.doe.gov

Brad Tomer
Director
Strategic Center for Natural Gas and Oil
National Energy Technology Laboratory
Morgantown, WV 26507-0880
Phone: (304) 285-4692
Fax: (304) 285-4216
Email: Brad.Tomer@netl.doe.gov

Authors

Section 1:

Daniel J. Driscoll (NETL)
Geo. A. Richards (NETL)

Section 2:

Daniel J. Driscoll (NETL)
Christopher J. Nichols (NETL)

Section 3:

E. David Huckaby (NETL)
Gilles N. Eggenspieler (ANSYS/FLUENT)

Section 4:

Michael H. McMillian, Steven W. Richardson, John S. Ontko (NETL)
Todd T. Worstell (RDS, Inc.)

Section 5:

Geo. A. Richards, Douglas L. Straub, Donald H. Ferguson (NETL)
Edward H. Robey (RDS, Inc.)

Section 6:

Jimmy D. Thornton, Steve K. Beer (NETL)
Lisa M. Porter, Yan Cao, Robert F. Davis, Jason Gu, Elias Towe,
David N. Lambeth, Bo Li (CMU)

Section 7:

Daniel J. Driscoll (NETL)
Brian Anderson (West Virginia University)

TABLE OF CONTENTS

1 EXECUTIVE SUMMARY 1-1
1.1 Pipeline Mixing 1-4
1.2 Reciprocating Engines 1-5
1.3 Stationary Gas Turbines 1-6
1.4 Sensors for Gas Composition 1-8
1.4.1 Gas Chromatography 1-10
1.4.2 Mass Spectrometers 1-10
1.4.3 Optical Spectroscopy (Dispersive IR, FTIR, Raman) 1-11
1.4.4 Electronic and Physical (Solid-State, Mass, Calorimetric) 1-11
1.5 Hydrocarbon Dewpoint 1-12
2 GAS AND EQUIPMENT DATABASE 2-1
2.1 Data Overview 2-1
2.2 Implications from the Database 2-3
3 PIPELINE MIXING 3-1
3.1 Part I: Steady Evolution of Compositional Discontinuities at a Pipe Junction 3-1
3.1.1 Pipe Junction Geometry 3-2
3.1.2 Reynolds Averaged Navier-Stokes Simulations 3-3
3.1.3 Large Eddy Simulation 3-9
3.2 Part II: Evolution of Streamwise Compositional Discontinuities in Gas Pipelines 3-13
3.2.1 Semi-Analytical Solution 3-14
3.2.2 Computational Fluid Dynamics of the Development of an Axial Discontinuity 3-16
3.2.3 Calculation of the Effective Diffusion (Dispersion) Coefficient 3-18
3.2.4 Analytical Solutions Results 3-18
3.2.5 Solution Sensitivity 3-19
3.3 Summary 3-22
4 NATURAL GAS ENGINES: FUEL VARIABILITY EFFECTS 4-1
4.1 Introduction 4-1
4.2 Engine Type 4-4
4.2.1 Stoichiometric/Exhaust Gas Recirculation 4-6
4.2.2 Automotive Applications 4-7
4.2.3 Direct Gas Injection/Pilot Ignition 4-8
4.2.4 Spark-Ignited Prechamber 4-10
4.2.5 HCCI 4-11
4.3 Aftertreatment 4-12
4.3.1 Three-Way Catalysis 4-13
4.3.2 Selective Catalytic Reduction 4-15
4.3.3 NO_x Traps for Lean-Burn Engines 4-15
4.3.4 Oxidation Catalysts 4-16
4.4 Natural Gas/Engine Combustion and Fuel Properties 4-17
4.4.1 Autoignition 4-17

4.4.2 Flame Speed 4-19
4.4.3 Pollutant Chemistry 4-20
4.4.3.1 Hydrocarbons 4-20
4.4.3.1.1 Aldehydes 4-22
4.4.3.1.2 Poly-Aromatic Hydrocarbons 4-24
4.4.3.1.3 Non-Methane Organic Gases 4-25
4.4.3.2 NO_x 4-25
4.4.3.3 Carbon Monoxide 4-26
4.4.3.4 Particulate Matter 4-27
4.4.4 Knock/Detonation 4-27
4.4.5 Thermodynamics/Engine Cycles 4-29
4.4.6 Simulation and Kinetics 4-31
4.4.7 A/F Metering 4-32
4.4.8 Methane Number/Wobbe number 4-34
4.5 Control Systems 4-38
4.5.1 Recent Studies of CNG/LNG Impact on Engine Control 4-38
4.5.1.1 Southern California Gas Study of CNG/LNG Impact on Cummins Engines 4-38
4.5.1.2 Southern California Gas Study on the Effect of Varying Fuel Composition on Fuel Supplied to DDC Gas Engines, May 4, 2005 4-40
4.5.1.3 Light-Duty CNG Vehicle Fuel Composition Study 2006 4-40
4.5.2 Oxygen Sensors 4-43
4.5.2.1 A/F Ratio Control 4-45
4.5.2.2 Other Control Strategies 4-47
4.5.2.2.1 Thermal Efficiency Control 4-47
4.5.2.2.2 Peak Optical Intensity Control 4-47
4.5.3 Sensor Techniques for Determining Natural Gas Properties 4-47
4.5.3.1 Thermal Conductivity 4-48
4.5.3.2 Solid-State Thermal-Wave Pyroelectric-Film Sensor 4-48
4.5.3.3 Spectroscopy 4-48
4.5.3.4 Acoustic 4-49
4.5.3.5 Dynamic Viscosity 4-50
5 GAS TURBINES 5-1
5.1 Gas Turbine Background 5-1
5.1.1 Gaseous Fuel Flow Control Systems 5-1
5.1.2 Turbine Combustion 5-3
5.2 Fuel Effects on Diffusion Flame Combustors 5-4
5.3 Fuel Effects on Premix Combustors 5-5
5.3.1 Fuel Effects on Flashback 5-5
5.3.2 Fuel Effects on Auto-ignition 5-8
5.3.3 Fuel Effects on Emissions 5-10
5.4 Fuel Effects on Lean Blowout 5-15
5.5 Fuel Effects on Dynamics 5-15
5.6 Description of Analysis and Experiments Reported 5-18
5.6.1 Lab-Scale Ring Stabilized Burner (< 15,000 BTUH) 5-18
5.6.2 Atmospheric Pressure Development Combustor (< 1x105 BTUH) 5-19

5.6.3 High Pressure Dynamic Gas Turbine Combustor (< 5x106 BTUH) 5-19
5.6.4 Simulations and Analysis 5-19
5.7 Results for Lab-Scale Ring Stabilized Burner 5-20
5.8 Premixer Performance 5-24
5.9 Analysis of Fuel Injector Dynamic Response 5-29
5.10 Atmospheric Pressure Development Combustor 5-37
5.10.1 Dynamic Pressure Amplitudes versus Fuel Composition 5-40
5.10.2 Dynamic Frequency and Flame Position versus Fuel Composition 5-43
5.10.3 Fuel Effect on Lean Blowout 5-49
5.11 Single-Injector High Pressure Combustor Apparatus 5-50
5.11.1 Data Analysis and Error Discussion 5-53
5.11.2 Dynamic Stability 5-56
5.11.3 Pollutant Emissions 5-60
5.11.3.1 Test Plan 5-61
5.11.3.2 Emissions Results 5-64
5.11.4 High Pressure Test Summary 5-67
5.12 Summary and Conclusions 5-68
5.13 Additional Information – Fuel Heating and Modified Wobbe Index 5-69
6 NATURAL GAS COMPOSITION: SENSOR REVIEW WITH APPLICABILITY FOR TURBINE CONTROL 6-1
6.1 Introduction 6-1
6.1.1 Objective 6-1
6.1.2 Natural Gas 6-2
6.1.3 Thermodynamic Considerations in Burning Hydrocarbons 6-3
6.1.4 Summary of Gas Composition Effects on Gas Turbine Performance 6-7
6.2 Gas Turbine Control 6-8
6.2.1 Potential Control Solutions 6-8
6.3 Gas Composition Sensors 6-10
6.3.1 General Comments Regarding Chemical-Sensing Technologies 6-10
6.3.2 Traditional Laboratory Sensor Technologies 6-10
6.3.2.1 Gas Chromatographs 6-11
6.3.2.1.1 Introduction and General Comments 6-11
6.3.2.1.2 Gas Chromatography Instrumental Components 6-12
6.3.2.2 Mass Spectrometers 6-12
6.3.2.2.1 Introduction and General Comments 6-12
6.3.2.2.2 Mass Spectrometer Instrumental Components 6-13
6.3.2.3 Hybrid Techniques 6-17
6.3.2.3.1 Gas Chromatography/Mass Spectrometry 6-17
6.3.2.3.2 Ion Mobility Spectrometry (IMS)/Mass Spectrometry 6-17
6.3.2.4 Example Commercial Devices 6-18
6.3.2.4.1 Quadrupole Mass Spectrometer (QMS) Products 6-18
6.3.2.4.2 Natural Gas Analyzer (NGA) – Agilent 6-18
6.3.2.4.3 Heated Hydrocarbon Analyzer – CAI 6-18
6.3.3 Exploratory Sensor Technologies 6-19
6.3.3.1 Infrared Optical Spectroscopy 6-19
6.3.3.1.1 Introduction 6-19

6.3.3.1.2 IR Spectrometer Instrumentation 6-22
6.3.3.1.3 Response Time, Sensitivity, and Selectivity 6-23
6.3.3.1.4 Application to Natural Gases Analysis 6-23
6.3.3.1.5 Commercial Availability 6-24
6.3.3.1.6 Infrared Semiconductor Light Sources and Detectors 6-24
6.3.3.2 Raman Spectroscopy 6-26
6.3.3.3 Chemical Sensors Based on Organic Materials 6-27
6.3.3.3.1 Conductometric Sensors 6-28
6.3.3.3.1.1 Conductometric Sensor Based On Conductive Polymers 6-29
6.3.3.3.1.2 Conductometric Sensors Based On Carbon Black-Polymer Composites 6-32
6.3.3.3.1.3 Conductometric Sensors Based On Carbon Nanotubes 6-32
6.3.3.3.2 Mass Sensitive Sensors 6-33
6.3.3.3.2.1 Surface Acoustic Wave Devices (SAW) 6-33
6.3.3.3.2.2 Quartz Crystal Microbalance (QMB) Mass Sensor 6-33
6.3.3.3.2.3 Micro Cantilever Based Mass Sensor 6-34
6.3.3.4 Calorimetric or Specific Heat Determination 6-35
6.3.3.5 Solid State Sensors for Hydrocarbon Detection 6-36
6.3.3.5.1 Metal Oxide Chemical Sensor 6-36
6.3.3.5.2 Metal Oxide Semiconductor Capacitors 6-39
6.3.3.5.3 Metal Oxide Semiconductor Schottky Diode 6-42
6.3.3.5.4 Metal Oxide Semiconductor Field Effect Transistor Sensors 6-44
6.3.3.5.5 High Electron Mobility Transistor 6-45
6.3.3.5.6 Electrochemical Cell 6-48
6.3.3.6 Hybrid Sensor Technology Concept 6-50
6.4 Summary of Sensor Technologies for Gas Turbine Control 6-51
6.4.1 Gas Chromatography 6-52
6.4.2 Mass Spectrometers 6-52
6.4.2.1 Detector Array Mass Spectrometers 6-53
6.4.2.2 Time-of-Flight Mass Spectrometers 6-53
6.4.3 Optical Spectroscopy (Dispersive IR, FTIR, Raman) 6-53
6.4.4 Electronic and Physical (Solid-State, Mass, Calorimetric) 6-54
7 ASSESSMENT OF HYDROCARBON DEW POINT, HYDROCARBON DROPOUT AND EQUATIONS OF STATE FOR NATURAL GAS CONTAINING LONG CHAIN HYDROCARBONS SUPPORT 7-1
7.1 TASK 1.0 – Identification of Gas Compositions for Assessment 7-1
7.2 TASK 2.0 – Literature Assessment 7-1
7.3 TASK 3.0 – Identification of Hydrocarbon Dropout Conditions 7-2
7.4 TASK 4.0 – Equation of State Modeling 7-3

LIST OF ACRONYMS

AC	alternating current
A/F	air-to-fuel
AFM	A/F module
AMU	Atomic Mass Unit
API	American Petroleum Institute
BAW	bulk acoustic wave
BMEP	brake mean effective pressure
BTDC	before top dead center
BTU	British Thermal Units
BWRS	Benedict-Webb-Ruben-Starling
CA	crank angle
CAI Inc.	California Analytical Instruments Inc.
CARB	California Air Resources Board
CEC	California Energy Commission
CFD	computational fluid dynamics
CHDP	Cricondentherm Hydrocarbon Dew Point
CI	compression ignition/chemical ionization
CNG	compressed natural gas
CO	carbon monoxide
COV	coefficient of variation
CPUC	California Public Utilities Commissions
CR	compression ratio
CRADA	Cooperative Research and Development Agreement
CRM	chemical reactor modeling
DC	direct current
DDC	Detroit Diesel Corporation
DEG	dimensional electron gas
DOE	Department of Energy
DPF	diesel particulate filter
DLE	dry low emission
ECD	electron capture detector
EGR	exhaust gas recirculation
EGO	exhaust gas oxygen
EI	electron ionization
EIA	Energy Information Administration
EMG	electromotive force
EPA	Environmental Protection Agency
ER	equivalence ratio
ERSABE	ER spark advance for best efficiency
FERC	Federal Energy Regulatory Commission
FID	flame ionization detector

FNHC	fuzzy neural hybrid controller
FPD	flame photometric detector
FTIR	Fourier Transform Infrared
FTNIR	Fourier Transform Near Infrared
FTP	Federal Test Procedure
FTMS	Fourier Transform Mass Spectrometer
GAMA	Gas Appliance Manufacturers Association
GC	gas chromatograph
GC/MS	gas chromatograph/mass spectrometer
GS	Grayson Streed
GTI	Gas Technology Institute
GVWR	gross vehicle weight rating
HC	hydrocarbons
H/C	hydrogen/carbon
HCCI	homogenous charge compression ignition
HEGO	heated exhaust gas oxygen
HEMT	high electron mobility transistor
HHV	higher heating value
ID	inside diameter
IGCC	integrated gasification combined cycle
IGHV	ideal gross heating value
IMEP	indicated mean effective pressure
IMS	ion mobility spectrometry
IR	infrared
IVC	intake valve closing
LES	large eddy simulation
LHV	lower heating value
LNG	liquefied natural gas
LNT	lean NO_x trap
LPG	liquefied petroleum gas
LPM	lean premix
MAD	mean absolute deviation
MBT	maximum brake torque
MCP	maximum combustion potential
MEMS	Micro-Electro-Mechanical-System
MN	methane number
MON	motor octane number
MOS	metal-oxide semiconductor
MOSFIT	metal-oxide semiconductor field-effect transistor
MPEG	miles per equivalent gallon
MS	mass spectrometer
MW	megawatt
MWI	Modified Wobbe Index
NETL	National Energy Technology Laboratory
NG	natural gas
NGA	natural gas analyzer

NGSA	Natural Gas Supply Association
NGV	natural gas vehicles
NIST	National Institute of Standards and Technology
NMHC	non-methane hydrocarbon
NMOG	non-methane organic gases
OC	oxidation catalyst
OEM	original equipment manufacturer
ON	octane number
PAHs	poly-aromatic hydrocarbons
PCC	precombustion chamber
PID	photoionization detector
PM	particulate matter
PR	Peng-Robinson
PSRK	Predictive Soave-Redlich-Kwong
QA/QC	quality assurance/quality control
QCM	quartz crystal microbalance
RANS	Reynolds Averaged Navier-Stokes
RMS	root mean squared
RON	research octane number
SAFT	Statistical Associating Fluid Theory
SAW	surface acoustic wave
SCR	selective catalytic reduction
SG	specific gravity
SI	spark ignition
SNG	synthetic natural gas
SRK	Soave-Redlich-Kwong
SOS	speed of sound
STD	standard deviation
SWNT	single-walled carbon nanotube
TCD	thermal conductivity detector
TDC	top dead center
THC	total hydrocarbons
TIT	turbine inlet temperature
TLHV	total lower heating value of intake
TOF	time-of-flight
TOFMS	time-of-flight mass spectrometer
TWC	three-way catalysts
UEGO	universal exhaust gas oxygen
UHC	unburned hydrocarbons
VCSEL	vertical-cavity surface-emitting laser
VDC	volts direct current
VOC	volatile organic compounds
WI	Wobbe Index
WKI	Waukesha knock index
YSZ	yttria-stabilized zirconia

1 EXECUTIVE SUMMARY

This project was initiated in October of 2005 in response to a request from the Federal Energy Regulatory Commission (FERC) to conduct a technical assessment of the effect of fuel variability on end-use equipment. The initial request was focused on questions regarding natural gas interchangeability; however, in subsequent discussions, the issue of liquid hydrocarbon drop-out (i.e., hydrocarbon dewpoint from minimally processed gas) was also raised.

The Department of Energy's National Energy Technology Laboratory (NETL) developed a research plan to address the topics of interest, and presented this plan to both DOE and FERC, as well as stakeholders like the NGSA, AGA, SoCal Air Emissions Advisory Committee, etc. The plan covered the following topics:

- **Database & Gap Analysis –** Develop a database of publicly available information on gas fuel composition and effects on end-use equipment and determine where additional testing is needed.

- **Pipeline Mixing –** Evaluate steady-state and transient mixing behavior where differing gas composition is blended into the pipeline to answer questions about how mixing in the pipeline affects a change in delivered gas composition.

- **Reciprocating Engines –** Review the effect of gas composition on reciprocating engines used for stationary power generation. A decision was made in February 2006 not to conduct testing on reciprocating engines because a relatively short test program would not add significantly to the existing literature.

- **Stationary Gas Turbines –** Document the literature on fuel effects in stationary gas turbines, and conduct experiments to address uncertainties on how fuel composition affects low-emission turbines.

- **Sensors for Gas Composition –** Review available sensor technology to allow rapid gas composition measurement to assess equipment control options to accommodate changing gas composition. This work parallels research at NETL sponsored by the Fossil Energy Advanced Research Program.

- **Hydrocarbon Dewpoint –** Questions about gas quality (hydrocarbon dewpoint) were added to this study in May 2006. A project was initiated to determine if recent advances in computational simulation could be used to improve dewpoint prediction.

Appliances were not a part of the study as there are multiple public studies that have looked at the impact of fuel variability on appliances. NETL did review available data on appliances reported by earlier investigators and simply documents these earlier studies in the database. Those studies show that properly tuned and maintained appliances can handle a broad range of fuel variability without any material impact.

Industrial burners were not a part of the study because these are currently being studied in a project supported by the California Energy Commission. NETL staff are participating in the CEC study as members of the advisory board.

The goal of this investigation was to report to FERC technical information on the topics listed above. This work was not planned or intended to provide a new approach to specifying acceptable gas composition standards.

In February, 2005, two comprehensive industry white papers on the LNG interchangeability and hydrocarbon dewpoints were issued by the NGC+. Consensus have been reached in the industry with regards to the use of a Wobbe Index based "interchangeability box" and Interim Guidelines to ensure interchangeability, and the use of control measures (e.g., cricondentherm or C6+ GPM) to address liquid drop out. Thus, there is an additional goal for this investigation to use the collected technical information in order to make an independent assessment of the findings of the NGC+ to see whether or not there are any realistic material concerns related to the NGC+ recommendations.

A draft of the final report was provided for technical review to 15 individual reviewers as well as reviews from AGA and NGSA. The final version of the report has been updated in response to reviewer comments.

The final report provides technical information related to fuel flexibility and on the basis of that information an assessment is made of any concerns related to realistic natural gas fuel flexibility within the NGC+ interchangeability box. This information and the assessment can be used to inform future decisions. Results from studies directed at the topics above are summarized below. Additional details can be found in the sections following this introduction.

Database & Gap Analysis – A database was developed that is searchable for gas property data, fuel composition effects, and some information about equipment populations. Significant data was located on some aspects of gas composition and equipment performance. The final database contains more than 50,000 individual entry lines. Generally, the database can be used to compare gas compositions in various locations and at different time span. Moreover the general information on equipment and its testing is adequate. However, in spite of the quantity of some available data, it was also recognized that limited public information was available on the effect of fuel composition on some larger equipment, especially stationary gas turbines. As another example, detailed data on heavy hydrocarbons needed for dewpoint prediction was also not widely available as part of the composition specification. Unless some consistent formats are mandated to be used for reporting gas quality in the industry in the future so that one can then make some correlations with gas quality data and end-use equipment performance, the current database will only provide limited use.

Pipeline Mixing – A combination of numerical models and mathematical analysis was used to assess two scenarios where different composition gases mix at a pipeline junction. For example, if LNG is added to a main pipeline, how long will it take to mix to some average composition with the main gas? First, it was shown that *steady* injection of a gas into a flowing main would mix to an average composition in a relatively short distance; typically within 100 pipe diameters.

Second, it was shown that during *transient* injection, (e.g., when a branch supply is activated) the interface between the new and old average composition would flow well-defined in the pipeline for very large distances (> 100 km). Thus, gases with different composition appear to move as "packets" though the pipeline. Abrupt changes in gas composition will be delivered through the pipeline with only modest attenuation. Reviewer comments on this work noted that the write-up was too brief, and suggested other approaches to calculation. The text has been revised to address these comments, but the general conclusions remain unchanged.

Reciprocating Engines – Fuel composition range is an established specification for gaseous fueled reciprocating engines. The gas composition can affect the engine emissions, power output, and knock/misfire behavior. Traditionally, varying composition range in natural gas fuel is handled during the engine specification through performance guarantees for a specific fuel range. The extent of the effect versus fuel composition depends on the type of engine (lean or stoichiometric) and type of control system employed. If the fuel exceeds the limits of the specification range then emissions and/or power and efficiency performance can be compromised. Thus, for changes in fuel composition, legacy systems without controls are most affected, but new OEM stationary engines with controls can accommodate wider fuel compositional changes. Most modern engines have A/F ratio control systems and knock sensors that can reduce or eliminate the impact of even larger variations in Wobbe Index and Methane Number.

Gas Turbines – Legacy gas turbines, using diffusion flame combustors, are known to be relatively insensitive to fuel composition. Correlations from turbine vendors can be used to predict how changes in fuel composition may affect engine emissions, but there are few other expected impacts. Modern low-NO_x turbine combustors, based on premix technology, have been introduced over the past 15 years. There are relatively few turbine studies on changing gas composition publicly available. Also, the physics and chemistry of premix combustion, with fuel variability, has not been widely published. For this reason, a review of literature on this technology was prepared and a series of tests were carried out to record the effect of fuel composition on premix turbine combustion. Tests covered the range from lab burners (15,000 BTUH), to full gas turbine injectors ($5x10^6$ BTUH).

From a theoretical and fundamental basis, premix combustors will be affected by fuel composition. However, the data presented here show that the effect of fuel composition is small unless the fuel composition change is very large (e.g., larger than expected for realistic natural gas blends). Both experimental and modeling results show that significant differences in the stability boundary and pressure amplitude are observed when there is an extreme switch in fuel composition, from natural gas to pure propane, or when propane is diluted with nitrogen to obtain the same Wobbe Index as the baseline natural gas, but for realistic natural gas composition ranges this is not a significant concern.

Compared to the draft version of this report, a key addition was the incorporation of improved emission sampling tests. These additional tests are included in the report, and affirm with greater confidence the draft information showing that that modest fuel composition changes do not significantly affect NO_x emissions. A review of the publicly available literature suggests that NO_x emissions will increase, if the concentration of higher hydrocarbon species (C2's and

higher) in the fuel increases. However, the data presented here do not show this result. Instead, the NO_x emissions are a stronger function of the flame temperature. We note that engine control systems that produce constant flame temperatures should therefore maintain good emissions performance with modest changes in fuel composition.

Sensors for Gas Composition – A review of gas composition sensor technology was prepared. The purpose was to define the existing capability, and define sensor and control developments that may allow turbine and reciprocating engine operation on wide fuel blends. Discussions with both gas turbine and reciprocating engine OEMs suggested that a rapidly responding, low cost gas composition analyzer may allow real-time engine adjustments to accommodate changing fuel blends. The review suggests several emerging approaches like catalytic sensor arrays, and novel "micro" Fourier transform IR (FTIR) techniques may be justified for development. This work complements activities at NETL to develop sensor and control technology for coal syngas. The actual sensor development is now occurring at NETL with funding from the Fossil Energy Advanced Research Program.

Hydrocarbon Dewpoint – This portion of the work was added late in the plan to address growing interest in improved prediction of hydrocarbon dewpoint. Concerns about hydrocarbon dewpoint are related to gas quality from minimally processed natural gas, not LNG. As of this writing, the study conducted with West Virginia University has identified 16 publicly available data sets showing how the dewpoint changes with relatively small additions of minor species, beyond C6. Work in progress is assessing how well the advanced simulations can be used to predict the change in dewpoint curves versus higher hydrocarbons.

1.1 Pipeline Mixing

A combination of numerical models and mathematical analysis was used to assess two scenarios where different composition gases mix at a pipeline junction. For example, if LNG is added to a main pipeline, how long will it take to mix to some average composition with the main gas? First, it was shown that *steady* injection of a gas into a flowing main would mix to an average composition in a relatively short distance; typically within 100 pipe diameters. Second, it was shown that during *transient* injection, (e.g., when a branch supply is activated) the interface between the new and old average composition would flow well-defined in the pipeline for very large distances (> 100 km). Thus, gases with different composition appear to move as "packets" though the pipeline. Abrupt changes in gas composition will be delivered through the pipeline with only modest attenuation.

A methodology has been demonstrated to estimate the downstream evolution of a compositional discontinuity in a pipe. Two situations were considered: steady state mixing, and transient mixing.

For steady mixing, the results show that gases mixed where a junction joins a main are mixed to an average composition in distances less than 100 meters for the cases studied here. In other words, steady- state gas blending is completed in a relatively short distance.

For transient mixing, the situation is different. Transient mixing refers to the situation where a different composition gas supply is abruptly "switched-on" at a pipe junction. While steady state conditions are rapidly established near the pipe junction, the interface between the old and new gas composition moves along the pipeline. Several methods were discussed to calculate or the dispersion of this interface. Estimation of the dispersion coefficient along with an analytical solution provide quick estimates of the time interval over which the composition will change at large distances away from the discontinuity. The results indicate that there is minimal mixing between the upstream and downstream gases, a behavior which mimics field evidence documented in a recent report [Apsen Environmental Group 2006]. Application of the solution procedure to a nominal operating condition (mass flow: 21.55 kg/s, pipe diameter: 0.762m pipe, operating pressure: 55 atm) indicates that if the supply is switched over a time period of less than two minutes, then the composition change 100 km downstream will occur over approximately two minutes. This analysis can used to provide estimates of how gas composition changes are transmitted along the pipeline. Reviewers suggested that more detailed calculations would be needed to provide specific solutions. The final document presents more details and rationale for using a combination of analytic and computational methods to develop the estimates of transient pipeline mixing. More exact analysis would require some combination of multidimensional CFD and pipeline network calculations of the specific scenario.

1.2 Reciprocating Engines

Fuel composition range is an established specification for gaseous fueled reciprocating engines. The gas composition can affect the engine emissions, power output, and knock/misfire behavior. Thus, traditionally, varying range in natural gas fuel is handled during the engine specification process through performance guarantees for a specific fuel range. The extent of the effect versus fuel composition depends on the type of engine (lean or stoichiometric) and type of control system employed. If the fuel exceeds the limits of the specification range then emissions and/or power and efficiency performance is compromised. Because of the importance of engine controls, legacy systems without controls are most affected by changing fuel composition. New OEM stationary engines with controls can accommodate wider fuel compositional changes.

The physical and chemical processes influenced by changing gas composition have been studied by various research groups. Generally, these studies show that engine behavior can be adequately characterized by two measures: the Wobbe Index and the Methane Number. Both Wobbe Index and Methane Number are dependent upon gas composition. Methane Number is used as indicator of knock resistance. The Wobbe Index is a measure of the fuel interchangeability with respect to its energy content and metered air to fuel ratio (A/F ratio). In engine applications, changes in the Wobbe Index are proportional to changes in stoichiometric A/F ratios. Low engine emissions are achieved by controlling A/F ratio through two designs:

- Lean burn engines reduce peak combustion temperatures.
- Stoichiometric engines reduce emission by using three-way catalysts.

The actual response of a given engine design will depend on the engine and control system.

Increased heating value tends to raise the Wobbe Index while increased specific gravity tends to lower the Wobbe Index. LNG will usually have higher heating value and specific gravity than domestic natural gas. However, LNGs anticipated to arrive at the US will have Wobbe Index not to exceed 1400 Btu/scf after blending with nitrogen or after NGL is being extracted in accordance with the NGC+ Interim Guidelines.

Most modern engines have A/F ratio control systems and knock sensors that can reduce or eliminate the impact of even larger variations in Wobbe Index and Methane Number. Therefore, the key findings from this literature review are:

- Engines with closed loop A/F ratio control can accommodate most LNGs without significant impact on emissions.
- Engines with open loop A/F ratio control will experience small changes in CO, NO_x and NMHC emissions due to changes in A/F ratio (typically < 3%).
- Most engines are certified to operate with natural gas having a Methane Number of 80 or higher. These engines are typically designed with safety margins and can likely accommodate most of the LNGs arriving the US, when
    - Engines with knock sensors will adjust engine timing, if required, to maximize efficiency while eliminating engine knock,
    - Even engines without knock sensors would likely accommodate most of the LNGs; however, simple in-field timing adjustment may be needed to avoid potential engine knock,
    - These timing changes may reduce fuel efficiency at most by 1-3% for an engine operating with retarded spark timing,
- Rapid on-line natural gas compositions sensors would be useful for control adjustments.

1.3 Stationary Gas Turbines

Modern, low-emission gas turbines are precisely tuned to maintain cool flame conditions that avoid the formation of NO_x pollutants. This precision comes with a cost. For example, these flames are susceptible to flashback, blow-off, and dynamic instabilities. The dynamic instabilities can be a serious problem, leading to pressure driven vibrations that can damage engines in a short time, or require adjustments that compromise the emissions performance of the engine. It is not widely appreciated how sensitive some turbine combustors are to changing operating conditions. In some engines, ambient temperature changes can lead to damaging oscillations unless the control system can take over and re-tune the engine. Retuning means changing the flow splits among the various fuel stages, and in some cases, adjusting the compressor inlet guide vanes, or bleeding air from the compressor to control primary zone temperature. The combination of these tuning adjustments is used to meet the competing demands of stable operation, and emissions performance. In some cases, these tuning adjustments are performed by engine operators in a trial and error manner until acceptable engine performance is achieved. To date, there is not a comprehensive theory of how combustion dynamics respond to changes in ambient conditions, and to a lesser degree an understanding of how engine dynamics are linked to fuel type. This explains why there has been controversy over the standards for new natural gas supplies in engines that have already been tuned to operate on a particular gas composition.

In this section, fuel interchangeability effects on gas turbine combustor performance have been described in considerable detail. The results presented in this section have focused on the underlying fundamentals of gas turbine combustion. As a result, the conclusions represent generalizations that have some scientific foundation, but may not necessarily cover every engine specific condition. Actual performance on operating engines could vary depending on individual design factors such as dynamic stability margin, flashback margins, control system design, etc. The following points are important outcomes of this work:

- Since the mid-1990's, lean premixed gas turbine combustor designs have become increasingly popular. It is believed that fuel interchangeability issues will be most prevalent in these combustion approaches. Since lean premixed approaches are relatively new to the industry, and very little information is available in the public literature, this effort has been focused toward premixed systems.

- If there is adequate flashback margin designed into the combustion system, it is believed that flashback issues can be avoided for realistic changes in fuel composition. Evidence suggests that although the laminar flame speeds for higher hydrocarbon species are higher than domestic natural gas, other work has shown that the turbulent flame speeds actually decrease with the addition of heavier hydrocarbon species. It is more likely that flashback events could be triggered by combustion instabilities which are discussed in more detail below.

- Others studies have operated a premixed combustors on relatively high heating value fuels without any autoignition problems , however, there is relatively little fundamental data on auto-ignition delay times for hydrocarbon fuels at conditions of interest to all gas turbines. Thus, it is recommended that operational data and OEM experience be gathered.

- Modeling results show that fuel jet penetration into a cross-flow is inversely proportional to the Wobbe Index of the fuel. However, for "realistic" range of fuel compositions and typical premixer residence times, variations of fluid dynamic mixing as result of fuel variability is not expected to have a significant effect on NO_x production.

- Combustion instabilities are a significant concern for lean premixed systems, and a significant level of effort has been directed toward this issue. The stability boundary and the observed pressure amplitude are not significantly affected by "realistic" variations in the fuel composition. This statement is based on data collected from a lab-scale ring-stabilized burner, a one-atmosphere swirl-stabilized combustor, and a pressurized swirl-stabilized single-nozzle test rig. As was pointed out by a reviewer, for engines operating right at the stability limit, this may indeed change the operating margin, but the effect observed here is small.

- Dynamic system modeling results suggest a small shift in the phase and gain of the open-loop response are observed when using fuels comparable to those expected in typical CNG and LNG blends. For systems operating well inside their stability window this

would suggest that changes in fuel composition may not pose a serious concern. However, systems that are marginally stable may experience difficulties in maintaining stability similar to those occurring as a result of typical variances in operating conditions (e.g., changing inlet air temperature).

- Both experimental and modeling results show that significant differences in the stability boundary and pressure amplitude are observed for pure propane and propane diluted with nitrogen to obtain the same Wobbe Index as the baseline natural gas, but for realistic natural gas composition ranges this is not a real concern.

A review of the publicly available literature suggests that NO_x emissions will increase, if the concentration of higher hydrocarbon species (C2's and higher) in the fuel increases. For diffusion flame combustors, it is believed that the NO_x increase will be proportional to the natural logarithm of the flame temperature relative to some reference (i.e., methane) flame temperature. For 100% premixed systems, it is believed that the NO_x emissions increase is some function of the higher hydrocarbon species. However, results from NETL's high pressure test facility show no significant changes in NO_x emissions as a function of adding as much as 5% propane to the baseline natural gas (i.e., a nominal Wobbe increase from 1380 to 1425 BTU/scf). It is noted that the data presented here are reported at constant flame temperature. Thus, when the control system can meter the fuel to produce constant flame temperature, modest changes in gas composition are less important than the flame temperature itself in determining the NO_x emissions. Details of the specific engine control system should be considered when assessing how fuel composition affects measured emissions, or even dynamics from a given engine.

1.4 Sensors for Gas Composition

The conversion of energy via industrial gas turbines requires control systems which optimize efficiency, minimize pollutants, and protect hardware. With these criteria in mind, the objectives of this white paper are to review the state-of-the-art gas composition sensors and to suggest potential sensor solutions to adequately determine gas composition for industrial gas turbine applications.

A summary of capabilities of the sensor technologies discussed is shown in the Table below.

Table 1-1: Summary of Detection Technologies.
It is noteworthy that the costs estimates for several technologies largely represent engineering development and not production costs.
(Used With Permission)

Sensor	Estimated Unit Cost ($k)	Size	Species	Gas Composition Update Rate (Data Sets/Second)
GC/Mass Spectrometer	> 10	Benchtop	Detector Dependent	< 0.1
Scanning Magnetic Sector Mass Spectrometer	40 -100	60" H x 30" x 30" (Typical)	H_2, He, CH_4, H_2O, N_2, CO, C_2H_6, O_2, H_2S, Ar, CO_2, C_3H_8, SO_2, COS, CS_2, and hydrocarbons > C4	< 0.1
Scanning Quadrupole Mass Spectrometer	10 - 100	Benchtop	Same as above	> 1
Time-of-Flight Mass Spectrometer	> 10	Benchtop	Same as above	> 10
Detector Array Magnetic Sector Mass Spectrometer	> 10	Benchtop	Same as above	1000
Dispersive IR	< 10	Benchtop to Compact	Requires IR absorption	< 1, SNR dependent
FTIR	> 10	Benchtop	Requires IR absorption	> 10
Raman	> 10	Benchtop	Requires IR absorption	~ 1
Conductometric Sensors	< 5	Compact	Chemical alterability dependent	~ 1
Mass-Sensitive Sensors	< 5	Compact	All	~ 1
Calorimetric of Specific Heat Determination	< 10	Compact	All	~ 1
Solid-State Sensors	< 5	Compact	Oxidizable materials	~ 1

For gas turbine control, the emphasis is placed on composition measurements within 1 second and with a 1% volume fraction accuracy. This table represents only an estimate of the sensor technology attributes for the application, and since some of these technologies could be designed more specifically for the application these estimates could change. For example, cost is highly dependent upon product volume as well as upon the configuration for the application. In high volume, one might anticipate integrated sensor technology such as MEMS-based or Solid State devices to be very inexpensive. High production volume accelerometers, as employed for automobile airbag systems, cost only a few dollars. While the manufacturing cost for such a device or other solid state devices could be quiet low, one would expect the system cost to be

dominated by system engineering issues and service. Likewise, for example, Raman spectroscopy is usually applied to solids, but due to the anticipated high gas pressure and concentrations it may very well be suitable for this application as a benchtop tool. As such, its cost and response time would very well be dominated by the laser system employed to achieve a satisfactory signal-to-noise ratio.

Depending upon how the information for such a sensor system might be employed, a more or less complex computer analysis and control system may be needed. Hence, once again the cost may be more accurately reflected by consideration of the system issues. If one simply desired a fixed embedded control system based upon a few channels of sensor information, then one could expect the unit cost to be low. However, if the device has to be so versatile as to be used on a large variety of customized turbines, then engineering costs will again dominate. It may be more appropriate to focus on the attributes of size, detection accuracy, and response time.

1.4.1 Gas Chromatography

Gas Chromatography is considered accurate and reasonably reliable and can be constructed for the analysis of a large variety of materials. However, it is usually slow, somewhat bulky, and the columns require considerable maintenance. By itself, it is not considered practical for this continuous on-line application where rapid measurements are required.

1.4.2 Mass Spectrometers

Mass spectrometers can be used to measure principal components and many minor components with varying accuracy, depending on the mass spectrometer design and the complexity of the gas mix. A stand-alone unit is usually rather large, and much of the cost is associated with the high engineering content. Its system complexity allows it to be used to obtain more information than may be needed for the control system. Most mass spectrometers have software that determines gas concentrations from peak intensities and allows the user to set up real-time calculations for the Wobbe Index, mass balances, and other items. A spectrometer appropriate for fuel gases should be capable of observing masses 1 through at least 100, and preferably 200 if there are C_8 or heavier hydrocarbons present. Expected components in fuel gas are H_2, He, CH_4, H_2O, N_2, CO, C_2H_6, O_2, H_2S, Ar, CO_2, C_3H_8, SO_2, COS, CS_2, and hydrocarbons C_4 and heavier, including straight-chain and branched hydrocarbons. Alkenes, alkynes, cycloalkanes, and hydrocarbons with heteroatom substituents (N,O,S) are assumed to be negligible. (The accuracy of this assumption is uncertain for coal-derived synfuels.)

A mix in which all of the expected species are present produces a complex spectrum with overlapping fragmentation patterns that require deconvolution. This necessitates the complexity of the computer software in most laboratory analysis applications, but a somewhat reduced amount of analysis should be allowed for the turbine control application. Lighter hydrocarbons (CH_4, C_2H_6, and C_3H_8) have only one isomer and one fragmentation pattern. Heavier hydrocarbons have more than one isomer, each one having its own unique fragmentation pattern. Butane, pentane, and hexane, for example, have 2, 3, and 5 isomers respectively. A mixture of the above components up to and including C_6 (as may occur in coal-derived synfuels) requires sampling a minimum of 25 different mass numbers (one for each component) to deconvolute the

individual fragmentation patterns. The sensitivity of calculated concentrations to slight variations in fragmentation patterns can produce significant errors, whether from calibration errors or from changes in gas composition during a sampling cycle. Accurate analysis requires a mass spectrometer that is both fast and accurate. Sampling 25 masses several times a second is beyond the reach of most commercially available scanning mass spectrometers but may be possible with TOF and detector array mass spectrometers.

1.4.3 Optical Spectroscopy (Dispersive IR, FTIR, Raman)

Benchtop dispersive IR optical spectroscopy, FTIR spectroscopy and Raman spectroscopy normally employ physical displacement of an optical element to perform the sensor channel (wavelength) scan. In order to achieve high resolution scanning over a large bandwidth, a long optical path and a bright source are required. Hence, they are rather bulky for the application and can be rather expensive. Their response to particular species is totally dependent upon the vibrational absorption bands of the species. Since the IR absorption bands are formed via the atomic bonding and because the bonding is similar for several natural gas species, they are not independent from each other. However, the spectra are perturbed by the secondary atomic bonding and so has a considerable degree of uniqueness. In this regard, after the spectra are taken, a mass-spectroscopy analogous software-based deconvolution is required. However, unlike the mass spectroscopy there are some species which are transparent in the IR and so produce no optical signal. Hence, all optical spectroscopy techniques are blind to some materials and the optical sensor channels must be supplemented with some complimentary sensor technology.

With a finite number of natural gas species to be detected, it is quite feasible to measure via only a finite number of a pre-selected measurement channels (wavelengths). Doing so could be accomplished with optical filters as the wavelength selection mechanism. This would significantly reduce the physical size, cost and measurement time. In the IR, black-body thermal detectors (thermal piles) have been traditionally utilized. These can easily be constructed via MEMS technology and be fully integrated with signal-conditioning electronics. More recently, MEMS technology, combined with new quantum well emitter/detector structures, is enabling the development of vertical-cavity surface-emitting laser (VCSEL) technology with a built-in voltage-tunable, wavelength-selectable etalon (Fabry-Perot interferometer) for precision wavelength selection. This technology could also be applied to the IR for detectors. Using MEMS technology, reflective parallel-plate etalons can be constructed with controllable spacing between the plates. These can therefore be tuned to the desired wavelength. This technology could enable individual, wavelength-specific, matched emitter-detector sensor pairs at the integrated circuit device size.

1.4.4 Electronic and Physical (Solid-State, Mass, Calorimetric)

While calorimetric sensor technology has been actively used for many years in flow controllers, it is an integrating technology with virtually no specificity. It is reasonably inexpensive and can be utilized with other technology as a complementary channel. Furthermore, calorimeters could be constructed via MEMS technology to further reduce size and cost. Likewise, gravimetric, or mass sensing, technology via QMB and SAW devices are purchasable technology. MEMS-

based devices, which should be integratable into multi-channel systems, are still largely in the research phase but the technology appears to be viable. All of these rely upon receptor chemistry coatings which are largely hydrocarbon-based. As such, they are limited in their operating temperature range. They may also be limited in the concentration range by the solubility of the receptor chemistry.

Electronic conductometric- and solid-state devices, which are being actively studied, fall into two very broad classes, which can be further bifurcated. Some are based upon organic receptor chemistries, which may have specificity via the chemical make up of the receptor. They would suffer from the same limitations associated with the hydrocarbon-based gravimetric sensors; however, they can be extremely simple to construct, are potentially very small, and lend themselves well to the multi-channel electronic-nose concept. As such, they are potentially inexpensive. They are also, integratable with on-board signal-processing technology and other sensor techniques that are compatible with MEMS.

A number of purely solid state technologies were discussed at length. They can be constructed as either passive (variable resistance) or active (transistor with internal gain) devices. They all appear to rely upon chemical reactions via surface catalytic activity to decompose the gas and inject carriers into the solid state materials. The decomposition rate is dependent upon the analyte, the catalysis, and the temperature. Hence, they too may lend themselves well to the electronic-nose concept. Even if a single catalytic material was used for several sensors, the temperature might be swept to generate analysis channels. If device response time is critical, an array of MEMS based devices might be constructed with individual heaters and temperature controllers. The response time of an individual channel device is anticipated to be very fast and primarily limited by the surface diffusion time of the gas to be broken down. Assuming the signal in such a sensor is limited by the analytic concentration or the response time, an active device, with gain, would be appropriate.

1.5 Hydrocarbon Dewpoint

A comprehensive literature assessment of hydrocarbon dew point and liquid dropout in natural gas has been conducted. A wealth of literature exists for measurements of single dewpoints at a given temperature or pressure, but most do not evaluate the dewpoint curve. To measure the Cricondentherm Hydrocarbon Dew Point (CHDP) requires measurement of many dewpoints. As a result of an extensive review of informational postings, academic literature, and any other available public data, sixteen different natural gas mixtures for which there has been an experimental dewpoint curve determined have been found and examined. Informational postings with compositional data for heavy hydrocarbons (C6+) were tracked in order to give validity to any potential natural gas mixture composition studied. Often, informational postings include the CHDP; however, in *all* cases this value is predicted using an equation of state.

A comprehensive literature assessment of the commonly used equations of state (e.g., Peng-Robinson and Soave-Redlich-Kwong, etc.) used to describe pipeline quality natural gas was conducted. To date seven common equations of state have been investigated to determine their predictive ability for the behavior of natural gas vapor-liquid equilibriums. The investigated equations of state were Peng-Robinson (PR), Soave-Redlich-Kwong (SRK), Predictive Soave-

Redlich-Kwong (PSRK), Statistical Associating Fluid Theory (SAFT), American Petroleum Institute (API)-SRK, Benedict-Webb-Ruben-Starling (BWRS), and Grayson Streed (GS). These seven equations were chosen based on perceived accuracy for hydrocarbon mixtures.

The included mixtures are representative of varying concentrations of higher hydrocarbons (C6+), and thus spans a wide range of CHDP's (-60 to +10 °C, -76 to +50 °F). The dependence of the experimental CHDP on the gas composition was determined. As one might expect, higher hydrocarbons (C6+) affect the CHDP much more strongly than the lower hydrocarbons. Given the variability in the 16 gas mixtures studied here, statistically significant (i.e., P-value < 0.05 corresponding to a 95% confidence interval) values for $\Delta T(K)/\Delta mol\%$ have been determined for many of the gas components.

The seven equations of state were evaluated based on their ability to accurately predict hydrocarbon dropout conditions of the 16 experimental mixtures. While the assessment of the ability of the various equations of state in predicting liquid dropout amounts would be useful, this study is limited to the prediction of the dewpoint curve. However, these two predictive abilities are directly linked and the evaluation of the prediction of the dewpoint curve should provide insight into the liquid dropout amount predictive capabilities of the various equations of state. Phase envelopes were calculated using each equation of state for every gas to determine how well the predicted values for hydrocarbon dewpoint match the reported experimental data. The Mean Absolute Deviation (*MAD*) was calculated by determining the difference in temperature at a given pressure, to quantify how well each of the equations predicted the vapor-liquid equilibriums.

All of the equations of states were tested for the first three gases; however, for gases 4-16 the BWRS equation of state was eliminated due to the poor prediction of the first three vapor-liquid equilibriums. Generally, the SAFT, SRK, API-SRK, and the GS equations of state were all very comparable and usually agreed best with the experimental data. Two molar ratios for C6 and larger hydrocarbons have been proposed by the Gas Processors Association (GPA 60/30/10) (C6/C7/C8) and the Natural Gas Council (NGC 47/36/17) to predict the behavior of different gas mixtures. These ratios were applied to 5 natural gas mixtures of known C1-C8 composition and the seven equations of state were used to predict the vapor-liquid envelopes that include cricondentherm and cricondenbar points. Using these data, an improved C6/C7/C8 ratio (68/28/4) was found to better fit the experimental data.

For most of the mixtures measured, the GPA ratio overestimated the dew point temperatures, contradicting the results from George et al. As one would expect, using the actual composition of the natural gas gives a better prediction of its phase envelope than using approximate ratios. The ratio with the best overall performance was the 68/28/4 ratio with an average absolute temperature deviation of 3.7 K using PR and 3.05 K using SRK. The GPA ratio had an average absolute temperature deviation of 5.95 using PR and 2.98 K using the SRK, insignificantly better using the SRK EOS but significantly worse using PR. The NGC ratio had the worst performance with an average absolute temperature deviation of 3.97 using Pr and 11.10 using SRK.

Modifications to the existing database of interaction parameters have been examined, but changes proved to be ineffective in improving the predictive ability of the equations of state.

Currently, molecular dynamics simulations are being designed and developed that will assist in determining the interactions between heavy hydrocarbons and the light hydrocarbons that determine the hydrocarbon dewpoint curve for these mixtures. The solvent effect of the methane phase on the confirmation of the large hydrocarbons will be determined, along with the change in free energy of the mixture due to introduction of large hydrocarbon molecules. These free energy changes will assist in the improvements over the existing equations of state.

2 GAS AND EQUIPMENT DATABASE

In response to recent issues regarding the interchangeability of liquefied natural gas with pipeline gas, the National Energy Technology Laboratory (NETL) began an effort to gather and generate data related to the effects of gas composition on those appliances and pieces of equipment which burn natural gas. In order to ensure that all available data was collected, a database was created to store and analyze the data collected. In this section, we describe the data that was gathered, as well as the implications for subsequent testing and analysis.

2.1 Data Overview

The database is approximately 56 MB in size, contains 25 separate data tables, 15 forms, 5 modules and over 50,000 rows of data.

Data of three main categories were collected for this effort:

- Gas compositions, tariffs, and specifications
- Natural gas-burning appliance and equipment information
- Data from previous tests and operational results related to the performance of equipment with respect to natural gas composition

Data on gas compositions are stored in the following tables:

- GasComp&Spec – contains 239 total entries in the following data types:
    - 85 actual gas composition readings
    - 21 specifications from equipment or appliance manufacturers
    - 29 LNG composition data records
    - 113 pipeline operator tariffs
    - 11 proposed gas compositions
    - 29 test gas compositions

- USGS_Database – contains over 13,000 entries of gas compositions from wells drilled in the U.S.

- GasVariability – contains daily data from April to September 2006 detailing gas compositions for the following pipeline segments:
    - Cove Point Sendout
    - Dominion - Cove Point
    - Dominion - Transco
    - Dominion - DTI
    - Duke Energy - East Tennessee
    - Duke Energy - Egan
    - Duke Energy - Everett Marine - Algonquin
    - Duke Energy - Everett Marine - Maritimes and Northeast
    - Duke Energy - Texas Eastern Transmission
    - El Paso - ANR Pipelines
    - El Paso - ANR Storage

- El Paso - Blue Lake Storage
- El Paso - SNG - Aiken
- El Paso - SNG - Bass Junction
- El Paso - SNG - Dalton
- El Paso - SNG - Elba Island
- El Paso - SNG - Macon
- El Paso - SNG - Port Wentworth
- El Paso - SNG - Wrens
- Florida Gas Transmission - Desoto
- Gulfstream - Station 200
- Lake Charles
- NW Pipeline - Spokane Lateral
- NW Pipeline - Moab
- SML - ELBA ISLAND SNG INTERCONNECT (GA)
- Trans Western Pipeline - San Juan Needles

- LakeCharlesHourly Data – contains hourly gas composition data for two time periods of LNG sendout from the Lake Charles LNG facility, 5/20-22/06 and 7/4-8/06 (this data table is not available in the public database)

- ExtendedCompositions – contains gas compositions from various sources where hydrocarbon compositions of C5 and above were recorded.

- USGS_ExtendedCompositions – contains gas compositions from USGS well records where hydrocarbon compositions of C5 and above were recorded.

Data on appliances and equipment are stored in the following tables:

- Equipment: 1391 total pieces of equipment
- Appliances: 3205 total appliances
- GasTurbines: Listing of the manufacturer, model number, location, install date and other attributes of all known gas turbines in electric power plants in the U.S. This table contains over 7,200 units (not available on the public database)

Data on test results and performance are stored in the following tables:

- Test results: 158 total from the Southern California Gas Company and GTI tests
- GasTurbineEmissions: Daily emissions data of NO_x, So_x, and CO_2 from gas turbine power plants in the vicinity of an LNG facility for the period of January to June, 2006

Following are some of the major data sources used in the database:

- Gas composition and specifications:
  - Tariffs: Federal Energy Regulatory Commission website
  - Actual gas compositions: Pipeline operators' website Informational Postings
  - LNG compositions: LNG terminal operators
  - Gas variability data: pipeline operators' Informational Postings on their websites, and data obtained from TMS' consultant

- Test gas compositions: Southern California Gas Company testing (2004) and GTI testing (2003)
- Appliance and equipment data: original manufacturers and the Gas Appliance Manufacturer's Association (GAMA)
- Gas turbine data: Platts PowerMap and PowerDat products
- Emissions data: EPA's Continuous Emission Monitoring website

The database is stored in a Microsoft Access format, and can be made available to interested parties. As example, Figure 2-1 shows an example of one of the user interfaces.

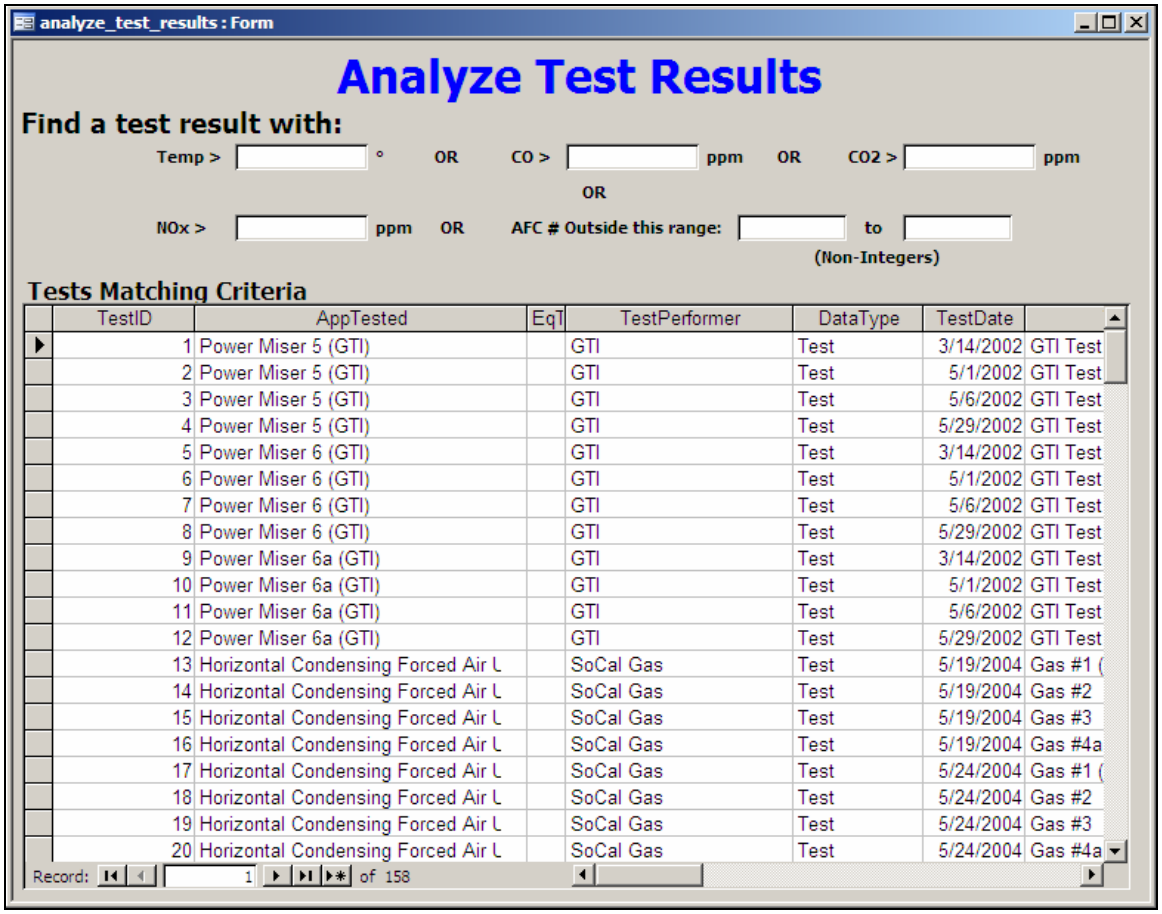

TestID	AppTested	Eq1	TestPerformer	DataType	TestDate	
1	Power Miser 5 (GTI)		GTI	Test	3/14/2002	GTI Test
2	Power Miser 5 (GTI)		GTI	Test	5/1/2002	GTI Test
3	Power Miser 5 (GTI)		GTI	Test	5/6/2002	GTI Test
4	Power Miser 5 (GTI)		GTI	Test	5/29/2002	GTI Test
5	Power Miser 6 (GTI)		GTI	Test	3/14/2002	GTI Test
6	Power Miser 6 (GTI)		GTI	Test	5/1/2002	GTI Test
7	Power Miser 6 (GTI)		GTI	Test	5/6/2002	GTI Test
8	Power Miser 6 (GTI)		GTI	Test	5/29/2002	GTI Test
9	Power Miser 6a (GTI)		GTI	Test	3/14/2002	GTI Test
10	Power Miser 6a (GTI)		GTI	Test	5/1/2002	GTI Test
11	Power Miser 6a (GTI)		GTI	Test	5/6/2002	GTI Test
12	Power Miser 6a (GTI)		GTI	Test	5/29/2002	GTI Test
13	Horizontal Condensing Forced Air L		SoCal Gas	Test	5/19/2004	Gas #1 (
14	Horizontal Condensing Forced Air L		SoCal Gas	Test	5/19/2004	Gas #2
15	Horizontal Condensing Forced Air L		SoCal Gas	Test	5/19/2004	Gas #3
16	Horizontal Condensing Forced Air L		SoCal Gas	Test	5/19/2004	Gas #4a
17	Horizontal Condensing Forced Air L		SoCal Gas	Test	5/24/2004	Gas #1 (
18	Horizontal Condensing Forced Air L		SoCal Gas	Test	5/24/2004	Gas #2
19	Horizontal Condensing Forced Air L		SoCal Gas	Test	5/24/2004	Gas #3
20	Horizontal Condensing Forced Air L		SoCal Gas	Test	5/24/2004	Gas #4a

Figure 2-1: Example of User Screen in Database.
This particular interface allows the user to find all the test data that meets the requirements specified above the data rows.

2.2 Implications from the Database

The purpose of generating the database was to identify gaps in what was known about the effect of fuel composition on various equipment, and guide the investigation. The database and survey of the literature shows that some early and recent studies of fuel effects on gas appliances are reported in the literature. The effect of gas composition for reciprocating engines has also been studied for situations where gas engines are used with fuel variability. In contrast, few published reports discuss the effect of gas composition on low-emission turbines. Low-emission *premixed*

combustors are a relatively recent development (within the last 15 years) and have not been used extensively with wide fuel variability. This is why NETL chose to focus experimental investigations on gas turbine combustion.

In discussions between DOE Office of Fossil Energy and the Federal Energy Regulatory Commission, it was decided that this study would not consider the effect of fuel composition on appliances and industrial burners. A separate investigation of industrial burners was recently commissioned by the California Energy Commission (CEC) and will investigate the effect of changing fuel type on the most common industrial burner applications in the state of California. NETL research staff are part of the advisory board for this CEC study, and will communicate findings to DOE as they are made available.

Another issue that was identified in the development of the database was the rate of changing gas composition. In particular, few studies have considered how completely a change in gas composition is transmitted along the supply pipeline. This motivated the study presented in Section 3, and also the review of sensor technology in Section 6. Where gas composition changes are expected, sensors may be integrated with control systems to accommodate rapid fuel variability.

Finally, during the course of collecting information for the database, more questions about gas quality were raised. Gas quality issues were included in this effort by investigating hydrocarbon dropout described in Section 7.

3 PIPELINE MIXING

A combination of computational fluid dynamics (CFD) and a closed form semi-analytical model[1] was used to illustrate two scenarios where different gases with differing compositions mix at a pipeline junction. For example, if LNG is added to a main pipeline, how long will it take to mix to some average composition with the main gas? First, it was shown that *steady* injection of a gas into a flowing main would mix to an average composition in a relatively short distance; typically within 100 pipe diameters. Second, it was shown that during *transient* injection, (e.g., when a branch supply is activated) the interface between the new and old average composition would flow well-defined in the pipeline for very large distances (> 100 km). Thus, gases with different composition appear to move as "packets" though the pipeline. Abrupt changes in gas composition will be delivered through the pipeline with only modest attenuation, assuming no additional flow disturbances occur along the length of the pipe. This type of behavior is documented in a California Energy Commission Report.[2] In the scenario described in the report, a monitoring station in Redding, CA measures an increase in the BTU content over a 5 hour period. A monitoring station in Pittsburg, CA, 200 miles (320 km) downstream then measures a similar increase in BTU content (composition) 8 hours later.

It should be emphasized that the results are intended to be illustrative generalizations. More accurate results will necessarily be situation dependent and thus require specific application of theory, simulation and experiment to more definitively characterize the scenario.

3.1 Part I: Steady Evolution of Compositional Discontinuities at a Pipe Junction

Several Computational Fluid Dynamics (CFD) simulations are performed to illustrate the flow and mixing in the vicinity of a pipe junction with two different compositions of gas feeding a single pipe. For the pipe geometry shown in Figure 3-1, two test conditions are simulated using the Reynolds Averaged Navier-Stokes (RANS) approach. The flow conditions and compositions of the two pipes are listed in Table 3-1 and Table 3-2. Additionally, a Large-eddy simulation (LES) is performed of the first test condition. The results are compared with the results of the less expensive RANS simulation to highlight additional flow structures not resolved by the RANS calculations. The results from either solution methodology can be extrapolated to distances beyond the simulated domain using an exponential function.

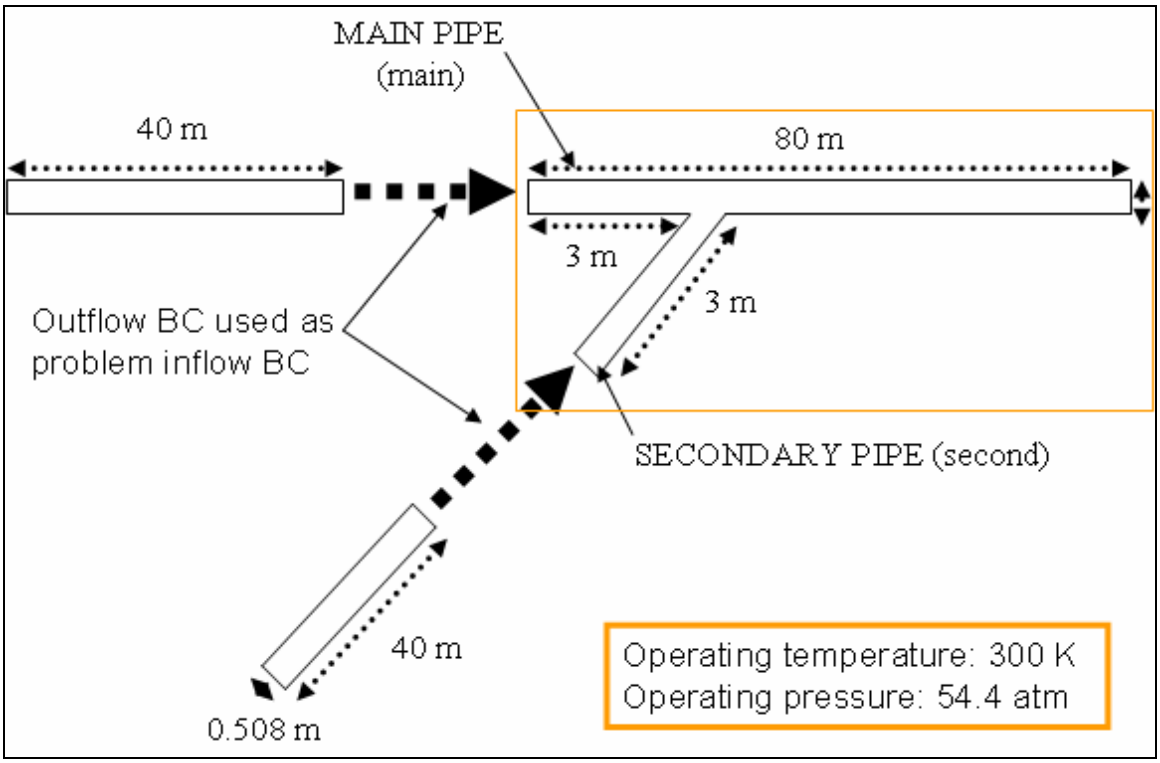

Figure 3-1: Schematic of Pipe Junction.

Table 3-1: Flow Rates.

	Case 1	**Case 2**
Primary (Main) (kg/s)	50.07	50.41
Secondary (kg/s)	36.11	34.04
Outlet (Total) (kg/s)	86.18	84.45

Table 3-2: Gas Composition.

	Case 1	**Case 1**	**Case 2**	**Case 2**
	Primary	Secondary	Primary	Secondary
CH_4	0.92	0.86	0.91	0.96
C_2H_6	0.03	0.08	0.04	0.03
C_3H_8	0.006	0.04	0.01	0.005
C_4H_{10}	0.003	0.015	0.006	0.001

3.1.1 Pipe Junction Geometry

The configuration and geometry of the pipe junction are shown in Figure 3-1. The domain simulated is the vicinity of a "Y-junction" in a hypothetical pipeline. The dimensions, flow rates, and compositions have been selected within the range typically found in the U.S. pipeline system, including both domestic and imported (LNG) natural gas compositions (see references of

Table 3-7). The nominal operating pressure of the system was 54.4 atm for all simulations. The primary pipe has a diameter of 30 inches (0.762m) with a operating velocity of (15 m/s), while the second pipe has a diameter of 20 inches (0.508m) and a velocity of (10 m/s). The flow conditions in terms of mass flow rates are listed in Table 3-1. The two cases studied differ in the compositions of gas through the two upstream legs of the pipe junction. The gases are composed of differing amounts of methane (CH_4), ethane (C_2H_6), propane (C_3H_8) and butane (C_4H_{10}). The mass fractions are listed in Table 3-2.

3.1.2 Reynolds Averaged Navier-Stokes Simulations

Several RANS simulations were performed of the above described configuration. Each result was generated from 3 simulations. First, a simulation was performed for each of the upstream sections of the pipe legs to provide fully developed inlet profiles for a third simulation which began approximately 10m upstream of the intersection point and various distances downstream of the intersection. The simulations were performed using the FLUENT™ CFD package. The simulations were solved using the steady segregated solver with the standard k-ε model.[3,4] All the turbulent scalar fluxes (energy, species, turbulent kinetic energy (k), turbulent dissipation rate (ε)) are modeled using the simple-gradient diffusion hypothesis (SGDH), though other closures have been proposed.[5,6] The approach used is similar to studies of mixing in "T-junctions" by Tang et al.[7] and Kok and van der Wal.[8] Results using the "realizable" form of the k-ε model[9] provided qualitatively similar results as did results using a finer grid resolution. The fine grid was obtained by refining the grid in the vicinity of the junction, resulting in 75% increase in cell count.

For the analysis of the results it is convenient to normalize the methane mass fraction, $\langle Y \rangle$ as

$$\langle Y \rangle = \left| \left(\frac{Y - \tilde{Y}}{Y_1 - Y_2} \right) \right|$$

where Y_1 and Y_2 are the methane mass fractions in the primary and secondary pipes, $\tilde{Y} = \frac{1}{\bar{\rho} A} \int_A \rho Y dA$ is the mass averaged mass fraction and $\bar{\rho} = \int_A \rho dA$ is the cross-sectionally-averaged density. The normalized mass fraction is analyzed at five lines parallel to the axis of the primary pipe. The locations are shown in Figure 3-2. The normalized mass fraction is used as an indicator of the degree of radial mixing in the pipe.

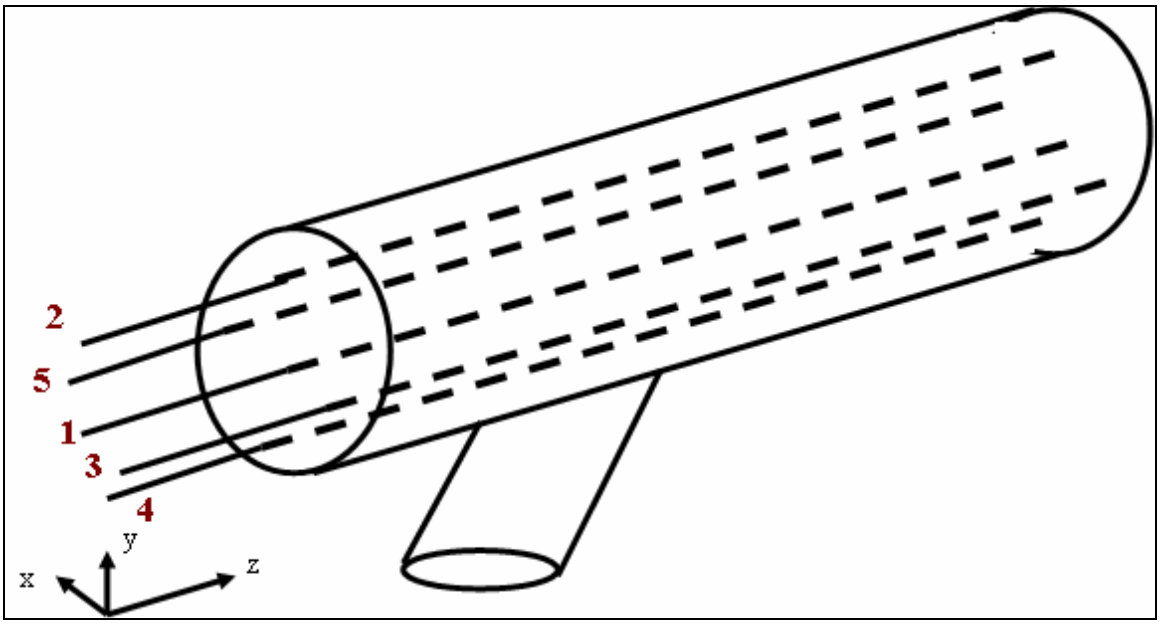

Figure 3-2: Axial Sampling Lines.

The evolution of the normalized mass fraction at the sampling lines for the first test case is shown in Figure 3-3 (Figure 3-4 – logarithmic). The evolution is quite similar for all the lines. By the end of the computational domain, 80m, the fluid in the pipe shows less than 1% of the peak un-mixedness for all lines. Figure 3-5 (Figure 3-6 – logarithmic) shows the corresponding lines for the second case. The exit un-mixedness for this case is also less than 1% of the peak. The evolution of the normalized mass fraction is quite similar for both cases, as can be seen more clearly in Figure 3-7 (Figure 3-8 – logarithmic). A sign change in the value of the normalized mass fraction is the cause of the non-monotonic variation in any of the sampling lines shown in the figures.

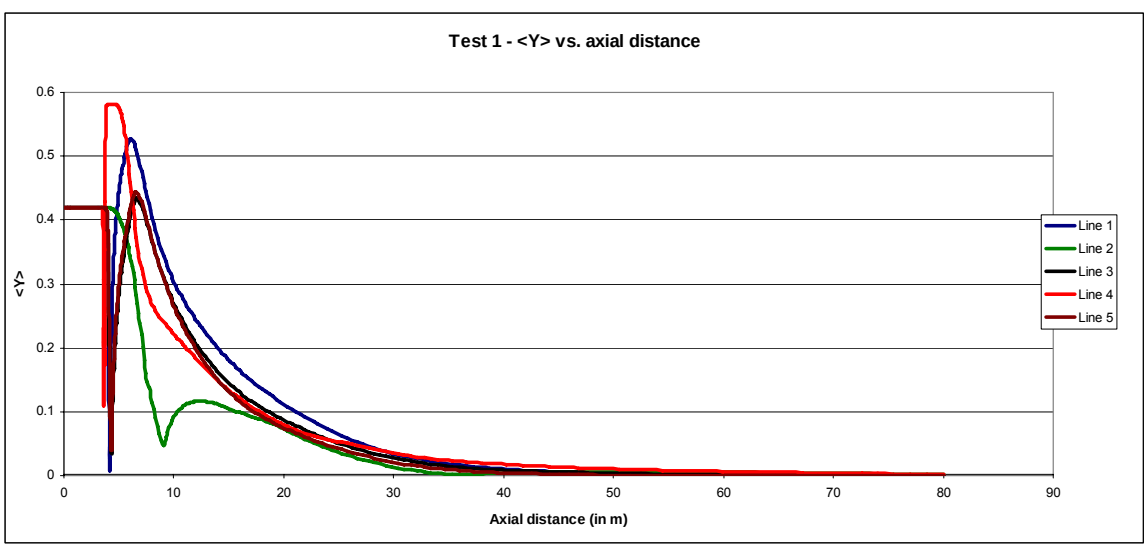

Figure 3-3: Streamwise Evolution of Normalized Methane (Case 1).

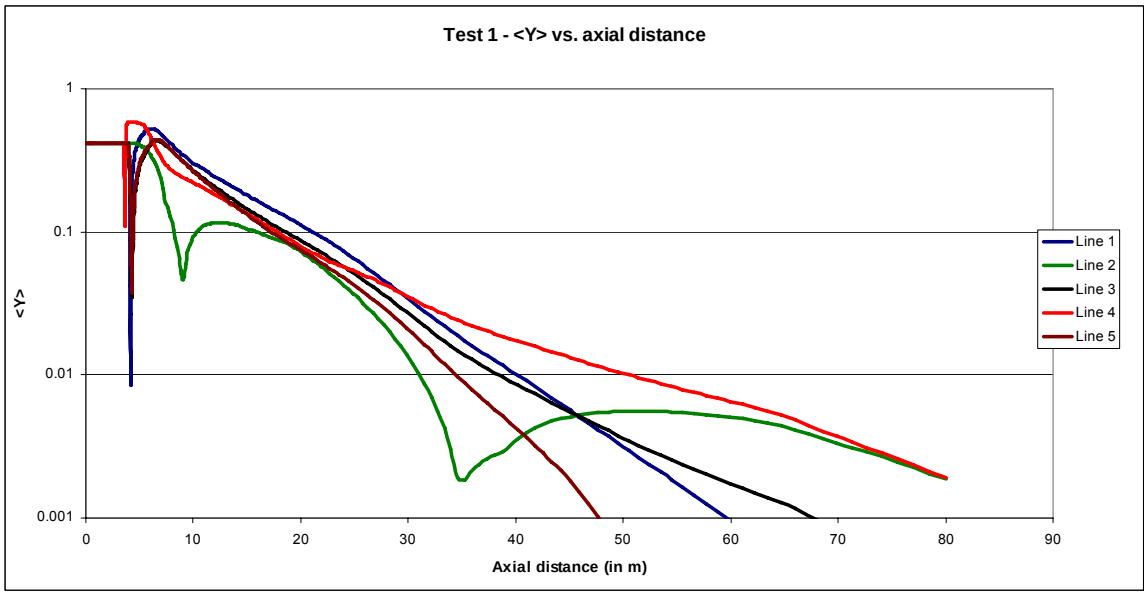

Figure 3-4: Streamwise Evolution of Normalized Methane (Case 1 - Log Scale).

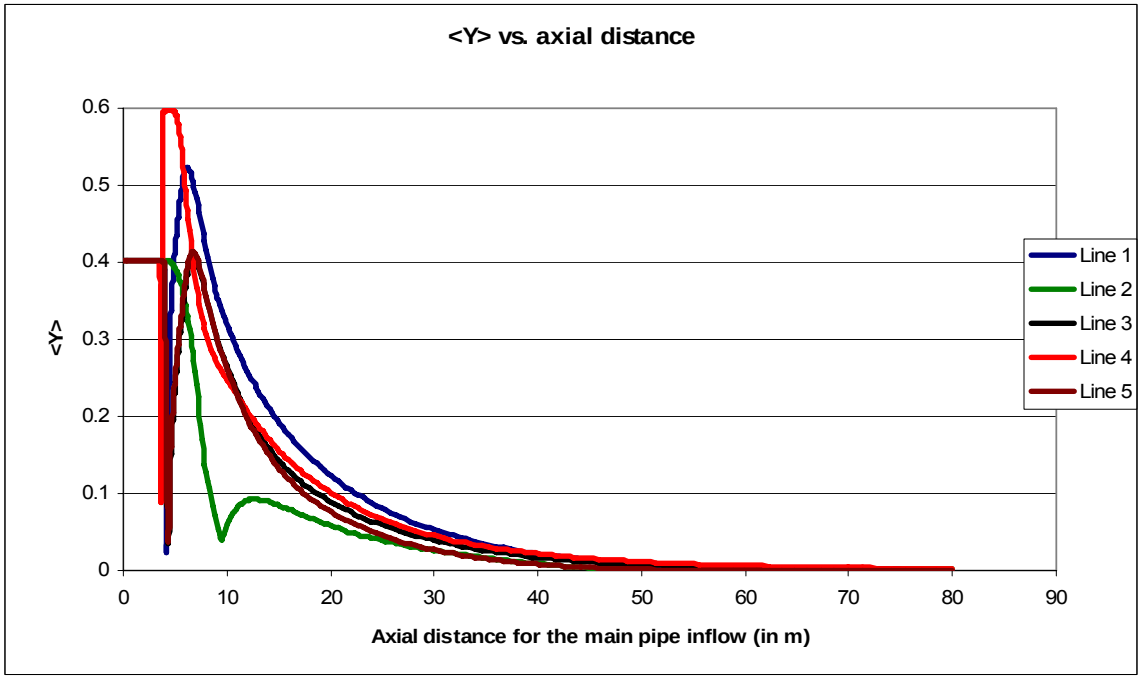

Figure 3-5: Streamwise Evolution of the Normalized Methane Mass fraction (Case 2).

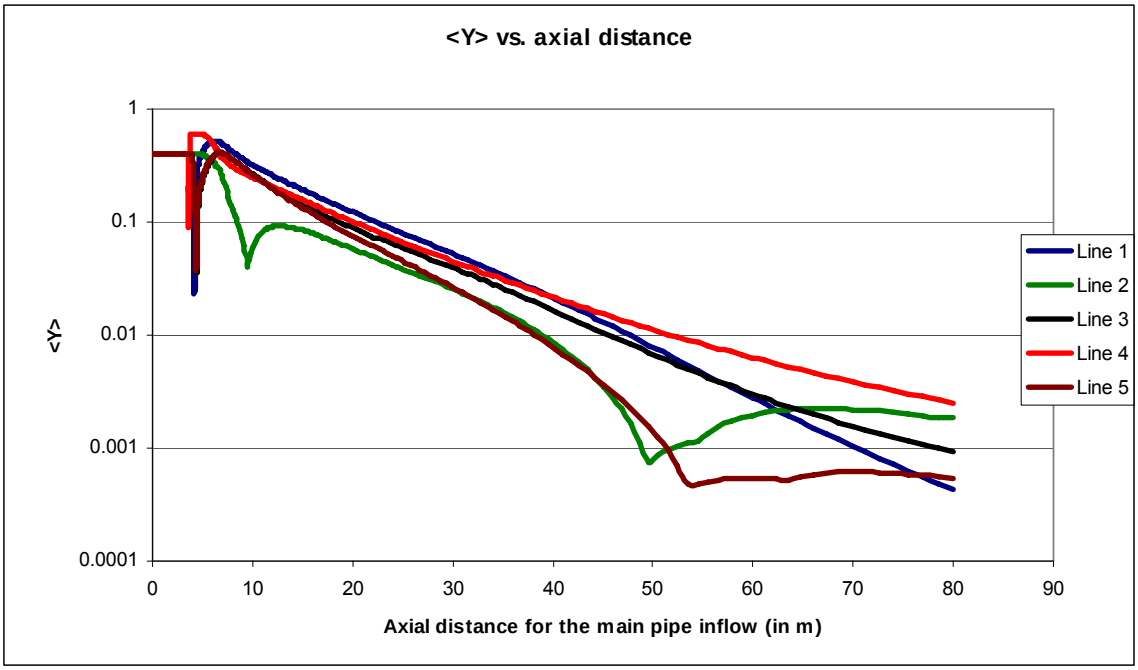

Figure 3-6: Streamwise Evolution of Normalized Methane Mass Fraction (Case 2 – Log Scale).

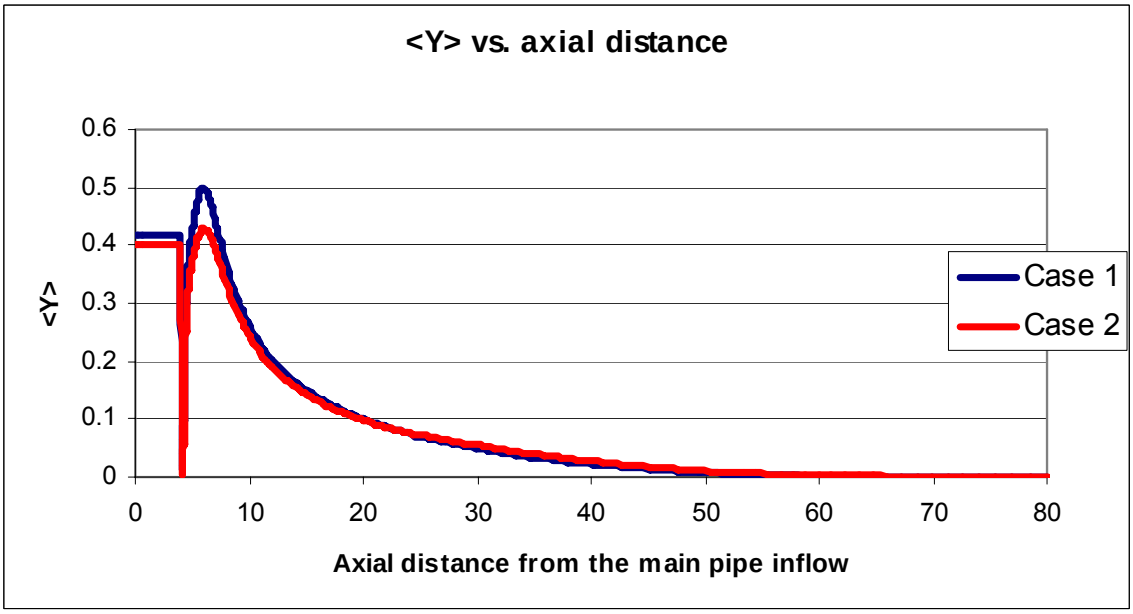

Figure 3-7: Comparison of Streamwise Evolution of the Normalized Methane Mass Fraction for Two Flow Conditions (Line 1).

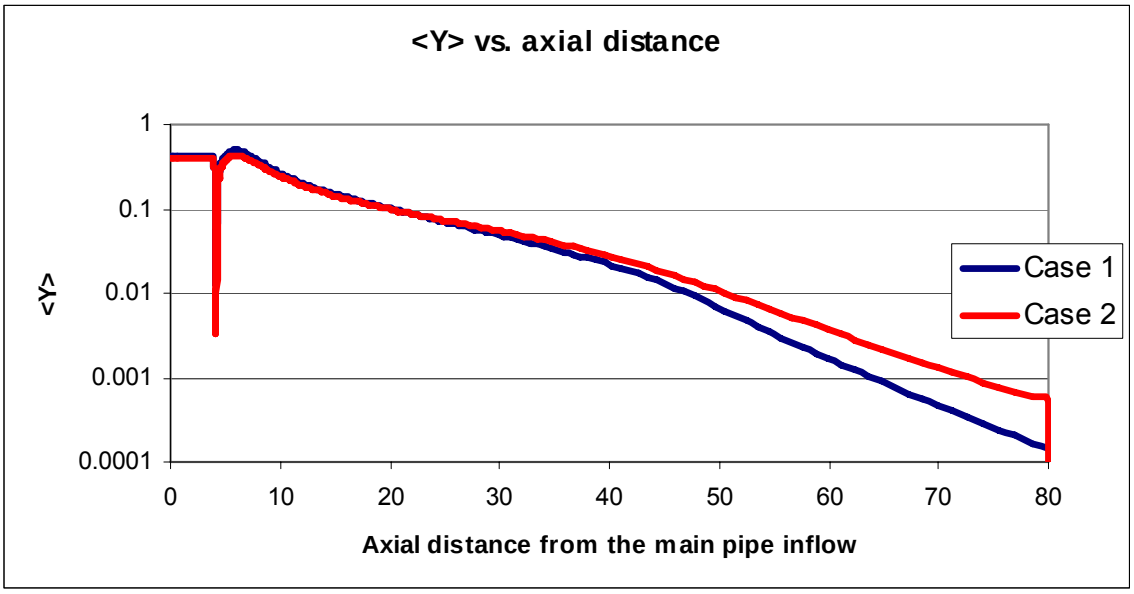

Figure 3-8: Comparison of the Streamwise Evolution of the Normalized Methane Mass Fraction for Two Flow Conditions (Line 1 – Log Scale).

The behavior of the profiles downstream of the junction suggests the following fit:

$$<Y>(x) = <Y>(x_0)\exp\left(-\frac{x - x_o}{L}\right)$$

Figure 3-9 (Figure 3-10 – logarithmic), shows the application of this formula to the numerical results. The first, labeled "Near Field" is calculated by matching un-mixedness at the junction and then adjusting L to best match the downstream values. The parameters for this fit are $x_0 = 0.58$m and L = 9m. For the second curve, labeled "Far Field", the parameters, $x_0 = 32.1$m and L = 18.5m were calculated to maximize the agreement the downstream behavior of the simulation at the expense of near field agreement.

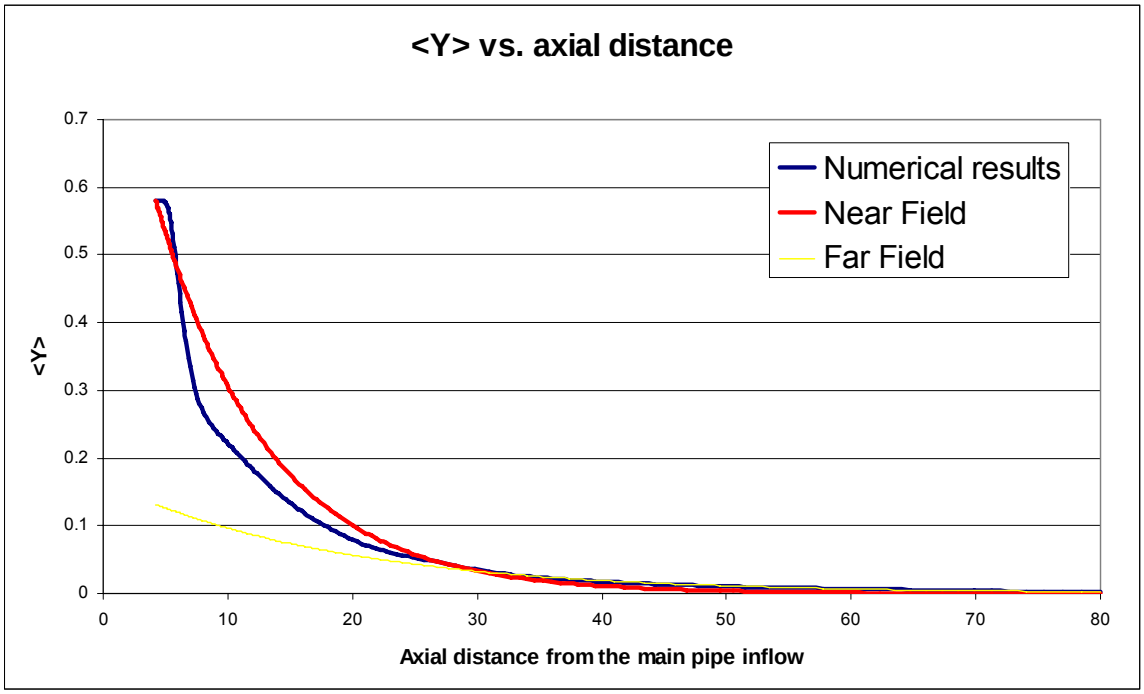

Figure 3-9: Normalized Mass Fraction Curve Fit.

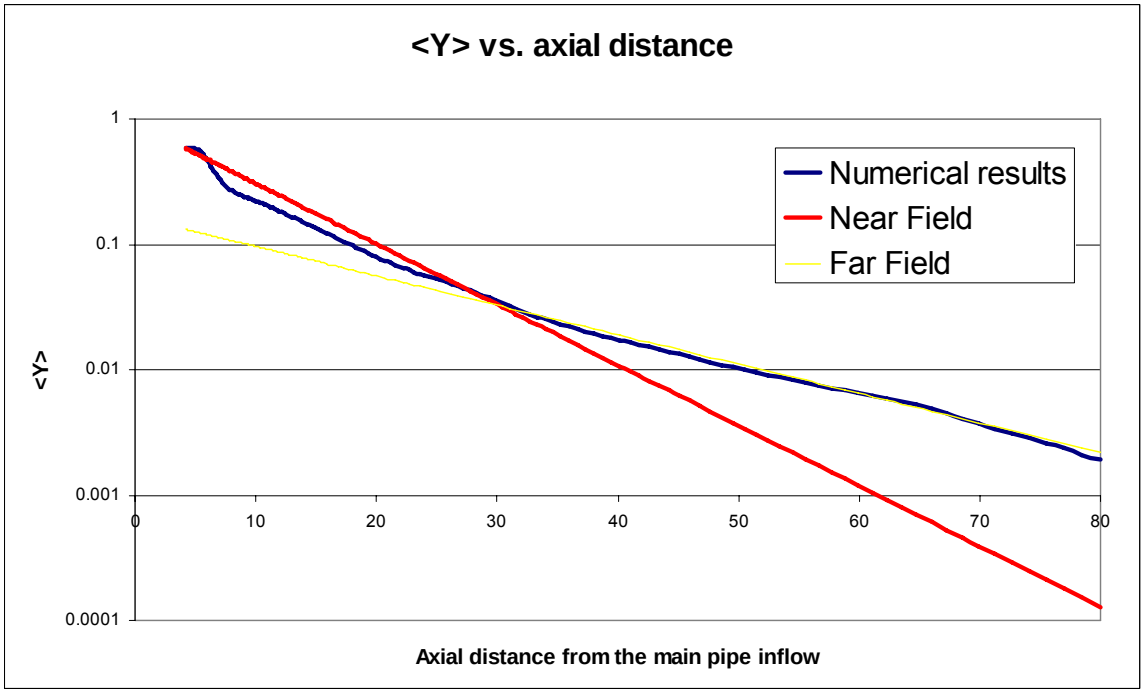

Figure 3-10: Normalized Mass Fraction Curve Fit (log).

3.1.3 Large Eddy Simulation

A Large Eddy Simulation (LES) was performed to illustrate the mixing process at the pipe junction for length scales finer than what is computed with the RANS simulations. LES should produce more accurate results since it resolves the large geometry/problem dependent fluid motions while applying the turbulence modeling procedure only to the small scale universal (geometry/problem independent) fluid motions.[3,4] The simulation was performed at the first operating condition (Table 3-1, Table 3-2, and Figure 3-1). The dynamic kinetic energy subgrid model[10] in FLUENT was used to perform the simulations. As with the RANS model, the simple gradient diffusion hypothesis is used to calculate the unresolved scalar fluxes. A fine mesh with approximately 1.4 million cells was used. The approximate distribution is illustrated in Figure 3-11. The mesh resolution is sufficient for LES in the junction region, but is likely too coarse in other regions. This distribution both damps reflections from the computational boundaries and makes efficient use of fixed computer resources.

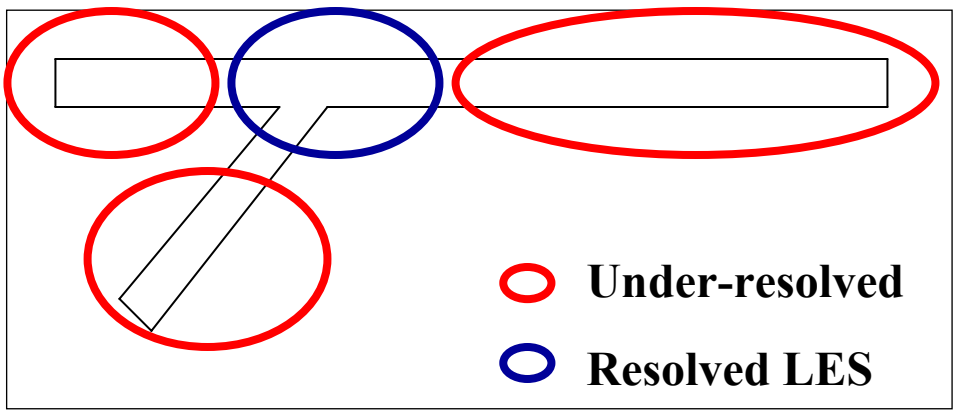

Figure 3-11 – Continuous Mixing LES Strategy.

The comparison of the streamwise evolution of the normalized methane mass fraction (Figure 3-12) indicates that the LES predicts more efficient mixing of the two gas streams. This can be explained by fact that the LES resolves in both time and space additional large scale vortices which enhance the mixing process. The LES results shown have been extrapolated using an exponential function, similar to what is described in the previous paragraph for the RANS simulations.

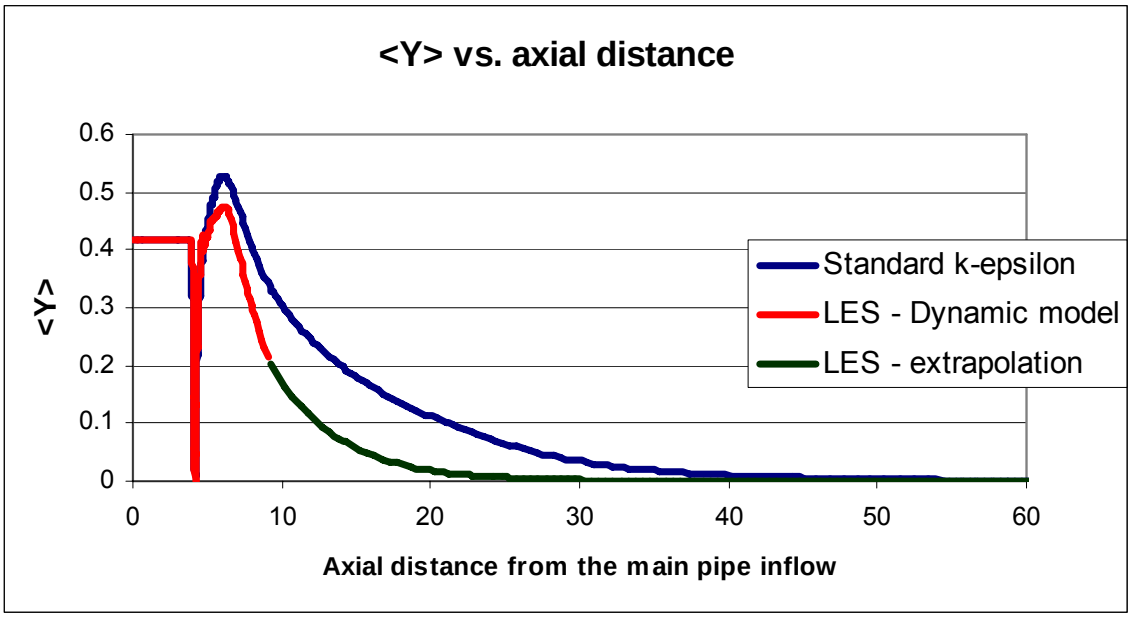

Figure 3-12: Normalized Methane Mass Fraction, LES verses RANS.

Figure 3-13 shows a "snapshot" of the methane mass fraction at a cut-plane of the pipe. The enhanced mixing provided by LES can be seen in Figure 3-13 by the pocket of relatively low methane mass fraction at the down-stream corner of the elbow and by the irregular interface along the centerline. The RANS results shown in Figure 3-14, in contrast, show a relatively smooth interface between the gas supplies. The mixing in the RANS simulation is only provided by unresolved fluid motions through the eddy-diffusivity. Figure 3-15 and Figure 3-16 show the corresponding velocity vectors. The recirculation region predicted by the LES downstream of the junction is quite evident in Figure 3-15. For this study the RANS calculations provide computationally efficient method of estimating the amount of mixing, and relative to the LES provide a more conservative estimate of the rate of mixing. For the scenarios simulated, either modeling technique predicts nearly complete mixing within 100 pipe diameters.

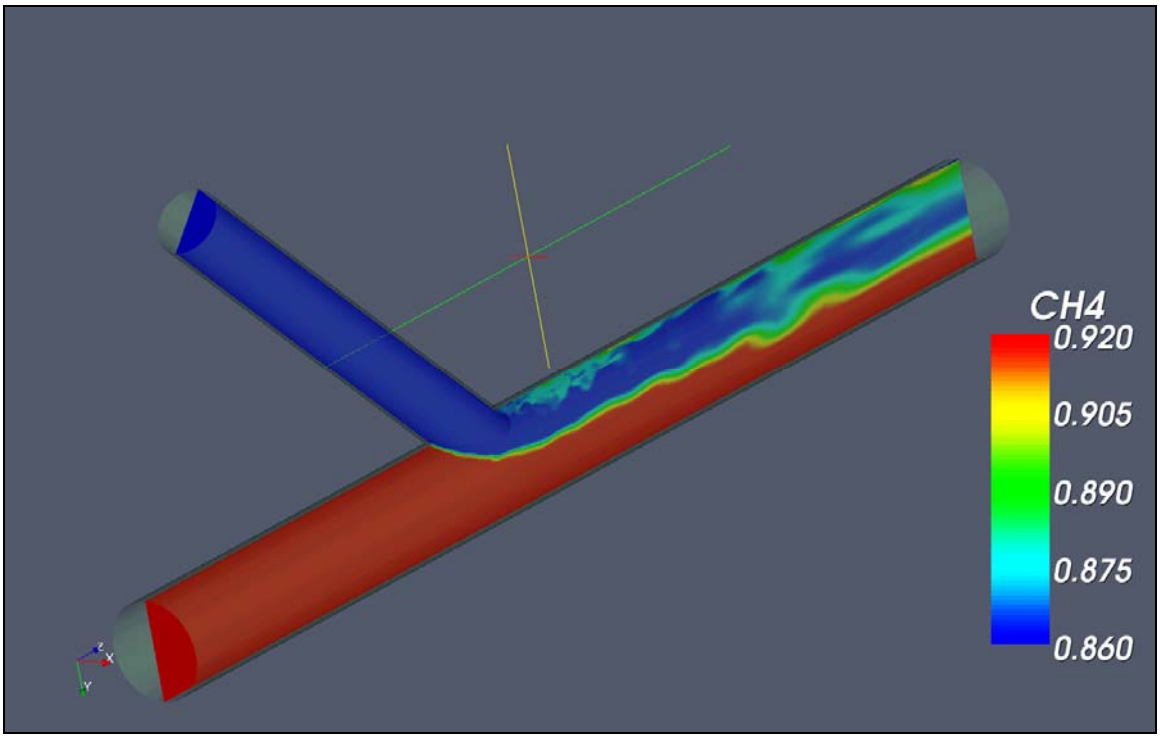

Figure 3-13: Methane Mass Fraction (LES).

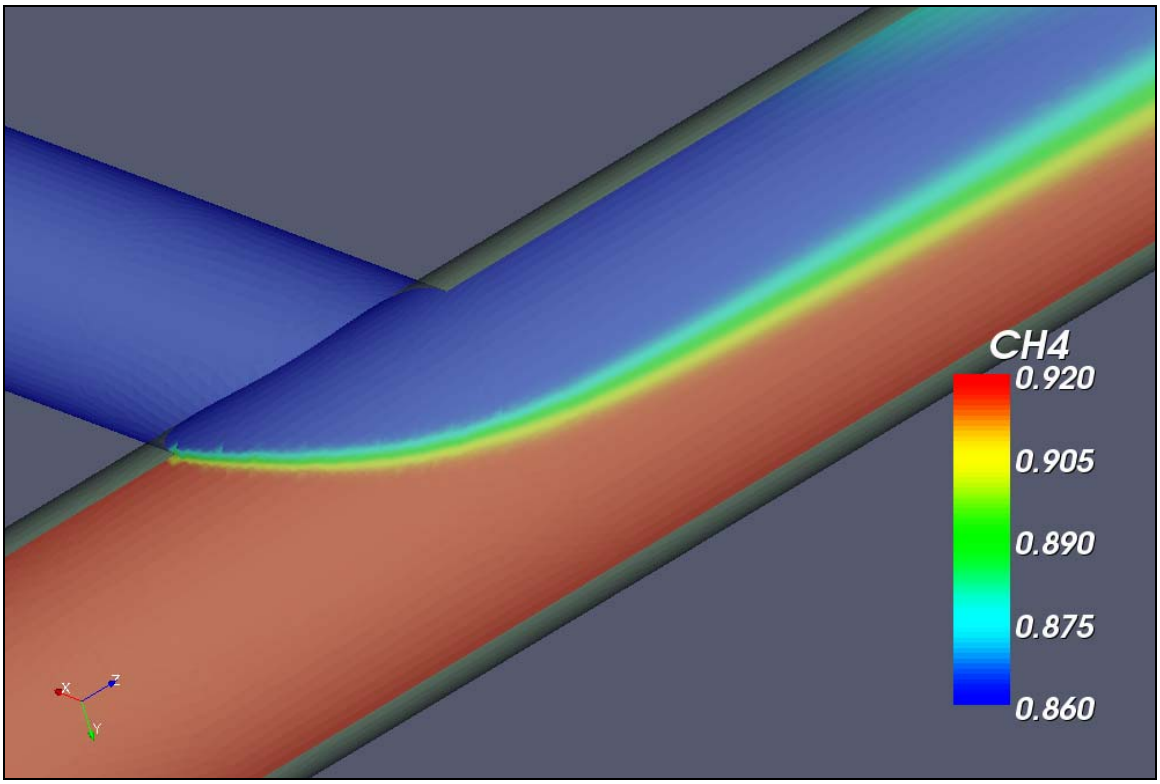

Figure 3-14: Methane Mass Fraction (RANS).

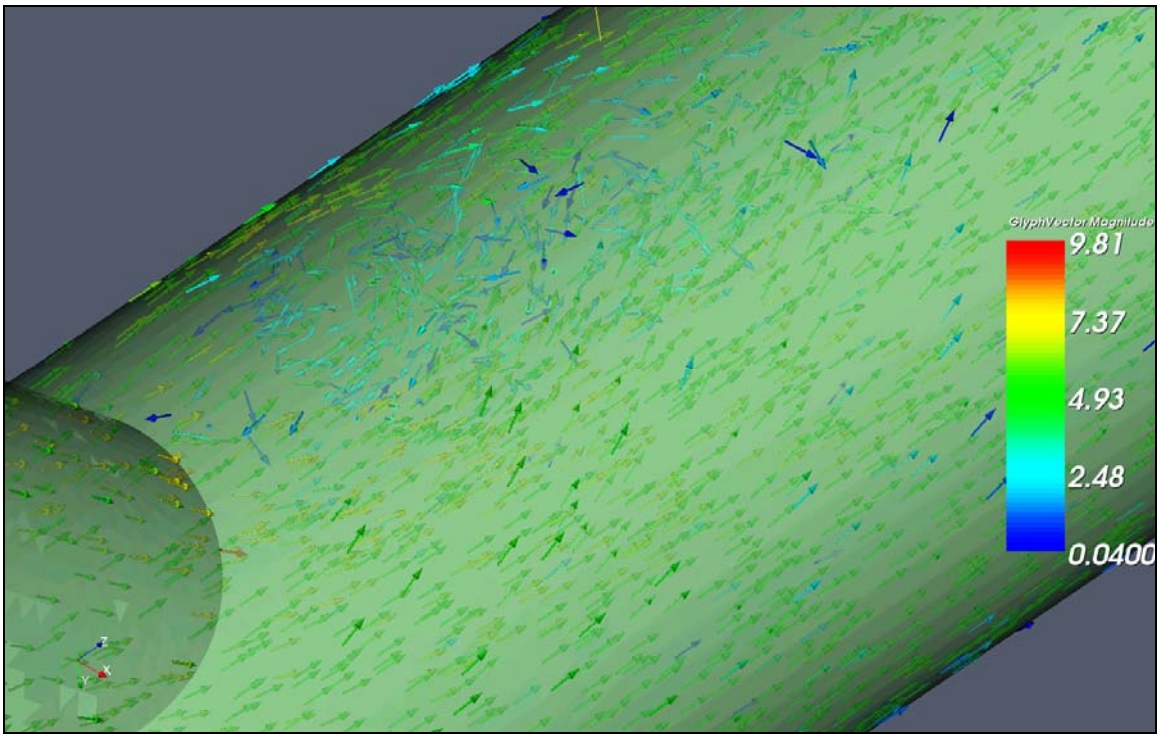

Figure 3-15: Velocity Vectors in Junction Recirculation Region (LES).

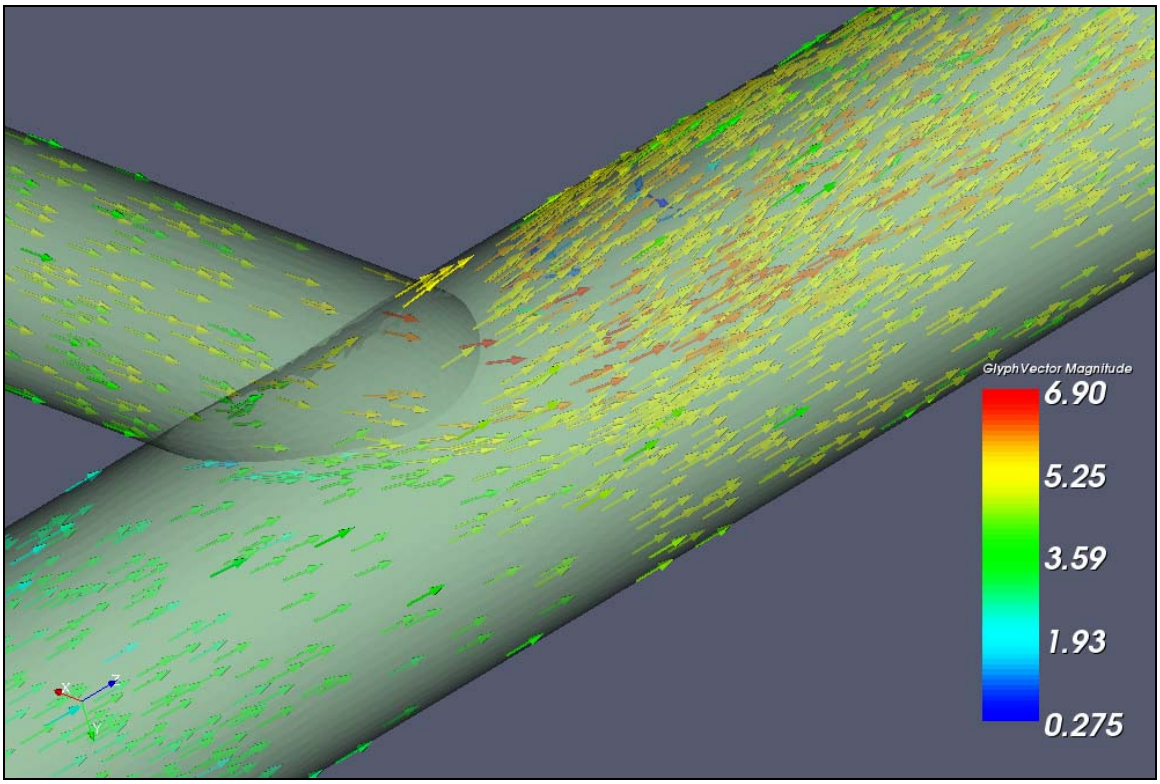

Figure 3-16: Velocity Vectors (RANS).

Table 3-3: Grid Resolution.

Mixture	Grid	Δy_{wall} (Main)	Y+ (Main)	Δy_{wall} (Secondary)	Y+ (Secondary)	Number of Cells
Case 1	A	0.0025 m	430	0.0025 m	480	**400k**
Case 1	B	0.0015 m	260	0.0015 m	300	**400k**
Case 2	A	0.0025 m	440	0.0025 m	500	**400k**

Table 3-4: Locations of Axial Sampling Lines.

Line	Y (in m)	Z (in m)
1	0	0
2	0.15	0
3	0	-0.15
4	-0.15	0
5	0	0.15

Table 3-5: Transient Mixing - Initial Conditions.

Species	Main	Second
CH_4	0.90	0.95
C_2H_6	0.03	0.025
C_3H_8	0.02	0.015
C_4H_{10}	0.01	0.005

Table 3-6: Transient Mixing - Inlet Conditions.

Species	Main	Second
CH_4	0.92	0.86
C_2H_6	0.03	0.08
C_3H_8	0.006	0.04
C_4H_{10}	0.003	0.015

3.2 Part II: Evolution of Streamwise Compositional Discontinuities in Gas Pipelines

The initial development and evolution of an streamwise gas discontinuity is illustrated using a generalization of an analytical solution first proposed by Taylor[1,11] and computational fluid dynamics (CFD) simulations.

The analytical solution for the propagation of a discontinuity in the axial composition is described in Section 3.2.1. This section is followed by a description of the CFD model and verification of the analytical formula (Section 3.2.2). In Section 3.2.3, the results of a "supply switching" event are presented as well as the procedure by which the parameters for the analytic solution are extracted from the CFD results. The final section, Section 3.2.5, describes the application of the analytical model including sensitivity to input parameters.

3.2.1 Semi-Analytical Solution

The equation for the evolution of the cross-sectionally-averaged mean mass fraction Y of a chemical constituent in a duct can be written as

$$\rho\left(\frac{\partial Y}{\partial t}+U\frac{\partial Y}{\partial x}\right)=\frac{\partial}{\partial x}\left(\rho D_{eff}\frac{\partial Y}{\partial x}\right)$$

where D_{eff} is the effective diffusivity or dispersion coefficient.[1,11] The effective diffusivity is in general a function of Reynolds number and also Schmidt number. The equation can be simplified by measuring distance from the center of the discontinuity, x_m, which moves at the speed of the bulk flow velocity, U.[12]

$$\frac{dx_m}{dt}=U(x)$$

The result is an equation,

$$\rho\left(\frac{\partial Y}{\partial t}\right)=\frac{\partial}{\partial s}\left(\rho D_{eff}\frac{\partial Y}{\partial s}\right)$$

which describes the thickening of the discontinuity during propagation. In this formula, $s = x - x_m$, is the distance from the center of the concentration transition zone. By assuming the dispersion coefficient is independent of position an analytical solution for this equation[1,11,13,14,15] with an initially infinitely sharp discontinuity is:

$$\theta(s,t)=\frac{Y(s,t)-Y_m}{Y_{up}-Y_{down}}=\frac{1}{2}erf\left(\frac{s}{2\sqrt{D_{eff}t}}\right)$$

where Y_{up} is the mass fraction of constituent upstream of the discontinuity and Y_{down} is the mass fraction of constituent downstream of the discontinuity and Y_m is the average, which is also the value at the discontinuity. Figure 3-17 shows a plot of this function.

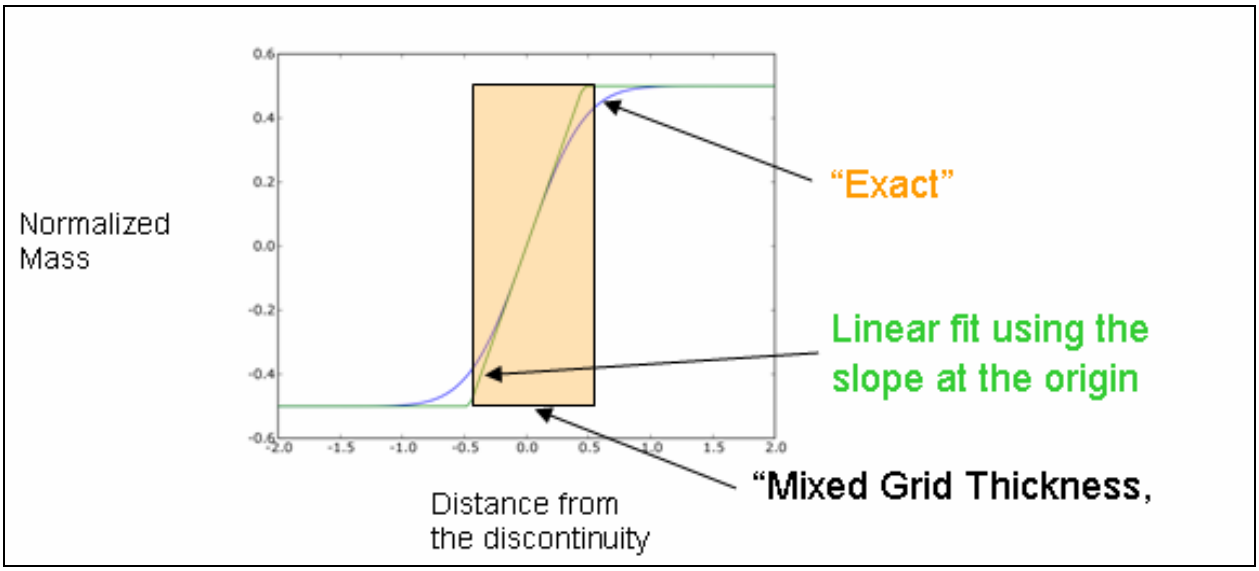

Figure 3-17: Analytical Mixing Zone.
***U* = 1 m/s, t = 100 s, D_{eff} = 0.1 m^2/s, δ_0 = 0 m**

The thickness of the average concentration transition zone, (Figure 3-17 shaded area), can estimated from the slope of the mass fraction at the center of the discontinuity (s = 0).

$$\frac{1}{\delta(t)} = \frac{\partial\theta}{\partial s}(s=0,t) = \frac{1}{2}\left(\frac{1}{\sqrt{\pi D_{eff} t}}\right)$$

The thickness of the transition (mixing) zone can then be used to estimate the *composition transient* or the time internal at which the composition will change from the initial value to the new value.

$$\tau(t) = \frac{\delta(t)}{U}$$

An infinitely thin composition discontinuity would correspond to an instantaneous temporal change in composition, which is not realistic. The equation can be modified as follows to account for a finite initial discontinuity, δ_0 and corresponding supply switching time, $\tau_0 = \delta_0/U$.

$$\theta(s,t) = \frac{Y(s,t) - Y_m}{Y_{up} - Y_{down}} = \frac{1}{2} erf\left(\frac{s}{\sqrt{4D_{eff} t + \frac{\delta_0^{\,2}}{\pi}}}\right)$$

This leads to the following expression for the thickness of the transition length.

$$\delta(t) = \sqrt{4\pi D_{eff} t + \delta_0^{\,2}}$$

3.2.2 Computational Fluid Dynamics of the Development of an Axial Discontinuity

CFD is used to provide an illustration of the initial development of an axial composition discontinuity, which is a highly-disorganized multidimensional flow.

Figure 3-18 describes the simulation in which the gas composition changes abruptly due to a switch in supply from one leg to a second. This is a simplification of the type of scenario which might occur when a pipeline "null point" moves across a T-junction. For this case, there are two inlets with different compositions (Table 3-7). Initially the flow in the pipe main pipe is supplied by the first inlet (Inlet 1). Over a specified time interval (1 s), the mass flow rate of the first inlet decreases linearly, while the flow rate of the second inlet increases to keep the flow rate to main pipe constant (21.55 kg/s). The diameter of all the pipe sections is 0.762m (30in) and the length of the outlet section is 50m.

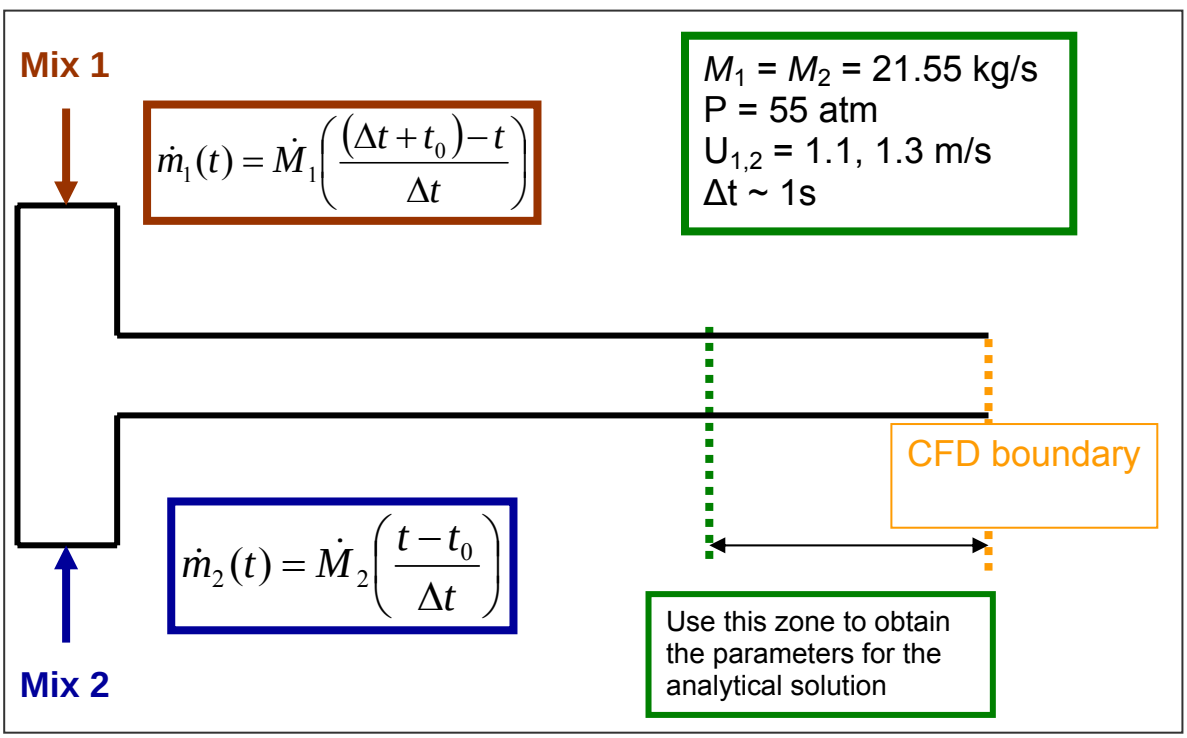

Figure 3-18: Transient Mixing Schematic.

The flow rates, composition (see Table 3-7) and operating pressure (55 atmospheres) were nominal values chosen from available data. The bulk velocity in the main pipe was initially 1.09 m/s, but increased to 1.3 m/s (2.9 mph). The switching time of 1 s was selected as an exaggeration of what is likely to occur in the field. The evolution of the initial discontinuity is

shown in Figure 3-19. After about 25 seconds, the flow is fully developed and the parameters for semi-analytical solution could be extracted. The standard k-ε model was used as with the previous simulations.

Table 3-7: Brief Survey of Natural Gas Compositions.

	Mix 1	**Mix 2**	**Union Gas[16]**	**Natural Gas Org[17]**	**GTI[18]**	**GTI[18] (LNG imported)**
Methane	**0.70**	**0.94**	87.0-96.0	70-90	89.6-96.5	86-96 (C1)
Ethane	**0.12**	**0.03**	1.8-5.1	0-20	1.5-4.8	3-10 (C2)
Propane	**0.08**	**0.01**	0.1-1.5	0-20	0.2-1.2	0.5-5 (C3)
Butane	**0.07**	**0.005**		0-20	0.1-0.6 (and other C_4)	0.0-2 (CX)
Nitrogen	**0.03**	**0.015**	1.3-5.6	0-5	1.0-4.3 (including CO_2)	< 0.5

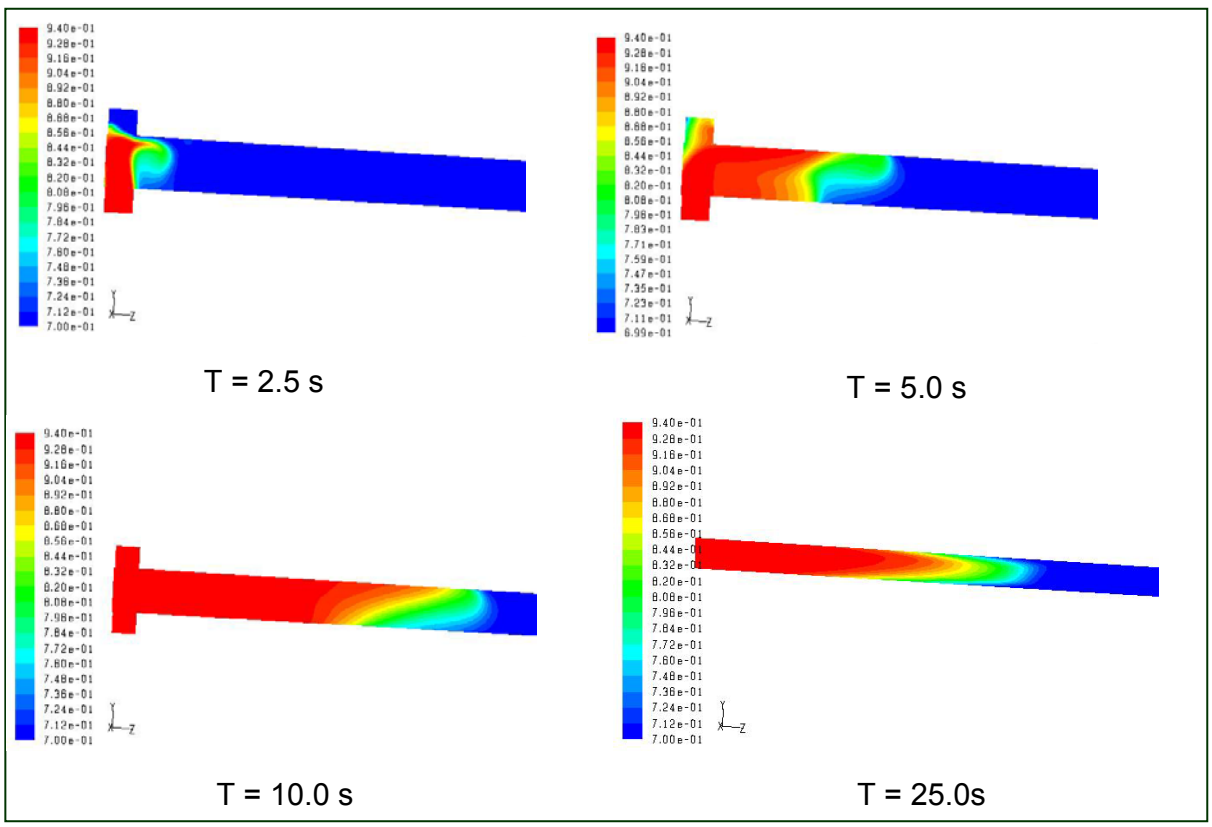

Figure 3-19: Evolution of the Initial Discontinuity.

3.2.3 Calculation of the Effective Diffusion (Dispersion) Coefficient

Numerous formulas to calculate the dispersion coefficient for flow in pipes have been developed starting with the work of Taylor.[11,1] Ekambara and Joshi[19] have cataloged several of these formulas. The formulas found in Taylor,[11] Tichacheck, Barklew, and Baron,[20] and Zitny and Thym[21] are used to estimate the dispersion coefficients for the flow rate, the operating pressure and the two compositions (Table 3-7) used in this study. The values are listed in Table 3-8.[*] The estimates calculated using Tichacheck et al.[20] formulas use Reichardt's generalized turbulent velocity profile and Prandtl's universal friction law.[22]

As alternative to the empirical formulas, the dispersion coefficients may be estimated from simulations or experiments using a time history of the cross-sectionally averaged concentration of one of the gas constituent at one or more axial locations. The equations to perform this type of analysis can be found in Levenspiel[23] and Folger.[24] The application of this procedure to CFD simulations has been described by Ekambara and Joshi.[25,19]

Table 3-8: Calculated Dispersion Coefficients.

	Dispersion Coefficient Mixture 1 (Re = 3.27 x 10^6)	**Dispersion Coefficient Mixture 2 (Re = 3.15 x 10^6)**
Taylor[11]	0.150	0.176
Tichacek, Barkelew, Baron[20]	0.108	0.126
Zitny, Thym[21]	0.172	0.203

3.2.4 Analytical Solutions Results

The analytical solution is applied using a supply switching time (initial composition transient), τ_0, of 1.0 s, a mean velocity, U of 1.09 m/s and a dispersion coefficient, D_{eff} of 0.115 m^2/s. The velocity is selected within the range of the velocities of the two mixtures (1.09 and 1.31 m/s). The dispersion coefficient is within the range of the two values in Table 3-8 obtained from the procedure developed by Tichacek et al.[20] These input values were used to determine how fast the composition will change (*compositional transient,* **τ)** as the discontinuity reaches various positions along the pipe (Figure 3-19 and Table 3-9). Even after 100 km, the composition will change in slightly less than five minutes, indicating that the two gas supplies remain relatively segregated at a significant distance. It should also be noted that rate that the gas composition change at any particular "point" in the flow could be faster than the mean.

[*] The dispersion coefficients (effective diffusivities) shown in Table 3-8 and used for the calculations in Sections 3.2.4 and 3.2.5 are larger than the values in the draft reports. This increase in the dispersion coefficient effects increase the layer thickness, but does not significantly alter the general conclusions.

Table 3-9: Downstream Evolution of the "Compositional Transient, τ".
D_{eff} = 0.115 m^2/s, U = 1.2 m/s, τ_0 = 1 s

Distance from "CFD Exit Plane"	Composition Transient
0 km	1.0 s
1 km	28.9 s
10 km	91.4 s
100 km	289 s

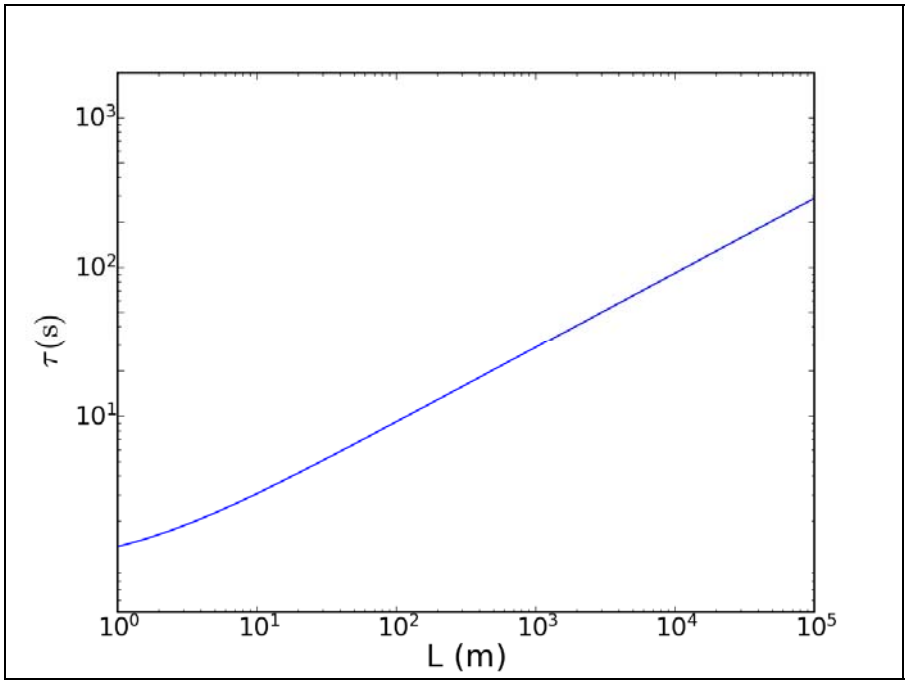

Figure 3-20: Downstream Evolution of the "Compositional Transient, τ".

3.2.5 Solution Sensitivity

The sensitivity of the composition transient to the initial composition transient (or layer thickness) is shown in Figure 3-21 and Table 3-10. The composition transient (layer thickness) at downstream locations becomes less sensitive to the initial condition as the mixing layer propagates. At 100 km downstream of the supply change, the composition transient would be about five minutes for any initial supply switching time which was less than 100 s.

Table 3-10: Composition Transient @ 100 km for different Supply Switching Times (Layer Thicknesses).

Layer Thickness @ 0 km	*Supply Switching Time* Composition Transient @ 0 km	Composition Transient @ 100 km
0.0 m	0.0 s	289.189 s
1.15 m	1.0 s	289.191 s
11.5 m	10 s	289.362 s
115 m	100 s	306 s
1150 m	1000 s	1041 s

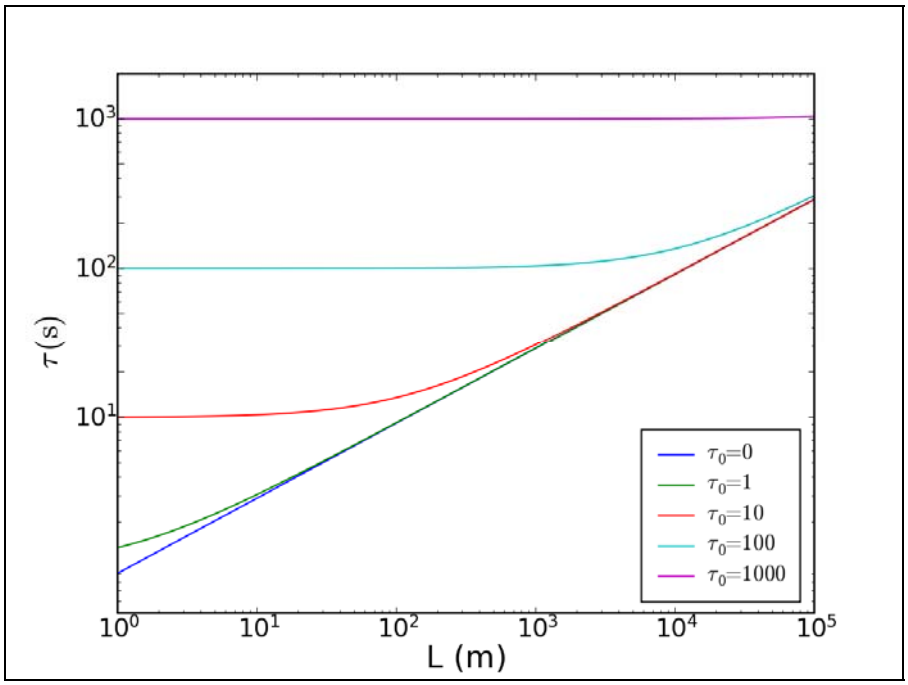

Figure 3-21: Variation of the Composition Transient for several different Supply Switching Times, τ_0 (s).

The composition transient at a downstream location is much more sensitive to the flow rate than the supply switching time (Figure 3-22 and Table 3-11). It should be noted however, the results shown are for fixed axial dispersion coefficient and fixed supply switching time. The analytical and experimental results in the literature indicate that for given a specific geometry (pipe diameter and pipe roughness in this case), the effective dispersion coefficient would increase with increasing flow rate (Reynolds number).[11]

Table 3-11: Composition Transient @ 100 km for Different Bulk Velocities.

Bulk Velocity	Composition Transient @ 100 km
0.5 m/s	1075 s
1.15 m/s	289 s
2 m/s	134 s
5 m/s	34 s
10 m/s	12 s
20 m/s	4.4 s

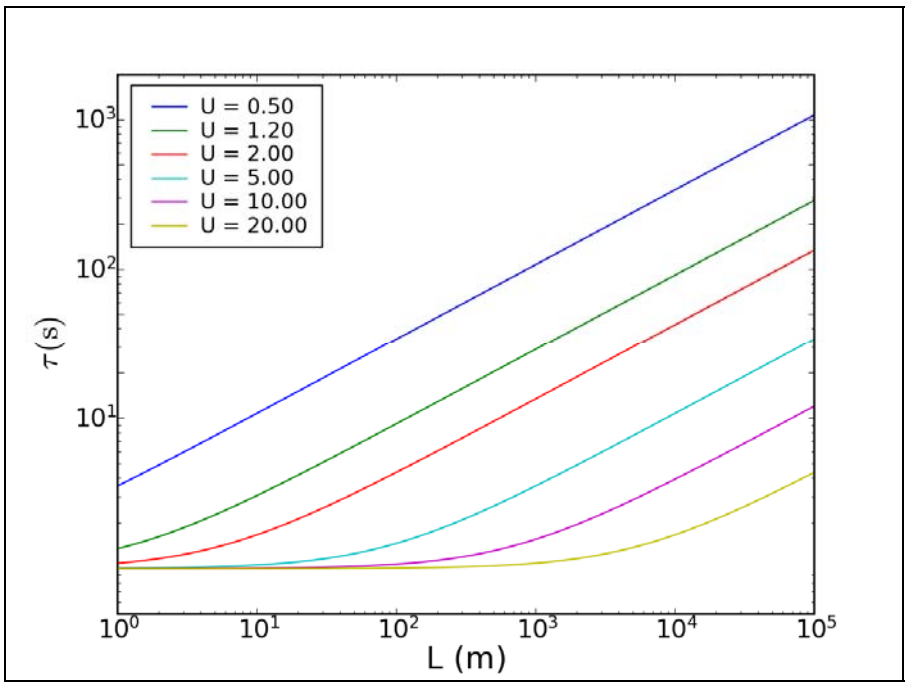

Figure 3-22: Variation of the Composition Transient for Different Bulk Velocities, *U* (m/s).

The results for different values of the dispersion coefficient with fixed velocity and fixed initial composition transient are shown in Figure 3-23 and Table 3-12. As the dispersion coefficient is increased, the composition transient increases, due to a faster thickening of the mixing layer. Through two orders of magnitude of dispersion coefficient change, the composition transient changes less than a factor of ten. It should be mentioned that the dispersion coefficient, or effective diffusivity, is not necessarily an independent parameter. In addition to being strongly affected by the bulk flow rate (Reynolds number), the value is also affected by other parameters including the surface roughness and mass diffusivity (Schmidt number).[11,12,20,21]

Table 3-12: Composition Transient @ 100 km for Different Dispersion Coefficients.

Dispersion Coefficient (m^2/s)	Composition Transient @ 100 km
0.0115	91.4 s
0.0575	204 s
0.115	289 s
0.23	409 s
1.15	914 s

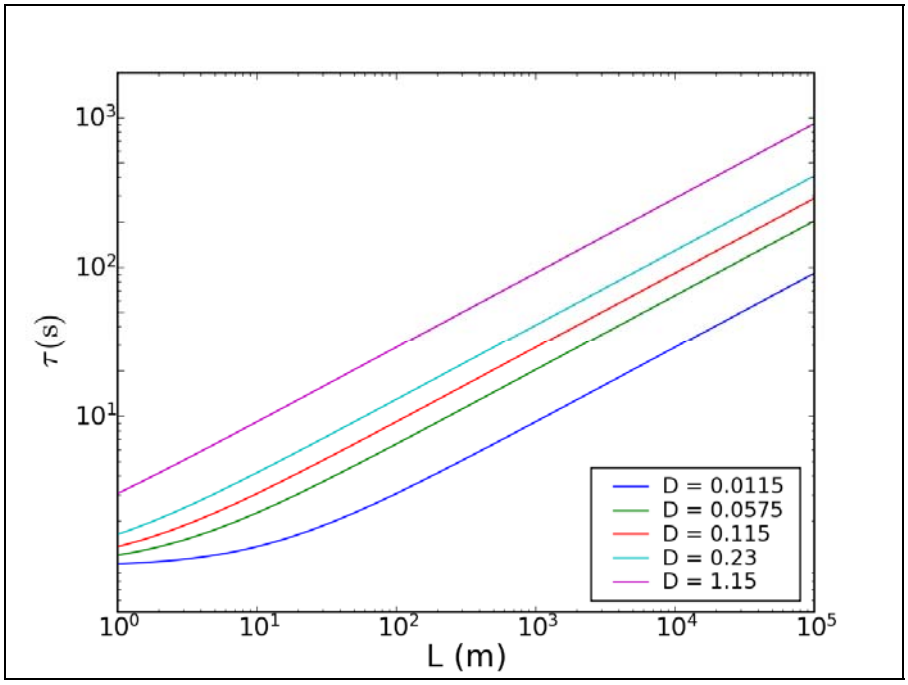

Figure 3-23: Composition Transient for Dispersion Coefficients, D (m/s^2) (*Effective Diffusivity).*

3.3 Summary

Computational fluid dynamics (CFD) simulations and calculations using an analytical formula[11] were used to illustrate continuous (steady) cross-sectional mixing and transient axial mixing of gases in pipe junctions.

For continuous mixing, the results show that two gases streams are mixed to an average composition within 90 to 100 meters downstream of the junction for the specific cases simulated in this report. In other words, steady-state gas blending is completed in a relatively short distance.

For transient mixing, the situation is different. Transient mixing refers to the situation where a different composition gas supply is abruptly "switched-on" at a pipe junction. While steady state conditions are rapidly established near the pipe junction, the interface between the old and new gas composition continues to propagate along the pipeline. Several methods were discussed to calculate or the dispersion of this interface. Estimation of the dispersion coefficient along with an analytical solution provide quick estimates of the time interval over which the composition will change at large distances away from the discontinuity. The results indicate that there is minimal mixing between the upstream and downstream gases, a behavior which mimics field evidence documented in a recent report.[2] Application of the solution procedure to a nominal operating condition (mass flow: 21.55 kg/s, pipe diameter: 0.762m pipe, operating pressure: 55 atm) indicates that if the supply is switched over a time period of less than a two minutes, then the composition change 100 km downstream will occur over approximately five minutes. This analysis can used to provide estimates of how gas composition changes are transmitted along the pipeline. More exact analysis would require some combination of multidimensional CFD and pipeline network calculations of the specific scenario.

---

[1] Geoffrey Taylor, 1953, "Dispersion of soluble matter in solvent flowing slowly through a tube", Proc. of the Royal Society of London, Series A, Mathematical and Physical Sciences, vol. 219, no. 1137, pp. 186-203.

[2] Aspen Environmental Group, 2006, "Natural gas quality: power turbine performance during heat content surges", California Energy Commission (CEC) Report CEC-700-2006-001.

[3] David C. Wilcox, Turbulence Modeling for CFD, DCW Industries, 1994.

[4] Steven Pope, Turbulent Flows, Cambridge University Press, 2000.

[5] Abe and Suga, Towards the development of a Reynolds-averaged algebraic turbulent scalar flux model, International Journal of Heat and Fluid Flow, vol. 22, pp. 19-29, 2001.

[6] S. Kenjereš and K. Hanjalić, "LES, T-RANS and hybrid simulations of thermal convection at high Ra numbers," International Journal of Heat and Fluid Flow, Volume 27, Issue 5, October 2006, Pages 800-810

[7] Donald Y. Tang, Jane J. Ou, Richard H. Heist, Shaw H. Chen, Alexander J. Dukat, Arthur C. Eberle, 1993, "Dynamics of fluid mixing induced at a T-Junction. 3. Experimental characterization and fluid dynamic computation of temperature distribution in space", Ind. Eng. Chem. Res., vol.32, pp.1727-1733.

[8] J. B. W. Kok, S. van der Wal, 1996, "Mixing in T-junctions", Applied Mathematical Modeling, vol. 20, pp. 232-242.

[9] Tsan-Hsing Shih, William W. Liou, Aamir Shabbir, Zhigang Yang, Jiang Zhu, 1995, "A new k-ε eddy viscosity model for high Reynolds number turbulent flows", Computers and Fluids, vol. 24, no.3, pp.227-238.

[10] S. Menon, P. -K. Yeung and W. -W. Kim, "Effect of subgrid models on the computed interscale energy transfer in isotropic turbulence", *Computers & Fluids*, *Volume 25, Issue 2*, *February 1996*, *Pages 165-180*

[11] Geoffrey Taylor, 1954, "Dispersion of matter in turbulent flow through a pipe", Proc. of the Royal Society of London, Series A, Mathematical and Physical Sciences, vol. 223, 446-468.

[12] F.B. Freitas Rachid, J.H. Carneiro de Araujo, R.M. Baptista, 2002, "Predicting mixing volumes in serial transport in pipelines", J. of Fluids Eng., vol. 124, pp.528-534.

[13] Frank P. Incropera, David P. De Witt, 1985, *Fundamentals of Heat Transfer*, (2nd Edition), Wiley and Sons.

[14] F.B. Freitas Rachid, J.H. Carneiro de Araujo, R.M. Baptista, 2001, "Mixing Volume Evaluation under Pumping Shut-down Conditions", Pipeline simulation interest group (PSIG), Paper 2001-11.

[15] James B. Rawlings, John G. Ekerdt, 2006, *Chemical Reactor Analysis and Design Fundamentals* (2nd Edition), Nob Hill Publishing.

[16] http://www.uniongas.com/aboutus/aboutng/composition.asp

[17] http://www.naturalgas.org/naturalgas/transport.asp

[18] William E. Liss, David M. Rue, "Natural Gas Composition and Fuel Quality, Information Report," William Boyer - Occidental of Elk Hills, Gas Technology Instittue, February 11, 2005 (http://www.energy.ca.gov/-2005_energypolicy/documents/2005027+18_workshop/comments/R0401025_Comments_Occidental_of_Elk_Hills.pdf)

[19] K. Ekambara, J.B. Joshi, 2004, "Axial mixing in laminar pipe flows", Chemical Engineering Science, vol. 59, pp. 3929-3944.

[20] L.J. Tichacek, C.H. Barkelew, Thomas Baron, 1957, "Axial mixing in pipes", A.I.Ch.E. Journal, vol. 3, no.4, pp.439-442.

[21] Rudolf Zitny, Jiri Thym, 2004, "Axial dispersion model in finite element analysis of heat and mass transfer in pipes", 16th International Congress of Chemical and Process Engineering, p.1-13.

[22] Burmeister, 1983, *Convective Heat Transfer*, Wiley-Interscience.

[23] Octave Levenspiel, 1972, *Chemical Reaction Engineering*, John Wiley and Sons.

[24] Scott Folger, 1999, *Elements of Chemical Reaction Engineering*, Prentice Hall International.

[25] K. Ekambara, J.B. Joshi, 2003, "Axial mixing in pipe flows: turbulent and transition regions", Chemical Engineering Science, vol. 58, pp. 2715-2724.

4 NATURAL GAS ENGINES: FUEL VARIABILITY EFFECTS

4.1 Introduction

Natural gas is basically a mixture of hydrocarbons in gaseous form, comprised predominantly of methane with other hydrocarbons, inerts and impurities as minor constituents. The composition of natural gas depends primarily on the production field from which it is extracted and its storage history. It is also dependent on processing for heating value control and hydrocarbon dewpoint reduction. A significant body of information exists concerning geographical compositional variations. Further, gases are mixed and distributed based on demand and availability creating significant temporal and geographic variations in natural gas.[1] As heavier hydrocarbons (HC) are substituted for methane, inerts must also be added to maintain a near constant fuel heating value per unit volume, since the higher HC have higher volumetric heating values than methane. Historically, domestic natural gas supplies have limited variation in quality.

However, decreasing domestic production and increasing use of natural gas means that LNG will provide an increasingly larger portion of future U.S. natural gas supplies. But, imported LNG may face several challenges to its broad acceptance into a specific U.S. market area. One of these challenges is the degree to which LNG in its gaseous form is interchangeable or compatible with existing utilization equipment. LNG is simply a natural gas that has been treated to remove impurities, and then condensed into liquid form. The economics of the LNG industry usually dictate that ethane, propane, and butanes are not removed to the levels commonly found in U.S. domestic pipeline gas. At the same time, LNGs usually contain few inerts (carbon dioxide [CO_2] or nitrogen [N_2]) and practically no heavier hydrocarbons beyond pentanes which are commonly present in domestic natural gases. The U.S. Federal Energy Regulatory Commission has taken the position that LNG is natural gas and has exercised its jurisdiction over LNG in the same way as it does over any natural gas.[1]

In specific areas of the country, high levels of propane and/or air are sometimes used to meet peak demand loads of the local distribution company. This is referred to as propane/air peak shaving.[2] Due to these and other compositional influences, limited variations in composition must be accepted. Three areas of engine operations; emissions, power characteristics and knock potential can be impacted by heavier HC or air which are present in distribution system gas when utilities peak shave.[3] On the contrary, methane is more difficult to catalytically remove from engine exhaust than higher HCs.

Liss and Thrasher have evaluated the natural gas composition changes in several areas of the country. They indicate variations of ±14% in heating value and density, ±20% in Wobbe number, and ±25% in stoichiometric A/F ratio may occur in different regions across the United States. On engines that are highly tuned for efficiency, these variations can impact engine performance and emissions.[4]

There are many codes, standards and recommended practices for CNG but few that actually address fuel composition. For a fairly comprehensive list of codes, standards and advisories applicable to natural gas vehicles and infrastructure, see the Clean Vehicle Education Foundation

website at www.cleanvehicle.org/technology/image/code.pdf. Current fuel guidelines for natural gas vehicles (NGVs) include SAE J1616, CARB Alternative Fuels Regulations[5] and brief guidelines for contaminants in NFPA 52.[6] The provisions contained in J1616 are intended to protect the interior surfaces of the fuel container and other vehicle fuel system components such as fuel injector and exhaust catalyst elements from the onset of corrosion, poisoning, the deposition of liquids or large dust particles or the formation of water, ice particles, frost or hydrates. The provisions contained in J1616 are not intended to address the composition of natural gas as delivered to a fueling station, but rather at the outlet of the fueling station as delivered to the containers on the vehicle. Limits on gas quality currently not included in J1616 may be added when data are available to substantiate them. J1616 presents the more important physical and chemical characteristics that address these issues. Because SAE Standard J161 is copyrighted, it is not reproduced here. However, copies of this Standard (Document J1616, "Recommended Practice for Compressed Natural Gas Vehicle Fuel) may be purchased via SAE's website (http://www.sae.org/technical/standards/J1616_199402).

As a footnote, there is an SAE standard, J2699, which is work in progress as of August 2006. It is intended to eventually provide definition and fuel specification for automotive quality LNG.

NFPA 52, Section 4.5.2.1 adds a limit of 0.5% O_2 and a water content less than 7.0 lb/MMscf (110 mg/M^3) but otherwise addresses fueling and container specifications and procedures. The CARB Alternative Fuels Regulations Article 3, Section 2292.5 is the California Standard for CNG composition for NGVs. The specifications are provided in Table 4-1 below.

Table 4-1: CARB Specifications for Compressed Natural Gas for NGV Applications.[5]

Specification	Value	Test Method
Hydrocarbons (expressed as mole percent)		
Methane	88.0% (min.)	ASTM D 1945-81
Ethane	6.0% (max.)	ASTM D 1945-81
C3 and higher HC	3.0% (max.)	ASTM D 1945-81
C6 and higher HC	0.2% (max.)	ASTM D 1945-81
Other Species (expressed as mole percent unless otherwise indicated)		
Hydrogen	0.1% (max.)	ASTM D 2650-88
Carbon Monoxide	0.1% (max.)	ASTM D 2650-88
Oxygen	1.0% (max.)	ASTM D 1945-81
Inert gases		
Sum of CO_2 and N_2	1.5-4.5% (range)	ASTM D 1945-81
Water	a	
Particulate matter	b	
Odorant	c	
Sulfur	16 ppm by vol. (max.)	Title 17 CCR Section 94112

a. The dewpoint at vehicle fuel storage container pressure shall be at least 10 °F below the 99.0% winter design temperature listed in Chapter 24, Table 1, Climatic Conditions for the United States, in the American Society of Heating, Refrigerating and Air Conditioning Engineer's (ASHRAE) Handbook, 1989 fundamentals volume.

Testing for water vapor shall be in accordance with ASTM D 1142-90, utilizing the Bureau of Mine apparatus.

b. The compressed natural gas shall not contain dust, sand, dirt, gums, oils, or other substances in an amount sufficient to be injurious to the fueling station equipment or the vehicle being fueled.
c. The natural gas at ambient conditions must have a distinctive odor potent enough for its presence to be detected down to a concentration in air of not over 1/5 (one-fifth) of the lower limit of flammability.

LNG is stored at very low temperatures (around -162 °C at atmospheric pressure). Although LNG tanks are heavily insulated, heat leaks will cause some LNG to be "boil-off" during transport or storage. The gasified LNG can be used to power propulsion engines.[7] Because the lighter hydrocarbons (e.g., methane) evaporate first, the remaining LNG cargo is enriched in higher hydrocarbons. This is called "weathering" of the stored LNG, and can lead to additional variability in fuel composition from LNG sources.[8]

Typically, design engineers are asked to focus on designing the gas engine such that optimized efficiency, power, and emission behavior can be obtained. It must further be ensured that even with changing gas properties the engine operates safely, preventing any damage to engine components due to increased knock, and that acceptable efficiency and power are obtained while complying with emission limits. Therefore, only designing the engine for the highest possible heating value, lowest possible MN gas may not be a practical solution. In these cases the control system must respond by interacting with engine timing, load, A/F ratio etc. For example, speed reduction would have a detrimental effect on knock in a stoichiometric engine but little effect on NO_x.[9]

Traditionally, engine derating has been the means to handle fuel composition variations. However, the demand for higher engine efficiency and tighter emission regulations have forced engines to narrower knock and misfire margins and tighter engine control, therefore relegating engine derating to a last resort. Modern engines use a variety of sensors and controls which tend to indirectly accommodate a reasonable degree of fuel quality variation. Examples of current fuel recommendations for several fuel manufacturers may be found in the International Association for Natural Gas Vehicles Report, December 2002.[10]

Several examples of the effect of fuel composition on engine performance are now discussed. In a cogeneration application, engine data from a CAT-3516 was collected over 24-months. The authors indicate that they needed to install equipment to measure fuel composition because it was important to engine operation.[11] For two gases supplied for automotive use in New Zealand, the optimum full throttle A/F ratios and ignition timing settings were so dissimilar that it made it impossible to achieve the maximum power output on both gases with the same tuning and timing setting. The Wobbe indices of the two natural gases were 1320 btu/ft^3 and 1154 btu/ft^3 with 6% and 14% inerts respectively.[12] Note that the inerts on the second fuel were outside the range of interim guidelines put forth by the NGC+ working group in 2005.[13] In spite of these examples, it is emphasized that gas engines can run on a wide range of gas compositions. One case in point is a commercial low-Btu gas engine developed by Jenbacher. This gas-fueled engine can operate on 16% hydrogen (H_2), 0.5% CO, 3.5% CO_2, and 80% N_2 with a lower heating value (LHV) of

only 50 Btu/scf. The energy value of this gas is only 5% that of natural gas. Ten-bar brake mean effective pressure (BMEP), and 36% thermal efficiency at a raw value of 2 ppm NO_x were reported.[14]

Even though engines can run on a wide range of fuel compositions, a given engine with a given tuning is limited to a range of compositions determined by the engine's misfire limit, knock limit, emission limits (usually imposed by air permitting) and the ability for the engine's control system to control within those limits with respect to fuel variability. Modern control systems have enabled engines to operate with wider changes in fuel composition. The Cummins heavy-duty B5.9 natural gas engine has been in production since 1994, and was the industries' first engine with closed-loop A/F ratio control. Cummins also developed (1999) a propane version of this engine called the B5.9LPG. It utilizes lean combustion, closed-loop A/F ratio control, and electronic engine management technologies. Although the engine is similar to natural gas version, extensive engine development was required to modify the engine for LPG operation. Engine performance was optimized for combustion, detonation, and lean misfire margins with LPG versus natural gas. For example, the optimal compression ratio for LPG was 9.1:1 compared to 10.5:1 for natural gas. Development and validation for operation on LPG required more than 10,000 laboratory test hours.[15]

There has been a trend in time from the early 80's toward increased BMEP because it produces higher efficiency and ultimately reduces cost.[16] On the most advanced engines, thermal efficiency is now as high as 45% at 20 bar BMEP For any engine size, 20 bar BMEP is hard to achieve in knock and misfire free operation. Higher BMEP levels result in higher efficiency as parasitic losses are smaller in proportion to engine power. Larger bore sizes are typically more efficient due to the reduction in surface to volume ratio and resulting heat loss through the cylinder, head and piston surfaces and less (relative) opportunity for crevice fuel quenching. Larger engines run slower than smaller bore engines with linear piston speed fairly constant across sizes. Slower speed engines also benefit from reduced friction in rotating components. Electric efficiencies of natural gas engines range from 28% LHV for stoichiometric engines smaller than 100 kW to more than 40% LHV for larger lean-burn engines (> 2 MW).[17]

Currently, the maintenance interval is dictated by the spark plug change interval. Market forces call for increased engine efficiency while regulations call for lower emissions on the future spark ignited natural gas engines. However, experiences indicate the use of traditional ignition systems on leaner A/F mixtures and higher charge densities requires stronger ignition spark which in turn reduces spark plug life.[18] This is a concern as it may represent a barrier to the continued trend toward higher engine efficiency.[19]

4.2 Engine Type

Engines that operate with near stoichiometric mixtures are more prone to detonate than lean mixtures. With the exception of some stand alone industrial applications, such as irrigation or gas compression where engines tend to be gasoline engine derived and unboosted, stoichiometric engines are typically designed with little knock margin to provide optimum performance. Fortunately, knock dependence on changes in fuel composition is secondary when considering the impact of fuel variability on emission in these engines. When fuel composition changes, any

deviations away from stoichiometric conditions reduces knock propensity. Changes away from stoichiometric affect exhaust oxygen (O_2) composition and can affect downstream aftertreatment performance.[2]

Lean-burn natural gas engines are designed to operate with lower peak combustion temperatures than stoichiometric engines due to the diluting effects of additional air. This leads to lower heat loss and reduced NO_x formation. Lean-burn natural gas engines usually run sufficiently lean that variations in equivalence ratio (ER) can either result in engine misfire or increased NO_x emissions. As a result, any variable which affects the metered ER to the engine will affect engine performance and emissions, whether it is stoichiometric or lean-burn combustion.

Lean-burn engine technology typically uses turbo-charging to compress combustion air and/or fuel to maintain high specific power output. However, lean-burn engines are more likely to experience pre-ignition or engine knock when higher-than-normal levels of propane and ethane components are present in the fuel. Ignition timing can be used to control combustion to avoid engine knock. Due to concerns regarding variations in fuel composition, some manufacturers have chosen to de-tune certain lean-burn engines by retarding spark ignition timing, resulting in some loss of performance and fuel efficiency.[17]

An increase in ER in a turbocharged lean-burn engine has a twofold effect. First, if fuel controlled, it provides additional heat energy to the engine so power is increased for a constant boost level. Secondly, the added heat energy increases the available exhaust energy which tends to increase boost pressure. Provided the turbocharger system has sufficient control capability, boost pressure can be maintained. In some instances the wastegate control may have insufficient flow capacity to bypass the excess exhaust energy resulting in an increase in boost above operational limits. In this potentially unstable situation, the increased boost means additional mass air flow to the engine accompanied by still more fuel. In many stationary applications the engine is equipped with a fuel governor which will reduce fueling to maintain set speed.

A universal exhaust gas oxygen (UEGO) sensor is one way to improve engine performance with variable fuel composition. For example, according to information contained in SAE Paper No. 920593 (1992),[2] the variation of hydrogen/carbon (H/C) ratio of common gas blends can be considerable (3.11 to 3.88). However, at a fixed ER, this produces less than a 5% variation in the free exhaust oxygen. Thus exhaust oxygen is a suitable parameter for feedback control, but NO_x controls also need to be considered.[2] Another type of feedback control uses the power generator signal to regulate air-fuel ratio as described in U.S. Patent Number 4,867,127, "Arrangement for Regulating the Combustion Air Proportions".[20]

For lean-burn engines, higher HC content (and, thus, lower MN) may cause the engine to reach the knock limit unless the control system adjusts engine operation. For stoichiometric engines, higher HC may change the UHC emission, and exhaust oxygen. In addition, because stoichiometric engines operate close to the knock margin, they also may be constrained to relatively high MN. To avoid knocking, extreme ignition retarding may be used to compensate for low MNs, but this compromises efficiency.[2,9]

A commercial example of a natural gas lean-burn stationary engine technology is the Jenbacher J620 GS-E. This lean burn engine was developed in 1998 with a maximum working pressure of 180 bar. On natural gas, the thermal efficiency is 43%. When engine knock is detected, the control responds by first retarding timing, then increasing the air-fuel ratio (to reduce combustion temperature), and then finally reducing engine power. The control system automatically tries to reestablish engine power output until knock reoccurs. This control approach allows the engine to operate with a wide range of gas composition without knocking problems. The engine's knocking limit is beyond the typical operating range at a MN of 95. However, with knock control, it may run as low as MN = 70. With a reduced BMEP, it can operate using fuel gases with MN down to 30.[21]

4.2.1 Stoichiometric/Exhaust Gas Recirculation

The use of exhaust gas recirculation (EGR) has become a popular emission control technique specifically for reducing engine NO_x levels. By using EGR, the intake mixture contains significant quantities of diluents such as CO_2, N_2, and H_2O. NO_x emissions are reduced by two factors: reduced oxygen concentration in the charge, and reduced temperature via changes in heat capacity.[22]

In work by Kim et al., 1996,[23] under part load operations, the optimal EGR rates were 5-10% and excess air ratio of about 1.3-1.35. The EGR reduced NO_x emissions while the lean mixture condition had a minimal effect on engine efficiency and UHC emissions.[23]

The effects of EGR on NO_x emission at stoichiometric operation were investigated by Raine et al.[24] These authors compared natural gas and gasoline fueling at constant engine torque, Engine speed (1500 rpm) and A/F ratio (stoichiometric) were held constant for all tests. EGR was seen to reduce NO_x emission in both natural gas and gasoline fueling, but increased the total hydrocarbon (THC) emission.[24] The THC had a different composition for the two fuels. For natural gas, methane forms approximately 80% of the THC emission and was approximately constant across the range of ERs tested. For gasoline, methane forms 5% to 8% of the THC emission. Although EGR produced a slight increase of THC, the increase was modest in comparison with the level of NO_x reduction.[24]

In stoichiometric NG engine work by Thiagarajan et al.[25] brake power, fuel conversion efficiency and before catalyst emissions of CO, NO_x, and HC were not affected by higher HC (propane) addition as long as stoichiometric combustion was maintained. N_2 dilution at stoichiometric conditions was shown to reduce NO_x before the exhaust catalyst.

Stoichiometric engines in light-duty vehicles may use EGR and three-way catalysts (TWC) to control emissions. The combination of exhaust oxygen sensors, and adaptive electronic fuel controls can allow these engines to operate with a relatively wide range of gas compositions while maintaining oxygen levels, and without experiencing damaging engine knock.[17]

4.2.2 Automotive Applications

Nationally, as estimated from the U.S. DOE-EIA, there are an estimated 133,000 NGVs of which approximately 68.6% are light-duty vehicles.[26] Natural gas use in vehicles increased from 2.9 billion ft^3 in 1996 to 8.3 billion ft^3 in 2000.[27] Gasoline engine are usually retrofitted to NGV use but produce about 10-15% less power compared to operation on gasoline. Emissions from these retrofitted engine are different than when using gasoline: reduced CO by ~80%, reduced HC by 50%, and increased NO_x by 33%.[28] Because of adaptive control algorithms, fuel composition variation has not been an important concern for vehicle driveability.[26] In a recent GRI study, they conclude that there is essentially no concern over knock problems occurring in light-duty (gross vehicle weight rating [GVWR] < 6,000 lbs) NGVs. Because the engines are retrofit from gasoline counterparts, the compression ratios and BMEP ratings of light-duty NGVs are similar to those of gasoline engines For this reason, there is little concern these vehicles will have problems with engine knock even at MNs as low as 65.[26]

NGV performance was investigated by Lee and Kim.[29] In their study, gas HC compositions varied from 100% methane to 75/22/2.5 methane/ethane/propane. MONs varied from 110-138 while LHV varied by approximately 17.5%. Note that based on CARB MN calculation[5] this MON range would have a MN range of 59.5-105. These variations are very significant, especially when compared to realistic natural gas compositions compliant with NGC+ interim quidelines.[13] Fuel economy, drivability, and exhaust emission were all evaluated in the study that included two recreational vehicles and one passenger car. A negligible effect on vehicle drivability (starting, stalling, hesitation, and audible knock) was reported, even with the large variation in fuel composition.[29]

In another vehicle study, Elder et al.[30] tested two New Zealand CNG gases and two LPG gases using a 1981 Mitsubishi 2000 GSL engine. The engine was retrofit to gaseous fuel operation using a Renzo Landi CNG conversion system. The CNG gases varied little in their HC content. Their inert content varied from 2.5% to 12.1% CO_2 while N_2 remained relatively constant. In one gas, the additional CO_2 produced a methane range from 81.3% to 73.4%. The authors reported no perceptible changes in drivability when operating on the two CNG gases. When tuned for each gas, the differences in fuel consumption were minor. Differences were larger comparing the gases with wider composition changes. When tuning was performed on a single gas, and then shifted to the other gas, emissions performance or fuel economy could be compromised.[30]

A survey of CNG compositions available near Houston, Texas was performed.[31] The data showed that the properties of local CNG was very similar to a previous national survey.[32] The following properties were considered: heating value, the energy density per cycle, the Wobbe number, and the fuel methane-to-hydrocarbon ratio. Drivability was not compromised by the difference in fuel composition. The fuel CH_4/HC ratio did influence tailpipe emissions. No seasonal trends, no city to city trends, and no trends within a given city were found for the Wobbe number history considered.[31]

Based on a review of the coefficient of variation (COV) (the standard deviation normalized by the mean) for various fuel properties,[31] it was noted that except for the CH_4/HC ratio, the COV is

typically small (< 5%), which shows that many fuel properties do not vary greatly, even when the fractions of the higher HC and inerts vary substantially.

While many fuel properties do not change substantially, the study indicates that an important property in terms of emissions is the methane to HC percentage of the CNG. All tests were performed using the Federal Test Procedure (FTP) driving cycle which described in the Code of Federal Regulations, Title 40, Parts 86 and 600. The effects of CNG composition on fuel economy and drivability were not significant concerns, although it was possible to correlate drivability with the inert fraction of the CNG, the LHV (per unit mass) and the stoichiometric A/F ratio. NO_x, CO, or the Emissions Index did not correlate well with the fuel composition. Based on equilibrium calculations for the initial mass that burns, the stoichiometric, adiabatic flame temperature (without EGR dilution) varied by 20 K for the CNGs considered.[31]

Merétei et al. tested an engine to meet European emission limits forecast for the year 2005. The tests also needed to meet performance, drivability, and reliability goals. They concluded that EURO 4 (2005) specifications could be met with CNG fuel in a lean-burn, aftercooled, turbocharged engine using an oxidation catalyst (OC).[33]

In a study with the West Virginia University mobile emission laboratory, four actual operating tractor trailers were tested on natural gas and diesel fuel. Two tractors were converted to natural gas operation. The other two trucks were operated on diesel for comparison. The natural gas fuel composition was constant, so the comparison was made between a fixed NG supply and diesel fuel. Fuel consumption for the two fuels was 5.17 mpeg (miles per equivalent gallon) for NG, versus 6.73 mpg for diesel. Thus, the natural gas fueled vehicles have significantly worse fuel economy. However, NO_x was reduced by 24% and 45% for the Urban Dynamometer Driving Schedule. Particulate matter (PM) was reduced by more than 90% for some conditions.[27] Note that mpeg is used to compare fuel economy on an energy equivalent basis.

In the mid 1990s researchers at the University of Texas and the Southwest Research Institute investigated CNG and LPG vehicle performance. Eighty-six different vehicles including heavy light-duty pick up trucks were a part of this study. The vehicles were converted to bi-fueled operation using CNG and LPG retrofit systems that are sold as aftermarket products. All retrofits used closed-loop control. In many cases, the retrofit engines produced greater emissions with CNG/LPG versus the baseline gasoline with most engines having greater NO_x output. The authors determined that some retrofit engines were operating too lean, or the control system responded too slowly. The data indicate that successful kits must produce at least a stoichiometric mixture, and establish other criterion for successful conversion to alternative fuels.[34]

4.2.3 Direct Gas Injection/Pilot Ignition

The dual-fuel, compression ignition (CI) engine has been employed in a number of applications utilizing various gaseous and pilot fuels. Duel-fuel operation can produce lower NO_x and PM emissions when compared to conventional liquid fueled engines. Natural gas is suitable for high compression ratio (CR) engines because it has a high octane number (ON) and ignition can be

achieved with the diesel pilot. Reduction of both NO_x and PM is possible because dual fueling avoids the inherent NO_x/PM tradeoff that exists in single-fuel diesel engines.[35]

Pilot injection of diesel fuel can provide an ignition source for natural gas engines. Because diesel fuel has a lower ignition temperature than natural gas, it can provide an ignition event timed by the diesel injection. Unlike a spark plug, diesel injection produces multiple ignition sites, with a relatively large flame kernels compared to a spark plug. This can provide good ignition, but the mixing must be designed to avoid excessive stratification of the diesel jet to achieve expected timing.[36]

Most dual-fuel engines retain the ability to operate on 100% diesel fuel. However, in dual-fuel mode, the diesel fuel is required only as an ignition source, requiring very small levels of pilot injection. The minimum diesel pilot level is often established by the turn-down ratio of the fuel-injection system. To achieve adequate spray penetration and atomization, older duel-fuel diesel fuel injection systems require a minimum of 5-10% of the maximum full-load fuel flow. A smaller fuel injection system can be used if it is also not required to operate on 100% diesel fuel. In this case, the minimum pilot fuel can be reduced to less than 1% of the total fuel energy. It is desirable to reduce the pilot because NO_x levels increase with pilot fuel level.[36,37] However, reduced pilot also increases cyclic variability, providing a second limit on the pilot quantity.[38]

Cyclic variations of in-cylinder flow contribute to cyclic ignition and combustion variations. Flow variations affect conditions in the diesel pilot-air mixture preceding ignition, and these in turn affect the surrounding natural-gas air mixture. These variations ultimately appear as variability in the cylinder pressure history.[37]

The diesel-air mixture does not ignite immediately if in-cylinder temperatures are not high enough to ensure fast diesel evaporation. A prolonged ignition delay (observed at advanced timing conditions) allows more time for diesel evaporation, better dispersion of the fuel in the cylinder, and greater diesel-air mixing prior to ignition.[38]

Zeng et al.[39] studied the effects of variable diesel injection timing using constant duration fuel injection. With advanced fuel injection timing, the volumetric efficiency decreased and the overall ER increased. The fuel injection timing had a large influence on the engine performance, combustion and emissions. Engine performance was most affected by late injection because of insufficient time for fuel-air mixing and lower temperatures and produced high emission levels.[39]

In another duel-fuel study, Kusaka[40] observed high THC emission and low thermal efficiency at low loads, but showed that intake air heating combined with EGR improved the part-load performance. NO_x levels were lower in dual fuel mode because it is possible to operate at leaner conditions. However, the injection timing must be optimized to achieve high efficiency and low CO and THC emissions.

Duel fuel studies with three gaseous fuels (methane, CNG, and LPG) are reported by Selim et al.[41] Diesel fuel was used as the pilot. LPG was reported as propane with some butane. When the engine used LPG as the main fuel, it started to knock at a much lower torque than with either CNG or methane: 8 N-m (Newton-meter) torque for LPG compared to 16 N-m for CNG.

Fuel variation can affect the ignition delay of the diesel pilot in part due to the change in compression temperature for the different main fuels. Because the specific heat of the different main fuel blends is different for LPG versus CNG, the temperature of the compressed mixture is also different.[41] Combustion noise variations were detectable but not significant from an operational perspective.[41]

Diesel fuel is not always used as the pilot fuel. Nwafor[42] investigated bio fuels (rape methyl ester and neat rapeseed oil) as pilot fuels. The test results indicate that engine performance on these alternative pilot fuels was satisfactory and compared favorably with the baseline test result on diesel fuel pilot.

4.2.4 Spark-Ignited Prechamber

Little information regarding fuel variability effects in spark-ignited prechamber engines is available. Here, we provide some basic background information about prechamber natural gas engines.

A common solution to stringent emission regulations has been lean-burn combustion. With very lean A/F ratios, both CO and THC emissions become unacceptably high with open chamber spark ignition due to misfires and combustion instabilities. Open chamber pilot ignition is limited by pilot quantity and mixedness. In order to combat this, a precombustion chamber (PCC) ignition system is often used to stabilize combustion at very lean A/F ratios. PCC ignition with natural gas is another common method for extending the lean limit and reducing combustion variability in large bore (36-56 cm) natural gas engines.

A PCC ignition system is a small chamber usually 1-2% of the clearance volume, in which a near-stoichiometric mixture of fuel and air are ignited by a standard spark plug. The igniting mixture is thrust into the main chamber, where lean conditions exist. This burning jet in effect provides an ignition source to the main chamber through a single-elongated source or multiple elongated sources. The resulting natural gas flame front generally has a shorter distance to travel to complete combustion, which shortens the combustion duration. Some PCCs get their mixture from passage of gases from the main chamber through its holes during the intake and compression stroke. In comparison with direct spark ignition, prechamber ignition intensifies and accelerates the combustion process, because ignition sources are distributed in the main chamber via the hot prechamber jet. The flame from surface area is significantly increased by the prechamber jet entering the main chamber.[43]

There are several advantages to this type of ignition system. Since the ignition source volume (i.e., the hot burning jets exiting the PCC) in the main chamber is larger, ignition is less affected by uneven fuel/air ratio, or flow variability. This reduces cycle to cycle combustion variation. Compared to a spark ignition, PCCs can ignite a leaner overall mixture which extends the lean limit of combustion and lowers NO_x while maintaining low cyclic variability. A disadvantage is that a significant amount of CO is formed in the PCC relative to what is formed in the main chamber. In one study, the PPC CO ranged from 42% to 54% of engine out CO emission depending on operating conditions. NO_x is also formed in the PCC, with about 22% of the total NO_x coming from the prechamber when operating at the lean limit.[44]

In some cases an auto-ignition process in the prechamber may be used. In this case, in order for natural gas ignition to take place effectively, high compression ratio, preheated inlet air and a thermally insulated prechamber are used.[45]

4.2.5 HCCI

Homogenous Charge Compression Ignition (HCCI) engines have been under intensive investigation for the over 25 years. This is a technology that is only now emerging in niche applications but may someday have wide applications including the natural gas market. To date, however, there are no known NG fueled HCCI engines in commercial operation. Other names have been applied to this concept such as detonation ignition, explosive ignition, etc. Whatever term is used, it describes a combustion process in which a well-mixed (homogenous) charge of fuel and air is brought to ignition by compression in a traditional reciprocating engine. It, therefore, combines features of traditional spark-ignited engines (initial homogeneous charge) and diesel engines (CI). HCCI combines the high efficiency of the diesel cycle (due to high compression ratios, low combustion temperatures and potential for unthrottled operation) with very low NO_x (< 10 ppm) (due to very lean homogeneous combustion) and essentially zero particulate emissions. Combustion is kinetically controlled, rather than mixing controlled, as in conventional engines. This produces very high heat release rates, and allows ignition to occur closer to top dead center (TDC). For this reason, the engine cycle more closely approximates and ideal Otto cycle, and has a greater potential for higher efficiency. There are two major drawbacks that have limited the use of HCCI. First, it is difficult to control ignition, and second, the engines have limited load/speed capability.[46]

As HCCI combustion is kinetically controlled, fuel composition variability is expected play a role in combustion timing. Åberg et al.[47] considered the effect of fuel structure on HCCI combustion. They blended varying amounts of ethane, propane and both iso and n-butane into methane at varying A/F ratios, boosts and EGR rates. The inlet air temperature required to properly phase the HCCI combustion was then measured for the different components in the fuel.[47]

They[47] concluded that:

- The change in the fuel MN is directly related to the change in required inlet temperature. The butanes have the largest impact on the inlet temperature, followed by propane and ethane.
- It was also noted that the inlet temperature affects the fuel/air mixture density. At lower inlet temperatures, the denser gas allows more mass to be induced into the cylinder, increasing the indicated mean effective pressure (IMEP).
- A lower inlet temperature also affects the overall cycle temperature, and this in turn affects the exhaust emissions.[47]

A modeling study by Flowers et al.[48] suggested that HCCI combustion may require active control to compensate for changing fuel composition. Because ignition is controlled by the chemistry, it is reasonable to expect that the HCCI process would be affected by fuel

composition.[46] Changes in natural gas composition may shift the peak heat release timing by as much as 10 CA degrees.

In another modeling effort, Soylu et al.[49] examined combustion characteristics, combustion phasing strategies and efficiency potential of a natural gas HCCI engine. Active fuel composition control, with blends of natural gas and propane, was discussed as a possible method to control combustion phase,[49] showing the importance of fuel composition on HCCI ignition.

Hiltner et al. modeled two-component fuels and as in the Flowers work showed higher HCs tends to lower the required intake temperature for peak thermal efficiency. This work showed as much as a 40 K change for a 15% vol. addition of Butane. Thus, it is likely that HCCI engines will require explicit development efforts for a given gas composition. This could be problematic for LNG fuel fluctuations as engines will likely be designed to a very precise fuel specification.[50]

Ohyana[51] investigated control of an engine which uses HCCI combustion at light load and conventional spark ignition at high load. The combination of an intake model, combustion model and engine thermodynamic model was investigated to accurately estimate intake air mass, burn rate, and auto-ignition delay. The combination of spark ignition and HCCI ignition is an option to enable wider operating range of HCCI engines, and may afford some flexibility for fuel composition since the ignition timing (at least for the spark ignited operation) can be controlled.

4.3 Aftertreatment

The type and level of pollutant treatment from gas engine exhaust (after-treatment) depends on many factors. However, the engine stoichiometry primarily determines the aftertreatment approach. There are two main catalytic exhaust aftertreatment approaches in current use. Stoichiometric engines use a three-way catalyst (TWC) to control exhaust emissions. Lean burn engines control NO_x via low combustion temperatures, and use an oxidation catalyst (OC) to reduce unburned products in the exhaust.[43]

Three-way catalytic reduction was developed by the automotive industry.[52] The TWC can remove CO, NO_x, and HCs in stoichiometric engines. Stoichiometric engines employing TWCs are commonly selected for use where emissions requirements are very strict. Lean-burn engine technology can produce higher efficiency, but cannot achieve emissions as low as the stoichiometric engine with TWC. Catalytic NO_x reduction is not very effective in the lean-burn engine because the high exhaust oxygen level competes to oxidize the HC present in the exhaust, preventing HC from participating in effective NO_x reduction.[53] More details on TWC are given in Section 4.3.1.

For lean-burn engines, the use of HC as reducing agents for NO_x was first reported in the 1970s.[54,55] Without a selective catalyst, these earlier catalysts oxidized HC and therefore required the use of excessive of HC to remove the oxygen. Iwamoto et al.[56] discovered that a copper based catalyst (Cu-ZSM-5) could produce NO decomposition under lean conditions. Relatively high efficiencies have been reported with NO_x reduction in the presence of excess oxygen with non-methane HC, e.g., propane, propene, and ethylene. Methane is the least reactive alkane and with exhaust gas temperatures ranging from 350 to 500 °C, NO_x and CH_4

reduction is usually low.[53] Unfortunately, methane is also the largest fraction of the exhaust HCs.

Recently, rising fuel costs have increased the desirability of lean-burn natural gas engines because of their efficiency advantage over stoichiometric engines. As a result, catalytic methods to reduce NO_x have gained a great deal of interest. Selective catalytic reduction (SCR) of NO_x with ammonia (NH_3) is now widely used.[57,58] High conversion of NO_x (> 95%) can be achieved at relatively low temperatures, but ammonia must be added. Small applications or vehicles would benefit from an alternative NO_x reduction technology that does not require adding ammonia. SCR of NO_x with available exhaust HC would be more desirable than SCR with NH_3, but the required activity and selectivity of a CH_4-SCR of catalyst is a major technical challenge.[59]

From a different environmental viewpoint, the large methane fraction of the HC exhaust emissions from NGVs is a concern because methane is a more powerful greenhouse gas than CO_2. Methane is the most difficult HC to oxidize catalytically, but palladium (Pd) catalysts are most active for methane oxidation. With a TWC, slightly rich air fuel control is needed for effective NO_x conversion.[60]

Variation of HC in the fuel can also affect the species composition and reactivity of the HC emissions in the exhaust. Non-methane organic gases (NMOG) such as aldehydes, ketones, alcohols, and other pollutants are considered precursors to ozone formation and are regulated pollutants.

4.3.1 Three-Way Catalysis

Stoichiometric engines rely predominantly on three-way catalytic aftertreatment for emissions control. Very precise mixture control is required to achieve simultaneous control of CO, HC, and NO_x emissions. It is generally understood and has been shown that the stoichiometric operating window for natural gas TWCs is narrower than for gasoline catalysts and at a slightly richer set point.[10,61,62] Natural gases with higher hydrocarbons content would provide a slightly wider TWC window of operation.

Subramanian et al.[63] showed that CO, NO, and CH_4 conversions exceeded 80% over a Pd-based catalyst when ER is between 1.0 and 1.2. This suggests that the engine has to be operated slightly rich of stoichiometry to remove all three constituents. The high CH_4 conversion under slightly reducing conditions appears to be the results of a higher catalytic activity for the CH_4-O_2 reaction, combined with the CH_4-NO reaction that removes CH_4.[63]

Experience with a conventional TWC (Pt/Rh = 5/1) designed for gasoline engine operation showed that THC conversion efficiency with natural gas fuel operation was much lower than with gasoline fuel operation. Methane, the predominant HC in typical natural gas emissions, could not easily be oxidized. When a (Pd/Rh = 25/1) TWC designed for natural gas was used, the THC conversion efficiency significantly improved.[60] These reductions are highlighted in Figure 4-1 for THC, NMHC, CO and NO_x. In the figure, UCC is the gasoline catalyst and CCC is the natural gas catalyst. CCC + UCC is the series combination of the two catalytic converters.

Thiagarajan et al. found that on a gasoline engine converted to operate on both gasoline and natural gas, CO levels were lower for natural gas than for gasoline due to the more homogeneous mixtures with natural gas. After catalyst NO_x emissions were higher for natural gas than for gasoline because the lower engine out CO levels that occurred in natural gas operation reduced the NO_x conversion efficiency. The engine out THC levels were similar for natural gas and gasoline. However, because the THC emission from NG is mostly methane, the post-catalyst emissions were higher for natural gas. Methane was difficult to oxidize in the catalytic converter, which was designed for gasoline operation.[24]

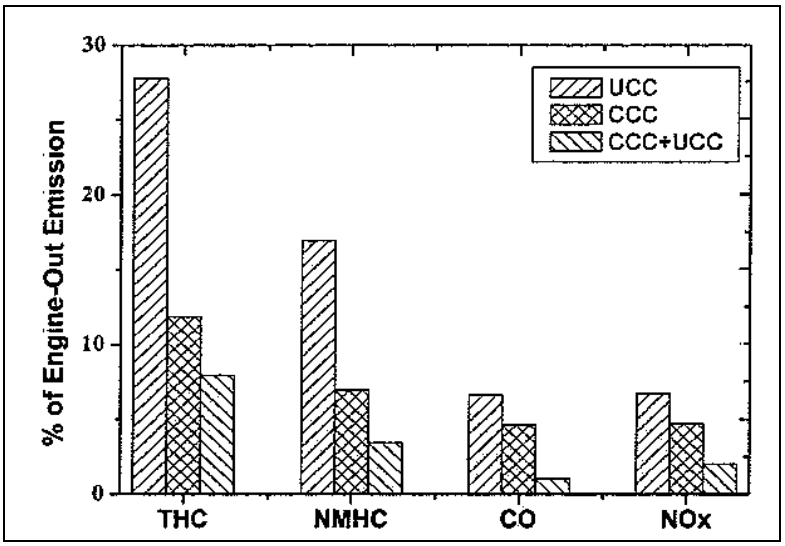

Figure 4-1: Comparison of NGV Emission Levels With Catalytic Converters (FTP-75 Mode, Fresh Catalyst).[60]
(Used With Permission)

Varde[64] found that at stoichiometric conditions in a NG engine, NO_x could not be reduced in a TWC to the levels found in gasoline fueled engines. As in the work by Thiagaranjan et al., these were automotive engines converted to natural gas operation using conventional gasoline catalytic converters. Reduced NO_x conversion was believed to be due to lower levels of CO emitted by natural gas fueled engines at stoichiometric condition relative to a gasoline fueled engine at the same ER. This was confirmed by injecting small amounts of CO upstream of the converter. The OC was Pt based with a noble metal loading of about 1.41 gm/cm^3 while the TWC was Pt/Rh based with the same noble metal loading of 1.41 gm/cm^3. The TWC also promoted a reduction reaction involving CO and NO according to

$$2NO + 2CO \rightarrow 2CO_2 + N_2 \tag{4-1}$$

The OC promotes oxidation reactions of the type:

$$HC + O_2 \rightarrow CO_2 + H_2O \tag{4-2}$$

$$2CO + O_2 \rightarrow 2CO_2 \tag{4-3}$$

$$CH_4 + 2O_2 \rightarrow 2CO_2 + N_2 \quad (4\text{-}4)$$

The two-way oxidation catalyst removed CO and HC from the engine exhaust. Since the presence of oxygen is necessary for the reactions to occur, it was necessary to supply secondary air to the catalyst depending on the A/F ratio supplied to the engine.

Because a sufficient concentration of CO is needed to yield high catalyst conversion efficiency for NO_x, it is necessary to control A/F ratios to yield appropriate exhaust gas composition. THC conversion efficiency for the natural gas fuel was about half of what was found for the gasoline fuel. Most of the reduction in HC conversion comes from the low oxidation of exhaust methane, and also because for NG engines, the exhaust temperature is lower compared to gasoline engines.[64]

In later work, Varde (2003)[65] investigated lean-burn natural gas engines for light-duty automotive applications. A three-way catalytic converter was applied to the engine while operating in the lean-burn mode. The conversion efficiency of CO was 90-99% at all conditions. In general, conversion of CO at stoichiometric or lean conditions is not difficult if the catalyst temperature is adequate. NO_x conversion was high near stoichiometric A/F ratio but decreased for lean mixtures. As already noted, reduction of NO_x in the exhaust of a lean-burn gas engine is not very effective due to the high oxygen concentration.

4.3.2 Selective Catalytic Reduction

Selective catalytic reduction (SCR) can be used to reduce the exhaust NO_x from lean-burn engines. The technique injects ammonia or urea (which converts to ammonia) into the exhaust stream prior to a catalyst. The catalyst and ammonia reduce the NO_x to nitrogen and water. The process temperature must be maintained (typically) between 450 and 850 °F, depending on the type of catalyst. SCR operation outside the planned operating temperature range, or with degraded catalysts, can lead to unreacted ammonia passing through the SCR device, and this is known as ammonia slip. SCR is most suitable for lean-burn engines operated at constant loads, and can achieve NO_x conversion efficiencies as high as 90%. Where operating conditions are widely variable, the SCR system and injected ammonia may not precisely match required demand, leading to period of excess or inadequate NO_x reduction.[66] Variations in fuel composition can affect exhaust temperatures due to changes in ER and hence engine timing or combustion duration. Engine out emissions may change somewhat but should have little effect on SCR performance.

4.3.3 NO_x Traps for Lean-Burn Engines

Lean NO_x trap (LNT) is an aftertreatment device used to reduce NO_x emissions for a lean-burn engine. NO_x is stored in the LNT during the lean operation of an engine. When the A/F ratio becomes rich, the stored NO_x is released and catalytically reduced by the reductants such as CO, H_2, and HC. This capture and release mechanism is shown schematically in "A Phenomenological Control Oriented Lean NO_x Trap Model," SAE Paper No. 2003-01-1164.[67]

Optimal modulation of lean and rich periods is required for high removal efficiency. The fuel must be low in sulfur, as the trap material can be damaged by sulfur. This is usually not an issue for natural gas, which has low sulfur levels. A control strategy must be used to determine when to switch between the lean and rich operating periods. During the lean period, NO_x is oxidized to NO_2 and then adsorbed on storage sites as barium nitrate. These reactions are given in Equations 4-5 and 4-6 below. Maximum storage capacity occurs at approximately 350 °C.

$$NO + \tfrac{1}{2}O_2 \rightarrow NO_2 \tag{4-5}$$

$$BaCO_3 + 2NO_2 + \tfrac{1}{2}O_2 \rightarrow Ba(NO_3)_2 + CO_2 \tag{4-6}$$

After the efficiency falls off, the trap must be regenerated (purged) during the rich period. The nitrate, $Ba(NO_3)_2$, becomes thermodynamically unstable under stoichiometric or rich exhaust conditions. This releases NO_2 and becomes BaO (Equation 4-7). BaO then reacts with CO_2 to regenerate to $BaCO_3$ (Equation 4-8).

$$Ba(NO_3)_2 \leftrightarrow BaO + 2NO_2 + \tfrac{1}{2}O_2 \tag{4-7}$$

$$BaO + CO_2 \rightarrow BaCO_3 \tag{4-8}$$

An important variable for the LNT control is the rich-period A/F ratio. Kim et al.[67] also theoretically investigated the effect of regeneration strategy on NO_x emissions and fuel consumption. Due to the sensitivity of regeneration A/F ratio, careful control is needed. Thus, changes to fuel composition that change stoichiometry may need careful adjustment for proper LNT operation.[67]

4.3.4 Oxidation Catalysts

The oxidation catalyst (OC) is effective for the control of CO, NMHC, volatile organic compounds (VOC), formaldehyde (CH_2O), and EPA classified Hazardous Air Pollutants from natural gas and LPG lean-burn engines. These catalysts are least effective for oxidizing methane compared to NMHCs.

McCormick et al.[68] studied the deterioration of oxidation catalysts performance for different exhaust HCs. A lean-burn CNG-fueled engine (Cummins B59G) was used in the study. A series of transient and steady state tests were used to age the catalysts. The catalysts were platinum/Pd on alumina and Pd on alumina. Carbon monoxide and ethylene conversions were nearly 100% at all conditions and did not decrease over time. However, methane conversion rates declined by more that 60% over the 10-hour experiment. Ethane and propane oxidation rates declined by roughly 40% and 20%, respectively. No decrease in activity was observed for heavier HCs, but the concentration of higher HCs is very low in NG engine exhaust.[68]

The mechanistic details of catalytic oxidation of methane in the exhaust are not completely understood. It has been proposed that the reaction proceeds through dissociative adsorption of methane to form methyl and methylene radicals. These adsorbed species can react directly with

adsorbed oxygen to form CO_2 and H_2O. Adsorbed species can also produce adsorbed formaldehyde, which dissociates to CO and H_2 which are further oxidized.[68] Researchers at the Danish Gas Technology Center tested lean burn engines and accumulated approximately two years of operation in field conditions with two catalyst types. Formaldehyde reduction ranged from 85% (aged) to 95% and from 40% (aged) to 60% with each catalyst.[69]

Strots et al. (1998)[70] investigated a novel catalytic converter technology, employing periodic reversal of gas flow through the OC monolith. This approach stores heat inside the catalyst support, and therefore can oxidize combustible components of the exhaust with even an ambient temperature inlet. Complete destruction of exhaust methane, is reported in simulation studies.[70]

In another investigation of converter technology, Creamer et al. (1993),[71] evaluated an oxidizing catalytic converter in the exhaust train of a 3.73-kW natural gas engine. A mathematic model was also used to study the effect of key variables on conversion. Methane conversion had the lowest of all HCs at 76%. Ethane was second lowest at 91.7%. All other HCs appear to be readily converted at the conditions tested. Tests showed that THC conversion increases as the spark is retarded because late ignition timing resulted in a higher converter inlet temperature.[71] In another study by the Danish Technology Center, poor methane oxidation was achieved with a full scale lean-burn engine fitted with an oxidation catalyst (2%-15%).[72]

4.4 Natural Gas/Engine Combustion and Fuel Properties

Effects of gas composition variations are due to the differences in the thermo-physical properties attributed to each gas component and their relative concentration in natural gas. Table 4-7 at the end of this section, gives some thermo-physical properties of select alkanes as well as two common diluents, N_2, and CO_2. LNG is expected to contain greater amounts of ethane, propane, and butanes than existing pipeline gas. Other components such as inerts also play a role in determining natural gas properties. Composition variations affect fluid dynamics, thermodynamics, combustion kinetics, etc. in ways that are predictable provided fuel compositions are known. This section briefly looks at flame speed, pollutant chemistry, engine knock, kinetics, thermodynamics and mixing in gas engine systems.

4.4.1 Autoignition

Autoignition occurs when pressure/temperature conditions lead to self-ignition of a fuel/air mixture, without any direct ignition source. Autoignition can occur in premixed systems, and also in systems where fuel and air streams are injected separately. By definition, the overall (or global) reaction is exothermic, but some key elementary and/or intermediate reactions can be endothermic.

In the past, researchers have conducted a number of experimental and numerical studies to understand ignition behavior in premixed methane/ethane or methane/propane mixtures; however many of these studies have been conducted at conditions that are not representative of engine conditions, (i.e., at atmospheric pressure or very high pressure).[73] A recent study by Turbiez showed that the combustion of natural gas can be appropriately represented by the combustion of methane/ ethane/propane mixtures.[74] This was also reported in jet stirred reactor

conditions, although at a lower temperature and higher pressure than the Turbiez study.[75] These findings allow for less chemically complex mixtures to act as surrogates in natural gas autoignition research.

Fraser et al. (1991)[76] measured the ignition delay (autoignition) time of methane and natural gas under simulated non-premixed diesel engine conditions in a constant volume combustion vessel. Measured ignition delay times for natural gas were very sensitive to temperature, but insensitive to gas pressure from 5 to 55 atm. They further observed that as the concentration of ethane increased, the ignition delay time decreased.[76]

Naber et al. (1994)[77] measured the ignition delay of pure methane and two blends of natural gas. This work was also performed in a constant volume combustion vessel under non-premixed diesel conditions. Similar to Fraser et al., higher concentrations of ethane and propane reduced the ignition delay time. At temperatures less than 1200 K, the ignition delay of natural gas had a first-order pressure dependence.[77]

Huang and Busch[78] measured the ignition delay of methane/air mixtures including small amounts of ethane and/or propane, at temperatures from 900 to 1400 K and pressures from 16 to 40 bar.[78] Below 1100 K, both propane and ethane had a similar promotion effect on autoignition. Similar conditions exist in an engine near TDC. Based on a detailed kinetic model, it was shown that at relatively low temperatures, the reactions between ethane/propane and methylperoxy (CH_3O_2) produce more OH radicals, promoting the initiation phase of the ignition. Based on the kinetic study the dominant ignition promoting mechanism for ethane/propane with changes with temperature. The CH_3O_2 and methylhydroperoxide chemistry are responsible for the promoting effect of ethane/propane at low temperatures ($T < 1100$ K).[78]

Fiveland et al. studied a lean premixed methane base fuel in an engine with either ethane, propane or butane as second fuel component. Typical fuel composition ranges were 85-97% methane, 2-10% ethane, 1-4% propane, and 0-2% butane. Sensitivity of minimum ignition temperature with fuel composition were measured and calculated, showing comparable temperature sensitivity between ethane and propane.[79]

Aesoy, et al.[80] conducted combustion bomb and engine testing to investigate the effect of higher alkane addition to methane. The studies were conducted in a diesel engine using glow-plug (assisted) ignition. Small changes in gas composition were shown to have significant impacts on ignition delay and also changed the required glow-plug surface temperature needed for ignition. Constant volume (bomb) ignition studies showed that propane had a greater promoting effect on methane ignition, Methane with 8% propane had a similar behavior as 20% ethane, reducing ignition temperature by 120 K.

Ignition property rating of fuels are normally estimated by standardized experimental methods, or by using simple correlations to physical known properties. Remarkably, for liquid HC fuels, the exact composition is usually not known because liquid fuels include many complex hydrocarbons that survive the refining process. By contrast, natural gas composition is relatively simple, and can be determined accurately. Thus, there is a good opportunity to predict fundamental ignition properties from the gas composition.[80] However, it should be recognized

that actual autoignition behavior depends also on details of fluid mixing and local temperature conditions in engines.

4.4.2 Flame Speed

The laminar flame speed of natural gas mixtures is slightly lower than that of most other HCs due to the low reactivity of the main constituent (methane). Flame speed will not be greatly affected by varying fuel hydrocarbon concentrations because the flame speeds are not greatly different for most alkane components (see Table 4-7). The effect of low flame speed is most important at lean conditions. For lean conditions, the charge turbulence and density may need to be increased to produce a faster burn rate.[81] A fast burn rate is important for several reasons:

- It enables a leaner mixture with comparable combustion time.
- For stoichiometric engines, where knock might be expected, a fast-burn combustion system decreases the chance for knock. This is because the flame front propagates through the end-gas before self ignition occurs.
- Faster burning lowers cyclic variability and increases efficiency.

Combustion chamber design is one of the key factors affecting the performance of a spark ignition engine. Multiple design considerations are involved, but a key parameter is the level of turbulence in the chamber just prior to ignition and during the combustion. The turbulence is controlled by the swirl level generated during the intake process, and by the "squish" as the piston approaches TDC. Higher turbulence levels improve mixing and usually increase burning rates, leading to greater efficiency and reduced emissions. For lean burn engines that minimize emissions and maximize efficiency, the combustion chamber design should be planned to achieve the highest possible combustion rate for all operating conditions.[82]

By modifying the chamber shape, compression ratio, and enhancing turbulence, a fast burning chamber for lean natural gas combustion was developed by Witze et al.[83] Brake thermal efficiency in excess of 40% was achieved, with better torque than when operating on gasoline. The chamber design used "tumble" (indicating the direction of swirling flow) to increase turbulence. The tumble vortex stores energy until late in the compression stroke. When the vortex breaks up, the turbulence result in fast burn rates.[83]

The squish motion generated during the compression stroke can be used to increase turbulence and produce other benefits. Squish forces the charge toward the center of the combustion chamber which decrease the distance the flame needs to travel to burn more of the fuel. The squish motion also breaks up swirling flow into small scale turbulence. The small-scale turbulence is generated when it can help the early phases of combustion. A disadvantage, however, is that the bulk motion associated with squish flow may also impinge directly on the spark plug, slowing the initial flame kernel growth and increasing ignition delay. However, in general, increased turbulence is an advantage.[81]

Evans et al. showed via covariance and mass fraction burned analysis that squish is most effective in the latter half of combustion. Their experimental studies showed that a small outlet passage directed into the central bowl in the piston crown generates high levels of turbulence.

The additional turbulence level provided significant levels of mass fraction burned rate reduction. This allowed a retarded timing adjustment (to get to maximum torque timing) to further improve NO_x reductions by 20%.[82]

In another work by Evans, combustion chamber geometry affected optimum spark advance, specific fuel consumption and specific emission levels via the burning rate in the combustion chamber. The burn rate is controlled by the intensity and scale of the mixture turbulence just prior to ignition and during the early combustion process. A comparison of two versions of the squish-jet combustion chamber and a conventional chamber design in a Cummins L10 engine, with and without enhanced swirl motion, showed the squish-jet configuration to be more effective in increasing thermal efficiency than the use of high swirl levels.[84]

A fast burn rate allows the use of a higher compression ratio by helping to avoid knock. This can reduce fuel consumption and increased power output.[85] For example, if the combustion duration were increased from 30 to 45 °CA, the efficiency of the cycle would be the same if the heat rejected fell from 26 to 21% of the fuel calorific value.[86] Fuel variability will impact burn duration when diluents are present as this is similar to "leaning" the fuel air mixture.[87]

Matthews et al.[31] conclude that differences in CNG composition over the ranges studied in the state of Texas do not have a significant effect on the flame propagation rate in that they did not significantly affect the combustion process. Test fuels ranged in Wobbe number from 1294 btu/ft^3 to 1381 btu/ft^3. All fuels were within NGC+ interim guidelines in both inerts and butane composition [33, 156]. It was concluded that engine control systems differences (e.g., spark timing and EGR schedules) plus catalyst differences dominate tailpipe NO_x emissions over the range of fuel composition studied.[31]

4.4.3 Pollutant Chemistry

The primary criteria pollutants from natural gas-fired reciprocating engines are NO_x, CO, VOC, and PM. The formation of NO_x is exponentially related to combustion temperature in the engine cylinder. Incomplete combustion produces CO and VOC species principally. PM emissions include trace amounts of metals, from engine wear and lube oil, non-combustible inorganic material, and condensable, semi-volatile organics which result from volatized lubricating oil, engine wear, or from products of incomplete combustion. Sulfur oxides are very low since sulfur compounds are removed from natural gas at processing plants. Only trace amounts of sulfur remain although small quantities of sulfur continuing odorants are added to natural gas at city gates prior to distribution for the purpose of leak detection. Sulfur is considered a poison for many exhaust catalysts.

4.4.3.1 Hydrocarbons

HC pollutants in any reciprocating engine are dependent on the fuel chemistry as most of the HC pollutants represent unburned fuel. Fuel chemistry represents a constraint to the initial birthing path of reactions leading to final quenched or equilibrium products. In natural gas engines the primary HC pollutants will be methane. Methane is, by far, the most stable alkane molecule. It

is because of its stability that it is a concern as a greenhouse gas. On the positive side, its stability minimizes it as a precursor to ozone formation.

Included in the pollutants commonly classified as VOC are multiple hydrocarbons that photoreact in the atmosphere. VOC emissions occur as the result of incomplete fuel combustion. With natural gas, some organics are carryover, unreacted, trace constituents of the gas. Other organics may be the result of pyrolysis of the heavier HC constituents. Multiple factors can lead to partially burned HC and in turn VOC emissions. These factors include poor fuel air mixing, incorrect fuel air ratio for the operating conditions, and reaction quenching at walls or in crevices.[66]

During fuel lean operation, two primary sources of HC emissions have been identified: storage of fuel in crevice volumes and dissolving of fuel in oil films. Both mechanisms contribute to HC emissions by shielding fuel from the passage of the flame in the combustion chamber resulting in unburned fuel in the engine out exhaust. In-cylinder sampling measurements have demonstrated that incomplete combustion in the bulk gas does not contribute to HC emissions at fuel lean conditions except at high dilution levels near the misfire limit. For HC less than C_6, the effect of an oil film is expected to be minimal since the solubility of these fuels in oils is small. Thus for natural gas fuels, storage in crevice volumes is the major source of HC emissions.[88,86]

Much of the observed experimental difference in total HC emissions for the C_1-C_5 fuels results from significant differences in fuel structure. Differing amounts of total carbon in the intake charge at a given equivalence ratio as a result of the different H/C ratios of the fuels and the extent of consumption of fuel that occurs upon its outflow from crevice volumes because of their different reactivity, diffusion rate, and flame temperature will affect total HC emissions. Under lean conditions, the remainder of the HC emission from alkane fuels consists primarily of olefins formed by breaking alkyl radical C-C bonds in higher molecular weight fuels. H_2 atom removal from alkyl radicals are also a likely source of olefins. This is especially the case for light HC fuels (e.g., C_3H_6 from C_3H_8 and C_2H_4 from C_2H_6).[88]

In the work by Kaiser et al.,[88] seven neat fuels (methane, ethane, n-butane, isopentane, isooctane, and toluene) were tested in a single-cylinder research engine at four operational conditions. They found that methane has roughly 50% larger HC emissions than ethane which is followed by monotonically increasing HC emissions as the carbon number of the fuels increase. Methane THC emissions were larger than ethane but less than C3 and above fuels. They also found the amount of CO and CO_2 in the exhaust is also directly related to the amount of carbon in the intake fuel.[88] As of now in the United States methane emissions from NG fueled engines are not regulated. There is need for concern since the higher hydrocarbon content of the NG there is greater likelihood of increased regulated non-methane hydrocarbon (NMHC) emissions. Though oxidation catalysts do well with higher hydrocarbons, methane reduction by catalytic methods has proven difficult.[88]

In NG combustion, the total hydrocarbon unburned fuel fraction of the engine out exhaust is largely methane. This can be explained by considering the differences in high-temperature oxidation pathways and kinetics of the relevant paraffinic fuels. Like other paraffins, methane undergoes dehydrogenation as a first step. However, unlike the primary radical product of other

paraffin dehydrogenations, the methyl radical (CH_3) is relatively hard to oxidize. Consequently, when a methyl radical is consumed, either by oxidation or CH_3-CH_3 recombination, the remaining sequential reactions oxidize the methyl products to CO and H_2O rapidly. Thus, the methane methyl reaction sequence limits the total reaction rate. The other paraffin oxidation paths do not contain dominant rate limiting reactions. This results in more even distributions of fuel and oxidation intermediate species.[73]

Generally, it is observed that THC emissions decrease with increasing engine speed. Changes in engine speed affect the amount of HC escaping the primary combustion process through crevice storage, and the extent of oxidation in the post combustion environment. This general trend suggests that the controlling process is the increased rate of oxidation associated with the higher temperatures.

Increasing exhaust temperatures as a result of spark timing, leads to a faster oxidation rate of the UHC in the post combustion environment. Hence, the potency of the crevice mechanism and the increased rate of post combustion oxidation could contribute to the observed reduction in THC volume fraction with retarded spark timing.[89]

HC emissions are minimized by compact combustion chambers in which the crevice volumes are minimized. In such an engine, HC levels should become significant only as the misfire limit is approached, as a consequence of inlet charge dilution by via excess air or EGR.[85]

4.4.3.1.1 Aldehydes

Formaldehyde is emitted from a number of natural and anthropogenic sources. It is an intermediate oxidation product resulting from the combustion of HC fuels. Emissions of formaldehyde from combustion processes are an environmental and health concern. Formaldehyde is carcinogenic, odiferous, and remains in the atmosphere sufficiently long enough to actively participates in tropospheric chemical reactions ultimately contributing to photochemical smog.[90]

Formaldehyde is a very reactive organic chemical with a high propensity to form ozone by photochemical oxidation. The widely accepted method to classify and compare the effect on ozone formation of an engine exhaust component is the maximum incremental reactivity developed by Carter and Lowi.[91] Aldehydes have very high maximum incremental reactivity values compared to other NMOGs. Aldehydes can directly impact human health by causing nausea; headaches; coughing; and irritation of eyes, nose, and throat.[92]

While bulk in cylinder conditions ensure rapid oxidation of formaldehyde, substantial amounts of formaldehyde may be formed in the outflow gases of relatively cold, protected regions of the engine such as crevice volume and quench zones during blow-down and later stages of the scavenging process in the engine.[90] Sources of formaldehyde include:[92]

- Unburned fuel-air mixture trapped in the piston top land and ring crevices.
- Absorption and adsorption of fuel by lubricating oil films and/or deposits in the combustion chamber followed by desorption of the fuel later in the cycle.

- Quenching of the advancing flamefront at cold wall surfaces in the combustion chamber.
- Gas-phase quenching when the engine is operating at the extremes of ER and spark timing.

Alzueta et al. conducted a computational study of chemical reactions in the exhaust system of natural gas engines. The study emphasizes the formation and destruction of formaldehyde. The results indicate a complex interaction between UHC formaldehyde and NO_x. At temperatures above 850 K, partial oxidation of UHC may occur resulting in net formation or destruction of formaldehyde depending on the UHC/formaldehyde ratio and the reaction conditions.[90]

There does not appear to be a complete combustion regime for which formaldehyde is favored thermodynamically in the amounts observed in the exhausts of operating gas engines. Equilibrium conditions predict less than 1 ppb. Thus observed formaldehyde exhaust emissions must come about as the result of chemical kinetic and fluid dynamic mechanisms which do not allow for complete oxidation. Relatively small amounts of C_2 and higher HC can have a strong impact on the low-temperature kinetic regime where formaldehyde formation is favorable. Unfortunately, all these mechanisms are complex. A reduced kinetic mechanism suitable for rapid prediction of formaldehyde formation is not currently available.[93] Shielded and protected crevices are a likely place of very significant levels of THC and formaldehyde formation. Mitchell and Olsen developed a schematic of likely paths for engine out formaldehyde.[93]

The data suggests that formaldehyde formation is closely tied to the shape of the bulk in cylinder gas temperature profile during the expansion stroke. Of particular significance and importance is the time that the combustion products spend in the net formaldehyde formation temperature window and the average slope of bulk temperature versus CA curve during expansion. Formaldehyde emissions are directly related to the time spent in the formation temperature window and inversely related to the absolute value of the average slope of the bulk temperature profile.[94]

With respect to formaldehyde emissions versus humidity ratio, humidity ratio is a mass based ratio of water vapor to dry air in the ingested air. The effects of humidity on formaldehyde emissions are significant. An increase in intake air humidity ratio increases formaldehyde emissions at all levels of boost pressure. One potential explanation of the influence of humidity is based on formaldehyde chemical kinetics. In the presence of UHC and oxygen there is a temperature window where a net positive formation rate of formaldehyde exists. That temperature window is approximately 700 to 1300 K. At temperatures greater that 1300 K formaldehyde is quickly destroyed. Below temperature of 700 K the formation reactions are quenched. The combustion products pass through this temperature window during the expansion stroke. For higher specific heat mixtures (as would be the case with a moist verses dry mixture) the gas temperature might spend more time in this temperature window during expansion thus resulting in higher HC concentrations.[94]

Aldehyde formation will be affected by fuel composition in several ways including changes in flame speed. Changes in flame speed will in turn affect and flame quenching distance. This affects the primary source of aldehydes which is crevice quenching. The degree of this effect has not been studied.

4.4.3.1.2 Poly-Aromatic Hydrocarbons

Poly-aromatic hydrocarbons (PAHs) are large agreements of benzene rings formed during the incomplete combustion organic substances. PAHs have been linked with cancer occurrences in both experimental animals and humans subject to exposure. The consequence of gaseous fuel variability on PAH emissions has been the subject of little investigation.

Gambino et al. looked at carbonyl and PAH compounds emitted from a heavy-duty CNG fueled engine. Compared to a tested conventional diesel engine, total PAH emissions were about a thousand times lower than those emitted from the diesel. Formaldehyde emissions from the CNG engine were about 10 times that of the diesel engine. Other carbonyl compound emissions of were considered comparable between the CNG and diesel fueled engines.[95]

Kado et al.[96] conducted chemical and biological (Ames) analysis to characterize the toxic air pollutants emitted from both CNG and low-sulfur diesel fueled heavy-duty transit buses. Tests were conducted on a chassis dynamometer over three transient driving cycles and a steady-state cruise condition. The engines used in the vehicles were Detroit Diesel series 50 engines. The CNG engine was a model year 2000 50G build. The diesel engines were model year 1998 build. The CNG bus had no after treatment. The diesel bus was first tested equipped with an oxidation catalyst (OC) aftertreatment system and then with a catalyzed diesel particulate filter (DPF). Emissions were analyzed for PM, VOC, PAHs, and mutagenic activity. Of the three vehicle configurations tested in this study, the lean-burn CNG-fueled bus had the highest emissions of 1,3-butadiene, benzene, and carbonyls (e.g., formaldehyde). The 1998 model year diesel bus equipped with an OC and fueled with low-sulfur diesel had the highest emission rates of PM and PAHs. The highest specific mutagenic activities (revertants/μg PM) were from the CNG bus over the New York Bus driving cycle. The 1998 model year diesel bus with DPF had the lowest VOCs, PAH and mutagenic activity. The emissions of toxic compounds from an in use CNG transit bus without an OC and from a vehicle fueled with low-sulfur diesel fuel equipped with DPF were lower than from the low-sulfur diesel fueled vehicle equipped with an OC. All vehicle configurations had generally lower emission of toxics than an uncontrolled diesel engine.[96] Fuel complexity in diesel engines has been linked to exhaust PAH speciation as well as overall reactivity and genotoxicity of the PM.[97]

In recent work, emissions from a spark ignited CNG fueled heavy-duty urban bus engine with a TWC were chemically analyzed and tested for genotoxicity. The results were compared to those obtained in a previous study on an equivalent diesel engine, fueled with regular diesel fuel and a blend of the same with 20% biodiesel (B20). The experimental procedures used in both cases were identical. The experimental design focused on carcinogenic compounds and genotoxic activity of the exhaust. The obtained results indicate that the SI CNG engine emissions, with respect to the diesel engine fueled with diesel fuel were nearly 50 times lower for carcinogenic PAHs, 20 times lower for formaldehyde and 30 times lower for PM. A 20-30 fold reduction of genotoxic activity was projected from the Salmonella typhimurium/mammalian microsome assay.[98]

4.4.3.1.3 Non-Methane Organic Gases

As the result of their contributions to ozone formation NMOG are an EPA regulated pollutant. In a recent automotive study using the FTP-75 transient mode, the light-end HCs (C_2-C5) accounted for vast majority (91%) of the total NMOG emissions. Formaldehyde was responsible for 82% of the aldehydes and carbonyl compounds measured.[60]

As ethylene has a large reactivity, any significant exhaust volume fraction tends to supply the most ozone forming potential in natural gas engine exhausts.[99,100] Typically the ethylene composition is sufficiently high enough that it is the dominate ozone precursor in NG engine exhaust. Kaiser et al. measured exhaust hydrocarbon mole fractions at four engine conditions using pure methane, pure ethane, pure propane, pure butane, and pure pentane. In each case, ethylene remained the dominate NMOG species. In many cases using C_2 or higher fuel ethylene was the dominant overall exhaust species save that of unburned fuel itself.

Data from Nine et al.[101] showed that THC production and specific HC species vary with the load and A/F ratio. Ethene exhaust levels indicated formation during the combustion process. One way to characterize the ethene production is to examine the ethene to methane ratio in the exhaust. According to a University of Dayton report, at temperatures in excess of 850 °C, thermal decomposition of methane produces significant amounts of ethene and propene byproducts. Yields approaching 10% for ethene and 1% for propene are reported. Ethene was destroyed at 1050 °C and propene at 1000 °C. This potentially explains the lower ratios of ethene to methane seen at high load operation.[101] Note that current emission standards use a weighted organic emission scale which considers the reactivity of individual HC species. Methane is by far the least reactive species and thus has been omitted form the scale. Only NMOG are limited under reactivity-based standards. The EPA and the European Union regulate NMOG.

The effects of engine operating conditions on the engine out HC emissions species from a 2-liter natural gas fueled spark ignition were examined by Paulsen et al. Methane was the dominate THC, as one might expect as it is the main component of natural gas. The NMHC consisted primarily of ethene, ethane, and acetylene. Ethene accounted for 80% NMHC reactivity. Over the speed range tested 95 to 98% of the THC reactivity is contributed to NMHC and ethene accounts for 83 to 90% of that reactivity.[89]

4.4.3.2 NO_x

NO_x is formed through three fundamentally different mechanisms. Thermal NO_x is produced in high temperature combustion regions where atmospheric nitrogen, injected during the intake stoke, reacts with oxygen. Prompt NO_x, the second mechanism, occurs via rapid reaction between N_2 molecules and HC radicals in the propagating flame-front. Fuel NO_x is the third mechanism. It occurs when fuel-bound nitrogen compounds react with oxygen during combustion. Natural gas has negligible fuel-bound N_2 (although some molecular N_2 is present), thus fuel-NO_x is not significant in natural gas engines. Prompt NO_x may be significant where HC radical concentrations are high. This can occur in rich-burn engines, but is typically not as prominent as thermal NO_x. Thus, thermal NO_x (also known as Zeldovich NO_x) is the major

mechanism for gas-fired engines. The rate of thermal NO_x formation is a strong function of the combustion temperature. Maximum thermal NO_x production occurs at conditions where combustion temperatures are greatest, i.e., near stoichiometric fuel/air ratio conditions.[66] It should also be noted that if the gas composition changes, the formation of NO_x is only affected if the peak temperature also changes.[17] Also consider that combustion phasing greatly affects peak temperature.

Uncontrolled NO_x emissions levels from NG fueled engines are generally significantly lower than diesel cycle engines. In test on the West Virginia University mobile emissions laboratory, vehicles were powered by 8.3-liter Cummins natural gas engines employing feedback control and by conventional 8.3-liter diesel engines. The vehicles were subjected to the Central Business District speed versus time cycle described by SAE J1367. NO_x emissions levels, by mass, were 12% lower for the 11 natural gas buses tested than for the three diesel control vehicles tested.[102] Although overall stoichiometry in diesel engines may imply leaner conditions relative to the spark ignited NG engines, the diesel combustion process is diffusion controlled and occurs at stoichiometric conditions. Thus even at reduced injection levels, unlike NG spark-ignited, throttled engines, diesels produce relatively high NO_x even at part load conditions. Kaiser et al.[88] investigated engine NO_x emissions from an engine fueled by pure $C_1 - C_5$ hydrocarbons. They discovered a weak increasing trend in NO_x emissions levels with increasing carbon number. They contributed this to a slight increase in adiabatic flame temperature and to slightly higher nitrogen partial pressure in the exhaust. This trend is not prominent and is often overshadowed by other engine operational effects and interactions. In their tests, timing and engine speed showed no effect on this trend further indicating a fuel effect.

4.4.3.3 Carbon Monoxide

CO is produced by localized combustion air scarcity and by flame quenching in the combustion chamber of the engine. It is minimally impacted by changes in fuel gas composition if the A/F ratio is held constant.[17] CO and THC emissions are each products of incomplete combustion of the fuel. Exhaust CO results from insufficient residence time at high temperature disallowing the completion of the final HC oxidation step. In reciprocating engines, CO emissions can be an indicator of early quenching of combustion gases on relatively cold cylinder walls or valves. It should be noted that the oxidation of CO to CO_2 is a slow reaction compared to most HC oxidation reactions.[66]

Rothlisberger and Favrat[43] studied the influence of specific engine geometric and design parameters to determine their propensity to reduce relatively high CO emissions levels. The parameters investigated were volumetric compression ratio, duration of the intake and exhaust valve overlap and the location of the first piston compression ring. The CR was reduced from 12 to 9. The decrease of cylinder pressure resulted in a slowing down of the combustion process which, in turn, decreased fuel conversion efficiency. Lower cylinder pressure reduces the amount of unburned mixture stored in the combustion chamber crevices at the end of the primary combustion process. Consequently the quantity of CO emissions generated through HC partial oxidation during the secondary combustion process is also reduced. The slower combustion process results in an increase of the average temperature during expansion stroke. This higher temperature promotes a more complete oxidation of the UHC emerging from the crevices. In

comparison with the baseline piston, these effects result in a simultaneous reduction of CO and THC emissions.[43] Thiagarajan et al. notes that cold start enrichment is a major source of CO emissions in gasoline fueled engines. Cold start enrichment is not required for NGVs.[25]

CO emissions were shown by Kaiser et al.[88] to be linearly dependent on an engine's total carbon intake. As higher hydrocarbons are introduced into the NG, slightly higher CO emissions may be expected under identical operating conditions.

4.4.3.4 Particulate Matter

Noncombustible trace constituents in the fuel and lubricating oil can produce PM emission in natural gas engines. These emissions are generally very low, producing fine filterable and condensable PM. Poor air-to-fuel mixing or maintenance problems may increase PM emission,[66] but little information has been published reporting the effect of NG fuel variability on PM emissions. Typically, engine PM emission testing is performed in concert with EPA methods as outlined in the Code of Federal Regulations 40, Part 86, Subpart N.

In a study conducted in Los Angeles, California PM emissions were consistently 2 orders of magnitude lower for the CNG vehicles and for the diesel fueled buses employing particulate traps than the baseline diesel buses. The test buses, late 2001 models with similar engine designs, were from in-service fleet mix.[103]

Ristovski et al.[104] conducted measurements to determine particle and gas emissions from two large bore CNG spark ignition engines. Particle size distributions ranging from 0.01–30 micron and gas compositions were measured for five distinct power settings between 35 – 100% of full power. Particle emissions in the size range between 0.5 and 30 microns measured by the aerodynamic particle sizer. Emissions in this range were negligible. Thus, they were not considered in the analysis. Both engines produced significant amounts of particles in the size range between 0.015 and 0.7 micron. A scanning mobility particle sizer was used to make the measurement. Maximum number concentrations of approximately 1×10^7 particle cm^{-3} were very similar for the engines. The count mean diameters were in the range between 0.020 and 0.060 micron. The observed levels of PM emission are similar in number to emissions from heavy-duty diesel engines.

4.4.4 Knock/Detonation

Knock in spark ignited reciprocating engines is the result of autoignition of the end-gases in the combustion chamber.[86] The autoignition results from the untimely development of chemical reactions in the fuel/air charge during the compression stroke prior to the arrival of the progressing flame front. The ranges of pressure and temperature experienced can be broad and as such the extent and variety of chemical reactions can also be extensive. Knock can occur so rapidly and with sufficient violence that the operator or engine controller cannot compensate fast enough to avoid engine damage. Damage from knock is directly related to the rapid energy release in the combustion chamber due to uncontrolled autoignition. The damage is not due to extreme temperatures or pressures. The pressures and temperatures developed in the autoignition process are elevated but are not overly acute. The rapid energy release of the

autoignition leads to pressure waves that reflect within the chamber. The high frequency pressure oscillations lead to very high convective heat transfer coefficients near the surfaces of the combustion chamber. This in turn leads to scouring and eventual melting of the solid surfaces. Elucidating the knocking phenomena in an actual engine is no easy task due to the speed, accessibility and cycle to cycle unsteadiness of the combustion and fluid dynamic processes.

Callahan et al.[105] took a fuel survey and designed a test program that allowed the development of predictive equations necessary to write a computer program that would allow accurate assessment of the knock characteristics of a typical natural gas fuel air composition. Tests were conducted on a single-cylinder, variable compression ratio research engine at a constant stoichiometric ER, engine speed, boost pressure, spark timing and an intake temperature. The experimental test matrix of natural gases was designed to represent typical field gases. These gases were rated for knock resistance using previously developed MN procedures. A quadratic response surface relating the MN of the gases to the gas composition was developed. The effects of individual gas components such as inerts, isomers, and heavier alkanes were also investigated. Using the developed tools and knowledge, a procedure was developed to predict the knock tendency of a gas based on composition. As this procedure does not correspond directly to the MN procedure, the estimated knock tendency of the fuel is referred to as the Waukesha knock index (WKI). In attempt to quantify the required amount of engine derating the WKI was used as a substitute for motor octane number (MON). The WKI provided a more linear derate curve that was less sensitive to small changes in gas composition.[105]

Engine derateing by compression ratio or boost reduction is a method for widening the margins for fuel compatibility. However, in work by Schiffgens et al. assuming constant NO_x output, a decreasing compression ratio was shown to directly reduce efficiency. At lower compression ratios, engine operation is characterized by a narrower lean operating margin and a reduced knock propensity. However, the operating range is markedly expanded from a fuel compatibility perspective. The results show that reducing MN requirements by lowering the compression ratio reduces efficiency to potentially unacceptable levels. This was true even if the supply of fuel mixtures with a low MN is restricted to short time periods.[9] The recent advent of high-boost, high-EGR stoichiometric engines have permitted replacement of some lean-burn engines even on applications where efficiency is paramount. These stoichiometric engines, as a result of their elevated EGR rates, can achieve high load and power density without engine knock. They also maintain suitable exhaust stoichiometry allowing the use of a TWC.

The knock intensity versus ER at different propane fraction in the natural gas increases considerably with ER. In addition, the knock intensity increases with the propane fraction of the natural gas even when the ER remains constant.[106]

Akansu et al., investigated knock limits associated with fuel mixtures containing different percentages of H_2 and CH_4, ERs and intake temperatures. When H_2 and CH_4 was blended in relatively small amounts the knock resistant qualities of methane are not diminished.[107,108]

In general lower engine speeds allow more time for end-gas reactions to take place prior to flame front arrival. This provides a more favorable environment for knock to occur. However, Zhang

et al., found that for an engine speed range of 1000-1500 rpm knock limit ignition timing is independent of the engine speed but dependent on BMEP.[109] As such, increases in power output due to gas composition variations impact engine knock.

Experiments (Brecq et al.)[110] were conducted on a single-cylinder SI engine fuelled by natural gas. ERs were varied from 0.7 to 1.0. Pressure data from 160 cycles were analyzed. It was found that coefficient of variation of peak pressure and standard deviation of the angle of occurrence of peak pressure can be used to tune the engine for knock free operation. These parameters show a sudden rise from a minimum value to an increased value when knock occurs. Various methods derived from in-cylinder pressure data were evaluated as means for early knock detection in stoichiometric and lean-burn natural gas engine applications.[110]

4.4.5 Thermodynamics/Engine Cycles

Natural gas engines typically operate at lower compression ratios than diesel engines. A natural gas/air mixture cannot be compressed to the pressure realized in most diesel engines without detonation or knock occurring. However, natural gas engines operate at higher compression ratios than gasoline engines, since a mixture of natural gas/air can be compressed to higher pressures than a gasoline/air mixture. Natural gas engines normally have more advanced ignition timing than gasoline engines. Volumetric efficiency of gas engines is generally lower than gasoline engines. The addition of fuel in the gaseous state displaces a relatively high volume of intake air.

Generally an increase in the CR results in increased pressure, temperature and mixture concentration of the compressed gases. This speeds up combustion reactions and results in an increase in the burn rate and tendency for knocking. However, increasing the CR at constant bore and stroke increases the surface to volume ratio of the combustion chamber by reducing clearance volume at TDC. This increases the heat transfer rate from the gases to the coolant and lube oil. The reduction in clearance volume also allows more efficient removal of post combustion exhaust gases. This reduces the residual gas in the cylinder and reduces any dilution effect that this gas would have on the subsequent intake of fuel and air, resulting in an increase in the flame temperature. As more HCs released from the crevice regions may be displaced into the exhaust, an increase in UHC may also be observed.[81]

For stoichiometric and lean-burn applications, NO_x and HC emissions have been found to increase with compression ratio at fixed spark timing. The effect is less pronounced at part load conditions. With optimized (MBT) spark timing, reductions of emissions have been be achieved at high compression ratio indicating a fully optimized natural gas fueled engine may be able to achieve high efficiency and low emissions.[111]

The impact of gas composition requires attention from the designer, developer, and operators of SI natural gas fueled engines. The demand for increasing thermal efficiency while maintaining control of emissions has emphasized that variability in natural gas composition must be given attention. It is necessary to accurately assess engine response to varying composition. Referring to a paper by Thomas et al.,[112] the fuel volume percent of higher hydrocarbons or hydrogen

dramatically decreases the knock limited engine load (BMEP) for stoichiometric and lean engine operation.

Min et al.[99] studied fuel gas composition affects on performance and emissions in CNG engines. From this study a measurement called the maximum combustion potential (MCP) was developed. Results show that THC emissions decrease with Wobbe number and MCP. In opposition, NO_x increase slightly as Wobbe number and MCP increase. The total lower heating value of intake is proposed as a potential index for compatibility of fuel gases in a CNG engine. They also experienced a variation in power up to 20% depending on the composition of gas with a fixed fuel air ratio and spark timing. MBT conditions were for each test gas. MCP is defined as

$$MCP = \frac{1.0H_2 + 0.6(CO + C_m H_n) + 0.3CH_4}{\sqrt{d}} \tag{4-9}$$

Where H_2, CO, C_mH_n, and CH_4 are volumetric fractions of the gaseous fuels, respectively and "d" is defined as the specific gravity of the fuel.

Yacoub and Atkinson, (1999),[113] performed a thermodynamic analysis of alternatives to conventional throttling. They considered throttled operation as a baseline and variable fueling, early intake valve closing, variable valve timing with boost and variable compression ratio as alternatives. A lean-burn engine employing variable timing of intake valve closing and variable boost was determined to offer the best strategy to control load. In this strategy, demanded load is met first by making use of available turbocharger boost. If no incremental boost is available, the intake valve closing timing is then delayed. Based on an air cycle analysis, this strategy provided the highest thermal efficiency. It also reduced peak cylinder pressure over a wide range of conditions when compared to a conventionally throttled engine. It also offered other benefits for gaseous fueled engines over similar liquid fueled engines.[113]

Charleton et al.[114] investigated knock at excess air ratios in the range of 1.2 to 1.6 times stoichiometric. Flame initiation and propagation, evaluated from the mass fraction burned, are delayed as the mixture is made more lean. Slower combustion lead to reduced cylinder pressure at fixed spark timing reducing NO_x emissions. The experimental results show that flame initiation and propagation times are reduced and knock tendency is increased as the percentage of higher HC is increased.[114]

Thomas et al.[107] conducted a computer modeling study to explore the possibility of fuel economy gains via various changes to a modern medium-duty gas engine. The objectives of the study were to identify techniques to improve part load fuel economy. Once identified, quantification of the potential gains using computer models of the engine and driving cycle operation was pursued. The Ricardo simulation code, WAVE, was used to model the effects of engine modifications. Fuel economy was determined using the Ricardo vehicle cycle simulation code CYSIM over a number of drive cycles applicable to transit buses which might employ the engine under consideration. After looking at six techniques for efficiency enhancement, they concluded that gains are individually small and that appreciable improvements to total efficiency must come from a number of sources collectively. One exception was utilization of the Miller cycle with intake valve closing at 30° before BDC and 14.5 CR. This resulted in a 5.3% improvement

in efficiency. The techniques considered included electronic actuation of turbocharger wastegate, part load EGR, Miller cycle, skip firing at low loads and reduced intercooling at part load.[107]

4.4.6 Simulation and Kinetics

In the United States the composition of natural gas varies significantly from location to location. Typical compositions range from 75 to 98% methane and 0.5 to 13% ethane. When subject to typical ranges of natural gas fuel composition, the early stages of combustion in a spark ignited engine are more sensitive to the characteristics of the ignition source than to large changes in fuel composition for constant ERs.[115]

The dominant heat release phase for a methane fueled engine takes place under highly turbulent conditions with considerable flame stretch. The heat release phase proceeds at rates similar to an equivalent gasoline-fueled engine. The early combustion phase is bound by the start of the ignition event to the onset of self sustaining combustion. This has also been termed the delay period. During this delay period, a pool of radicals and intermediate species must be established to provide for the subsequent main heat release reactions. For methane, the early phase is strongly endothermic and typically the delay is substantially longer than in gasoline engines. The progression of the early combustion phase is closely linked to the detailed chemistry and is highly dependent upon the local heat and mass transfer environment.[115]

Nabor et al.[116] modeled combustion with four fuel blends. In addition to pure methane, a capacity weighted mean based on Liss et al., 1992, a high ethane mixture representing an extreme typical of Colorado natural gas fuels and a peak shaving gas fuel with high propane content were modeled. The gas blends cover a range of Methane numbers from 75–100.[77,116]

The kinetic mechanism used to model these gases was the mechanism of Pitz et al.[117]. Typically, the model showed a relatively isothermal period, followed by a steep rise in temperature, with the induction or delay time defined as the time at which the steep rise occurs. This is typical of the ignition period in NG fuels. Experiments, conducted in a constant volume combustion bomb, were performed over a range of conditions centered on the TDC conditions of a diesel engine. Ignition delay, as a function of temperature for the four natural gas blends, varies by approximately 1 ms, depending on the gas composition.

Increasing concentrations of ethane, propane and n-butane reduce ignition delay of the natural gas.[116] However there may be practical limits to fuel injection boost pressure due to higher HC condensation effects in direct injection engines. Finally, measured and predicted effects of natural gas composition variations on ignition did not correlate well with the MN determination used. This is likely due to that fact that the experiments used to determine MN correlations use premixed fuel and oxidizer while the experiments conducted here were done under the more diesel like conditions of directly injecting the fuel in to the air mixture in the combustion bomb. It is evident that the experimental correlation represented by MN cannot be extrapolated to describe ignition under conditions significantly outside the ranges used to derive that correlation.[116]

Turbiez et al. looked at fuel effects in low pressure stoichiometric premixed flames. Their study produced detailed laminar premixed flat flame burner experimental data at stoichiometry on the identity and concentration of both stable and reactive species produced by oxidation of various representative natural gas blends. The mole fractions of stable intermediate and reactive species were measured in addition to reactants and major products. Ethane and propane were shown to significantly increase intermediate species. Olefins were particularly prevalent as an intermediate species and were strongly dependent on ethane and propane concentration in the fuel. Further, the higher alkanes (up to C_6 were studied) were determined to play a minor role in natural gas oxidation. Their work supports the notion that the combustion of methane/ethane/propane surrogate mixtures appropriately represent natural gas combustion.[74]

Comparing the calculated values of natural gas ignition delay to that of methane under adiabatic constant volume combustion conditions can serve as a guideline for required changes to engine operating conditions to avoid the onset of knock. The "propane equivalent" concept proposed by Khalil and Karim[17] can serve as a tool for the combustion simulation of natural gas fuel mixtures in engine modeling calculations. Even thought eh approach is not widely used, such an approach demonstrates the impact of small changes in the concentration of the higher HC components of the natural gas through the resulting substantial inflation of the concentration of propane, a more reactive fuel than methane in a surrogate mix.[17]

Yossefi et al.[115] modeled the effect of fuel composition on early premixed flame kernel development. Their work uses large-scale three-dimensional computational fluid dynamic simulations, and detailed chemical kinetics to describe the early stages of natural gas combustion in a SI engine. The results of the study show that fuel ethane concentration enhances combustion propagation rate and reduces ignition delay time. CO_2 as a diluent had the reverse effect.[115]

Zheng et al.,[45] used a detailed chemical kinetics mechanism with a computational fluid dynamics code, to show that auto ignition of natural gas occurs when local mixture temperatures reach approximately 1300 K. Engine performance had a strong dependency on natural gas composition. Data from the Zheng et al. study shows the effect of higher alkanes on in cylinder pressure. Peak pressure increases and ignition delay decreases as the concentration of ethane in the fuel mixture increases. This is due to increased reaction speed due to a greater concentration of radicals, again, resulting from increased amount of fuel ethane concentration. This study also considered the effect of ethane concentration on NO. Increasing the amount of ethane in the fuel results in higher NO formation due to increased peak in-cylinder pressure resulting advanced start of combustion.[45]

In the work by Khalil and Karim, the presence of small concentrations of n-heptane added to methane also produces very substantial changes in autoignition and combustion behavior. Their results show that small changes in higher hydrocarbon natural gas composition particularly in relation C4 and higher, can produce significant changes in natural gas reactivity.[17]

4.4.7 A/F Metering

A/F ratio of either the volumetric or mass flow of air to volumetric or mass flow of fuel supplied to the engine is given as:

$$A/F = M_{air} / M_{fuel} \text{ or } A/F = V_{air} / V_{fuel} \quad (4\text{-}10)$$

Variables affecting metered A/F ratio may include but are not limited to: ambient air temperature, barometric pressure, fuel higher heating value, fuel pressure and load.[118] The stoichiometric A/F ratio is the ratio at which all available oxygen is combusted with fuel.[119]

The equivalence ratio (ER) is defined as the ratio of the stoichiometric air/fuel ratio to the actual air/fuel ratio and is given in Equation 4-11.

$$ER = A/F_{sto} / A/F_{act} \quad (4\text{-}11)$$

For a stoichiometric mixture $ER = 1$, for a lean mixture $ER < 1$ and for a rich mixture $ER > 1$. We note here that lambda (λ) (also commonly used both in this paper and in the engine community) is the inverse of the ER.

The method in which fuel is introduced or metered into a gas engine is important because it significantly constrains the level of controllability. Three primary methods for fuel control and introduction in natural gas engines are used. They are carburetion, port injection and direct injection. Carburetion is primarily used in open-loop controlled engines and can take on various forms. One such form is a venturi in combination with a fuel regulator, operating on Bernoulli's principle. For a carbureted engine, the volumetric air flow creates a pressure drop at the throat of a restriction. The reduced pressure draws a fuel volume into the air stream which is proportional to the pressure drop. The air and fuel flows are typically subsonic. Carbureted fuel flow is therefore directly proportional to the air flow (given constant size orifice) and the volume flow rate to the engine is constant for a given speed and load assuming volumetric efficiency is constant. Port injection and direct injection are primarily used in closed-loop controlled engines. Port injected engines fuel flow rate is metered based on predetermined response to engine operating conditions, such as speed, manifold pressure, throttle position and can be controlled electronically. Fuel flow is, therefore, dependent on a known calibration of the engine and indirectly dependent on air flow. Similarly, for the direct injected engine, the fuel flow is indirectly dependent on the air flow as one of possibly several control system input variables. The fuel flow also may be choked during part of the injection since in many cases significant fuel pressure is needed to inject the fuel in the small time interval available for the injection event. Also for the direct injected engine, the air flow is independent of the fuel flow since the cylinder inducts and traps only air prior to the injection event.[2]

For stoichiometric operated engines, open-loop control will have no compensation for changes in fuel composition. Closed-loop control will be able to compensate for fuel composition by keeping the percent oxygen in the exhaust close to zero.

For lean-burn operated engines, ER is controlled at a value less than one. Open-loop control will have no compensation for changes in fuel composition. Closed-loop exhaust gas oxygen (EGO) concentration controlled engines will have some compensation for this. However, when controlling to a desired ER the control scheme must assume a stoichiometric EGO concentration. A change in fuel composition changes this value and therefore there will be some error in ER. If

the natural gas composition is measured, the correct value of stoichiometric EGO concentration can be determined, allowing the control loop to control the ER more accurately. However, in most control scenarios residual oxygen concentration is the control variable. In that case, fuel composition will not induce bias in the control point.

Fuel and air mixing and its uniform distribution to each cylinder has long been a concern to engine manufacturers. Upstream mixing methods utilize available turbulence or jet mixing phenomena. High turbulence leads to increased pumping losses and is independent of the gaseous fuel type at the macro level. However, it is suspected that micromixing is dependent on diffusion, which would differ for each gas species.[120]

4.4.8 Methane Number/Wobbe number

The H/C ratio is the ratio of hydrogen to carbon atoms in a natural gas. Inerts (such as CO_2) and other non reactants are not included as indicated in ASTM D 3588.[121] The operating ER of an engine can be determined from its oxygen concentration (typically measured with a UEGO sensor) and knowledge of the fuel H/C ratio. This is important in lean-burn operation where the ER is to be controlled using the both knowledge of oxygen concentration as the primary feedback and the H/C ratio. Typically, controlling to a given ER, control loop logic uses a static value of the H/C ratio as initially determined during engine installation or periodic fuel composition measurement. LNG will generally have a lower H/C ratio and, therefore, any calculated value of ER, based on the original static H/C ratio, will have some error. The amount of error that can be tolerated will depend on the operational criteria of the engine. If the error is not acceptable, the control loop will need to be retuned with a new static value of the H/C ratio. In cases of unacceptable H/C variation, some means of continuously monitoring the H/C ratio and making it available to the ER calculation in the control loop may be required. Again, in most control scenarios residual oxygen concentration is the control variable. In that case fuel composition will not induce bias in the control point.

In stoichiometric engine operation, the control system is simplified by only seeking to maintain stoichiometric conditions in the cylinder to produce a zero O_2 concentration in the exhaust. Typically, a simple exhaust oxygen sensor is used as feedback to the controller. It measures oxygen concentration as does the UEGO sensor but its response is so rapid that it acts as a step change effectively only indicating the transition point. The output step change signal at the transition from no oxygen to a small concentration of oxygen or vice versa is an indication of stoichiometric operation.

The heating value of natural gas is given by the sum of each component multiplied by its heating value where:

$$HHV = \sum xj \cdot Hj \qquad (4\text{-}12)$$

x_j is the % molar volume in the gas of a component j
H_j is the heating value per mole for that component j

LNG will likely have increased higher HC and therefore a higher heating value. Heating values for common LNG and natural gas components are given in Table 4-2. Concentrations less than 0.2 mole percent do not appreciably influence the heating value of natural gas.[122]

Table 4-2: Natural Gas Components Higher Heating Value (HHV) and Specific Gravity at 60 °F and 1 atm.

Component	HHV (Btu / ft^3)	Specific Gravity
Methane	1016	0.555
Ethane	1779	1.0405
Propane	2541	1.5256
i-Butane	3304	2.0111
n-Butane	3304	2.0111
i-Pentane	4067	2.4965
n-Pentane	4067	2.4965
n-Hexane	4830	2.9817
N_2	-	0.9692
CO_2	-	1.5253

A fuel anti-knock rating is a measure of its resistance to auto-ignition or detonation (knock). Of the methods commonly used, the higher the anti-knock rating, the more resistant the fuel is be to knock. The anti-knock properties of liquid fuels are measured by their ON, but for gaseous fuels MN is more commonly used. Methane, the main component of natural gas, LNG and many other gaseous fuels is highly resistant to knock and is given the highest ranking on the methane number scale (i.e., a MN of 100). H_2, also present in some gaseous fuels, is very knock prone, hence given an MN of zero. MN of a gas can be determined by the volume percentages of components in the mixture and their known MN.

When selling an engine, gas engine manufacturers define a MN requirement for their engine, which is the minimal MN required for knock-free operation. The MN of the customer's fuel gas should be equal to or greater than the engine's MN requirement. The MN of fuel gases depend on the constituent gases, and can be more than 100, if constituents with high MN, and diluents such as CO_2 and N_2 are present. Table 4-3 shows the MN, motor octane number (MON), butane number (BN), and Wobbe number for some common gaseous fuels.[123] There are two methane numbers presented. One is based on an assignment based on a procedure described by the GRI/SWRI report[124,125] and the other based on CARB.[126]

Another method, which is no longer used, is the butane number (BN) method. Its scale is based on molar blends of methane and butane with neat methane equal to 0 BN. It appears that the BN technique provides the most sensitive scale for rating natural gases. It should be noted, however, the relationship between carbon number and BN is much more nonlinear than either the octane or the MN scales and that the inverse is true to what was earlier stated regarding scale, (i.e., the lower the BN the higher a fuels knock resistance). The significance of this observation, besides its historical value, is that the knocking propensity of natural gas displays a non-linear relationship and increased sensitivity with both higher alkane concentration and carbon number. The greater the concentration of the higher carbon number constituents, the more sensitive the fuel is to knock.[4]

Table 4-3: Knock Rating and Wobbe number for C_1 to C_4 Normal Paraffin.

Gas	Motor Octane No.	Methane No.[127,128]	Methane No.[129]	Butane No.	Higher Wobbe No.	Lower Wobbe No.
Methane	122	100	108.4	0	1431	1287
Ethane	101	44	44.3	7.5	1832	1678
Propane	97	34	38.4	10	2177	2002
Butane	89	10	34.3	100	2480	2285

Several correlations have been developed to describe the relationship between gas composition and the ON of a fuel. These allow prediction of the motor ON if gas composition is known. In particular, a good correlation was found between the H/C ratio of the fuel and the ON. Correlations have also been derived between measured motor ONs and measured MNs, as well as between motor ONs and predicted MNs.[124]

There is a linear relationship[125] ($R^2 = 0.9996$) between the octane and methane scales where

$$MON = 84.9 + 0.37MN \tag{4-13}$$

The attainable shaft efficiency of Otto-cycle engines depends to a large extent on the compression ratio and power density often measured as the BMEP. Both are limited by the knock resistance of a mixture of fuel and combustion air and the structural integrity of the engine. Since the composition of the fuel is an important factor for determining the knock resistance, the attainable performance of an engine is directly coupled to fuel gas composition. The knock resistance is generally so high for natural gas fuels that the octane scale commonly used for liquid fuels is inadequate. One should bear in mind that for gaseous fuels, the knock resistance is dependent on process conditions and engine type.

As described, knock resistance has been characterized by several methods using a variety of reference mixtures. Some more common indicators are MON and research octane number (RON), BN, and MN. Models based on MN work use knock limited compression ratio and mixtures of H_2 and CH_4 as the reference fuel. The MN method has the best range and resolution and has been most commonly used by engine manufactures to adapt engines to fuels.

According to Kubesh et al.,[126] the MON can be converted to MN by:

$$MN = 1.624 \cdot MON - 119.1 \tag{4-14}$$

This method of determining the MN of natural gas has been adopted by the California Air Resources Board[130] and was developed based on linear regression of MON testing in a CFR engine of 12 blends of gaseous fuels consisting of C_1–C_4 alkanes, CO_2 and N_2. The MN may also be determined based on the weighted molar weight % of each component and their associated MN. The MON is not typically obtained in this manner for NG mixtures whereas MN is often obtained through gas analysis and the described weighting method.

Another test method for obtaining MN of gaseous fuels is the AVL method. It uses a small bore engine with an adjustable compression ratio. The engine is provided a fuel reference mixture of methane and H_2. The percentage of methane in the reference fuel is the MN since by definition

H_2 has a methane number of zero. For fuels with a MN exceeding 100, a blend of CO_2 and methane is used as the reference fuel. Here the percentage of CO_2 added to 100 (in a neat blend of methane) is the MN. The increasing effect on MN of another common inerts in natural gas, N_2, is considered to be 1/3 that of CO_2 in the AVL method. The stated error in MN using the AVL method is 1.5%.[131]

The ER can vary as gas composition (hence, the MN) changes with a carburetor/open-loop system. A lower MN usually results in a higher ER (richer operation) for a given carburetor setting due to the change in molecular weight of the fuel.[132] Because of the greater percentage of higher HC in LNG, the H/C ratio of the blend will decrease and the MN will decrease resulting in increased knock propensity.

For stoichiometric engines that rely on a TWC for emissions control, the metering effect of fuel composition variation may be controlled by monitoring exhaust oxygen concentration. Changes in stoichiometry affects not only engine-out emissions, but usually forces the catalyst to operate outside its the high-efficiency operating performance window. UEGO based stoichiometry controls avoid this situation.

Thomas et al.[112] investigated fuel variability effects on engine operation over a range of fuel gas composition relevant to the Tokyo area.[112] The purpose of their investigation was to improve part load engine efficiency. To do so, they tested more than 100 gas compositions with the engine tuned to MBT timing. As power density (represented by BMEP) increased, heat losses per unit energy output decreased and efficiency increased. Therefore, fuel HC composition may directly affect engine efficiency through its knock propensity by not allowing high load (high BMEP) operation. Thomas et al.[112] investigated the effect of component additive in methane. Based on this work, a significant reduction in knock limited BMEP with higher HC and MN was apparent. There were indications from both engines that the influence of H_2 on knocking is greater at lean conditions than at stoichiometric. The HC gases did not show this difference.[112]

Khalil et al. indicated that engine response to changing fuel composition can be satisfactorily characterized by the Wobbe number and the MN. The Wobbe number is a measure of the fuel interchangeability with respect to its energy content and metered A/F ratio assuming that the metering technique is by orifice or pressure loss device. In engine applications, changes in the Wobbe number are proportional to changes in stoichiometric A/F ratios.[17]

The Wobbe number is derived from fuel energy (higher heating value) and density properties and is given by:

$$WI = HHV / sg^{0.5} \tag{4-15}$$

HHV is higher heating value.
sg is the specific gravity of fuel with reference to air.

According to Khalil and Karim,[17] gas delivered in the range of 1289 to 1383 Wobbe will most likely not pose any problems in terms of engine performance or emissions for new or even old (existing) stoichiometric and lean-burn engines. A Wobbe number range of 1300 to

1420 Btu/scf was their recommendation, although a range of 1200 to 1250 was indicated to have been found acceptable for use on existing equipment in high altitude areas.

Increased heating value tends to raise the Wobbe number while increased specific gravity tends to lower the Wobbe number. LNG will usually have higher heating value and specific gravity than domestic natural gas. However, the increase in heating value from mixing LNG and natural gas usually increases the Wobbe number as carbon number also increases. Wobbe number is used as an indicator of energy flux though an orifice.[133] Thus, for an open-loop control system which does not monitor stoichiometry (via exhaust oxygen), variations in Wobbe Index may produce variations in the A/F ratio.[134] Liss and Thrasher[32] note that "variations in Wobbe number for the bulk of U.S. natural gas will effect, at most, a ± 3% change in ER for an uncontrolled engine." With appropriate engine control, reasonable Wobbe number variations can be accommodated because the feedback control compensates for variations in A/F ratio.[17] Similar in-cylinder pressure histories have been reported for similar Wobbe fuel, but with different composition.[135] In general, MN and Wobbe number are correlated and inversely proportional. Nevertheless, some values of MN independent of Wobbe number could cause damaging engine knock. Thus, there is still a need to control MN excursions.

4.5 Control Systems

Engine control systems in large part focus on fuel and air metering as well as timing control based on various input parameters. This section attempts to highlight some recent engine control studies as well as discuss some sensor techniques to shed light on the importance of engine control systems in to accommodate varying fuel quality effects.

4.5.1 Recent Studies of CNG/LNG Impact on Engine Control

Recently, in anticipation of increasing imports of CNG and LNG, several engine studies have been performed to assess the impact of varying fuel composition on gas engine operation. These studies were intended to provide information to the sponsors but are also recognized as potential input for possible future regulatory decisions by regulating agencies. As these studies represent dedicated analysis of fuel effects in existing commercial engines, they warrant special consideration. This section highlights three of the most recent efforts in this area.

4.5.1.1 Southern California Gas Study of CNG/LNG Impact on Cummins Engines[130]

A paper study was conducted to examine the effect of varying fuel composition on Cummins natural gas engines. The Cummins engines studied were chosen because they represent a majority of the engine technology and manufacturers in the California market. The study considered a fuel composition range which was bounded by the specification in California Public Utilities Commissions (CPUC) Rule 30 and a composition expected to represent LNG imports. and given in Table 4-4. The richest case gas was considered to be representative of LNG imports and was limited by the maximum energy content.

Table 4-4: California Public Utilities Commissions (CPUC Rule 30).[130]

Specifications	Min	Max
Btu/cu ft	970	1150
Wobbe number	1272*	1437*
MN	NA	NA
Methane (%)	NA	NA
Ethane (%)	NA	NA
Propane (%)	NA	NA
Inerts (%)	0	4

* Theoretical min and max based on CPUC Rule 30 Gas Quality Specification.

The two engines with a carburetor/open-loop system are the Cummins L10G Phase 1 and L10G Phase 2. Both of these engines use an Impco carburetor for fuel induction and fuel metering. The model years for the Phase 1 engines are 1991-1993 and for the Phase 2, 1994-1995. The Cummins fuel standard for these two engines is CES 20067. CES 20067 specifies a Wobbe number of 1300 to 1377, with methane content as low as 78% and the remainder ethane or propane.

In these engines, MN changes usually cause an ER change since they employ a carburetor/open-loop system. A lower MN usually results in a higher ER (richer operation) for a given carburetor setting due to the change in molecular weight of the fuel. The typical ER in this carburetor/open-loop system is 0.70. It is not recommended to set the ER less than 0.70 for such open-loop systems due to possible lean misfires. The author found that actual ER information for these engines was not available.

They report that power can also vary due to the energy density changes of the fuel in carburetor/open-loop systems. Assuming the efficiency of the engine does not change, the study determined that there will be an 11.1% increase in power with an open-loop system when changing from the CARB gas to the richest case gas used in the study.

Changes in combustion or "burn rate" affects combustion phasing when open-loop/carburetor system encounters varying gas composition. Burn rate increases with increasing ER in lean burn engines. Increasing the burn rate at a constant ignition timing effectively advances the combustion process which decreases the knock margin of the engine.

The Cummins L10G Phase 1 engine has a BMEP rating of 12.8 bar. With a change from CARB specification gas to the richest gas case in the subject study, the BMEP increases to 14.2 bar; the effective ER increased from approximately 0.750 to 0.835 for such a fuel change. The authors expect this engine type to knock at the richest cases.

A manual carburetor readjustment is one way to remediate increase in power when changing from CARB gas to the richest gas case. The authors state that if the carburetor was adjusted to the recommended oxygen % in the exhaust using the richest case gas, the ER would be 0.752 and the power would remain essentially unchanged. However, the engine would still likely knock due to decreased MN. Retarding the ignition timing and/or reducing the ER is expected to provide enough knock margin to operate on the richest case gas.

The authors conclude that engine operation on both the high and low MN gas cases would require an electronic fuel valve and a closed–loop fueling system. Adding a knock detection system would also enable the ignition timing to be retarded only when needed and perhaps continuously on low MN gas. Retarding ignition timing reduces the tendency to knock, but also reduces power, which reduces engine efficiency and negatively affects emissions. Power loss depends on the severity of knock and the particular engine and MN of the fuel. The authors estimate that the ignition timing will be retarded by 1 degree to operate on the richest case gas. A 1 degree ignition timing retard would result in approximately a 2% power loss.[130]

4.5.1.2 Southern California Gas Study on the Effect of Varying Fuel Composition on Fuel Supplied to DDC Gas Engines, May 4, 2005[132]

Detroit Diesel Corporation (DDC) Series 50G engines produced before October 1998 use an open-loop carburetor fuel system without a knock detection system. There will be an increase in power by 11.1% with an open-loop system when changing from CARB gas to the richest case gas assuming constant engine efficiency. Assuming the target ER for this engine is 0.700 the richest case gas will increase the ER to 0.779. The authors expect that knock would be experienced at the richest gas case. The authors predict that the lowest MN that this engine could run is 84.7 (CARB method) or 77.9 (AVL Method).

DDC engines produced after October 1998 use UEGO based closed-loop control systems. Because of richer operation, the combustion rate will also increase causing effective timing advancement in the direction of engine knock. However, these engines also have knock detection systems which prevent engine damage. The authors expect that the lowest MN that this engine could run is predicted to be 76.4 (CARB method) or 70.8 (AVL Method).

The ignition timing is retarded first, and if required, power is reduced when knock is detected. The DDC engine will need to retard timing by approximately 3 degrees at the richest case gas resulting in approximately a 3% power loss. A fuel with a CARB MN of 67.7, which is within the DDC fuel specifications, will result in a power loss of 7% with timing retard as the only knock mitigation technique.

4.5.1.3 Light-Duty CNG Vehicle Fuel Composition Study 2006[136]

The Gas Technology Institute (GTI) performed a study for the Southern California Gas Co. to investigate potential CARB NGV fuel specification modifications. Vehicle operational impact on air quality in California was one of the primary concerns with any proposed NGV fuel quality changes. Gas properties vary within California and will depend on natural gas production fields and the amount of LNG mixing. Composition ranges considered in the study are given in Table 4-5 and current California fuel specifications are given in Table 4-6. Low technology (bi-fuel with aftermarket systems) retrofits and high technology original equipment manufacturer (OEM) dedicated light-duty CNG NGVs were identified. Retrofitted NGVs have less sophisticated control systems than OEM NGVs. There are about 21,000 NGVs in CA, about 133,000 nationwide.

In the study, the impact of gas composition on a vehicle was analyzed as to impact in three primary areas: (1) Vehicle drivability (i.e., start-up problems, rough idle, acceleration, torque and horsepower); (2) engine knock potential; and (3) vehicle emissions impact.

Advanced OEM control systems include air temperature and pressure sensors used in feed-forward control logic, fuel pressure and temperature sensors used in feedforward control logic, pulse-width modulated fuel injectors, and dual upstream/downstream oxygen sensors used in feedback control logic. These inputs are used accurately calculate parameters for A/F ratio control, including adaptive control in response to air properties (humidity) and (potentially) fuel properties. As changes in natural gas fuel properties occur, the control system undergoes an adaptive learning process where it adjusts internal parameters to optimize operation without direct knowledge of fuel chemistry. The authors conclude that the state of adaptive control algorithms being used in new CNG light-duty vehicles alleviate vehicle drivability as a primary concern.

Typical natural gases have a much higher ON than gasoline. The compression ratios and BMEP ratings of light-duty NGVs in the market are basically the same as those of gasoline vehicles. Therefore, there is little concern that new vehicles will experience engine knock with natural gas mixtures having higher HC even at MNs as low as 65.

Table 4-5: Gas Composition and Properties for Average Natural Gas and Increasingly Rich Natural Gas.[136]
(Used With Permission)

Component	Average Natural Gas	Rich Natural Gas	Richer Natural Gas
Methane	93.40	86.00	81.60
Ethane	3.20	7.75	10.40
Propane	0.69	2.50	4.00
n-Butane	0.25	0.25	0.00
i-Butane	0.00	0.00	0.00
n-Pentane	0.10	0.00	0.00
i-Pentane	0.00	0.00	0.00
Hexanes (+)	0.06	0.00	0.00
N_2	1.50	3.50	4.00
H2	0.00	0.00	0.00
CO_2	0.80	0.00	0.00
H_2O	0.00	0.00	0.00
Air	0.00	0.00	0.00
Total	100.00	100.00	100.00
Higher Heating Value (Btu/scf)	1032.3	1076.8	1108.9
LHV (Btu/scf)	931.0	927.9	1003.0
LHV (Btu/lb)	20,363	20,035	19,836
Specific Gravity	0.5971	0.6338	0.6596
Ideal Density (lb/scf)	0.04557	0.04837	0.05034
Real Gas Density (lb/scf)	0.04565	0.04844	0.05041
Wobbe Number (HHV)	1336.0	1352.6	1365.3
Wobbe Number (LHV)	1204.9	1221.1	1235.0
H/C Ratio	3.884	3.755	3.678
Est. Octane Rating (MON) (Gas Data)	131.0	120.9	115.9
Est. Octane Rating (MON) (H/C ratio)	130.8	122.4	118.3
MN (CARB)	93.3	79.6	73.0
Stoichiometric A/F ratio	16.736	16.438	16.294
Molecular Weight	17.292	18.356	19.103

Table 4-6: Current CARB CNG Fuel Specifications.[5]

Specification		Value
Hydrocarbons (expressed as mole percent)	Methane	88.0% (min.)
	Ethane	6.0% (max.)
	C3 and higher HC	3.0% (max.)
	C6 and higher HC	0.2% (max.)
Other Species (expressed as mole percent unless otherwise indicated)	Hydrogen	0.1% (max.)
	Carbon Monoxide	0.1% (max.)
	Oxygen	1.0% (max.)
	Inert gases	
	Sum of CO_2 and N_2	1.5-4.5% (range)
	Water	a
	Particulate matter	b
	Odorant	c
	Sulfur	16 ppm by vol. (max.)

a. The dewpoint at vehicle fuel storage container pressure shall be at least 10 °F below the 99.0% winter design temperature listed in Chapter 24, Table 1, Climatic Conditions for the United States, in the American Society of Heating, Refrigerating and Air Conditioning Engineer's (ASHRAE) Handbook, 1989 fundamentals volume. Testing for water vapor shall be in accordance with ASTM D 1142-90, utilizing the Bureau of Mine apparatus.
b. The compressed natural gas shall not contain dust, sand, dirt, gums, oils, or other substances in an amount sufficient to be injurious to the fueling station equipment or the vehicle being fueled.
c. The natural gas at ambient conditions must have a distinctive odor potent enough for its presence to be detected down to a concentration in air of not over 1/5 (one-fifth) of the lower limit of flammability.

In contrast to NGVs, heavy-duty natural gas engines are highly turbocharged to increase their BMEP rating. They don't experience engine knock at high levels of BMEP because they operate at lean-burn combustion conditions. The excess air acts as a diluted to lower peak cylinder temperatures thereby lowering the propensity for auto ignition (or knock). Advanced controls and, in many cases, by using knock sensors, allow lean-burn heavy-duty engines to use natural gas compositions with a MN as low as 65 with manufacturer warranties. Even so, there is room to improve. The authors indicate that their survey of manufactures revealed that more testing is required to determine the effects of gas variability. The survey also indicated that the OEM's would generally be comfortable with the ability of their NGVs to accommodate a broader range of fuel compositions than currently experienced in the market.[136]

4.5.2 Oxygen Sensors

A steady-state closed-loop control strategy is often used to maintain the engine's A/F ratio in stationary, industrial, four-cycle, natural gas reciprocating engines (i.e., rich-burn engines). Oxygen sensors are the most commonly used devices in closed-loop A/F ratio engine controls.

An exhaust gas oxygen (EGO) sensor located upstream of the catalyst is used as the closed-loop control signal in stoichiometric engines. The EGO has a rapid but effective step change response around the point lambda = 1 (stoichiometric). Variables independent of the A/F ratio, including age of the EGO sensor, sensor contaminants, catalyst performance, engine performance, and exhaust gas temperature may affect the signal. These variables introduce uncertainties in the feedback control loop. For example, as the EGO sensor ages, the voltage response diminishes, requiring periodic recalibration to maintain exhaust emission compliance.

The A/F ratio for an open-loop controlled industrial, natural gas, rich-burn engine can typically be tuned within a range of 0.3% (lambda = 0.97) to 1.8% (lambda = 1.09) exhaust oxygen content through adjustments to the fuel pressure and carburetor.[118] A TWC requires an exhaust oxygen content of 0.3% to 0.5%, which is slightly rich of stoichiometry within an operating window of lambda = 0.99 ± 0.005.[118]

The standard EGO output produces a stable output voltage less than 0.15 VDC (volts direct current) at lean conditions and greater than 0.80 VDC under rich conditions. A sharp change in voltage offset is experienced when transitioning from lean to rich conditions at a point slightly lean of stoichiometry. A/F ratio control strategies typically switch back and forth rich to lean at 1 to 5 Hz, averaged slightly rich. The optimum oxygen concentration target is selected by monitoring the post catalyst emissions and is typically around 0.99 lambda.[118]

The EGO sensor gives a signal most useful for control near stoichiometric conditions because of the sharp signal change around lambda = 1. This performance characteristic is not useful in lean-burn operation. Lean-burn control is typically implemented with a UEGO sensor, also called a wide range sensor. The response of the UEGO sensor is a continuously varying current signal. Provided that the fuel H/C ratio is well known, this sensor gives information about the exact ER or lambda value, which for lean-burn applications, will be less than one.

Besides standard EGO sensors, automotive systems which use stoichiometric engines also use a heated exhaust gas oxygen sensor (HEGO). The use of a HEGO downstream of the catalyst was first used in the automotive industry. The sensor uses an integrated heater element to maintain constant reaction temperature greater than the exhaust temperature and independent of the exhaust temperature gradients. This increases sensitivity, repeatability and reduces contamination by preventing gas phase condensation and thermophoretic deposition.

HEGO sensors are still widely applied in automotive applications although the application of wide range sensors is slowly increasing. Due to sensor characteristics, together with control loop delay, the control system exhibits constant oscillations of the engine ER (or A/F ratio). Adjustments to controller response determines (somewhat) the amplitude and frequency of oscillation. However, not all control strategies remain fully linked to the UEGO or EGO during rapid transients.

Pollutant control is usually good when the downstream signal indicates stoichiometry. A fuel rich reading indicates that reducing gases are exiting the converter (CO, HC). When the signal indicates fuel lean it is very likely that there is some NO_x in the exhaust. The signal from the HEGO sensor downstream of the catalyst does not remain at stoichiometry although the inlet

signal oscillates around it, after a disturbance takes place. Therefore if high-performance control is desired, the dynamic behavior of the catalytic converter should be taken into account.

When a control scheme uses a HEGO sensor downstream of the TWC it is less prone to thermal aging, and the exhaust gas mixture is better equilibrated than upstream of the converter. The HEGO signal can also be used as an on-board-diagnostic (OBD) tool to monitor the catalyst.

In a typical EGO/UEGO feedback stoichiometric A/F ratio control, the control system components include: the engine and the catalytic converter, which act as the process; fuel injectors, which are the actuators; and various sensors (engine speed, throttle position, intake manifold pressure, coolant temperature).

The injected fuel is metered based on a calculation by the controller with inputs from measured O_2 concentration in the exhaust and estimated air flow. The engine state, such as the engine speed, coolant temperature and intake manifold pressure must also be measured. Automotive engine A/F control systems were made possible by the introduction of EGO sensors.

4.5.2.1 A/F Ratio Control

Accurate control of A/F ratio can be implemented in many ways. Classical controllers are based on static measured engine maps and are designed in part using frequency domain control theory. They were developed primarily for steady-state control of A/F ratio and often require an engine model that can be difficult to obtain or that become obsolete as the engine ages. The following are some common control strategies for A/F ratio control.

Weige, et al. 2002[119] developed an artificial intelligence (fuzzy neural network) controller based on a UEGO sensor (as output is proportional to the actual A/F ratio). The time delay between the formation of the air fuel mixture and measuring point is significant and requires a control scheme with feedforward and feedback elements. The feedforward loop drives the fuel injection based on current operating status (state). The feedback control loop drives the fuel injection based on the oxygen sensor (A/F control) and is implemented with a FNHC (Fuzzy Neural Hybrid Controller).

Weige et al.'s tests performed on an engine using the FNHC based controller were near the lean limit of the engine. The injection system controller's response was observed during torque transients at constant throttle and with air throttle transients at constant torque. These transients were selected because they are the most common engine transients and have a fast and greatest influence on A/F ratio. The FNHC control loop maintained precise A/F ratio control during both steady-state and transient operation. In addition, controller parameters can be adjusted with a gradient decent learning curve to maintain this control quality over time. Their results demonstrate FNHC as a promising strategy for A/F ratio control.[119]

Pre-turbocharger temperature has been shown to be a reliable sensor for A/F ratio control.[137] It turns out that for a given fuel heating value, air manifold pressure and engine load, the pre-turbocharger temperature is repeatable. Due to these dependencies changes in heating value and constant load will induce changes in the A/F ratio and pre-turbocharger temperature. If, for

example, after some transient the air manifold pressure is adjusted to return the pre-turbocharger temperature to its original value, the A/F ratio will also closely return to the correct ratio enabling proper exhaust emissions. Thus, by adding the pre-turbocharger temperature to the control scheme, the controller will also be able to compensate for heating value changes.

A controller with a two-level cascaded system which can adjust A/F ratio by bypassing exhaust gas, via a wastegate, around the turbocharger was developed by Eckard et al. 1987. Field tests were performed on two Superior Cleanburn 8GTLA engines, one running on processed natural gas and the other running on well gas. Correct A/F ratio control was determined by comparing the gas manifold pressure and air manifold pressure to the known values on A/F curves for the engine. Within the range of fuel blends tested, the controller was able to maintain stable emissions as the fuel heating value increased.[137]

Advanced techniques for ER control for a heavy-duty on-highway natural gas engine are detailed in Podnar et al. 1996.[138] Their work used a John Deere 8.1L lean-burn spark ignited natural gas engine. A flexible prototyping control system was used in lieu of the original control system. Engine instrumentation was added to measure intake pressure, exhaust pressure, fuel pressures and temperatures, and air flow and fuel flow rates. Steady-state, step and ramp throttle transients were tested. The authors found it difficult to calibrate the volumetric efficiency map of the engine (or the mass flow air sensor) closely enough to allow accurate ER control over all engine operating conditions using the open-loop control strategy. Due to this experience a closed-loop compensator was added which used a variable time delay in order to compensate for time delays of the fuel moving through the engine systems relative to the time of measurement of the UEGO sensor. The flexible prototyping control system also used an adaptive algorithm which allows active compensation to be learned as a function of intake manifold pressure and engine speed providing, on-line compensation of the open-loop fueling calculations.

Traditionally, a common approach for calculating engine air flow is a speed density algorithm. The calculation is, based on engine speed and mixture density to determine the volumetric flow rate displaced by the engine. Air flow can also be measured with a commercially available sensor. The system developed by Podnar et al.[138] allowed determination of air flow using a real time model of the engine's intake system. Models typically provide a signal that is smoother and cleaner than sensor signals with no time response penalty or signal conditioning required, however their accuracy may degrade over time due to engine and component wear or during abnormal operation. Models do require significant computation ability and add complexity to the control system.[138]

Waukesha developed an engine control A/F module (AFM) design to control the A/F ratio for all Waukesha carbureted, gaseous fueled (methane base), industrial engines. The AFM uses an oxygen sensing system, intake manifold pressure transducer, electronic control module, actuator, and exhaust thermocouple. The system is claimed to permit correct operation of Waukesha engines in spite of changes in fuel pressure or temperature, engine load or speed, and fuel composition. The system makes significant use of the exhaust oxygen concentration in closed-loop control.[139]

4.5.2.2 Other Control Strategies

4.5.2.2.1 Thermal Efficiency Control

Franklin, et al.[140] investigated a novel method to control ER and spark advance for best efficiency (ERSABE). The study was conduction on a lean-burn, heavy-duty, industrial, natural gas, Hercules G1600 engine. The approach used small disturbances to spark timing and air flow to produce perturbations in engine efficiency. The control system can then adjust ER and timing in the direction of increasing efficiency. This approach could be an advantage for adjusting to changes in fuel composition, because the engine response itself is monitored while accounting for current ambient conditions, engine wear, or other factors that are not otherwise easy to account for in a fixed control system.

4.5.2.2.2 Peak Optical Intensity Control

If optical signals from the combustion chamber can be accessed using a fiber optical port, it may be possible to use the optical signal in a feedback control loop. Previous research has determined that the 50% mass fraction burned and peak pressure occur at a fixed cyclic location (fixed crank angle [CA]) on any engine operating at MBT regardless of engine speed, load or A/F ratio. Thus, by relating these parameters to peak optical intensity, an ignition timing control scheme could be developed which requires no additional sensors.[141] This could allow adjustment of timing to accommodate different composition fuels.

The optical probe signal can easily be filtered to known specific wavelength of combustion radicals. Two radicals, such as a unique fuel and a unique air radical, can be measured simultaneously so that their ratio can be used to calculate A/F ratio, etc. From the results, a control scheme can be implemented to control ignition timing to optimize the combustion process.

4.5.3 Sensor Techniques for Determining Natural Gas Properties

Depending on the actual change in fuel composition, some engine applications may be relatively unaffected by new fuel blends, while others may require substantial modification or addition of sensors and controls. If natural gas suppliers change their compositional specifications, the properties can be calculated and operational effects can be determined. Knock, for instance, can be calculated using various formulas involving MN, but this is an estimation. The ultimate determination of knock susceptibility may have to be determined from actual OEM engine testing. Some remedies may only require adjustment of an existing control or operating point. For example, an open-loop carbureted engine may only need adjustment to bring operation back in line with requirements. However, if there is too much variability of natural gas over time the carburetor may require constant adjustment. In this case, in may be more practical to install an A/F ratio controller using an EGO feedback sensor to keep the engine under control.

If the component concentrations of a natural gas are known, then all of the natural gas properties, as discussed in Section 4.4.1, can be directly calculated. However, the instruments required for complete and accurate compositional analysis, such as chromatographs and spectrometers can be

expensive, bulky, require maintenance, have long analysis times and other undesirable characteristics. Knowledge of gas composition or properties would allow feed forward engine control even with a high degree of fuel variability. The following section provides a few examples of novel sensors and techniques for future consideration in engine control scenarios. *For an in-depth analysis of natural gas composition sensors, the readers are directed to the Sensors section of this report.*

4.5.3.1 Thermal Conductivity

The MN of natural gas can be determined based on its thermal conductivity.[142] Puente et al.[142] developed a device that measures thermal conductivity using a small microelectronic sensor. The sensor is inexpensive and can be placed in situ with the gas. The sensor has a sensitivity of 0.95 mV/MN over the range of 60-100 MNs. Using this device, Puente et al. tested several compositions and measured their MN, observing that MN generally decreases with increasing higher HC. The n-type silicon design used in the sensor was somewhat slow to reach thermal equilibrium in field tests.

Rahmouni et al.[143] measured thermal conductivity at two temperatures and developed a method to determine MN and LHV of natural gas from those measurements. The gas is first considered as a ternary mixture of the most important components. Using a method known as principle component analysis, it was found that the two thermal conductivity measurements describe 97% of the variation of MN and almost 100% of LHV of a test matrix of 30 natural gases.[143]

Determination of multiple physical or chemical properties, typically using multiple sensors, of a natural gas provides greater accuracy in gas quality determination. There are a number of properties that could be measured including pressure, temperature, thermal conductivity, dielectric constant, viscosity and others. Other combustion-relevant fuel properties can be determined from a multiple measurement system including stoichiometric oxygen demand and density. One measurement approach uses changes in electrical quantities in a sensing element in contact with the fuel. These signals are used to determine properties such as thermal conductivity, specific heat, temperature and pressure. These quantities can be used with correlations to determine gas properties of interest.

4.5.3.2 Solid-State Thermal-Wave Pyroelectric-Film Sensor

A novel sensor based on a pyroelectric thin-film transducer under thermal excitation was developed by Garcia et al. to detect a wide range of natural gas and methane concentrations in N_2. The system maintains a linear response with increasing concentrations for both gasses with a 15 second response time. It uses a lock-in amplifier to achieve high signal to noise ratio. This ability to detect different concentrations of natural gas allows its use in gas quality and concentration monitoring for NGVs.[144]

4.5.3.3 Spectroscopy

Absorption spectroscopy involves transmission of electromagnetic radiation through an absorptive media (i.e., here a NG sample) and measuring the subsequent radiant absorption. The absorption lines or bands (spectra) represent unique signatures of the gaseous components in the

sample gas. In a waveband centered near 6.83 microns, many of the common paraffinic HCs found in natural gas, with the exception methane, exhibit radiant absorption in near linear proportion to their heating value. By scanning the absorption spectra, the heating value can be estimated by measuring methane at one wavelength, and the other higher HC at another wavelength.[145]

Fourier transform Infrared (FTIR) spectroscopy is one such spectroscopic technique. More details can be found in the sensors section of this report. It is cheaper, faster, and more portable than a GC. A study by Fodor, 1997,[146] used FTIR to determine methane, ethane, propane and butane in N_2 (each having distinct in the infrared region). The measured values were well correlated ($R^2 > 0.98$) to GC analysis values. Measurement accuracy to 1% mole concentration was deemed feasible. Once gas composition is determined, it is a simple task to calculate in real-time critical parameters such as heating value which can in turn be used in a feedback/feedforward control system.[146]

Kastner et al. 2002[147] developed an IR spectrometer for the measurement of natural gas quality needed for gas pipeline applications. The system uses an IR-filter photometer and a heat conductivity sensor. It is reported to have an overall measurement uncertainty of 0.2%. It is important to note that all major components of natural gas, besides N_2, are absorbed strongly in the IR. The higher HC have strong cross sensitivities, meaning that absorption bands and spectra tend to overlap so that their molar fraction can not easily be separately determined. However, the gas composition for the major components can be resolved using common deconvolution techniques. Algorithms were developed to measure volumetric calorific value, density, compression factor, compressibility factor, and molar fraction CO_2. A measured full scale accuracy of less than ± 0.2% and a repeatability of about 0.1% is reported.[147]

4.5.3.4 Acoustic

The speed of sound (SOS) can in theory be used to measure gas composition since the SOS in a gas changes with the molecular weight of the gas. This works since each component has a unique molecular weight. However, the SOS is in the end a function of gas density. Therefore, other state parameters such as temperature and pressure must also be known. Methane has a low molecular weight and a high SOS. Other common NG components such as ethane, propane, N_2, and CO_2 have a lower SOS. Lueptow et al.[133] built and tested a bench-top prototype SOS sensor. Tests were done on 12 natural gas mixtures at temperatures ranging from -30 °C to 65 °C. SOS measurements were well correlated with theoretical values. An attempt was made to correlate SOS to several compositional and combustion properties including the percentage methane composition, molecular weight, density, volume stoichiometric A/F ratio, volumetric higher heating value, Wobbe number and lower flammability limit. Only very rough correlations were obtained between SOS and fraction of methane, but fairly linear correlations between SOS and molecular weight, density, and lower flammability were determined. The stoichiometric mole A/F ratio, volumetric higher heating value and Wobbe number demonstrated a weaker correlation with SOS. The sensor was not capable of precision measurements of natural gas physical or combustion properties. However, it can be used as an indicator for gas composition changes.[133]

4.5.3.5 Dynamic Viscosity

A useful correlation between the Wobbe Number and the dynamic viscosity of fuel gases has been developed.[148] This correlation has been used to measure Wobbe Number.[148,149] The correlation was developed from testing of natural gases from different sources, mixtures of natural gases and higher HC (to C_4H_{10}), H_2, air, N_2, and CO_2 as well as LPG/air mixtures.

The uncertainty of the correlation function primarily results from the large compositional variety of fuel gases used in its determination. The uncertainty can be reduced substantially by limiting the range of gases to natural gas mixtures. The measurement technique uses a dynamic viscosity sensor (capillary tube) and a density sensor (orifice plate) so that if the pressure drop across one of the sensors is controlled, the pressure drop across the second sensor is a measure of the heating value. System accuracy was improved by including temperature and pressure measurements of the fuel gas in the calculation of the heating value. Measurements were generally within ± 1.5% of measurements from GC data of the same gases.

Table 4-7: Thermophysical Properties of Select Natural Gas Alkanes and Common Diluents.

	Cp kJ/kg °C (gas) @ 25 °C Heat Capacity	Mol. Wt	Heat of Combustion (kJ/kg)		Theoretical A/F (molar)	Max. Flame Speed (m/s)	Enthalpy of Formation kJ/kmol	Minimum Ignition Energy (Φ=1, 10^{-5} J)	Flammability Limits (Limits in air by fuel vol. concentration, %)		Quenching Distance (mm) (Φ=1)
			HHV	LHV					Fuel Lean	Fuel Rich	
Methane	2.21	16.043	55,528	50,016	9.52	0.34	-74,850	33	5	15	2.5
Ethane	1.75	30.069	51,901	47,489	16.66	0.4	-84,680	42	3	12.5	2.3
Propane	1.62	44.096	50,368	46,357	23.8	0.4	-103,850	30.5	2.2	11.2	2
Butane	1.64	58.123	49,546	45.742	30.94	0.37	-126,150		1.86	8.41	
Pentane	1.62	72.15	49,032	45,355	38.08	0.37	-146,440		1.4	7.8	
Hexane	1.62	86.177	48,696	45,105	45.22	0.4	-166,883		1.25	7	
Heptane	1.61	100.203	48,456	44,926	52.36	0.4	-187,326		1	6	
CO_2	0.84	44					-393,520				
N_2	1.04	28									
Reference	Borman and Ragland[154]	Perry ChE HB[153]	Turns, table B.1[152]	Turns, table B.1[152]	Zink[151]	Zink[151]	Zink[151]	Turns, table 8.4[152]	Lefebvre, GTC[150]	Lefebvre, GTC[150]	Turns, table 8.4[152]

[1] GRI-03/0159, "Gas Interchangeability Tests: Evaluating the Range of Interchangeability of Vaporized LNG and Natural Gas," Final Report, Gas Research Institute, April, 2003.

[2] King, S. R., "The Impact of Natural Gas Composition on Fuel Metering and Engine Operating Characteristics," SAE Paper No. 920593 (1992).

[3] Pehrson, N. C. "Using LNG to Meet the Challenge of Gas Composition," Petro-Safe 95: 6th Annual Conference and Exhibition for the Oil, Gas and Petrochemical Industries, January 31 – February 2, 1995.

[4] GRI-91/0054, "Effects of Gas Composition on Engine Performance and Emissions," Topical Report GETA 91-13, Gas Research Institute, Prepared by Southwest Research Institute, December, 1991.

[5] CARB Alternative Fuel Regulation, Article 3, "Specification for Alternative Motor Vehicle Fuels," December 10, 1998.

[6] National Fire Protection Association NFPA 52 "Vehicular Fuel Systems Code," 2006.

[7] http://www.intertanko.com/pubupload/curt.pdf.

[8] Gibbs, J. L., Bechtold, R. L., and Collison, C. E., "The Effects of LNG Weathering on Fuel Composition and Vehicle Management Techniques," SAE Paper No. 952607 (1995).

[9] Schiffgens, H.-J., Endres, H., Wackertapp, H., and Shrey, E., "Concepts for the Adaptation of SI Gas Engines to Changing Methane Number," Journal of Engineering for Gas Turbines and Power Vol. 116, October 1994.

[10] Ly, H., "Effects on Natural Gas Composition Variations on the Operation, Performance, and Exhaust Emissions of Natural Gas Powered Vehicles, "International Association for Natural Gas Vehicles Report, December 2002.

[11] Bidini, G., Grimaldi, C. N., and Mariani, F. "Experimental Analysis of the Actual Behavior of a Natural Gas Fueled Engine Caterpillar (CAT)-3516" Applied Thermal Engineering, 20 (2000) 455-470.

[12] Jones, K., Raine, R. R., and Zoellner, S., "A Study of the Effects of Natural Gas Composition on Engine Performance, Emissions and Efficiency."

[13] Independent Source, "White Paper on Natural Gas Interchangeability and Non-Combustion End Use," NGC+ Interchangeability Workgroup, February 28, 2005.

[14] Gruber, F., and Herdin, G. R., "The Use of H_2-Content Process Gas in Gas Engines," Paper No. 97-ICE-60 ASME 1997 Fall Technical Conference (1997).

[15] Branner, J. L., Dunnuck, D. L., Kamel, M. M., and Mahon, J. A., "The B5.9 Propane Gas Engine Development," Paper No. 99-ICE-175 1999 Spring Technical Conference, 1999.

[16] Callahan, T. J., "Survey of Gas Engine Performance and Future Trends," Proceedings of ICES03, 2003 Spring Technical Conference of the ASME Internal Combustion Engine Division, Salzburg, Austria, May 11-14, 2003.

[17] Khalil, E. B., and Karim, G. A., "A Kinetic Investigation of the Role of Changes in the Composition of Natural Gas in Engine Applications," ASME Journal of Engineering for Gas Turbines and Power, Vol. 124, April 2002.

[18] Chan, A. K., and Waters S. H., "Ignition System Designed to Extend the Plug Life and the Lean Limit in a Natural Gas Engine," Proceedings of ICEF03, 2003 Fall Technical Conference of the ASME Internal Combustion Engine Division, September 7-10, 2003.

[19] McMillian, M. H., Woodruff, S. D., Richardson, S., and McIntyre, D., "Laser Spark Ignition: Laser Development and Engine Testing," Proceedings of ASME ICE Division 2004 Fall Technical Conference Long Beach, CA, USA, October 24-27, 2004.

[20] U.S. Patent No. 4,867,127, "Arrangement for Regulating the Combustion Air Proportions."

[21] Herdin, G. R., Henkel, W., and Plohberger, D., "New High Efficiency High Speed Gas Engine in the 3 MW Class," Paper No. 98-ICE-147, ICE-Vol. 31-3, 1998 ASME Fall Technical Conference, 1998.

[22] Abd-Alla, F.H., "Using Exhaust Gas Recirculation in Internal Combustion Engines: A Review," Energy Conversion and Management 43 (2002) 1027-1042.

[23] Kim, S. S., Kim, C. G., Kim, C. U., Pang, H. S., Han, J. O., and Cho, Y. S., "A Study on Efficiency and Emission Enhancements on a Four-Stroke Natural Gas Lean Burn Engine," SAE Paper No. 960849 (1996).

[24] Raine, R. R., Zhang, G., and Pflug, A., "Comparison of Emissions from Natural Gas and Gasoline Fuelled Engines – Total Hydrocarbon and Methane Emissions and Exhaust Gas Recirculation Effects," SAE Paper 970743 (1997).

[25] Thiagarajan, S., Midkiff K. C., Bell, S. R., and Green, M. N., "Investigation of Fuel Composition Effects on a Natural Gas Fueled Spark-Ignited Engine," ICE-Vol. 24, Natural Gas and Alternative Fuels for Engines ASME 1994.

[26] GRI Topical Report, Light-Duty CNG Vehicle Fuel Composition Study," GTI Project Number 20245, April, 2006.

[27] Kamel, M., Lyford-Pike, E., Frailey, M., Bolin, M., Clark, N. N., Nine, R., and Wayne,S., "An Emission and Performance Comparison of the Natural Gas Cummins Westport C-Gas Plus Versus Diesel in Heavy-Duty Trucks," SAE Paper 2002-01-2737 (2002).

[28] Aslam, M. U., Masjuki, H. H., Kalam, M. A., Abdesselam, H., Mahalia, T. M. I., and Amalina, M. A., "An Experimental Investigation of CNG as an Alternative Fuel for a Retrofitted Gasoline Engine," Fuel 85 (2006) 717-724.

[29] Lee, Y-J., and Kim, G-C., "Effect of Gas Composition on NGV Performance," Seoul 2000 FISITA World Automotive Congress, June 12-15, 2000, Seoul, Korea.

[30] Elder, S. T., Jones, K., and Raine, R. R., "Effects of Varying Fuel Composition on the Performance of CNG and LPG Fuelled Vehicles," Professional Engineers of New Zealand Transcripts, Vol. 12, No.3/EMCh, November, 1985.

[31] Matthews, R. Chiu, J., and Hilden, D. "CNG Compositions in Texas and the Effects of Composition on Emissions, Fuel Economy, and Drivability of NGVs" SAE Paper 962097.

[32] Liss, W., Thrasher, W., Steinmetz, G., Chowdiah, P., and Attari, A., 1992, "Variability of Natural Gas Composition in Select Major Metropolitan Areas of the United States," Final Report to GRI, Report No. GRI-92/0123, March 1992.

[33] Merétei, T., van Ling, J. A. N., and Havenith, C., "Urban air quality improvement by using a CNG lean burn engine for city buses," Int. J. Vehicle Design, Vol 20, No. 1-4, 1998.

[34] Chiu, J., and Matthews, R. "The Texas Project: Part 2 – Control System Characteristics of Aftermarket CNG and LNG Conversions for Light-Duty Vehicles" SAE Paper 962099.

[35] Papagiannakis, R. G., and Hountalas, D. T., "Combustion and exhaust emission characteristics of a dual-fuel compression ignition engine operated with pilot Diesel fuel and natural gas," Energy Conversion and Management, 45 (2004) 2971-2987.

[36] GRI-94/0094, "Duel-Fuel Natural Gas/Diesel Engines: Technology, Performance and Emissions," Topical Report, Gas Research Institute, Prepared by Engine, Fuel and Emissions Engineering, Inc., November 1994.

[37] Srinivasan, K. K., Krishnan, S. R., Singh, S., Bell, S. R., Gong, W., Fiveland, S.B., and Willi, M. "The Advanced Injection Low Pilot Ignited Natural Gas Engine: A Combustion Analysis" Journal of Engineering for Gas Turbines and Power, January 2006, Vol. 128 213.

[38] Krishnan, S., Srinivasan, K., Singh, S., Bell, S., Midkiff, K., Gong W., Fiveland, S., and Willi, M. "Strategies for Reduced NO_x Emissions in Pilot-Ignited Natural Gas Engines" Journal of Engineering for Gas Turbines and Power, July 2004, Vol. 126, pp. 665-671.

[39] Zeng, K. Z., Huang, Z., Liu B., Liu, L., Jiang, D., Ren, Y., and Wang, J., "Combustion characteristics of a direct-injection natural gas engine under various fuel injection timings," Applied Thermal Engineering 26 (2006) 806-813.

[40] Kusaka, J., Okamoto, T., Daisho, Y., Kihara, R., and Saito, T., "Combustion and exhaust gas emission characteristics of a diesel engine duel-fueled with natural gas," JSAE Review 21 (2000) 489-496.

[41] Selim, Mohamed Y. E., "Sensitivity of Duel Fuel Engine Combustion and Knocking Limits to Gaseous Fuel Composition" Energy Conservation and Management 45 (2004) 411-425.

[42] Nwafor, O. M. I., "Effect of choice of pilot fuel on the performance of natural gas in diesel engines," Renewable Energy 21 (2000) 495-504.

[43] Roethlisberger, R. P., and Favrat, D., "Comparison between direct and indirect (prechamber) spark ignition in the case of a cogeneration natural gas engine, part I: engine geometrical parameters," Applied Thermal Engineering 22 (2002) 1217-1229.

[44] Olsen, D. B., Adair, J. L., and Willson, B. D., "Precombustion Chamber Design and Performance Studies for a Large Bore Natural Gas Engine," Proceedings of ICDS2005, ASME Internal Combustion Engine Division 2005 Spring Technical Conference, April 5-7 2005.

[45] Zheng, Q. P., Zhang, H. M., and Zhang, D. F., "A computational study of combustion in compression ignition natural gas engine with separated chamber," Fuel 84 (2005) 1515-1523.

[46] Flowers, D., Aceves, S., Westbrook, C. K., Smith, J. R., and Dibble, R., "Sensitivity of Natural Gas HCCI Combustion to Fuel and Operating Parameters Using Detailed Kinetic Modeling," Proceedings of the ASME Advanced Energy Systems Division, 1999, 465-473.

[47] Åberg, K. "An Experimental Study of Different Hydrocarbon Components in Natural Gas and Their Impact on Engine Performance in an HCCI Engine," Report ISRN LUTMDN/TMVK-5335—SE, Lund Institute of Technology (2000).

[48] Flowers, D., Aceves, S., Westbrook, C. K., Smith, J. R., and Dibble, R., "Detailed Chemical Kinetic Simulation of Natural Gas HCCI Combustion: Gas Composition Effects and Investigation of Control Strategies," Journal of Engineering for Gas Turbines and Power, April, 2001, Vol. 123, 433-439.

[49] Soylu,S., "Examination of combustion characteristics and phasing strategies of a natural gas HCCI engine," Energy Conversion and Management 46 (2005) 101-119.

[50] Hiltner, J., Agama, R., Mauss, F., Johansson, B., and Christensen, M. "Homogeneous Charge Compression Ignition Operation With Natural Gas: Fuel Composition Implications," Journal of Engineering for Gas Turbines and Power, July 2003, Vol. 125, pp. 837-844.

[51] Ohyama, Y., "Engine Control Using a Combustion Model," Seoul 2000 FISTIA World Automotive Congress, June 12-15, 2000, Seoul, Korea. Paper No. F20000A033.

[52] Mondt, J. R., "Cleaner Cars: The History and Technology of Emission Control Since the 1960's," Society of Automotive Engineers, 2000.

[53] Armor, J. N., "Catalytic Reduction of Nitrogen Oxides with Methane in the Presence of Oxygen: A Review," Catalysis Today 26 (1995), 147-158.

[54] Y. Murakami, K. Hayashi, K. Yasuda, T. Ito, T. Minami, and A. Miyamoto, Nippon Kagaku Kaishi (1977) 173.

[55] J. W. Ault, and R. J. Ayen, AIChE J., 17 (1977) 265.

[56] M. Iwamoto, H. Furukawa, Y. Mine, F. Uemura, S. Mikuriya, and S. Kagawa, J, Chem. Soc., Chem. Commun. (1986) 1272.

[57] G. Busca, L. Lietti, G. Ramis, and F. Berti, Appl. Catal. B 18 (1998) 1.

[58] V. I. Parvulescu, P. Grange, and B. Delmon, Catal. Today 46 (1998) 233.

[59] Pieterse, J. A. Z., Top, H., Vollink, F., Hoving, K., and van den Brink, R.W., "Selective catalytic reduction of NO_x in real exhaust gas of gas engines using unburned gas: Catalyst deactivation and advances toward long-term stability," Chemical Engineering Journal [**ARTICLE IN PRESS**].

[60] Jang, C., and Lee, J., "Experimental investigation of the effects of various factors on the emission characteristics of Low-emission natural gas vehicles," Proc. IMechE Vol. 219 Part D: Journal of Automobile Engineering (2005).

[61] White, J. J., "Low Emissions Catalyst for Natural Gas Engines," GRI-91/0214 (1991).

[62] Klimstra, J., "Catalytic Converters for Natural Gas Fueled Engines – A Measurement and Control Problem," SAE Paper 872165 (1987).

[63] Subramanian, S., Kudla, R. J., and Chattha, M. S., "Treatment of Natural Gas Vehicle Exhaust," SAE Paper 930223 (1993).

[64] Varde, K. S., Cherng, J. C., Bailey, C. J., and Majewski, W. A., "Emissions and Their Control in Natural Gas Fueled Engines," SAE Paper 922250 (1992).

[65] Varde, K. S., "Fueling System Control and Exhaust Emissions from Natural Gas Fueled Engines," Journal of Scientific and Industrial Research Vol. 62 January-February 2003, 13-19.

[66] EPA AP-42. "Compilation of Air Pollutant Emission Factors," http://www.EPA.gov/oms/ap42.htm.

[67] Kim, Y.-W., Sun, J., Kolmanovsky, I., and Koncsol, J., "A Phenomenological Control Oriented Lean NO_x Trap Model," SAE Paper No. 2003-01-1164 (2003).

[68] McCormick, R. L., Newlin, A. W., Mowery, D., Graboski, M. S., and Ohno, T. R., "Rapid Deactivation of Lean-Burn Natural Gas Engine Exhaust Oxidation Catalysts," SAE Paper 961976 (1996).

[69] Kristensen, P. G., "Formaldehyde Reduction by Catalyst, Full-Scale Testing on Gas Engines," Project Report PSO project 5230, February 2007.

[70] Strots, V. O., Bunimovich, G. A., Matros, Y. S., Zheng, M., and Mirosh, E. A., "Novel Catalytic Converter for Natural Gas Powered Diesel Engines," SAE Paper 980194 (1998).

[71] Creamer, K. S., and Saunders, J. H. "Evaluation of a Catalytic Converter for a 3.73 kW Natural Gas Engine" SAE Paper 930221.

[72] Wit, J., and Mofid, I., "Methane Oxidation Catalyst for Gas Engines," Danish Technology Center, February 2005.

[73] Westbrook, C. K., and Pitz, W. J., "High Pressure Autoignition of Natural Gas/Air Mixtures and the Problem of Engine Knock," Topical Report, GRI-87/0264, 1987.

[74] Turbiez, A., El Bakali, A., Pauwels, A. F., Rida, A., and Meunier, P., "Experimental Study of a Low Pressure Stoichiometric Premixed Methane, Methane/Ethane, Methane/Ethane/Propane and Synthetic Natural Gas Flames," Fuel 83 (2004) 933-941.

[75] Dagaut, P., Luche, J., and Cathonnet, M., Proceedings of the Combustion Institute 2000; 28:2459.

[76] Fraser, R. A., Siebers, D. L., and Edwards, C. F., "Autoignition of Methane and Natural Gas in a Simulated Diesel Environment," SAE Technical Paper 910227, 1991.

[77] Naber, J. D., Siebers D. L., Di Julio, S. S., and Westbrook, C. K., "Effects of Natural Gas Composition on Ignition Delay under Diesel Conditions," Twenty-Fifth Symposium (International) on Combustion, 31 July-5 August 1994.

[78] Huang, J., and Bushe, W. K., "Experimental and kinetic study of autoignition in methane/ethane/air and methane/propane/air mixtures under engine-relevant conditions," Combustion and Flame 144 (2006) 74-88.

[79] Fiveland, S. B., Agama, R., Christensen, M., Johansson, B., Hiltner, J., Mauss, F., and Assanis, D. N. "Experimental and Simulated Results Detailing the Sensitivity of Natural Gas HCCI Engines to Fuel Composition," SAE 2001-01-3609.

[80] Aesoy, V., and Valland, H. "The Influence of Natural Gas Composition on Ignition in a Direct Injection Gas Engine Using Hot Surface Assisted Compression Ignition" SAE Paper 961934 (1996).

[81] Das, A., and Watson, H. C., "Development of a natural gas spark ignition engine for optimum performance," Proc. IMechE Vol. 211 Part D (1997).

[82] Evans, R. L., and Blaszczyk, J., "Fast-Burn Combustion Chamber Design for Natural Gas Engines," Transactions of the ASME, Vol. 120, January 1998.

[83] Witze, P. O., Martin, J. K., and Borgnakke, C., "Measurements and Predictions of the Precombustion Fluid Motion and Combustion Rates in a Spark Ignition Engine," Trans. SAE, 1983, 93, 786.

[84] Evans, R. L., "Lean-Burn Natural Gas Engines for High Efficiency and Low Emissions," Paper No. 99-ICE-177 ASME 1999 Spring Technical Conference (1999).

[85] Stone, C. R., and Ladommatos, N., "Design and evaluation of a fast-burn spark-ignition combustion system for gaseous fuels at high compression ratios," Journal of the Institute of Energy, December 1991, pp 202-211.

[86] Heywood, J. B., "Internal Combustion Engines Fundamentals," McGraw-Hill Publishers, 1988.

[87] Smith, Jack A., Bartley, and Gordon J. J. "Using Syngas in a Heavy-Duty, Lean-Burn Natural Gas Engine as a Means of NO_x Reduction" ASME 97-ICE-64, ICE Vol. 29-3. 1997 Fall Technical Conference.

[88] Kaiser, E. W., Siegl, W. O., Henig, Y. I., Anderson, R. W., and Trinker, F.H., "Effect of Fuel Structure on Emissions from a Spark-Ignited Engine," Environ. Sci. Technol., Vol. 25, No. 12, 1991.

[89] Poulsen, J. H., and Wallace, J. S., "Operating Parameter Effects on the Speciated Hydrocarbon Emissions from a Natural Gas Fueled Engine," SAE Paper No. 942007 (1994).

[90] Alzueta, M. U., and Glarborg, P., "Formation and Destruction of CH_2O in the Exhaust System of a Gas Engine," Environmental Science and Technology, Vol. 37, No 19, 2003.

[91] Lowi, A., and Carter W. P. L., "A Method for Evaluating the Atmospheric Ozone Impact of Actual Vehicle Emissions," SAE Paper No. 900710 (1990).

[92] Wagner, T., and Wyszyński, M. L., "Aldehydes and ketones in engine exhaust emissions – a review," Proc. Instn Mech Engrs, Vol 210, 1996.

[93] Mitchell, C. E., and Olsen, D. B., "Formaldehyde Formation in Large Bore Natural Gas Engines Part 1: formation Mechanisms," Journal of gas Turbines and Power, Vol. 122, October 2000.

[94] Olsen, D. B., and Willson, B. D., "The Effect of Parametric Variations on Formaldehyde Emissions from a Large Bore Natural Gas Engine," Paper No. 2002-ICE-446, ICE-Vol. 38, 2002 ICE Spring Technical Conference, ASME, 2002.

[95] Gambino, M., Cericola, R., Corbo, P. and Innaccone, S., "Carbonyl Compounds and PAH Emissions fro CNG Heavy-Duty Engine," Journal of Gas Turbines and Power, Vol. 115, October, 1993.

[96] Kado, N. Y., Okamoto, R. A., Kuzmicky, P. A., Kobayashi, R., Ayala, A., Gebel, M. E., Rieger, P. L., Maddox, C., and Zafonte, L., "Emissions of Toxic Pollutants from Compressed Natural Gas and Low Sulfur Diesel-Fueled Heavy-Duty Transit Buses Tested over Multiple Driving Cycles," Environmental Science and Technology 2005, 39, 7638 – 7649.

[97] Kweon, C. B., Okada, S., Stetter, J. C., Christianson, C. G., Shafer, M. M., Schauer, J. J., and Foster, D. E., "Effect of Fuel Composition on Combustion and Detailed Chemical/Physical Characteristics of Diesel Exhaust," SAE Paper No. 2003-01-1899 (2003).

[98] Baldassarri, L. T., Battistelli, C. L., Conti, L., Crebelli, R., De Berardis, B., Iamiceli, A. L., Gambino, M., and Iannaccone, S., "Evaluation of Emission Toxicity of Urban Bus Engine: Compressed Natural Gas and Comparison with Liquid Fuels," Science of the Total Environment, 355 (2006) 64-77.

[99] Min, B. H., Bang, K. H., Kim, H. Y., Chung, J. T., and Park, S., "Effects of Gas Composition on the Performance and Hydrocarbon Emissions for CNG Engines," SAE Paper No. 981918 (1998).

[100] Min, B. H., Chung, J. T., Kim, H. J., and Park, S., "Effects of Gas Composition on the Performance and Emissions of Compressed Natural Gas Engines," KSME International Journal, Vol. 16, No. 2, 219-226 (2002).

[101] Nine, R. D., Clark, N. N., Mace, B. E., and ElGazzar, L., "Hydrocarbon Speciation of a Lean Burn Spark Ignited Engine," SAE Paper No. 972971 (1997).

[102] Clark, N. N., Mott, G. E., Atkinson, C. M., deJong, R. J., Atkinson, R. J., Latvakosky, R., and Traver, M. L., " Effect of Fuel Composition on the Operation of a Lean-Burn Natural Gas Engine," SAE Paper No. 952560, 1995.

[103] Homen, B. A., and Qu, Y., "Uncertainty in Particle Number Modal Analysis during Transient Operation of Compressed Natural Gas, Diesel, and Trap Equipped Diesel Transit Buses," Environ Sci. Technol. 2004, 38, 2413-2423.

[104] Ristovski, Z. D., Morawska, L., Hitchins, J., Thomas, S., Grenaway, C., and Glbert, D., Particle Emissions from Compressed Natural Gas Engines," J. Aerosol Sci. Vol. 31, Nol 4, 403-413 (2000).

[105] Callahan, T. J., Ryan, T. W., Buckingham, J. P., Kakockzi, R. J., and Sorge, G., "Engine Knock Rating of Natural Gases – Expanding the Methane Number Database," ICE-Vol. 27-4 Proceedings from the 18th Annual Fall Technical Conference of the ASME Internal Combustion Engine Division, 1996.

[106] Soylu, S., and Van Gerpen, J., "Fuel Effects on the Knocking Limit of a Heavy-Duty Natural Gas Engine," SAE Paper No. 981401 (1998).

[107] Thomas, J. R., and LaPointe, L. A., "Potential for Part Lad Fuel Economy Improvement of Spark-Ignited Natural Gas Engines," Paper No. 97-ICE-61 ASME 1997 Fall Technical Conference (1997).

[108] Akansu, S. O., Dulger, Z., Kahraman, N., and Veziroglu, T. N. "Internal Combustion Engines Fueled by Natural Gas-Hydrogen Mixtures" International Journal of Hydrogen Energy 29 (2004) 1527–1539.

[109] Zhang, F., Okamoto, K., Morimoto, S., and Shoji, F., " Improving Performance and Reliability of Natural Gas Engines for Power Generation – A Concept of Realizing Lower Temperature and Higher Pressure Combustion," SAE Paper No. 1990-01-3511, 1999.

[110] Brecq, G., Ramesh, A., Tazerout, M., and Le Corre, O., "An Experimental Study of Knock in a Natural Gas Fueled Spark Ignition Engine," SAE Paper No. 2001-01-3562 (2001).

[111] Takagaki, S. S., and Rane, R. R., "The Effects of Compression Ratio on Nitric Oxide and Hydrocarbon Emissions from a Spark-Ignition Natural Gas Fueled Engine," SAE Paper Number 970506 (1997).

[112] Thomas, J. R., Clarke, D. P. Collins, J. M., Sakonji, T., Ikeda, K., Shoji, F., and Furushima, K., "A Test Program to Evaluate the Influences of Natural Gas Composition on SI Engine Combustion and Knock Intensity," ICE-Vol. 22, Heavy-Duty Engines a Look at the Future, ASME, 1994.

[113] Yacoub Y., and Atkinson C., "An Air Cycle Analysis of Alternatives to Throttling in the Otto Cycle Engine," Paper No. 99-ICE-164 ASME 1999 Spring Technical Conference (1999).

[114] Charlton, S. J., Tawfig, M. E., and Shooshtarian, A., "The Response of an Open-Chamber Natural Gas Engine to Gas Composition," Institution of Mechanical Engineers Conference Seminar on Gas Engines for Cogeneration, June 17, 1993.

[115] Yossefi, D., Belmont, M. R., Ashcroft, S. J., and Maskell, S. J., "A comparison of the relative effects of fuel composition and ignition energy on the early stages of combustion in a natural gas spark ignition engine using simulation," Proc. Instn. Mech..Engrs., Vol 214, Part D (2000) 383-393.

[116] Naber, J. D., Siebers, D. L., Caton, J. A., Westbrook, C. K., and Di Julio, S. S., "Natural Gas Autoignition Under Diesel Conditions: Experiments and Chemical Kinetic Modeling," SAE Technical Paper 942034, 1994.

[117] Pitz, W. J., Westbrook, C. K., and Leppard, W. R. "Autoignition Chemistry of C_4 Olefins Under Motored Engine Conditions: a Comparison of Experimental and Modeling Results" 1991 SAE Paper 912315.

[118] Cottrill, J., "Evaluation of Automotive Oxygen Sensors for Steady-State Air/Fuel Ratio Control and Its OBD Characteristics on Natural Gas Engines," ASME Paper No. 99-ICE-173, 1999.

[119] Weige, Z., Jiuchun, J., Yuan, X., and Xide, Z., "CNG Engine Air-Fuel Ratio Control using Fuzzy Neural Networks," Proceedings of the 2nd Annual International Workshop on Autonomous Decentralized Systems, 2002.156-161.

[120] Marsee, F. J., and Olree, R. M., "Distribution Factors that Influence Emissions and Operation of Lean Burn Engines," International Journal of Mechanical Engineering (1979) 129-136.

[121] D 3588-98 (2003) Standard Practice for Calculating Heat Value, Compressibility Factor, and Relative Density of Gaseous Fuels.

[122] "GRI-85/0248, "Low Cost Gas Btu Meter Using Physical Property Measurements, 1985."

[123] Zareh, A, "Gas Engines," Lubrication Vol. 81, No. 4 (1995).

[124] GRI-92/0150, "Effects of Gas Composition on Octane Number of Natural Gas Fuels," Topical Report GETA 92-01, Gas Research Institute, Prepared by Southwest Research Institute, May, 1992.

[125] Ryan, T. W., Callahan, T. J., and King S. R., "Engine Knock Rating of Natural Gases - Methane Number," Journal of Engineering for Gas Turbines and Power, October 1993, Vol. 115, 769-776.

[126] Kubesh, J. T., King, S. R., and Liss, W. E., "Effect of Gas Composition on Octane Number of Natural Gas Fuels," SAE Paper No. 922359 (1992).

[127] GRI-92/0150, "Effects of Gas Composition on Octane Number of Natural Gas Fuels," Topical Report GETA 92-01, Gas Research Institute, Prepared by Southwest Research Institute, May, 1992.

[128] Ryan, T. W., Callahan, T. J., and King S. R., "Engine Knock Rating of Natural Gases - Methane Number," Journal of Engineering for Gas Turbines and Power, October 1993, Vol. 115, 769-776.

[129] Kubesh, J. T., King, S. R., and Liss, W. E., "Effect of Gas Composition on Octane Number of Natural Gas Fuels," SAE Paper No. 922359 (1992).

[130] Independent Source, "Paper Study on the Effect of Varying Fuel Composition on Cummins Gas Engines," http://www.socalgas.com/business/gasquality/docs/library/Legacy_Cummins.pdf, May 4, 2005.

[131] Klimstra, J., Hernaez, A. B., Bouwman, W. H., Gerard, A., Karll, B., Quinto, Y., Graham R. R., and Schollmeyer, H., "Classification Methods for the Knock Resistance of Gaseous Fuels – An Attempt Towards Unification," ASME Paper No. 99-ICE-214, 1999.

[132] Independent Source, "Paper Study on the effect of Varying Fuel Composition on Fuel Supplied to Detroit Diesel Gas Engines," http://www.socalgas.com/business/gasquality/docs/library/Legacy_Cummins.pdf, May 4, 2005.

[133] Lueptow, R. M., and Phillips, S., "Acoustic Sensor for Determining Combustion Properties of Natural Gas," Meas. Sci. Technol. 5 (1994) 1375-1381.

[134] Blazek, C. F., Grimes, J., Freeman, P., Bailey, B. K., and Colucci, C., "Fuel Composition Effects on Natural Gas Vehicle Emissions," 207th ACS National Meeting of the Division of Fuel Chemistry, March 13-17, 1994.

[135] Clark, N. N., Gautam, M., Wang, W., Boyce, J. A., Lyons, D. W., "Emission Performance of Natural Gas and Diesel Fueled School Buses With Cummins 8.3 Liter Engines," Paper No. 99-ICE-176, ASME Spring Technical Conference, 1999.

[136] Liss, W. E., "Light-Duty CNG Vehicle Fuel Composition Study," Topical Report, GTI Project No. 20245, April 2006.

[137] Eckard, D. W., and Serve, J. V., "Maintaining Low Exhaust Emissions With Turbocharged Gas Engines Using a Feedback Air-Fuel Ratio Control System," Journal of Engineering for Gas Turbines and Power 109 (1987) 487-490.
[138] Podnar, D. J., Kubesh, J. T., and Colucci, C. P., "Development and Application of Advanced Control Techniques to Heavy-Duty Natural Gas Engines," SAE Technical Paper Series Paper No. 961984, October 1996.
[139] Moss, D. W., "Design and Development of the Waukesha Custom Engine Control Air/Fuel Module," ICE-Vol. 27-4, 1996 Fall Technical Conference, Volume 4, ASME 1996.
[140] Franklin, M. L., Kittelson, D. B., and Leuer, R. H., "The Application of a Thermal Efficiency Maximizing Control Strategy for Ignition Timing and Equivalence Ratio on a Natural Gas-Fueled Hercules G1600," Transactions of the ASME 118 (1996) 872-879.
[141] Nwagboso, C. O., Pendlebury, M. A., and Mukarram, S. K., "Design of Combustion Sensory Based Controller for Natural Gas Engines," Meas. Sci. Technol. 15 (2004) 303-317.
[142] Puente, D., Gracia, F. J., and Ayerdi, I., "Thermal Conductivity Microsensor for Determining the Methane Number of Natural Gas," Sensors and Actuators B 110 (2005) 181-189.
[143] Rahmouni, C., Le Corre, O., and Tazerout, M., "Online determination of natural gas properties," C. R. Mecanique 331 (2003) 545-550.
[144] Garcia, J. A., Dorojkine, L. M., Mandelis, A., and Wallace, J. S., "Thermophysical Response of a Solid-State Thermal-Wave Pyroelectric-Film Sensor to Natural Gas and Methane," Int. J. Hydrogen Energy 21 (1996) 761-764.
[145] Dewey, C. F., Jr., "Measuring the Heating Value of a Fuel in the Gaseous State: Method and Apparatus," United States patent 3,950,101, April 1976.
[146] Fodor, G. E., "Analysis of Natural Gas by FTIR; Calibrations and Validations," Interim Report TFLRF No. 324, AD A324665, May 1997.
[147] Kastner, J. F., and Schley, P., "Novel Optical Techniques for Process Analysis of Natural Gas Quality," VDI-Berichte NR. 1667 (2002) 105-110.
[148] HeB, R., and Altermark, D., "Flameless System for the Measurement of the Gross Calorific Value and the Wobbe Number of a Fuel," 1986 International Gas Research Conference, Toronto, Canada, September 1986.
[149] Bonne, U., "On-Line Combustionless Measurement of Gaseous Fuels Fed to Gas Consumption Devices," United States Patent 5,311,447, May 1994.
[150] LeFebvre, A. H., "Gas Turbine Combustion," 1983.
[151] The John Zink Combustion Handbook, Charles E. Baukal, Editor, CRC Press, 2001.
[152] Turns, S. R., "An Introduction to Combustion," McGraw-Hill, 1996.
[153] Perry's Chemical Engineers' Handbook, McGraw-Hill, 1984.
[154] Bormon, G. L., and Ragland, K. W, "Combustion Engineering," McGraw-Hill, 1998.

5 GAS TURBINES

5.1 Gas Turbine Background

Modern, low-emission gas turbines are precisely tuned to maintain cool flame conditions that avoid the formation of NO_x pollutants. This precision comes with a cost. For example, these flames are susceptible to flashback, blow-off, and dynamic instabilities. The dynamic instabilities can be a serious problem, leading to pressure driven vibrations that can damage engines in a short time, or require adjustments that compromise the emissions performance of the engine. It is not widely appreciated how sensitive some turbine combustors are to changing operating conditions. In some engines, ambient temperature changes can lead to damaging oscillations[1] unless the control system can take over and re-tune the engine. Retuning means changing the flow splits among the various fuel stages, and in some cases, adjusting the compressor inlet guide vanes, or bleeding air from the compressor to control primary zone temperature. The combination of these tuning adjustments is used to meet the competing demands of stable operation, and emissions performance. In some cases, these tuning adjustments are performed by engine operators in a trial and error manner until acceptable engine performance is achieved. To date, there is not a comprehensive theory of how combustion dynamics respond to changes in ambient conditions, and to a lesser degree an understanding of how engine dynamics are linked to fuel type. This explains why there has been controversy over the standards for new natural gas supplies in engines that have already been tuned to operate on a particular gas composition.

It should not be suggested that engines cannot be adjusted or tailored to operate with widely different fuel composition. Kurz[2] notes that some engines may allow as much as a 10% variation in fuel heating value, while others can accommodate less than 2-3%. Although engines may be adjusted/designed for different fuels, a key question is whether engines that have been designed to meet emissions standards on domestic natural gas can accommodate sudden changes in fuel composition, without causing machine upsets, excess emissions, or component damage. Before considering this question, a review of what is known about fuel effects in turbine combustion is provided.

5.1.1 Gaseous Fuel Flow Control Systems

The authors have chosen to add this section on gaseous fuel control because it is important to understand that gaseous fuel control may be a factor in how the engine responds to changing fuel type. In actual gas turbine conditions, the fuel flow can be controlled to maintain a constant turbine inlet temperature or power setting. Therefore, if the fuel composition change is slow enough such that the control system can adjust, the system should react to maintain a fairly constant overall flame temperature. However, the actual response may depend on the fuel metering approach. This issue is complicated by the many different types of staged fueling schemes that exist on real engines, so it is difficult to make a general statement, but the following information is provided as background.

In the past, volumetric flow devices (i.e., orifice plates, venturi meters, etc.) have been widely used throughout many industries to monitor process flows. These devices operate by measuring a pressure drop across an internal flow restriction, and require information about the properties of the flowing media to convert the measured pressure drop to units of flowrate. These volumetric flow devices may be used in a feedback controlled flow loops to maintain the same fuel flow rate in the presence of variations in fuel delivery pressure or other process variations. Although these volumetric devices have a considerable knowledge-base throughout many industries, other technologies are becoming increasingly competitive with volumetric flow devices. Therefore, let's consider whether a fuel flow measurement approach, other than a volumetric device would be more, or less, sensitive to changes in fuel composition.

Let's consider two fuel compositions. First, a methane fuel has a carbon number of 1.0 and a hydrogen-to-carbon ratio of 4.0. Methane also has a Wobbe Index of 1360 BTU/scf (50.6 MJ/m^3) and an air-fuel stoichiometric ratio of 9.52 (molar basis) and 17.2 (mass basis). Note that a molecular weight of 16.0 has been assumed for the methane fuel.

For comparison, let's consider a second fuel (actually used experimentally in this report, see Section 5.11.3) that has an average molecular weight of 19.3 and a Wobbe Index of 1424 BTU/scf (53.0 MJ/m^3). This second fuel has an averaged carbon number of 1.2 and a hydrogen-to-carbon ratio of 3.65. The air-fuel stoichiometric ratio for this second fuel is 10.94 (molar basis) and 16.4 (mass basis).

The stoichiometric air-fuel ratio on a molar (volume) basis increases by 13-14 percent when the fuel changes from methane to the second fuel. Assuming that the fuel flow control device can respond fast enough to provide the same volume of flow for each fuel, the second fuel gas will still be operating at a much hotter condition (i.e., for a constant air flow, the fuel-air equivalence ratio and flame temperature are directly related to the stoichiometric air-fuel ratio). While this is an extreme example (methane to NG), it demonstrates that volumetric metering schemes may need to be changed to adjust flow splits, for example, if the fuel composition changes.

In contrast, the stoichiometric air-fuel ratio on a mass basis decreases by about 4.5 percent when the fuel changes from methane to the second fuel. On a mass basis, if a fuel flow device is able to maintain a constant mass flow, the second fuel type will be operating at a slightly cooler condition. It should be noted that mass flow devices such as Coriolis meters can measure mass flow independent of the properties of the flowing media. However, volumetric devices require some knowledge of the fluid properties to maintain accurate flow measurements. Generally speaking, if a volumetric flow control device does not have on-line corrections for the density, density changes could result in proportional changes in the actual flow rate.

In summary, this description of turbine combustion control systems is not intended to be comprehensive, but emphasize that the type of control system is important in understanding the engine response to changing fuel composition.

5.1.2 Turbine Combustion

A turbine combustor flame is much different than an appliance flame. Early designs used so-called "diffusion" flames that mixed the fuel and air into a primary combustion zone, while combustion was sustained by back-mixing hot products of combustion. Figure 5-1 (a) shows a schematic of a diffusion flame combustor. Fuel is injected at one point, and air is injected both at the front and sides of the combustor. The combustion reactions are so fast that the reaction rate is controlled by the rate of mixing between fuel and air, hence the name "diffusion" flame. In a classic diffusion flame, reactions proceed at nearly stoichiometric conditions, producing very high local temperatures. While this produces very stable combustion, and can be very efficient, it also has a major drawback: NO_x production is high.

Because of regulations on NO_x emissions, engines built over the last decade have increasingly used "premix" combustion approaches in which the fuel and air are mixed upstream of the combustor. The flame is established in the combustor where the velocity slows to the local flame speed. Figure 5-1 (b) shows a schematic of a premix combustor. In essence, the flame is stabilized in the combustor because of the lower velocity and back-mixing of hot products of combustion. Based on discussions with the Edison Electric Institute, a survey of gas turbine operators and equipment manufactures indicates that more than 85% of the gas fired capacity built since 1995 (> 200,000 MW) has some version of a lean-premixed combustion system.[3] In the following paragraphs, the issues surrounding fuel interchangeability for both diffusion and premixed combustors are described.

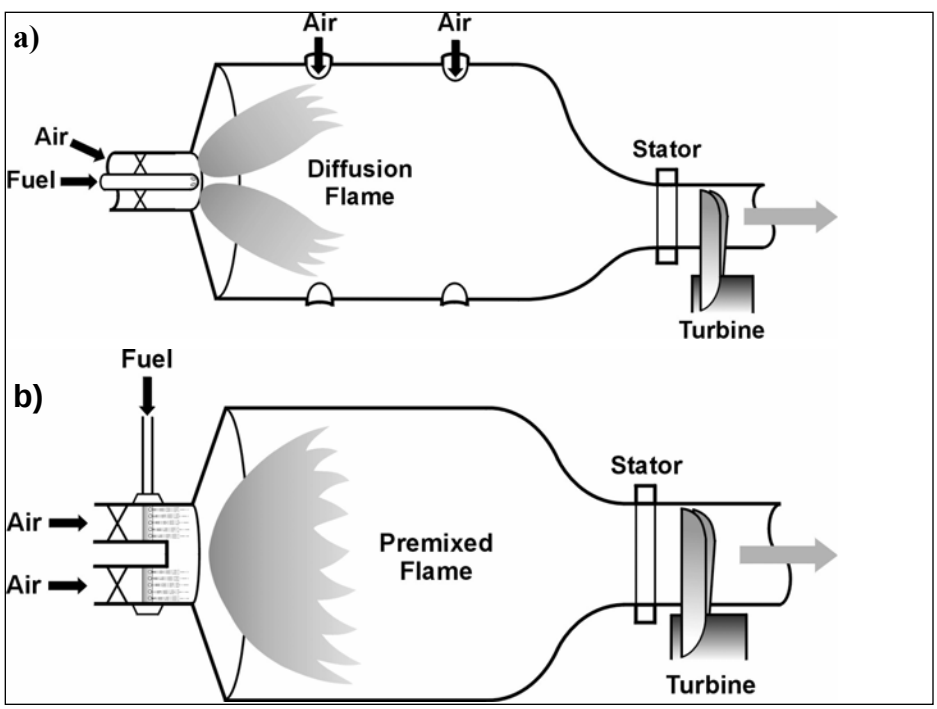

Figure 5-1: a) Diffusion Flame Combustor b) and Premix Combustor.

5.2 Fuel Effects on Diffusion Flame Combustors

Most of the subject matter that is discussed in this report addresses premixed combustors, because fuel composition is a greater consideration in premixed combustors. However, many legacy turbine installations use diffusion flame combustors, and an important question is how fuel composition will affect these earlier machines. There is not a common way to answer this question for all machines, since it depends on the actual combustor configuration, but in general terms, it is expected that NO_x emissions will rise slightly with greater concentration of higher hydrocarbons. This occurs because diffusion flame reactions occur near stoichiometric conditions, with associated flame temperatures being greater for higher hydrocarbons. The effect of temperature on NO_x is documented in emissions correlations presented by commercial engine manufacturers.[4,5,6] The NO_x correlation is expressed as a ratio between the NO_x on a given fuel, and the NO_x produced on methane (CH_4):[4]

$$\frac{NO_x}{NO_{x_{CH_4}}} = 1 + 10 \cdot \ln\left(\frac{T}{T_{CH_4}}\right) \tag{5-1}$$

On the right side, T is the adiabatic flame temperature of the fuel of interest, compared to methane (T_{CH4}), and 'ln' is the natural logarithm. The change in NO_x can be conveniently express as:

$$\Delta NO_x(\%) = \left(\frac{NO_x}{NO_{x_{CH_4}}} - 1\right) * 100\% \tag{5-2}$$

Using this definition, a change of 1% on a baseline of 100ppmv would be a NO_x value of 101ppmv. To use Equations 5-1 and 5-2, it is only necessary to know the value of the flame temperature on a given fuel compared to methane. Table 5-1 compares various fuels labeled A thru K, and calculated values of Wobbe Index #,* stoichiometric flame temperature, and ΔNO_x from Equation 5-2, above. Flame temperatures are calculated from standard equilibrium codes,[7] assuming initial conditions of 300 K for the reactants at one atmosphere.

* The Wobbe number is the ratio of fuel higher heating value to the square root of fuel higher heating value and is a widely used parameter to characterize natural gas.

Table 5-1: Calculated Wobbe (HHV BTU/scf), Flame Temperature, and NO_x for Pure Fuels A (Methane) and K (Propane), and Representative Blends B-J.

Fuel:	A	B	C	D	E	F	G	H	I	J	K
CH4 (%)	100	96.2	87.1	86	90	85	87.1	92.2	88.8	86.0	0
C2H6	0	3.4	10.7	9	5	15	10.7	6.5	7.4	8.7	0
C3H8	0	0.3	1.3	5	5	0	2.1	0.9	2.6	3.5	100
C4H10	0	0.08	0.3	0	0	0	0.0	0.4	1.2	1.8	0
CO2	0	0	0	0	0	0	0	0	0	0	0
N2	0	0.01	0.5	0	0	0	0	0	0.03	0.02	0
Wobbe#	1360	1377	1409	1435	1419	1420	1420	1398	1424	1443	2023
Stoich Temp (K)	2226	2229	2233	2236	2234	2235	2234	2231	2234	2234	2267
Delta NOx(%)	0%	1.6%	3.4%	4.7%	3.8%	4.2%	3.8%	2.5%	3.8%	3.8%	18.3%

Note there is a relatively modest change in temperature among the different fuels, with the most extreme case being +40 K when pure propane is exchanged for pure methane. In this extreme situation, the NO_x is predicted to increase by 18%. For the other fuels, the NO_x increase is much smaller. Thus, based on this correlation, the effect of fuel interchangeability is relatively modest. It should be emphasized that Equation 5-1 has been documented for one family of commercial engines, and the correlation does not represent the stack emissions on engines outfitted with NO_x control measures like SCR or water injection. In those cases, the slight increase in NO_x could be compensated for with adjustments to the SCR, or added water injection. In some cases, adjustments may not be possible. For example, an engine operating right at the NO_x permit level, using water injection may not be able to accommodate added water without compromising CO emissions. These situations would need to be considered on a case-by-case basis. It is not clear how many engines operate this close to permit levels.

5.3 Fuel Effects on Premix Combustors

As already stated, premix combustors are the preferred design for modern gas turbines, and have been widely installed since the early 1990's. The premixed combustor design must meet several criteria. The flame must not flashback into the premixer and the fuel and air mixture must avoid "autoignition", a condition in which combustion occurs spontaneously upstream of the main flame zone. To keep NO_x emissions very low, the entire combustor must operate at relatively cool temperatures, or near the lean extinction limit. However, the CO must be completely oxidized in the combustor, therefore excessively cool regions must be avoided. These competing requirements are only compounded by the additional requirement for dynamic stability – the flame must not oscillate. For many reasons, premix combustor flames are susceptible to oscillations that can destroy engine hardware, can trigger flashback, and compromise emissions. Avoiding dynamics has become an important consideration in engine design and operation.[8] A brief review of what is known about these various topics is presented next.

5.3.1 Fuel Effects on Flashback

Flashback occurs when a flame propagates backward into the premixer through a shear layer, a boundary layer, or the central recirculation formed in the combustor (i.e., the vortex core). The

flame may anchor behind a fuel injector or swirl vane, leading to thermal failure. Flashback is possible when the flame speed of the fuel air mixture exceeds the local gas velocity in the premixer, allowing flame propagation against the premixer flow. Early attempts to build and operate premix combustors were sometimes confounded by flashback due to marginal aerodynamic design, producing slower velocities than required in the premixer. This can be addressed, and in many instances has been solved. Premixer bulk air velocities are typically designed to be more than 40m/s to provide a wide margin and prevent flame flashback problems.

Will flashback be aggravated by changing fuel composition? Flashback depends partially on the flame speed of the fuel air mixture. Figure 5-2 is a plot of the laminar flame speed of several different NG blends studied in Europe.[9]

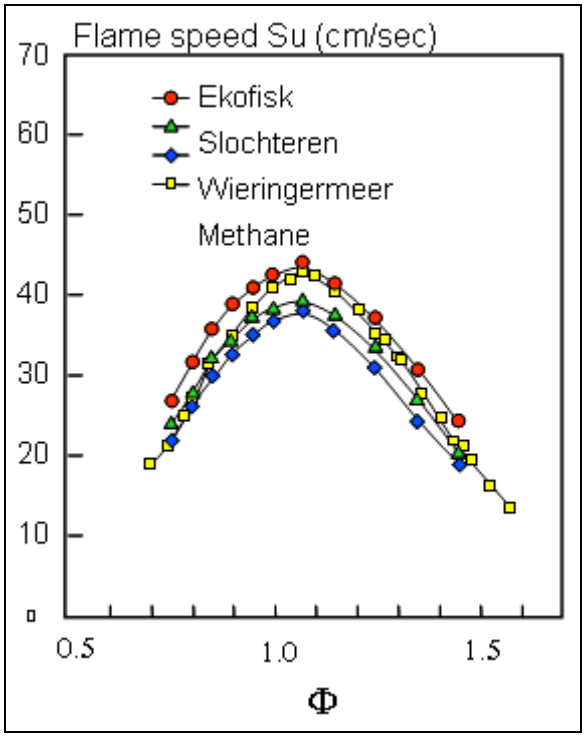

Figure 5-2: Laminar Flame Speeds of Several Natural Gas Blends and Methane.[9]
The x-axis is the Equivalence Ratio (Normalized Fuel/Air Ratio).
Premix Gas Turbines Operate at Lean Conditions, with Equivalence Ratios Φ < 0.8.

As can be seen, there is a modest change in the flame speed for the different hydrocarbons, with less than 25% change at the lean conditions. This would appear to indicate a level of "margin" for setting the necessary premixer velocity to avoid flashback, but there are several other issues to consider regarding flashback. First, it has recently been shown that the *turbulent* flame speed of different hydrocarbons is uniquely enhanced by combined features of the turbulent flow, and the transport properties of the hydrocarbon itself. This is important because practical premixers are characterized by turbulent flow, meaning that the turbulent flame speed must be considered in premixer design. The usual assumption is that the turbulent flame speed is directly related to the laminar flame speed. Figure 5-3 shows the measured turbulent flame speed of methane mixed with progressively greater quantities of propane, reported by Kido and co-workers.[10] The fuel/oxygen/nitrogen composition was established so that the *laminar* flame speed of all the

mixtures was the same at a common equivalence ratio $\Phi = 0.8$. The graph shows that turbulent acceleration of flame speed is greatest for pure methane, and decreases with higher levels of propane addition. Thus, the turbulent flame speed responds differently for different fuels, in contrast to the usual assumption that the turbulent flame speed is simply proportional to the laminar flame speed. The proposed explanation is that the preferential diffusion of methane relative to propane causes locally higher equivalence ratio (and increased burning rates) on the distorted turbulent flame surface. Perhaps unexpectedly, the added propane actually inhibits the turbulent flame speed compared to the pure methane flame, and this would help prevent a flame from moving into the premixed flow.

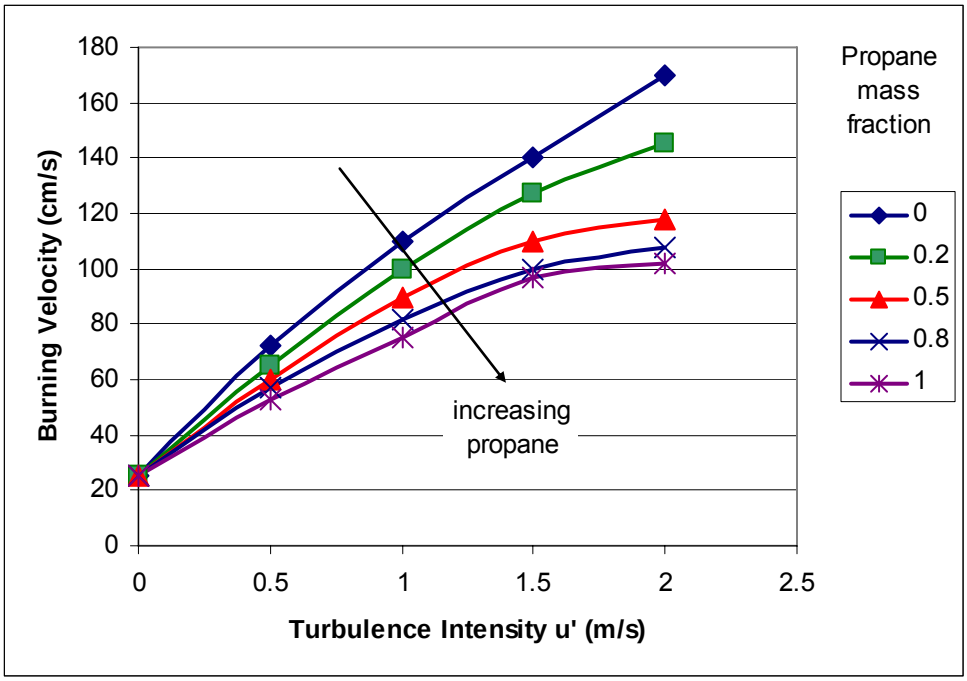

Figure 5-3: Turbulent Flame Speeds[10] of Methane/Propane Mixtures Having the Same Laminar Flame Speed. The x-axis is the magnitude of the turbulent velocity fluctuation. Data is shown for different mass fraction of propane/methane blends.

There are additional considerations in evaluating flame flashback. The mechanisms of flame flashback are not restricted to simple passage of the flame through slow-moving boundary and wake flows in the premixer. It has been shown that other mechanisms can lead to flame flashback, including a slow repositioning of the flame in the swirling flow ("slow flashback").[11] Unless the changes in fuel composition lead to a noticeable change in the flame geometry, it is not likely that this mechanism would accompany a change in fuel composition. Visual images of swirl stabilized laboratory flames discussed in Section 5.10.2 show that the flame geometry is not significantly altered by modest changes to fuel composition.

It is also important to note that flashback is sometimes triggered by combustion dynamics. Combustion dynamics can be sensitive to fuel composition, and the damage produced by dynamics/flashback can be quite serious. Angelo and Castaldini[12] describe an example of how dynamics produced a flashback event that severely damaged a fuel injector during engine tuning

at cold ambient conditions. This emphasizes the importance of monitoring dynamics even apart from changes in fuel composition.

In summary, if one assumes that the fuel control system can respond to a change in fuel composition such that the fuel-air equivalence ratio does not change significantly, the laminar flame speed is not expected to change significantly due to modest changes in the fuel composition. Other factors such as turbulence, contaminants, and aerodynamic design of the premixer could impact the flashback margins for some premixers. The interactions between these factors and variations in fuel properties are an area that could be developed in more fundamental studies. Thus, it appears that the greatest flashback risk associated with fuel composition arises from dynamics problems, and not the modest changes in flame speed or flame geometry.

5.3.2 Fuel Effects on Auto-ignition

Auto-ignition occurs when fuel is injected into an airstream having a temperature high enough to start combustion without any other flame present. This is technically different from flashback, where the flame in the combustor moves into the premixer, but the practical consequences can be just as bad. Auto-ignition requires time for combustion reactions to cascade and produce a flame, and this is known as the ignition delay time. As a result, fuel-air premixers are designed such that mixing occurs at a time scale that is shorter than the ignition delay time. Thus, it is necessary to understand how fuel composition affects the auto-ignition time. Unfortunately, there is not enough fundamental data on ignition delay times at conditions of interest to gas turbines. It is widely understood that ignition delay is shorter at higher temperatures, at higher pressures, and for higher hydrocarbons. For pure fuels, Cowell and Lefebvre[13] report measured auto-ignition times for methane and propane at typical industrial gas turbine conditions. Their results show that the ignition delay differs by almost an order of magnitude for these two (pure) fuels, but mixtures of the fuels were not studied. Spadaccini and Colket[14] report the ignition delay time for hydrocarbon mixtures, and compare the ignition delay for several types of natural gas, showing a factor of seven difference among different natural gas compositions. The correlation of data was applicable only to temperatures and pressures which are higher than in most stationary engine premixers. Data for natural gas reciprocating engines presented by Naber et al.[15] report measured ignition delay times from 7-12 milliseconds at temperatures and pressure which are *higher* than exist in current gas turbines. These delay times should be considerable longer at lower temperatures and pressures that exist in turbine premixers, but data at specific turbine conditions are admittedly lacking. Gas turbine premixer (bulk flow) residence times are often in the range of 2-4 milliseconds, suggesting some margin, but it should be understood that secondary flows in a premixer may produce longer residence times.

Concerns about auto-ignition are greater where fuel must be mixed with high temperature air. The highest premixer temperatures are produced in engines having recuperation, or high pressure ratios. Recuperated engines are not in wide use, with a few notable exceptions such as the Solar Turbines Mercury 50, and micro-turbine generators. In this regard, it is interesting to note that Hack and McDonell[16] tested high concentrations of ethane and propane in a recuperated micro-turbine generator, without noting any operation problems from auto-ignition. Based on discussions with engine manufacturers, it was learned that some industrial engines are currently

sold to operate on unprocessed, or so-called "associated" gas (produced along with oil recovery), which contains appreciable propane, butane and higher hydrocarbons. Some industrial engine premixers have been tested using vaporized diesel fuel.[17] The large hydrocarbons in diesel are more prone to auto-ignition than natural gas constituents, but testing showed that auto-ignition was not a problem. While these observations suggest that auto-ignition should not be a concern for natural gas fuel variability, experience with industrial engines cannot be translated with absolute confidence to other classes of engines, as explained next.

For non-recuperative engines, the compressor discharge temperature of gas turbines is a function of the engine pressure ratio. Figure 5-4 shows the calculated temperature of air compressed isentropically to pressure ratios that are typical of industrial, frame, and aeroderivative gas turbines. The indicated range of pressure ratio for these different machine types is only approximate, and the calculated temperatures are presented in kelvins (red line) and degrees Fahrenheit (blue line).

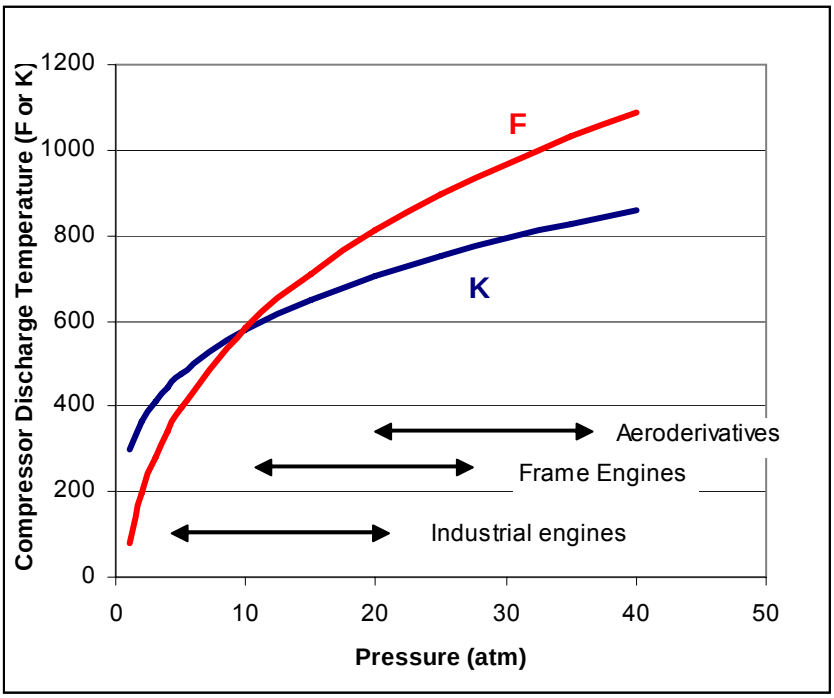

Figure 5-4: Calculated Compressor Discharge Temperature versus Engine Pressure Ratio (Isentropic Compression, Constant Ratio of Specific Heat = 1.4). The approximate range of pressure ratio for different engine types is indicated.

Figure 5-4 is included here to emphasize that future studies on auto-ignition would ideally cover the range of temperature and pressure conditions relevant to all three engine classes. Very recent studies by Kalittan et al.[18] cover parts of this range, but for mixtures of hydrogen/CO/methane fuels. Similar studies would be useful for expected natural gas blends. A study on natural gas fuels, sponsored by DOE, has been initiated to cover these conditions and fuels, but experimental difficulties prevented collection of a wide range of data on these gas compositions.[19]

Several points can be added to the preceding discussion. First, it is true that the autoignition, if it occurs, could be very damaging – even if limited to just a few specific installations. Some reviewers of this report suggest that particular operating conditions may provide conditions that lead to autoignition events, but NETL did not find public data available to define these conditions. Other reviewers noted (correctly) that there are engines operating today with premixed combustors, and using variable composition fuels including gasified LNG, without known problems. As noted above, definitive data sets do not cover the range of conditions needed for all engines.

A second point of clarification is that the presence of hydrocarbon droplets or contaminants may trigger either flame anchoring or autoignition. These are real possibilities, but they are not particularly related to interchangeability. Heavy hydrocarbons and impurities (even solids) from inadequate gas processing may indeed cause problems, but these issues exist for current gas supplies.

5.3.3 Fuel Effects on Emissions

Lee[20] studied the effect of different hydrocarbons on NO_x and CO emissions in a flame that is partially representative of low-emission gas turbine practice. Fuels were premixed upstream of a jet-stirred reactor to a practical level of premixing. Combustion in the jet-stirred reactor (JSR) represented the conditions of strong back-mixing that is typical of swirl-stabilized gas turbine flames. In this JSR experiment, no plug-flow reactor region was included downstream of the JSR, so the CO oxidation that typically occurs along the flow axis of a real combustor was intentionally neglected for this study. In contrast, non-thermal NO_x, which is known to be formed in the flame zone, was represented. The tests data are collected at atmospheric pressure, but at firing temperatures that represent modern gas turbines (1790 K = 2762 °F). Atmospheric pressure emissions data are not as reliable as full, high-pressure data sets. The discrepancy is often the result of un-characterized heat losses (which can be considerable in low-pressure rigs) but this is accounted for in Lee[20] by controlling the temperature of the JSR. Apart from heat losses, the non-thermal component of NO_x is thought to be pressure independent,[21] suggesting that trends with fuel type in this atmospheric pressure data are representative. Figure 5-5 shows data from Lee[20] for a 2.3ms JSR residence time, using the first three alkanes as pure fuels (e.g., not mixtures). Results are shown for two different premixing strategies (mixer 1&2), demonstrating that the degree of premixing was not ideal, but the practical effect was small. Note that for both premixers, the NO_x emissions increase modestly with the fuel carbon number.

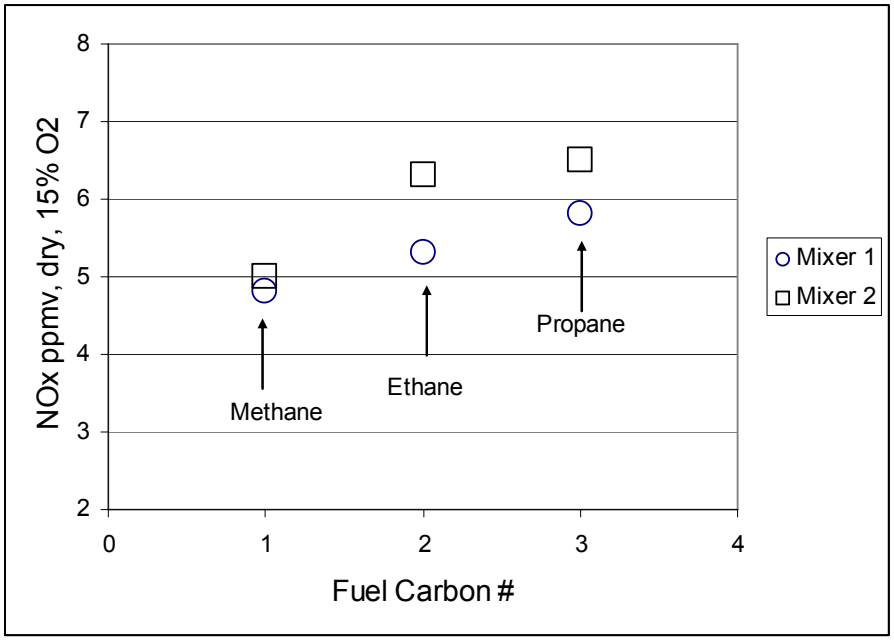

Figure 5-5: Comparison of NO_x Emissions from Jet-Stirred Reactor for Three Fuels (2.3 ms Residence Time, 1790 K Temperature, 1 atm).[20]
(Used With Permission)

Given the relatively small change going from *pure* methane to propane (~+20%), the NO_x changes from varying small levels of higher hydrocarbons in natural gas would be expected to be modest when based on this data alone. This is confirmed by kinetic modeling. Klassen[22] uses chemical reactor modeling (CRM) to predict the effect of natural gas composition on NO_x emissions, based on kinetic schemes that have been "tuned" to a limited set of engine data. No actual experimental validation of the fuel effects is presented. Nevertheless, the model predictions show that NO_x levels do not change for natural gas compositions 1 and 2. Calculations only show an impact on NO_x emissions at ethane and propane levels that are much larger than exist in expected natural gas supplies (compositions 3, 4, & 5).

Figure 5-6 shows a *replot* of some of the predicted data in Klassen. The original calculation data were presented normalized against an unspecified NO_x baseline. Because the calculations were prepared for a commercial client, specific NO_x levels, and combustion temperatures were normalized to avoid divulging proprietary data. In Figure 5-6, a baseline value of 5ppmv NO_x was assumed just to give the data a range that is comparable to Figure 5-5. The data represent NO_x levels at a fixed combustion temperature, but with five different fuel types. Comparing the data, the calculations suggest a much stronger dependence of NO_x on fuel type than the experimental data in Figure 5-5. In these model calculations, propane has a much stronger effect on NO_x than ethane – note that the highest NO_x originates with the higher propane content. It is emphasized that the calculations only show an impact on NO_x for compositions that are beyond current expectations for natural gas. It is also emphasized that these are calculations from available kinetic models; they should be subject to experimental validation.

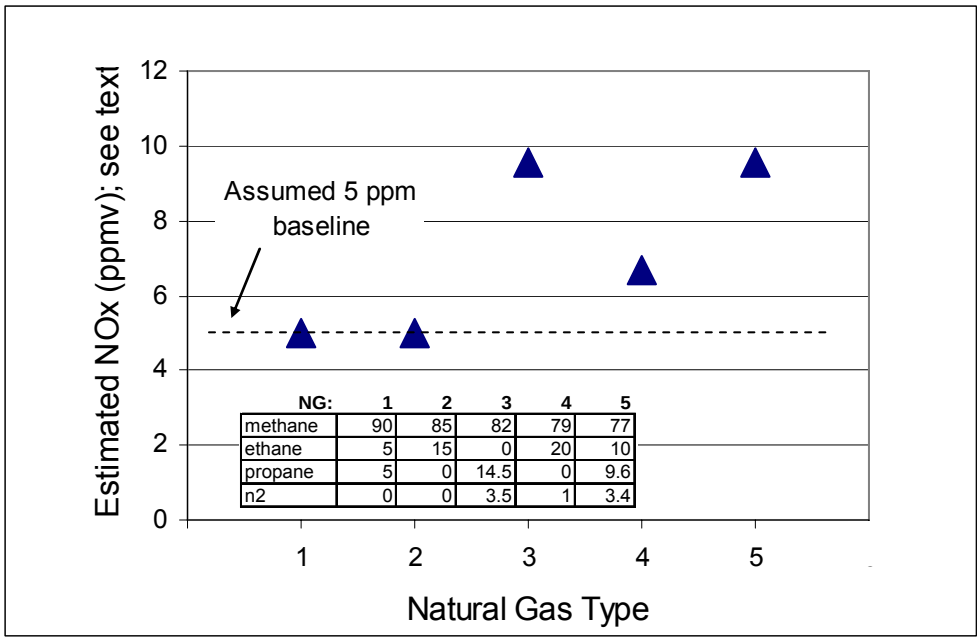

Figure 5-6: Replot of Data Presented by Klassen.[22] Five gas compositions are considered, and an assumed baseline of 5 ppmv NO_x is used to scale the normalized data sets; see the text – the actual NO_x levels are not reported.
(Used With Permission)

Flores et al.[23] experimentally investigated the emissions from a premix, swirl stabilized combustor, using fuel blends of natural gas with as much as 15% ethane and 20% propane. The data were limited to 1 atm pressure, but used realistic air preheat temperatures. Depending on the approach to premixing the fuel and air, the NO_x response to fuel composition was negligible in some instances. With other fuel premixing distributions, NO_x levels covered the range from 2.5 to 4 ppmv for the extreme change from 100% methane to 80/20 methane/propane fuel.

Hack and McDonnel[16] conducted tests of a recuperated 60kW micro-turbine, using fuel blends with 78 – 100% methane, 0 – -17% ethane and 0 – 22% propane. While LNG will not have propane levels anywhere near this high, the data range should clearly demonstrate the effect of higher hydrocarbons. These studies were conducted at fixed engine operating conditions (100% load) and the firing temperature was therefore constant. Thus, the only variable was the fuel composition. Over the range of fuel blends studied, the NO_x ranged from 4 – 7 ppmv (15% O_2). There was no statistically significant variation in CO emissions versus fuel type. The NO_x emissions could be correlated with the fuel composition using the following equation:

$$NO_x\ [15\%O_2] = 0.0351*C1+0.147*C2+0.225*C3 \qquad (5\text{-}4)$$

In this equation, C1, C2 and C3 are the percentage of methane, ethane and propane, respectively. For comparative purposes, this expression can be used to predict the micro-turbine performance on the same fuels that were considered in Table 5-1. Table 5-2 reports the NO_x performance using Equation 5-4, ignoring the small concentrations of butane which was not studied by Hack and McDonell. The ΔNO_x (%) is again reported relative to the baseline on methane alone:

Table 5-2: Predicted NO_x (ppmv @15% O_2) and ΔNO_x (%) Relative to Methane for the Correlation of Microturbine Data from Equation 5-4. The correlation was not tested for pure propane fuel (Column K) and does not account for butane.

Fuel:	A	B	C	D	E	F	G	H	I	J	K
CH4 (%)	100	96.2	87.1	86	90	85	87.1	92.2	88.8	86.0	0
C2H6	0	3.4	10.7	9	5	15	10.7	6.5	7.4	8.7	0
C3H8	0	0.3	1.3	5	5	0	2.1	0.9	2.6	3.5	100
C4H10	0	0.08	0.3	0	0	0	0.0	0.4	1.2	1.8	0
CO2	0	0	0	0	0	0	0	0	0	0	0
N2	0	0.01	0.5	0	0	0	0	0	0.03	0.02	0
Wobbe#	1360	1377	1409	1435	1419	1420	1420	1398	1424	1443	2023
Predicted NOx	3.5	4.0	4.9	5.5	5.0	5.2	5.1	4.4	4.8	5.1	n/a
Delta NOx(%)	0%	12.6%	40.7%	55.7%	43.0%	47.9%	45.7%	25.1%	36.4%	44.6%	n/a

These data show that there is a noticeable percentage increase in NO_x particularly when propane is present. Expressed as parts per million, the absolute increase is not as large, but is significant when expressed as a percent of the (small) baseline. Considering the coefficients in Equation 5-4, propane as a percentage produces more NO_x than does ethane in this gas turbine. If correlations like Equation 5-4 were demonstrated to be applicable to different gas turbines, it would provide a method to estimate the effect of fuel composition on NO_x. Data from laboratory tests (see Section 5.11.3) indicate that this correlation overpredicted the effect of propane on NOx for the premixer/combustor studied at NETL.

The reasons for the NO_x increase with fuel composition can be attributed to two possible mechanisms. First, the change in Wobbe Index among fuels may change the premixer performance. In essence, the smaller volume flow of higher heating value fuel degrades the jet penetration used to premix. This issue is considered in detail in Section 5.8, and will show that premixer performance is not dramatically changed for the fuels presented in Table 5-2. Hack and McDonell[16] also discuss this possibility, and likewise conclude that premixer performance was not significantly degraded using the higher hydrocarbon fuels. For this reason, it is expected that the change in observed NO_x output is due to the chemistry of the fuel itself. This is supported in principle by the fundamental studies of Lee[20] described earlier (see Figure 5-5), but the magnitude of the change observed on the micro-turbine engine tests is larger than might be anticipated from fundamental jet-stirred reactor studies.

The effect of fuel quality on larger gas turbines was recently studied in a report to the California Energy Commission.[24] Four turbine installations along a Pacific Gas and Electric natural gas pipeline were monitored during an excursion in heat content. The turbines included early DLN equipped machines, but all four engines were equipped with exhaust after-treatment (ammonia based SCR, or SCONOx on one machine). The heating value excursion was from 1025 to 1075 BTU/ft^3, approximately a 5% rise over a three day period. In those cases where NO_x was measured before after-treatment, the general trend was an increase in NO_x. However, the scatter in the data makes it hard to draw definite conclusions. For example, at the highest heating value, the spread in the measured data at the Redding power plant ranges from 25 to 28 ppm, but the change attributed to the natural gas heat content ranges from 26 to 27 ppm (see reference 24). In spite of the data spread, the report shows that the best linear fit of the data demonstrates NO_x

rises with fuel heating value. Ammonia injection for the SCR was also tracked during the excursion and suffered from considerable data spread as well. Accepting this data spread, the linear fit of the data in two cases showed an increase in ammonia use during periods of higher heating value, but this was not consistent for all the turbines. A key point to note is that in all instances, the post SCR/SCONOx emissions of NO_x were not influenced by the heating value excursion, and no operational problems were noted on these machines.

There are only a few other publicly available papers that report turbine emissions as a function of fuel variability.[25,26] In these references, emissions and stability were recorded during normal day-to-day ambient fluctuations, as well as relatively small variations in pipeline natural gas composition. These studies did not include a wide variation in natural gas composition, but considered the range of gas composition that has been typical of domestic gas. For example, propane varied between 0.2 and 0.5% (volume basis) of the natural gas, with similar small variations in CO_2 (1.5 – 2.7%), nitrogen (0.17 – 0.22%) and methane content (94.5 – 96.5%).[26] The authors concluded that these small variations in gas composition could not be correlated with observed machine performance in terms of emissions, or combustion stability. However, the authors caution that larger changes in gas composition could lead to different performance.

During the preparation of this report, discussion with various gas turbine owners, developers, and operators was initiated concerning so-called "brown-plume", which is attributed to high levels of NO_2 in turbine exhaust. No definitive case studies were identified that could be reported (e.g., no voluntary reports of visible plume occurrences). Nevertheless, anecdotal descriptions of visible plumes have consistently been connected with part-load or start-up operation. This is technically plausible. During part load, premixed combustors will necessarily change the fuel distribution, leading to some regions of air that deliberately pass through the combustor without premixing. The edge of these unmixed regions could quench hydrocarbon oxidation, leaving trace levels of hydrocarbon in the combustor exit. These hydrocarbons are present in the turbine exhaust along with the NO produced in the combustion process. The NO itself is not a visible emission, and must be oxidized to NO_2 to contribute to the brown plume. It has been shown[27] that this oxidation is dramatically accelerated by hydrocarbons in the temperature range 800 – 1000 K, and this has been proposed as the mechanism for fuel composition changes leading to brown plume. Chemical kinetic studies show that the conversion to NO_2 is very dependant on the type of hydrocarbon, with higher alkanes being most efficient.[28,29,30] Because LNG is expected to have higher levels of ethane and propane than domestic gas, it has been suggested that these un-oxidized fuels may catalyze the formation of NO_2 in the turbine exhaust, producing more visible NO_2 than from domestic natural gas. While this is technically plausible, it has not been experimentally verified, and a detailed analysis would need to be performed on a specific engine, confirming the presence of hydrocarbons in the temperature range needed to form NO_2 from NO. Such a study was beyond the scope of the current investigation, and would only be relevant at part load where NO_2 is already known to be a problem.

In summary, based on the available data, it seems that NO_x production in premixed combustors will rise with higher hydrocarbon fuels, but the extent and cause of the increase has not been completely documented. This issue is addressed by analysis and tests reported in Section 5.11.3.

5.4 Fuel Effects on Lean Blowout

The blowout limit is usually characterized by the fuel equivalence ratio. The equivalence ratio ϕ is the fuel/air mass ratio (f/a), normalized by the stoichiometric value of (f/a):

$$\phi = \frac{(f/a)}{(f/a)_{st}} \tag{5-5}$$

The lean-blowout (LBO) limit of most premixed combustors operating on gas turbines occurs near $\phi \sim 0.5$ for natural gas. The precise blowout equivalence ratio depends on the geometry of the combustor, the flow rate, and the chemistry of the fuel. Although no detailed theory has been developed to describe all aspects of lean blowout it is generally true that blowout data can be correlated with a characteristic combustor time scale, and a chemical time scale which is related to the flame speed of the fuel. Again, because the flame speed does not vary dramatically with compositions that are typical for most domestic as well as imported LNG supplies, it might be anticipated that the lean blowout margin will not change dramatically. However, this point needs to be quantified for LNG. Recent studies have done the same for mixtures of natural gas and hydrogen.[31,32,33] A quantitative knowledge of how the blowout equivalence ratio changes with fuel type will help engine operators recognize how to refine fuel staging schedule to avoid blowout during load changes. The engine control system is set so that fuel transition among stages can avoid getting any stage lean enough to trigger blowout. Some engines have control systems developed to immediately re-pilot burners that are near the blow-out limit.[34] Not all engines have these features, some recent techniques have been proposed using pressure, or ionization sensors to detect the onset of lean blowout.[35,36]

Data from NETL lab tests (see Section 5.10.3) demonstrates that modest changes in fuel composition did not significantly change the lean blowout condition. However, somewhat surprising, a direct change from natural gas to propane did noticeably increase the equivalence ratio where LBO occurs. This result is contrary to traditional blowout correlations based on time scales derived from laminar flame speeds, which are not dramatically different for hydrocarbons (see Figure 5-2). Recently, improved correlations, based on stirred reactor models, have shown better success in describing lean blowout for hydrogen fuels.[33] More discussion will be provided in the discussion of the lab data (Section 5.10.3). This technical issue needs further investigation to insure that no future problems are encountered with more extreme changes in fuel composition.

5.5 Fuel Effects on Dynamics

It is known that relatively small changes in turbine engine ambient conditions[1] and fuel composition[37] can affect the combustion dynamics of operating engines. Combustion dynamics are a form of oscillating combustion that produces pressure oscillations at hundreds of cycles per second. If left uncontrolled, these oscillations can be very damaging, cracking metal combustion liners, triggering flashback, and producing thermal failure from enhanced heat transfer. Currently, it is not known how to confidently predict the effect of fuel composition, or the effect of ambient conditions on dynamics. In actual operation, engines are re-adjusted to meet the combined requirements of power setting, emissions levels, and stable combustion. This process

of re-tuning is done empirically, based on experience with a given engine. Theories of combustion dynamics have provided a qualitative picture of the processes involved in oscillating combustion, but can seldom provide quantitative predication of the occurrence of damaging dynamics.

A brief description of combustion dynamics is provided for background. This text was borrowed from a recent book chapter[38] authored by some of the NETL researchers, and has been adopted for the present discussion; more details can be found in reference 38.

Combustion dynamics are the result of an interaction between acoustic pressure (p') and heat-release perturbations (q'). This interaction can be described as a closed-loop feedback, shown schematically in Figure 5-7. Acoustic pressure p' interacts with the flame and can produce a variation in the heat-release rate q'. The heat-release perturbation can generate acoustic waves as described by Chu.[39] In a physically closed volume, such as a combustor, the boundary conditions will establish standing waves which can produce a periodic disturbance in the heat-release rate, q'. The system will be unstable, if the timing (phase) and the amplitude (gain) of these variations in pressure and heat-release rate produce constructive feedback. This feedback process is analogous to conventional feedback control systems, where the processes shown in Figure 5-7 would correspond to control system components. The G and H nomenclature, as well as the summation circle shown on the left side of Figure 5-7, follow directly from the control system literature and it is typical to refer to dynamics as a feedback process. Many factors control the combustion response G, and may include periodic fluid mechanic perturbations (vortex shedding), periodic variation in fuel flow, or mixing, and changes in the flame itself.

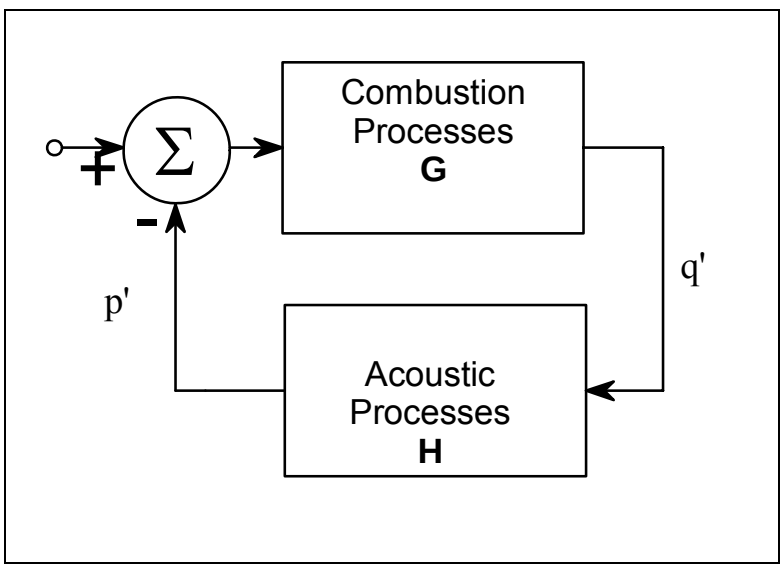

Figure 5-7: Schematic of the Feedback Loop Responsible for Combustion Dynamics. The pressure perturbation p' and heat release perturbation q' are analogous to signals in a tradition feedback Control model.

To understand how the fuel can affect the dynamics, it is helpful to follow the fuel into the combustor and enumerate the things that may change with the fuel composition. Figure 5-8 shows the main points to consider; these are some of details which comprise box G in Figure 5-7.

Fuel enters the injector stem, and enters a fuel manifold which divides the fuel into numerous individual jets and injects the fuel into the air stream. Premixing with the air is accomplished as the fuel jets penetrate the air stream, and the subsequent fuel-air mixture enters the combustion region.

The fuel/air mixing process is characterized by the pressure drop at the point of fuel injection. The pressure drop determines the momentum of the fuel jet, and this in turn controls the steady jet trajectory that mixes the fuel with the air stream. If the Wobbe Index increases, the pressure drop will go down because it takes less volume flow of fuel to provide the same heat input. As shown schematically in Figure 5-8, this means that high or low Wobbe fuels will have different jet trajectories. The premixing will change slightly, and this may lead to a difference in the output NO_x.

In addition to the steady jet trajectory, the fuel jet will respond to pressure perturbations associated with combustion dynamics. The response includes fluctuations in the fuel flow rate, and the trajectory of the fuel jet. The magnitude and timing of these fluctuations is part of the feedback process that contributes to oscillations. The fluctuation response is characterized by the acoustic impedance of the fuel system. If the impedance is high, the fuel fluctuations are small, and conversely a low impedance fuel jet has a large response. Model data will be presented in Section 5.9 to show how changing fuel composition affects the impedance.

Also in Figure 5-8, the flame itself plays a role in the dynamic response. The shape and position of the flame are critically important in determining if the combustion will remain stable, or oscillate. If fuel composition affects the shape, it is not possible to directly calculate the effect on dynamic stability, but it should be recognized as playing a role. Experimental data presented in Section 5.10.2 will show how fuel composition affects the mean position of the flame.

Even if the flame position and shape are constant, it is also possible that the dynamic response of the flame itself may change with fuel composition. For example, Figure 5-3 has already shown that the turbulent burning rate is different with different fuel types at constant laminar flame speed. Thus, the transport properties of individual fuels play a role in the dynamic behavior of flames, yet how this couples with oscillating combustion is an open question. In this study, laboratory Bunsen flames have been used to explore this question, and do indeed show some differences in the dynamic flame response for large changes in fuel composition. Tests in larger, more practical combustors are also reported, and may show a similar effect, but it is difficult to isolate the various features of the total response in practical combustors.

As pointed out by a reviewer of this document, experiments and analysis presented in this report do not cover the class of dynamics problems typically referred to as “screech”. Dynamics with frequencies in the kilohertz frequency range are typically described as screech, and it is not clear whether these type of oscillations will be more sensitive to fuel type than the lower frequency oscillations studied here. More work is needed to understand both the science behind screech problems, and their relative occurrences on fielded engines.

Dynamics problems are often addressed in commercial applications by changing the “split” of fuel to various injectors,[12,40] or with other types of active control methods[41,42,43] applied or being

developed. A recent paper describes how one engine manufacturers is developing a control system that can adjust fuel splits to accommodate wider ranges of fuel blends than in the past.[44] These recent developments show that manufacturers are developing methods to increase the fuel flexibility of premixed combustion systems.

In summary, multiple individual factors which contribute to dynamics and are related to fuel composition have been described. Tests and analysis described in the next section are used to address many of the issues noted above.

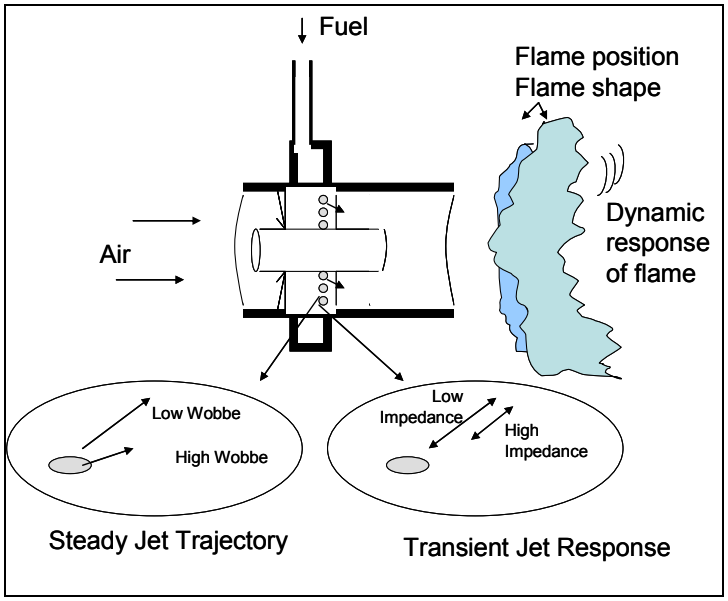

Figure 5-8: Schematic of Combustion Dynamics Processes that may be affected by Fuel Composition. Fuel enters via the premixer stem at the top and is injected into the air stream by jets which may be part of the swirl vanes as shown.

5.6 Description of Analysis and Experiments Reported

A combination of numerical models and experimental testing have been used at NETL to address the issues described above. The rationale and relationship between these different tests is explained next.

5.6.1 Lab-Scale Ring Stabilized Burner (< 15,000 BTUH)

NETL uses this lab-scale burner to study features of how flames oscillate. Tests in this device are very easy to conduct, and data on different fuel types can be obtained in just a few hours of testing. The flame is a (nearly) laminar ring stabilized flame and is ideal for studying the response of the flame to changes in fuel type. If significant changes in flame response versus fuel type are observed in this burner, it would be especially important to consider how to account for fuel type in more complicated flames. For example, if a propane flame was shown to exhibit local extinction during oscillations, but a natural gas flame did not, the situation in large scale flames would need to account for such differences. As will be seen, some differences for

extreme fuel composition changes were observed, but not for the typical composition changes associated with LNG versus traditional U.S. natural gas.

5.6.2 Atmospheric Pressure Development Combustor (< 1x105 BTUH)

This device is used to study the interaction between the flame and fuel injection. The combustor uses a swirl-stabilized flame, with a fuel-air premixer that shares features with full-scale hardware. Significant dynamic instrumentation is used to diagnose acoustic behavior. Because the combustor operates at atmospheric pressure, it is relatively easy to modify the hardware, and gather visual images. If significant changes in flame response versus fuel type were observed in this burner, the role of fuel injection on these changes could be clearly determined. On this experiment it is possible to measure and quantify the change in fuel injection versus fuel Wobbe Index. This is important because adjustment to the Wobbe Index can be achieved by simply heating the fuel, or adding nitrogen. Data from this experiment shows that Wobbe Index alone will not describe the flame response versus fuel composition. Furthermore, the actual change in flame response for modest Wobbe variation was relatively small.

Although many features of combustion could be studied in the atmospheric pressure development combustor, the effect of operating pressure is an important consideration. For example, atmospheric pressure combustion emissions are not representative of high-pressure turbine flames. For this reason, emissions data were recorded only in the high-pressure combustor described next.

5.6.3 High Pressure Dynamic Gas Turbine Combustor (< 5x106 BTUH)

This combustor is used to study both research and commercial gas turbine fuel injectors. The NETL facilities can supply preheated, pressurized air at conditions that are typical of gas turbine operation. The high-pressure operation requires pressure vessels that limit instrumentation access, and complicate controlled addition of higher hydrocarbons. To conduct this study, a considerable effort was required to install a system capable of adding propane to the natural gas supplied to the experiment. As part of this research effort, a propane blending facility was developed to meet all relevant safety codes and is described in this report.

Combustion testing at high pressure has been conducted using a fuel injector has been manufactured by Woodward Industrial Controls for a separate NETL Cooperative Research and Development Agreement (CRADA). This fuel injector is an analogue of premix injectors used in commercial engines. The experiment is also outfitted with dynamic pressure transducers and all relevant emissions monitors. Tests in this combustor have focused on affirming that the change in flame response versus fuel type followed expectations from low-pressure testing, as well as recording emissions data at realistic high-pressure conditions.

5.6.4 Simulations and Analysis

Before discussing experimental results, it is useful to consider what aspects of the fuel interchangeability can be predicted from numeric or analytic models. Some details of the flame behavior remain difficult to predict. In a recent review article, Lipantnikov and Chomiak[45]

comment that it is not presently possible to confidently predict even the flame speed of two mixtures A and B subject to different turbulent length scales and intensities. This is why experimental testing is needed to determine the response of the flame with different composition fuels. However, some question can be assessed numerically, providing a greater definition to what can be isolated in experiments. These are discussed below.

Premixer Behavior – Low emission turbine operation relies upon fuel/air premixing prior to combustion. Premixing is achieved using variations of jet mixing, often in a cross-flow configuration, upstream of the flame. The simplest jet/cross-flow geometry can be predicted using the correlations in Hautman et al.[46] As discussed below, this provides a simple way to demonstrate how the fuel Wobbe Index will affect premixing, but it does not directly predict the effect of emissions, or flame structure. It is also important to note that these simple correlations have been developed based on specific fuels. When using these correlations are used to predict behavior of different fuels, effects like preferential diffusion are neglected. In some fuels this assumption should be validated. Nevertheless, conventional analysis of the jet mixing problem suggests that experiments conducted at constant Wobbe, but with different fuel composition, will have the same mixture profile at the flame, removing one variable in the combustion response.

Fuel Injection Dynamic Response – In addition to premixing, fuel injectors in low-emission gas turbines are usually designed for a particular dynamic response, and examples of how this is done are found in the literature.[47] The dynamic response is defined by how acoustic pressure perturbations modulate the flow of fuel. In some circumstances, this fuel modulation can trigger damaging combustion oscillations. It is therefore necessary to consider how changes to fuel composition affect the fuel modulation. While fuel modulation does not determine the whole combustion response, it is again important to determine what can be done experimentally to measure changes in the dynamic response as a function of fuel composition so that testing can be conducted to isolate this parameter.

5.7 Results for Lab-Scale Ring Stabilized Burner

The lab-scale burner is a ring-stabilized premixed burner that is inserted into a quartz-tube. The quartz (Rijke) tube has an 8.0 cm diameter and an 80 cm length (see Figure 5-9). This Rijke tube arrangement produces acoustic feedback that interacts with the heat-release rate in the flame to drive combustion instabilities.[48] The combination of ease of operation, 360° optical access, and strong acoustic resonance makes the Rijke tube combustor an excellent experimental platform to study the fundamental properties of combustion dynamics. This burner arrangement has been described in previous work.[49,50,51] The burner nozzle is a stainless steel tube with an inside diameter of 2.18 cm and a wall thickness of 1.8 mm. The premixing tube and ring stabilizer are positioned 20 cm (¼L) into the quartz main body in order to produce peak resonance. The flame is anchored on a ring (2.0 cm OD x 1.8 cm ID) located at the top of the nozzle.

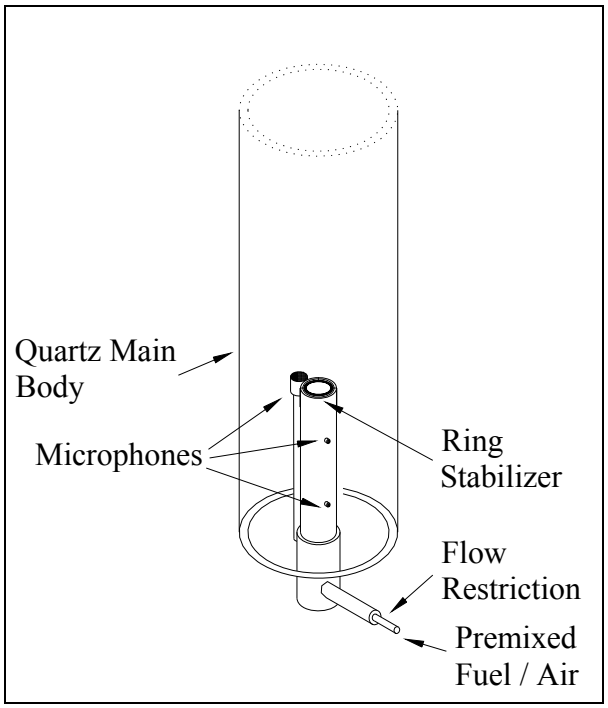

Figure 5-9: Schematic of Lab-Scale Ring Stabilized Burner.

This study included fuel blends of methane, ethane and propane which were prepared using mass flow controllers, and are summarized in Table 5-3. Included in the table is the Wobbe Index which is a parameter commonly used by the gas industry to assess fuel interchangeability.

Table 5-3: Fuel Blends Tested In Rijke Tube Burner.

	Fuel A Base Case	**Fuel F Case 1**	**Fuel C Case 2**	**Fuel E Case 3**	**Fuel K Case 4**
Methane (%)	100	85	87.14	90	0
Ethane (%)	0	15	10.74	5	0
Propane (%)	0	0	2.12	5	100
Higher Heating Value (MJ/m3) (BTU/scf)	39.76 1067	44.53 1195	44.53 1195	44.53 1195	94.0 2523
Wobbe Index (MJ/m3) (BTU/scf)	50.4 1353	52.7 1414	52.7 1414	52.7 1414	75.8 2034

As previously mentioned, combustion instabilities (dynamics) are a concern for gas turbine systems utilizing lean pre-mixed combustion. Strong dynamics can produce pressure oscillations as much as 10% of the operating pressure. RMS pressure levels within the burner provide a means of characterizing the magnitude of the dynamic, or unstable, response of the burner to changes in fuel composition. The base case represents the observed response with 100% methane fuel. The other cases represent fuel blends with various levels of methane, ethane and propane. Although fuels given in Cases 1, 2, and 3 have different fuel compositions, the Wobbe Index for each of these cases was kept constant (Wobbe ≈ 52.7 MJ/m^3) in order to independently vary the hydrocarbon content. Figure 5-10 is a plot of the RMS pressure levels measured as a

function of equivalence ratio for each of the fuel combinations. The plot suggests that for fuels containing higher concentrations of heavier hydrocarbons (above C1 methane) the dynamic response was slightly higher at richer operating conditions. This is particularly evident for the 100% propane case (Case 4) in which both the amplitude and operating range at which instabilities occur are both increased. Note that all the fuel blends have smaller amplitudes on the rich side, where diffusion burning stabilizes the flame dynamics.

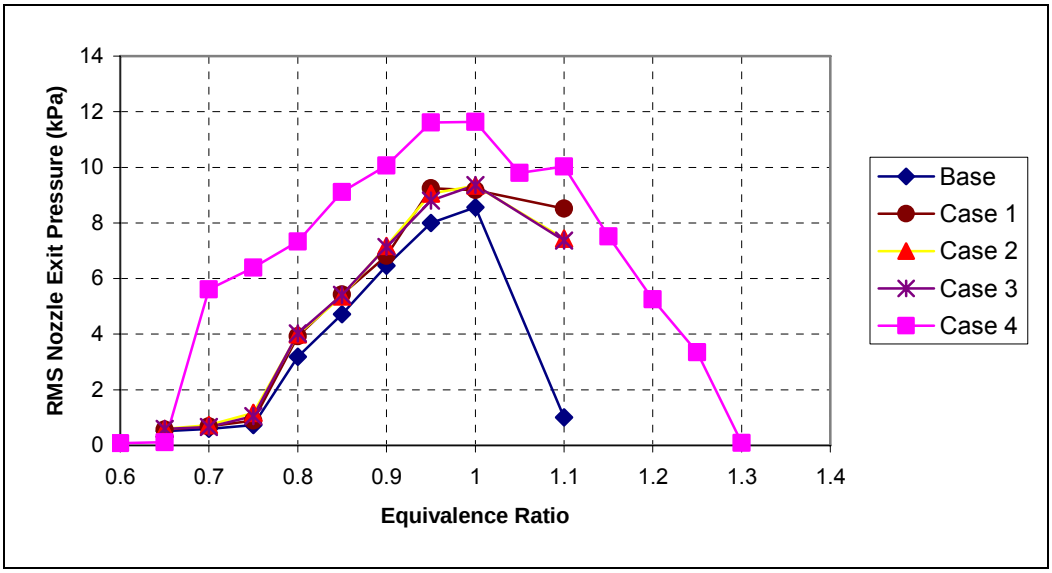

Figure 5-10: RMS Pressure Levels Observed in Lab-scale Rijke Tube Burner as a Function of Fuel Equivalence Ratio.

Gas turbine operators typically control fuel and air mixtures in order to produce a desired flame temperature or turbine inlet temperature. Figure 5-11 plots the same measured dynamic response as shown in Figure 5-10 but shown as a function of the theoretical adiabatic flame temperature. This plot (Figure 5-11) would appear to suggest that the dynamic response of the burner was less affected by the actual fuel composition and more dependent upon the resultant flame temperature. A particular finding shown here is that for the Base fuel and Cases 1 - 3 there is no difference in the measured RMS pressure over the operating range investigated although there was a difference in the Wobbe number. These fuels had large methane and ethane content variations with 85 - 100% and 0 - 15% respectively, but a difference of propane percentage of only 5%. As the propane percentage is increased to 100% there is a significant change in the overall dynamic response in terms of both amplitude and range of instability. However, it should be noted that in the Rijke tube combustor, mechanisms known to influence combustion dynamics are limited to flame dynamics only, whereas other mechanism may become dominant in a full-scale combustor. In particular, equivalence ratio fluctuations are prevented from occurring in the Rijke tube combustion through the use of upstream pre-mixing and flow restrictions. In full scale systems, acoustic perturbations may propagate upstream into the fuel nozzle and through variations in the gas density and speed of sound (characteristic impedance). As a result of changes in the gas composition, the acoustic response of the fuel injector may change which could potentially alter the overall response of the combustor.

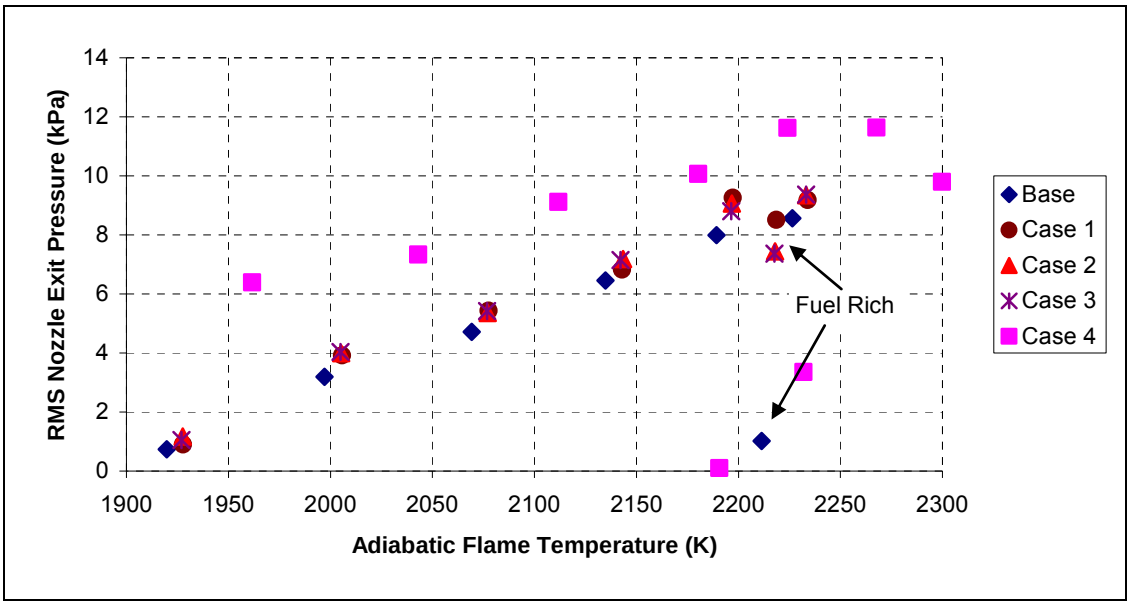

Figure 5-11: RMS Pressure Levels Observed in Lab-scale Rijke Tube Burner as a Function of Flame Temperature.

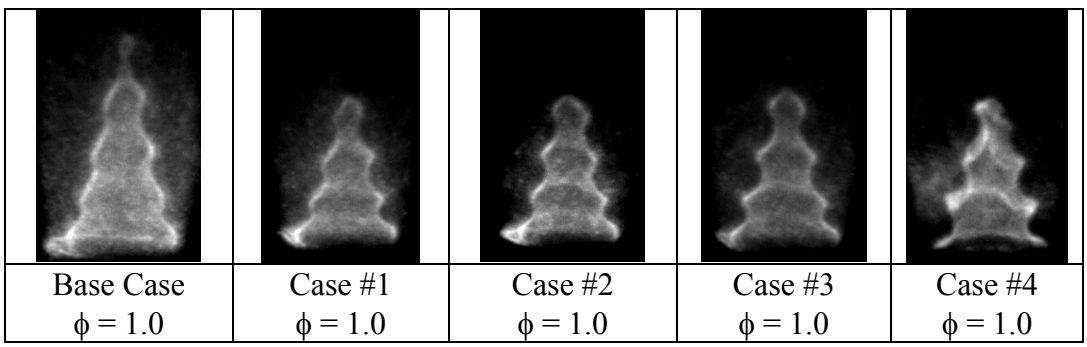

Base Case	Case #1	Case #2	Case #3	Case #4
$\phi = 1.0$	$\phi = 1.0$	$\phi = 1.0$	$\phi = 1.0$	$\phi = 1.0$

Figure 5-12: Flame Images for Fuel Blends Studied in the Lab-scale Burner.

The flame structure (i.e., length, area and shape) can also have a significant effect on the dynamic response of the flame,[52] and hence these effects could result in changes to the dynamic behavior of a premixed burner. For these reasons, images of the flame have been collected at various operating conditions. Examples of the instantaneous images for each blend of fuel are shown in Figure 5-12. These instantaneous images capture the cusps that form along the surface and contribute to changes in the immediate heat release from the flame. The images shown here were taken at various locations within the period of oscillation, and it is difficult to conclude whether differences in the flame shape exist when using the different fuel blends.

Comparisons made over the entire cycle between the Base Case and Cases 1 – 3 revealed very little difference in the observed flame structure. When the burner was operated under extreme changes in the fuel composition (100% propane, Case 4) there was a modest change in the flame structure with an observed reduction in the overall flame volume (measured volume enclosed by the flame surface and burner exit nozzle). This is most likely the result of difference in the laminar flame speeds between methane (~ 40 m/sec) and propane (~ 45 m/sec). Although these results tend to indicate that experimental fuel blends comparable to those commonly found in

domestic and imported natural gas supplies produced little if any change in the overall flame structure, more analysis is needed in order to fully understand how differences in fuel composition may influence the instantaneous heat release from unstable flames.

In summary, tests in this lab scale burner indicate that the flame dynamic response is minimally affected by modest changes in fuel composition, even when comparing pure methane to a blend of 90/5/5 methane/ethane/propane. However, *pure* propane produced a noticeable increase in the magnitude of dynamic oscillations, and shortened the flame length, presumably due to the increase in laminar flame speed. These results suggest that large-scale tests may need to focus on physical features of the dynamic response, such as the fuel injector dynamic response, considered next.

5.8 Premixer Performance

The resultant pollutant and dynamic response from lean-premixed gas turbine systems relies heavily on adequate mixing of the fuel and air prior to reaching the reacting zones within the combustor. Turbine manufactures often choose some variation of a crossflow jet configuration to achieve the desired degree of mixing. Figure 5-13 shows a simple example of a jet crossflow mixing system in which fuel is injected into a stream of air.

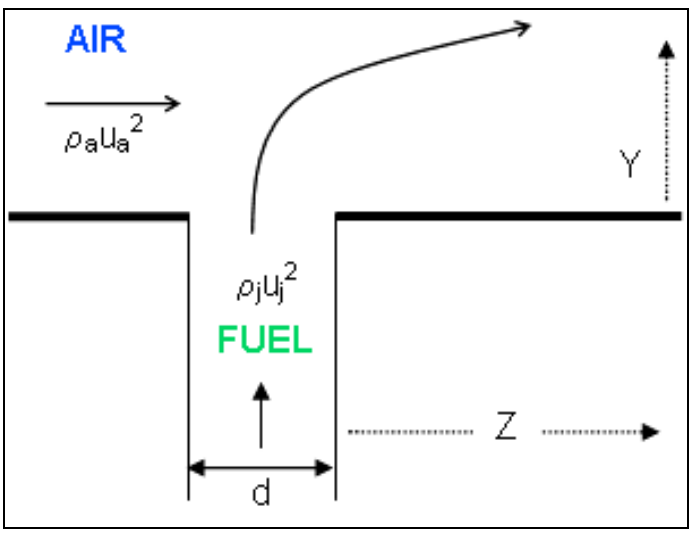

Figure 5-13: Schematic of Simple Jet Crossflow Mixing Configuration.

For this discussion it is useful to consider the fuel Wobbe Index, defined as:

$$Wobbe = \frac{HHV}{\sqrt{SG}} \tag{5-6}$$

where HHV is the fuel higher heating value (on a gaseous standard volume basis, e.g., MJ/m^3) and SG is the specific gravity.* As described by Baukal,[53] different fuels with the same Wobbe

* The Wobbe index can also be defined based on the lower heating value, leading to confusion when comparing fuels. The gas heating industry usually uses HHV, but the turbine industry often uses LHV.

Index will produce the same heat input for a given fuel orifice size and fuel pressure drop. The Wobbe Index is widely used as an interchangeability parameter for self-aspirating fuel nozzles in atmospheric pressure burners because the line pressure is usually fixed, and the desired heat input is often constant. In gas turbines, the heat input is controlled by the engine throttle, not the fuel pressure/orifice size, so the Wobbe Index does not play the same role as in atmospheric burners. Instead, the Wobbe Index may affect the premixer performance as described next.

Consider the simplified premixer geometry shown in Figure 5-13. Fuel is injected vertically from the wall into the air stream flowing left to right. The heat release originating from combustion of the fuel jet is the product of the jet mass flow and the heat release per unit mass of the fuel, ($HHV/\rho_{f,std}$). The jet flow is calculated from the standard orifice flow equation, leading to an expression for the heat release produced from the fuel jet:

$$Q = K \cdot A_j \cdot \left(\frac{HHV}{\rho_{f.std}} \right) \cdot \sqrt{\Delta P_j \cdot \rho_j} \tag{5-7}$$

where K = the orifice coefficient. A_j = jet area, ΔP_j = pressure drop associated with the fuel jet, and ρ_j is the density of the fuel jet upstream of the orifice. The subscript 'std' represents standard conditions, and subscript 'f' corresponds to the fuel. Noting that both densities in this expression can be written as the product of specific gravity and a corresponding density of air at the same P and T, this equation can be re-written as:

$$Q = \frac{K \cdot A_j}{\rho_{air.std}} \cdot \left(\frac{HHV}{\sqrt{SG}} \right) \cdot \sqrt{\Delta P_j \cdot \rho_{air,j}} \tag{5-8}$$

Note the appearance of the Wobbe Index inside the brackets. If this expression is written for two fuels A and B, assuming ideal gas density, the ratio of the heat release between fuels is:

$$\frac{Q_A}{Q_B} = \frac{WI_A \cdot \sqrt{\Delta P_A \cdot P_A}}{WI_B \cdot \sqrt{\Delta P_B \cdot P_B}} \tag{5-9}$$

This equation demonstrates the utility of the Wobbe Index. If the fuel line pressure and pressure drop are the same for two different fuels, the heat release will be equal if both fuels have the same Wobbe Index. This is why the Wobbe Index is useful as an interchangeability parameter in naturally aspirated burners, where the line pressure is usually fixed. For gas turbines, the Wobbe is related to the premixer jet mixing.

Returning to Figure 5-13, the coordinate Y denotes the vertical height of the peak fuel concentration, and Z is the horizontal distance downstream. From the jet mixing correlations reported by Hautman et al.,[54] then:

$$\frac{Y}{d_j} = 0.56 \cdot \sqrt{\left(\rho_j u_j^2 / \rho_a u_a^2\right)} \cdot \left(Z / d_j\right)^{0.33} \tag{5-10}$$

The subscripts a and j refer to the air and fuel jet. Note that the first term in the square root is the ratio of the fuel jet momentum, to air jet momentum. Because the air jet momentum is unchanged for two fuels A and B, the center of the jet trajectory at any Z position is:

$$\frac{Y_A}{Y_B} = \sqrt{\frac{\rho_{jA} \cdot u_{jA}^2}{\rho_{jB} \cdot u_{jB}^2}} \tag{5-11}$$

The fuel jet momentum is twice the kinetic energy of the fuel jet, which in turn is a function of the pressure drop across the orifice that creates the fuel jet. From the orifice equation,

$$\rho u_j^{\ 2} = 2 \cdot C_D \cdot \Delta P_j \tag{5-12}$$

If two fuels A and B are to produce the same heat release in an engine, from Equation 5-9, $Q_A = Q_B$, and assuming that the change in fuel pressure drop ΔP is much larger than the change in pressure (i.e., $P_A/P_B \sim 1$), combining Equations 5-9 thru 5-12,

$$\frac{Y_A}{Y_B} = \frac{WI_B}{WI_A} \tag{5-13}$$

Equation 5-13 shows that the penetration distance is inversely related to the Wobbe number, suggesting that jet flows for higher Wobbe number fuels will not penetrate as far as lower Wobbe fuels. The actual effect on resultant NO_x emissions will depend not only on the jet penetration, which aids in mixing, but also turbulence intensity.

To better understand these effects, the geometry shown in Figure 5-13 was utilized to develop a simple two-dimensional CFD model of a jet crossflow mixing system and evaluate the effects of varying fuel composition on downstream mixing. Two fuel compositions were investigated: 100% methane and a blend similar to that used for Case 3 discussed previously (see Table 5-3). The Case 3 fuel has a Wobbe number of 1414 compared to the 100% methane fuel with a Wobbe number of 1360. For this analysis, the air flow rates are held constant while the fuel flow rates are varied in order to maintain a constant adiabatic flame temperature at the flame location which is maintained at x = 0.03.

Figure 5-14 (a) & (b), are the results of the analysis and show the fuel mass fraction distribution downstream of the injection point at x = 0.0025. Although these fuels had Wobbe numbers that differed by almost 100 points, there is not a significant difference in the fuel mass fraction at the prescribed flame location, and thus there appears to be little effect on NO_x emissions due to mixing of these two different fuel compositions.

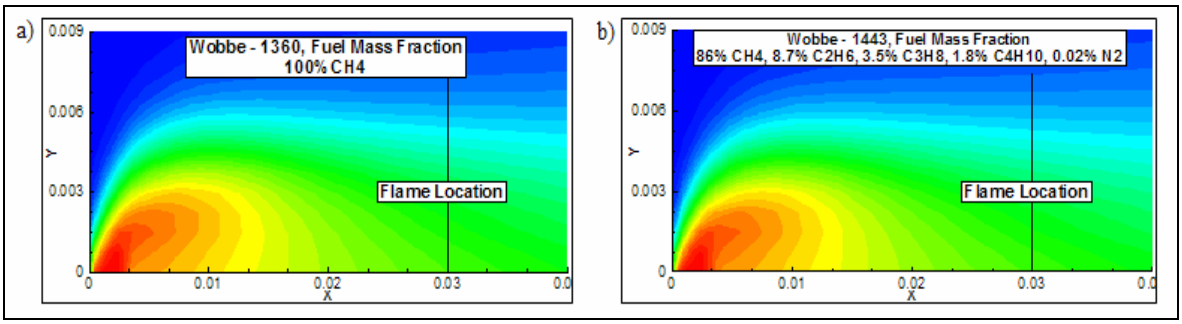

Figure 5-14: Fuel Mass Fraction Contours for 100% Methane Fuel and Typical LNG Composition Fuel for Jet Crossflow Mixing.

In a realistic combustor, mixing occurs not only as a result of a jet crossflow but typically some additional mechanism such as swirling flow which increases the turbulence intensity. This increase in flow turbulence allows the fuel and air to have a shorter mixing time. Swirl also helps to stabilize the flame at the combustor dump plane. As shown previously in the two-dimensional models, varying the Wobbe number had only a small impact on the level of "mixedness" within the desired reaction zone. It is expected that the addition of swirl (or increased turbulence) would further reduce the effects of varying fuel composition on fuel-air mixedness, and ultimately engine-out emissions.

To evaluate the effects of fuel composition on fuel mixedness in more realistic combustor geometry, a full three-dimensional CFD mixing study has been performed. The geometry considered for this analysis is shown in Figure 5-15 (a) & (b). Air is injected through a 30° swirl vane just upstream of a series of fuel spokes which injects the fuel tangential to the primary axis of the premixer. Fuel mixes with the air as the flow continues through the premixer until it reaches the dump plane where the flame is stabilized.

In order to examine extreme differences in fuel composition, 100% methane and 100% propane were chosen as the fuels for comparison with Wobbe numbers of 53.3 (1360) and 76.0 (2023), respectively. This constitutes a much larger difference than expected between various natural gas supplies. Thus it is anticipated that typical fuel blends will produce mixing profiles within the boundaries identified in this analysis.

The mass flow of air was held constant as in the 2-D analysis, while the fuel mass flow was varied in order to obtain a consistent adiabatic flame temperature in the combustor. The effects of reacting gases in the combustor were neglected for this cold flow analysis, since the primary consideration was pre-combustion mixing in the premixer and at the dump plane.

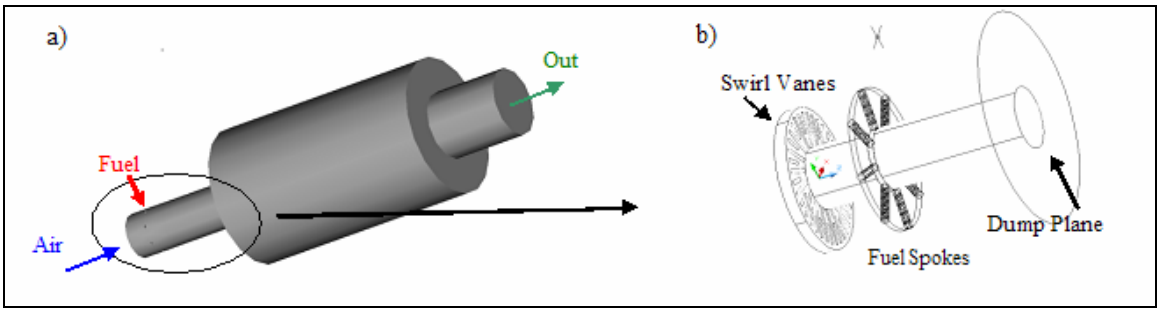

Figure 5-15: Full 3-D gas Turbine Premixer and Combustor Geometry Including Swirl Vanes and Downstream Fuel Spokes.

Results from the analysis are shown in Figure 5-16 (a) & (b) as the respective distributed fuel mass fraction. Figure 5-16 (a) & (b) shows the radial distribution of fuel immediately downstream of the fuel spokes for 100% methane and 100% propane, respectively. As previously predicted with Equation 5-13, the lower Wobbe number (i.e., methane) case (Figure 5-16a) produces deeper penetrating flow thus rapidly mixing with the incipient swirling air stream. The radial distribution of the 100% propane case shown in Figure 5-16b displays a narrower distribution of the fuel thus a higher mass fraction persists further downstream than the previous methane case.

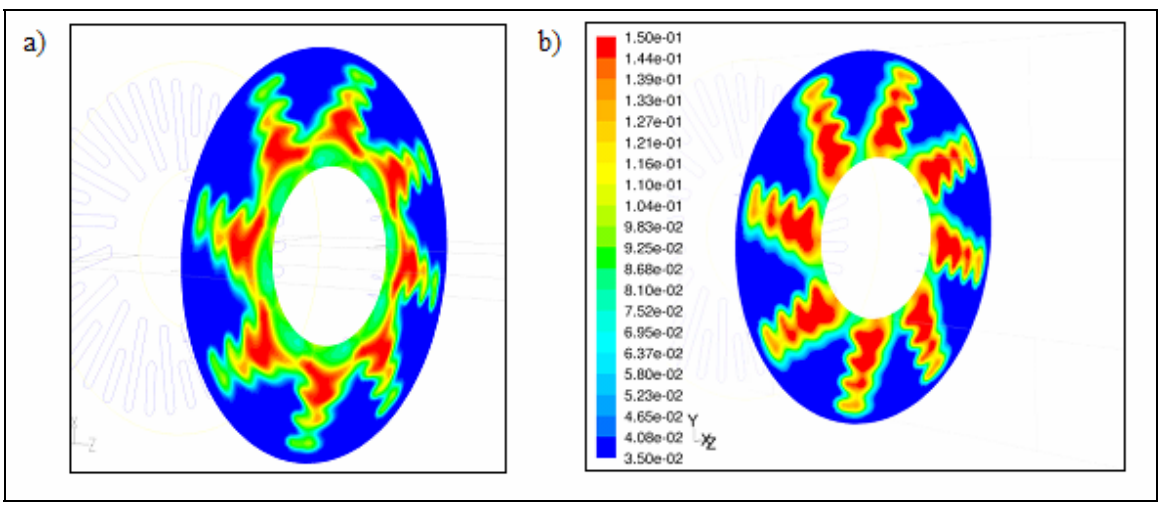

Figure 5-16: Radial Distribution of Fuel Mass Fraction Just Downstream of Fuel Spokes. a) 100% Methane, b) 100% Propane.

The axial fuel distributions are shown for a mass fraction range of 0.035 – 0.15 for both 100% methane and 100% propane in Figure 5-17 (a) & (b), respectively. The actual shape of the contour of constant mixture ratio is different between the two cases, because less propane is mixed than methane. However, upon reaching the dump plane, the mixture is fairly uniform in both cases. Once the flow reaches the combustor the overall mass fraction through the volume equalizes near 0.03. It should be noted that high reaction temperatures would alter the flow distribution at the combustion dump plane due to regions of re-circulating gas that back-mixes with the cold reactant flow.

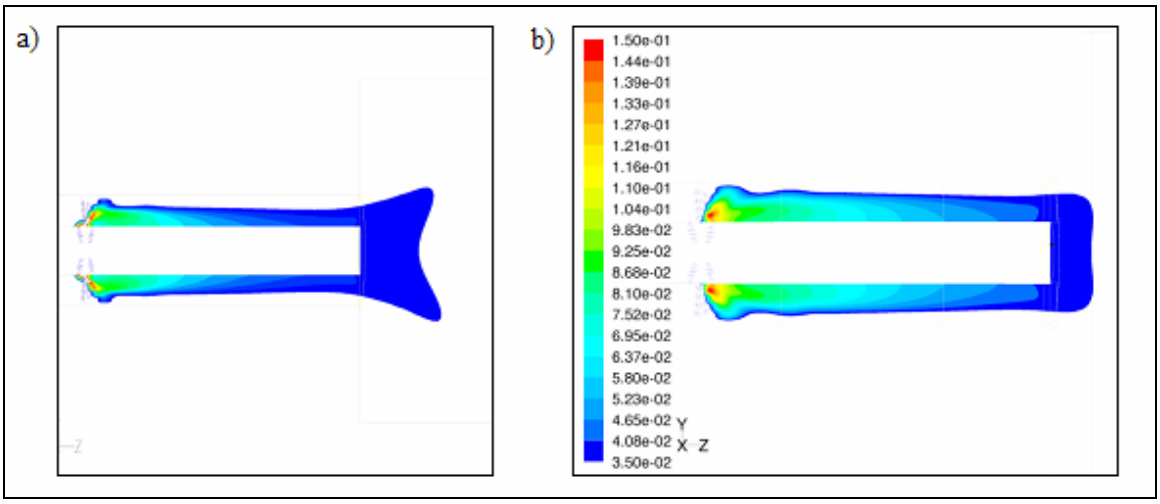

Figure 5-17: Axial Distribution of Fuel Mass Fraction Just Downstream of Fuel Spokes. a) 100% Methane, b) 100% Propane.

Results from both the 2-D and 3-D computational analysis, along with the analytical solution given in Equation 5-13, suggest that little effect on mixing is expected for fuel compositions typical of domestic natural gas and imported LNG. Even for the extreme fuel compositions utilized for the 3-D analysis, which provides a mixedness boundary for the expected fuel composition, only a slight variation in the level of fuel mixedness was observed. This would suggest that fuel variability effects on fluid dynamic mixing would not have a significant effect on NO_x. However, this does not address the more significant chemical mechanisms contributing to NO_x production that may change as a result of fuel variability. Experimental results at turbine like conditions investigating fuel variability on NO_x emissions are presented in Section 5.11.

5.9 Analysis of Fuel Injector Dynamic Response

Before considering experimental results from larger combustors (Sections 5.10 and 5.11) it is valuable to analyze what features of practical fuel injectors may participate in the combustor dynamics, and how these will change with fuel composition. As shown in this section, certain features of the response versus fuel type can be predicted analytically, meaning these can be controlled or measured in subsequent experiments.

Thermoacoustic instabilities (combustion dynamics) are the result of variations in the heat release from the flame (q') coupling with pressure perturbations (p') that form as a result of the acoustic characteristics of the combustion chamber, fuel and air injectors and premixing regions within the turbine. This closed-loop feedback system was shown previously in Figure 5-7 and is shown in slightly more detail in Figure 5-18, where G(s) is a transfer function representation of the combustion processes that interact with the acoustic processes, H(s), to form the feedback loop.

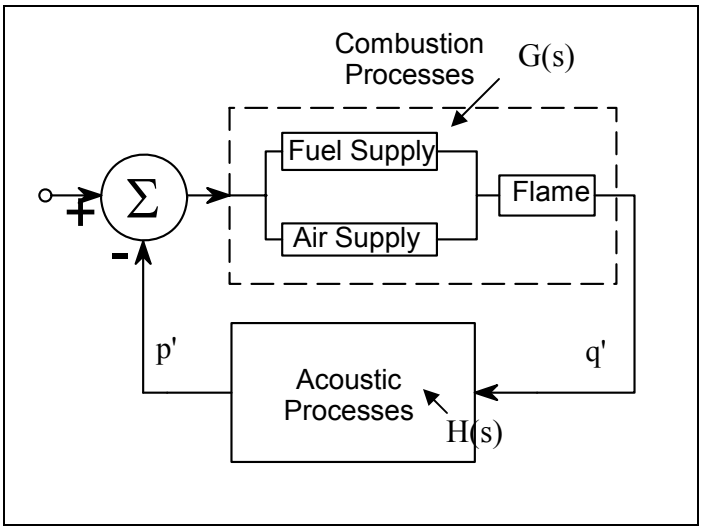

Figure 5-18: Schematic of the Feedback Loop Representing Processes in Combustion Dynamics.

The acoustic processes H(s) are defined by a combination of the system geometry, boundary conditions, and operating conditions, including fuel composition. Changes in the acoustic properties of any of the components that form the closed-loop system could alter the coupling between pressure and heat release perturbations which could lead to a reduction, or possibly an increase in the amplitude of the combustion dynamics.

The combustion response G(s) is divided into physical responses of the air supply, fuel supply, and the flame itself. Section 5.7 considered the response of the flame in an idealized lab situation. The fuel and air supply response is analyzed here. The acoustic characteristics of a given system may be described by its acoustic impedance (Z), which is the ratio between the acoustic pressure (p) and acoustic velocity (ν) (i.e., $Z = p/\nu$). This parameter describes the complex combination of incident and reflected waves and is dependent upon the geometry and boundary conditions of the respective volume, as well as the gas or medium in which the wave is propagating. Changes in the acoustic impedance within a given volume can act to drive or dissipate energy by either changing the amplitude of the reflected / traveling wave or by changing the phase angle (time lag) between the acoustic pressure and acoustic velocity.

Prior research[38,39,40] demonstrated that by changing the acoustic impedance of the fuel system through altering the length of a resonator attached to the fuel plenum it was possible to considerably reduce the amplitude of the RMS pressure measured in the combustor over a range of operating conditions (equivalence ratios and bulk flow velocities). It was determined that this control was achieved primarily by changing the phase (convective time delay) of the fuel/air perturbations brought on by the acoustic velocity, and to a lesser extent by changing its magnitude. This would also suggest that for systems that are marginally stable, small changes in the operating conditions (including fuel composition) that result in a change of the acoustic impedance at particular locations within the combustion system may be sufficient to drive an unstable dynamic response.

Changes in the operating conditions, such as variations in the equivalence ratio, fuel composition or even the gas temperature, alters the speed of sound (c_o) and the density of the medium (ρ). The product of these parameters is the characteristic impedance of the medium (fluid)

$$Z_{ch} = \rho c_o \tag{5-14}$$

The characteristic impedance is a measure of the resistance of the medium inside a volume to reflect and transmit acoustic waves. The impedance at any position for a one-dimensional, propagating wave is as follows:

$$Z = \frac{p}{\upsilon} = \frac{Ae^{-ikz} + Be^{ikz}}{Z_{ch}\left(Ae^{-ikz} - Be^{ikz}\right)} \tag{5-15}$$

The terms A and B are constants described by the boundary conditions on the up- and downstream side of the volume of interest, z is the spatial coordinate, and k is the wave number which is dependent on the speed of sound, c_o, and the frequency.

To investigate the effects of fuel composition on the acoustic response of a model gas turbine, a computational model of the combustor shown in Figure 5-19 was utilized and changes in the magnitude and phase of the acoustic impedance in the injector and downstream reaction zone (prior to combustion) were evaluated for a number of different fuel compositions. The geometry shown in Figure 5-19 is a simplified version of the injector used in tests of the low-pressure development combustor (Section 5.10).

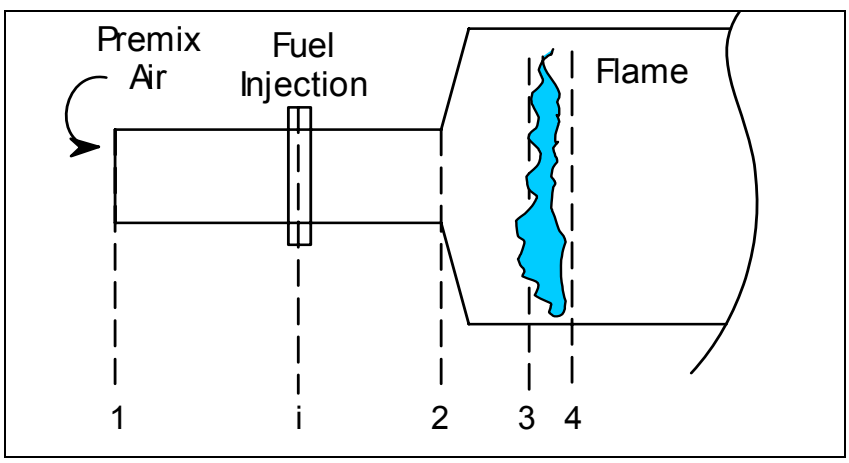

Figure 5-19: Geometry of Model Combustor.

An acoustic model of the combustor shown in Figure 5-19, developed previously[38,39,40], was used to express the closed loop feedback that produces variations in the heat release from the flame as a function of pressure perturbations in the combustor and the impedance of various components. Heat release perturbations were defined as follows:

$$\frac{q'}{Q} = \left[\frac{1}{\gamma} + \frac{P_{3.avg}}{m_{3.avg}} \cdot \left(\frac{1}{q_{st} \cdot \phi \cdot Z_{fi}} - \frac{1}{Z_{ai}} \right) \cdot \left(\Psi_{0,0} + \Psi_{0,1} \cdot \frac{1}{Z_3} \right) \cdot e^{-j \cdot \omega \cdot \tau} + \frac{P_{3.avg}}{Z_3 \cdot m_{3.avg}} \right] \cdot \frac{p'_3}{P_{3.avg}} + \frac{A'_{fl}}{A_{fl.avg}} \quad (5\text{-}16)$$

The Ψ terms are the elements of an acoustic transfer matrix,[55] and are defined by the acoustic geometry between station i and station 3. The first term inside the square brackets is the reciprocal of the specific heat which represents the change in reaction rate that accompanies the increasing density produced by pressure perturbations. The term multiplied by $e^{-j\omega\tau}$ represents the production and transport of fuel/air ratio perturbations. Notice that this term is an effective difference between the (reciprocal) air and fuel impedance at station i. If the impedance of these terms is large, the response is small, meaning the fuel/air perturbations are small. For example, choking both the fuel and the air supply would correspond to large impedance, such that pressure perturbations could not modulate the flow of fuel or air. However, practical injectors cannot use a choked supply of air, so that the air flow will typically be modulated in accordance with Z_{ai}. The concept of varying the fuel system characteristic impedance enters through the term Z_{fi}, which is controlled by the geometry of the fuel system as well as the fuel gas properties. In order for Z_{fi} to have an impact on the overall dynamics it must be comparable to the value of $Z_{ai}/q_{st}\phi$.

The last term inside the square brackets, $P_{3.avg}/Z_3 m_{3.avg}$, represents the variation of flow entering an (assumed) fixed flame position. The mass flow of fuel/air entering the flame is inversely proportional to the impedance at station 3. If the impedance at this position is low, small pressure perturbations will produce relatively large acoustic velocity perturbations. It is likely that this term would need to be modified to account for translation or distortion of the flame in the oscillating flow.[56] Direct translation of the flame would reduce the magnitude of this term, while distortion could be accounted for in the flame area term $A'_{fl}/A_{fl.avg}$. While the exact contribution of these terms is difficult to quantify, it has been shown that adjustments to the fuel impedance,[39,57] or fuel time lag[58] play a significant role in stabilizing the flame. For this reason, in the present analysis, it is most useful to consider just the *change* in the term multiplying $e^{-j\omega\tau}$ as the fuel system impedance is modified through changes in the fuel composition.

To evaluate the effects of varying the fuel composition, a number of fuel combinations were investigated and are shown in Table 5-4. The Base Case and Cases 1 – 4 are similar to those tested in the Rijke tube discussed earlier. As before, Cases 1-3 have the same Wobbe number although a different chemical composition. Cases 4 and 5 are extreme cases composed of primarily propane gas with Case 4 being 100% propane and Case 5 is a blend of propane and nitrogen. Although Case 5 is not a natural gas, the nitrogen was added as a means of controlling the Wobbe number and provides a means of evaluating the ability of Wobbe number in predicting the combustor response.

Included in Table 5-4 is the equivalence ratio, ϕ, at which the computational of the overall system stability was conducted as well as the speed of sound in the fuel gas and in the fuel-air mixture at an ambient temperature of 298 K. At the same temperature the speed of sound in air is approximately $c_{o_air} = 346$ m/sec. The equivalence ratio was selected in order to produce a flame temperature of approximately $T_f \approx 1750$ K which is representative of a lean-premixed turbine during typical operation.

Table 5-4: Fuel Blends Tested In Fuel Injector Impedance Variability.

	Base Case	Case #1	Case #2	Case #3	Case #4	Case #5
CH_4 (%)	100	85	87.14	90	0	0
C_2H_6	0	15	10.74	5	0	0
C_3H_8	0	0	2.12	5	100	62.3
C_4H_{10}	0	0	0	0	0	0
N_2 (fuel)	0	0	0	0	0	37.7
Wobbe#	50.36	52.69	52.68	52.66	75.73	50.80
ϕ	0.65	0.65	0.65	0.65	0.65	0.65
co_mix (m/sec)	345	344	344	344	338	338
co_fuel (m/sec)	450	421	421	421	252	279
Zch_mix (Pa.sec.m-1)	406	407	407	407	414	414

Given the lean fuel-air mixture typical of today's LPM turbines, even with a modest change in fuel composition, the reactant mixture will remain predominantly air, and very little change in the characteristic impedance ($Z_{ch\text{-}mix}$) downstream of the premixer is expected as shown in Table 5-4. However, pressure perturbations generated inside the combustor can produce resonance that propagates upstream to the fuel injector. The magnitude and phase of the fuel response is determined by the fuel system acoustic impedance. Prior to mixing, the fluid in the fuel injector is 100% fuel, thus changes in the fuel composition will have a significant impact on the characteristic impedance, and therefore the acoustic response, inside the fuel injector. It is well known that resonance in the fuel system can drive perturbations in the equivalence ratio that subsequently produces variations in the heat release within the combustor.

Calculations of the acoustic impedance of the fuel injector were made using Equation 5-15 and acoustic relationships as specified in Munjal[42]. The acoustic impedance is a function of the characteristic impedance and properties of the volume. Figure 5-20 and Figure 5-21 show the magnitude and phase, respectively, of the acoustic impedance inside the fuel injector for the various fuel combinations shown in Table 5-4. Comparisons of the magnitude between the 100% methane case (Base) and Cases 1-3 exhibit a peak in amplitude at approximately the same frequency, although the Wobbe number differs from 50.4 to 52.7. The phase angle shown in Figure 5-21 for these cases follows the same trend as all four cases produce similar results. These findings are in agreement with experimental results from the Rijke tube discussed previously.

Experimental results from operating on fuels of Case 4 and 5 produced dynamic responses that differed from those of the Base Case in terms of both amplitude and phase even though Case 5 has a similar Wobbe number (50.8) as the 100% methane (50.4) used as the Base fuel. The propane / nitrogen blend of Case 5 has a Wobbe number close to that of the Base Case, however the speed of sound in the fuel is considerably different between the Base Case and the two high percentage propane fuels. This could contribute to the strong difference in gain and phase that is exhibited here. However, it should be noted that the high percentage propane fuels utilized here are not representative of commercially available CNG or LNG fuel blends, but were utilized to help differentiate between physical and chemical effects of the fuels on combustion dynamics.

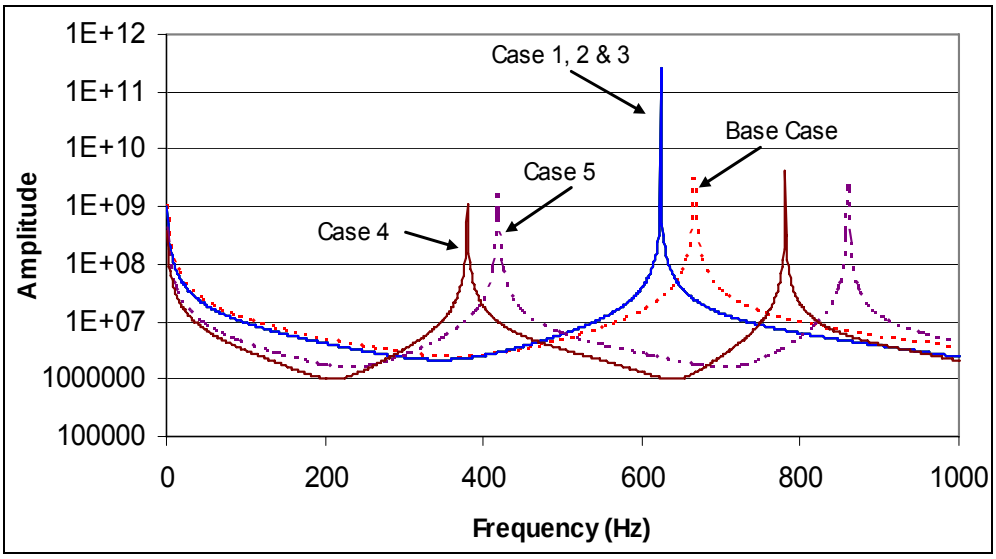

Figure 5-20: Magnitude of the Acoustic Impedance of the Fuel Injector under Varying Fuel Composition.

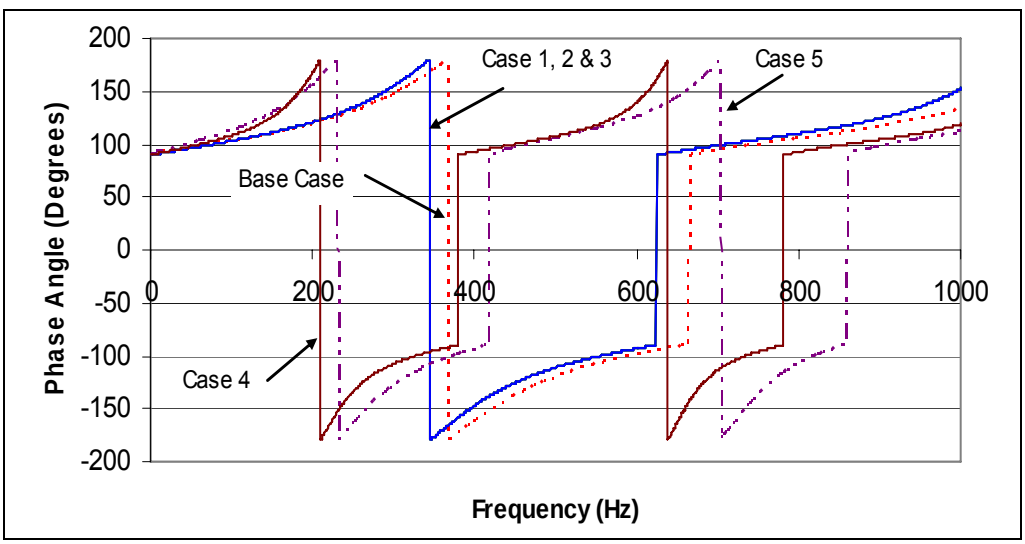

Figure 5-21: Phase Angle of the Acoustic Impedance of the Fuel Injector under Varying Fuel Composition.

In addition to general changes in the characteristic impedance due to fuel composition, variability also alters the transmission and reflection of acoustic waves at the interface between fuel and air in the pre-mixer. This may help account for the vast differences in the response between the Base Case and Cases 1-3 compared to Cases 4 and 5. For the Base Case and Cases 1-3 the ratio of fuel characteristic impedance to the characteristic impedance of the air at the fuel injector / pre-mixer interface is $Z_{fuel} / Z_{air} = Z_{int} = 0.7 – 0.76$ and for Cases 4 and 5, $Z_{int} \approx 1.05$. Assuming that a wave propagating from the combustor encounters the impedance difference at the interface within the pre-mixer, for $Z_{int} < 1$ a positive pressure in the incident wave is reflected as a positive pressure (no change in phase). However, when $Z_{int} > 1$ a positive pressure is reflected as a negative pressure producing a 180° phase shift. Additionally, when $Z_{int} = 1$ there is complete transmission and no waves are reflected. If an acoustic wave was permitted to

propagate through the combustor upstream to the pre-mixer and fuel injector, it is the latter case in which $Z_{int} = 1$ and little energy is reflected at the interface, that would permit the largest amplitude wave to travel into the fuel injector and produce the greatest fluctuations in the equivalence ratio.

Although the driving mechanisms that produce thermoacoustic instabilities are the result of a closed loop feedback, acoustic perturbations that result in large shifts in the acoustic response in the fuel injectors (as shown in Figure 5-20 and Figure 5-21) may not necessary propagate downstream to influence variations in the heat release rate at the same phase and gain. Evaluating the open-loop response of the system, G(s) H(s), it is possible to estimate the closed loop dynamic response to fuel variability and observe the impact of the gain and phase shifts observed in the fuel injector shown in Figure 5-20 and Figure 5-21. The open-loop response is given by G(s) H(s), where

$$G(s) = \frac{\frac{q'}{Q_{avg}}}{\frac{p'_3}{P_{3.avg}}} \quad \text{and} \quad H(s) = \frac{\frac{p'i}{P_{i.avg}}}{\frac{q'}{Q_{avg}}} \tag{5-17}$$

Figure 5-22 is a plot of the magnitude and phase of the open-loop response from the Base Case in which the fuel is 100% methane. This plot shows a peak gain for oscillations of approximately f = 300 Hz, which is accompanied by a sudden shift in phase. Although having varied concentrations of methane, ethane and propane, the open-loop response from Case 1-3 were identical and shown in Figure 5-23. The open-loop response produced from these fueling options displayed considerable agreement to the Base Case as well. The three cases (Cases 1-3) were composed primarily of methane with small percentages of the remaining other constituents and the Wobbe Index did differ from that of the Base Case (see Table 5-4).

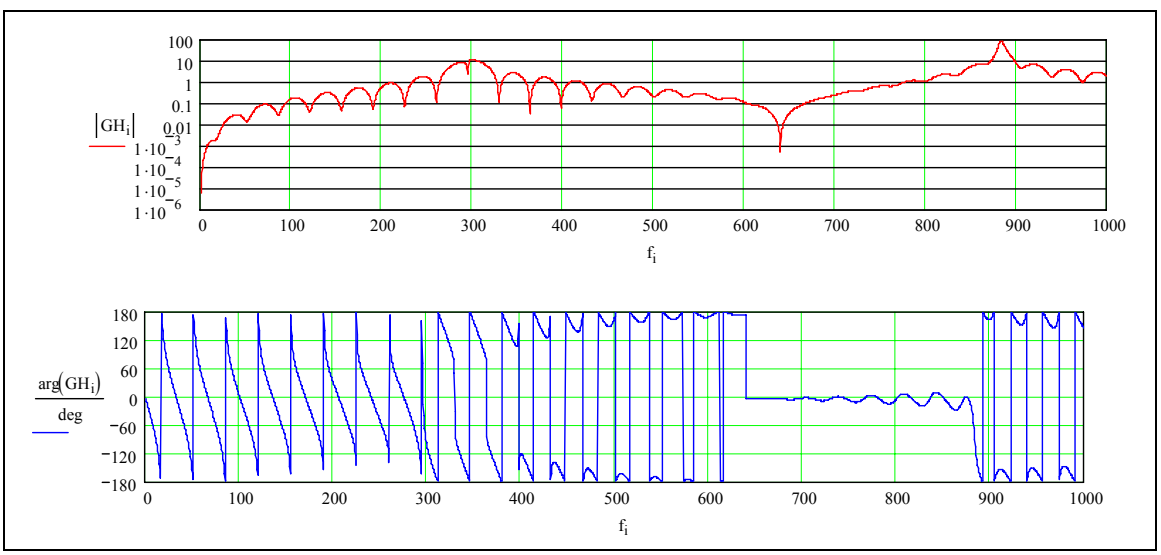

Figure 5-22: Open-Loop Magnitude and Phase from Base Case.

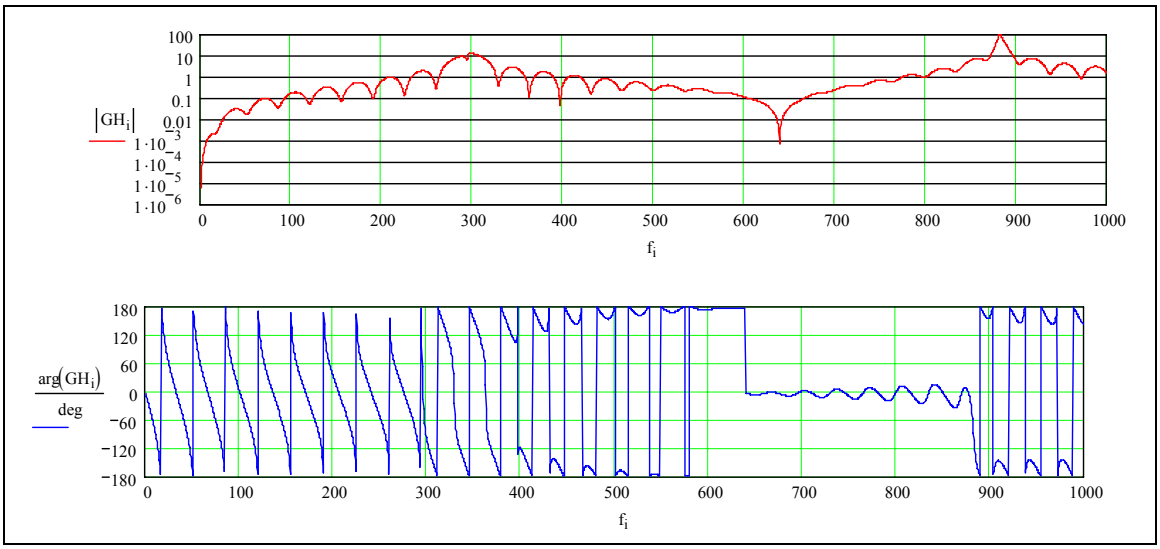

Figure 5-23: Open-Loop Magnitude and Phase from Case 1–3.

Case 5 utilizes a combination of propane and nitrogen in order to produce a fuel that has a Wobbe number similar to the Base Case. Although the composition may not be representative of typical natural gas supplies, it does provide a means of evaluating the physical and chemical nature of fuel variability on the dynamic response. Figure 5-25 is a plot of the gain and phase of the open-loop response of the combustor while operating on Case 5 fuel. Observe the changes in gain at the peak frequencies, and the similar trend which is seen for the 100% propane case shown in Figure 5-24. There is also a shift of approximately 60° and 100° in phase for Case 5 and 4 respectively when compared to the Base Case at approximately 300 Hz. This shift in the overall response for high percentage propane fuels is in agreement with experimental results and is supported by the significant change in acoustic impedance observed in the fuel injector.

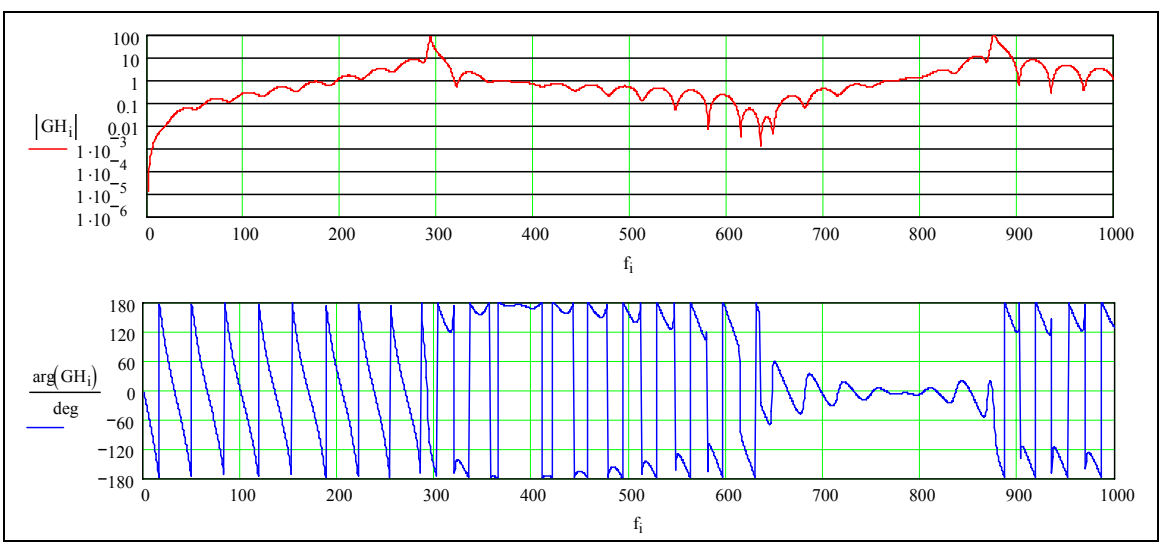

Figure 5-24: Open-Loop Magnitude and Phase from Case 4, Pure Propane.

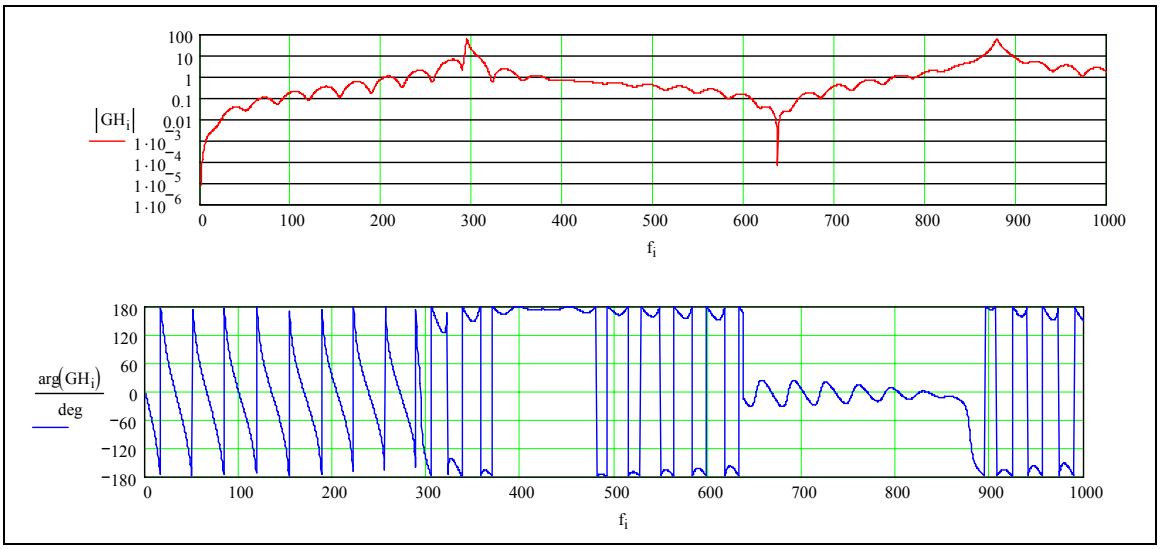

Figure 5-25: Open-Loop Magnitude and Phase from Case 5, Propane + N_2.

In summary, this analysis has considered how fuel variability is expected to change the overall dynamic response of premixed combustor. Based on this analysis, even with a constant *flame* dynamic response, the acoustics of fuel injection will change the *overall* dynamic response with changing fuel composition. Significant changes in the dynamic response were observed for extreme changes in fuel composition, however only a small shift in the phase and gain of the open-loop response were seen when evaluated using fuel comparable to those expected in typical domestic and imported natural gas supplies. For systems operating well inside their stability window this would seem to suggest that changes in fuel composition may not pose a serious concern. However, systems that are marginally stable may experience difficulties in maintaining stability similar to those occurring as a result of typical variances in operating conditions (e.g., changing inlet air temperature). These theoretical results are limited to the case studied here, and again, assume a constant flame dynamic response. In the next section, the atmospheric development combustor will be used to address the same questions experimentally, and will show similar behavior as the analytic model.

5.10 Atmospheric Pressure Development Combustor

This experimental setup has been described in previous work.[59,60] The combustor is shown in Figure 5-26, and a close-up of the fuel injector resonator assembly is shown in Figure 5-27.

Air enters the 12.7 mm x 26.6 mm premixer annulus at the left through a sintered metal plate. This plate serves as an acoustic termination at the upstream end of the combustor. The air is swirled by a slotted disk that is 6.4 mm thick along the flow axis. Fuel is injected into the premixing annulus using the fuel injector shown in Figure 5-27. The tip of the premixer centerbody is fitted with a conical expansion made from a commercial compression-fitting ferrule. The ferrule axial length is 7.3 mm with a larger OD of 17.3 mm. This ferrule serves to provide flow acceleration at the tip of the premixing annulus, and prevents flame anchoring inside the premixer passage. This insures consistent flame anchoring at the step expansion, and has been shown to improve data repeatability.

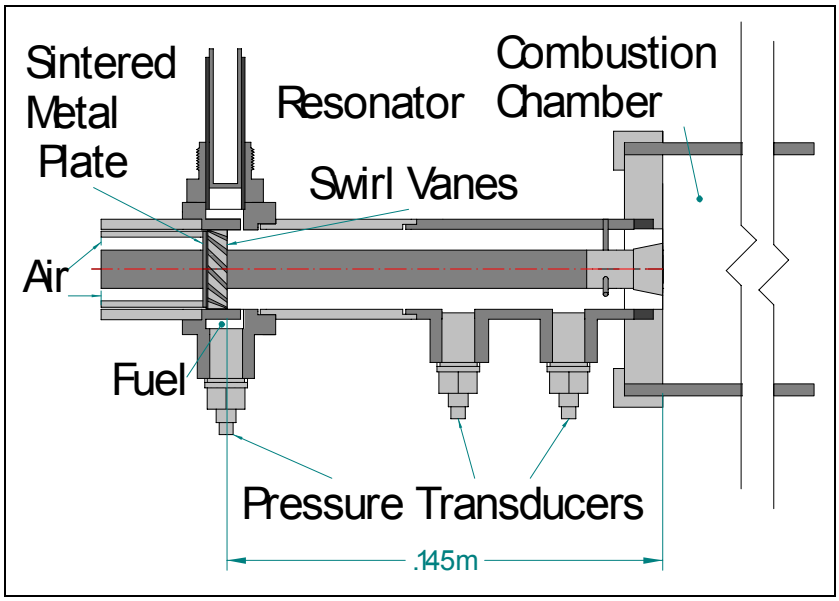

Figure 5-26: Schematic of Atmospheric Pressure Development Combustor.

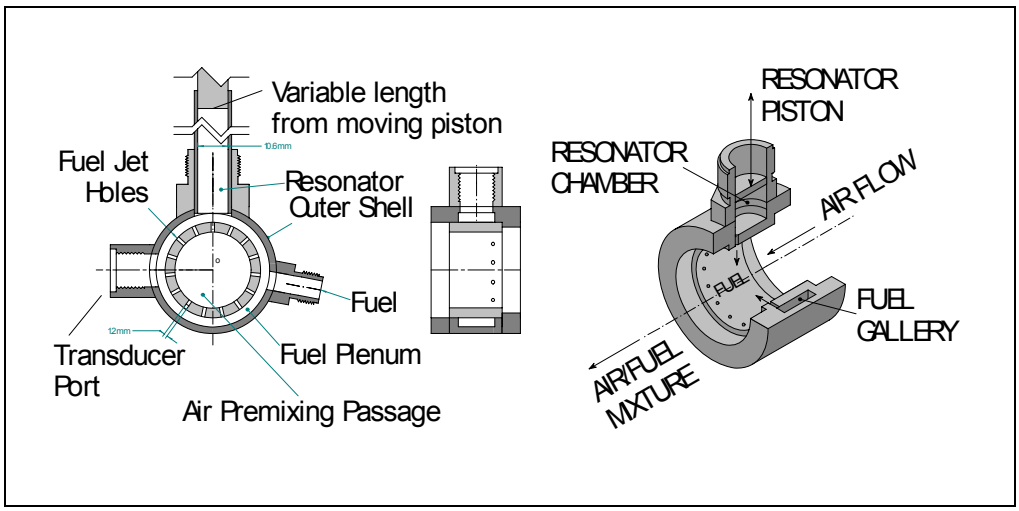

Figure 5-27: Cross-section of Fuel Injector/Manifold.

The combustor wall is a quartz tube with an 80 mm inside diameter and a 0.6m length. The entire combustor is located inside an exhaust duct, supplied with dilution air, and equipped with a silencing muffler system. The exhaust duct diameter (35 cm ID) is significantly larger than the tube combustor. Acoustic analysis demonstrates almost no coupling between the exhaust plenum and the combustor acoustics at observed instability frequencies.

Dynamic pressures are recorded using Kistler Model 206 pressure transducers. Pressure transducers mounted directly in the premixer annulus are used to record the magnitude of acoustic velocity in the premixer, affirming the relative size of both fuel and air flow fluctuations. Methods to calculate the acoustic velocity from pressure signals can be found in previous work[61] or any standard acoustics textbook.[62] Dynamic pressures in the combustor are recorded with a pressure transducer mounted on a short section of tubing on the back of the combustor dome.

Signals are acquired and analyzed with an HP35670A Dynamic Signal Analyzer, and recorded for later analysis using a TEAC Model LX-10 high-speed data recorder. The transducers and data acquisition/processing have been verified for consistency by mounting all the transducers in a common plane perpendicular to the axis of a 7.5 cm duct. By using plane waves generated by a loudspeaker in the duct, all transducers have demonstrated essentially the same gain and phase relative to the input signal. Over the range 0-400Hz, the phase angles differ from –3 to +5 degrees, and the gains are 1 ± 0.06 relative to one of the transducers.

The combustor has been operated on natural gas fuel with a nominal composition of 93.7 % CH_4, 4.3 % C_2H_6. The remainder is inert or higher hydrocarbons as determined by GC analysis. The average Wobbe Index was 51.5 MJ/m^3. Fuel and air are metered with flow loops that are designed following standard protocols, and are within 1% of the flow measured by calibration standards. The combustor was operated over a nominal range of heat inputs from 15 to 45 kW (50 to 150 x 10^3 BTUH).

Experiments to investigate the effects of fuel composition on combustion dynamics were performed as follows. The fuel-air ratio, bulk premixer velocity, and fuel composition were controlled as input variables. The dependent variables included RMS pressure levels, OH* chemiluminescence, flame images, stability margins, and acoustic impedance changes in the fuel manifold. A series of tests were first completed for the reference case (i.e., natural gas) at reference velocities of 20.0, 22.5, 25.0, 27.5 and 30.0 m/sec and equivalence ratios starting from 0.90 and decreasing in increments of 0.02 until the flame detached from the tip of the premix injector. Three other fuel blends were tested: propane (commercial grade), propane blended with nitrogen to match the Wobbe Index of the reference case natural gas, and a 90% natural gas / 10% propane blend (Table 5-5).

Table 5-5: Fuel Blends Tested in Fuel Injector Impedance Variability.

	Case #1	**Case #2**	**Case #3**	**Case #4**
Site NG	100	0	0	90
Propane	0	100	62	10
Nitrogen	0	0	38	0
Wobbe (MJ/m^3) (BTU/scf)	51.5 1382	76 2039	51.5 1382	59.5 1597

The combustion air flow rates for these tests were fixed at the same flow rates used in the natural gas tests. The fuel flow rates were set such that the adiabatic flame temperatures (via standard equilibrium codes[7]) matched the adiabatic flame temperatures of the natural gas reference cases. Results that are typically expressed as a function of reference velocity and equivalence ratio will be expressed here as a function of reference velocity and adiabatic flame temperature because gas turbine control systems typically operate at a fixed firing temperature.

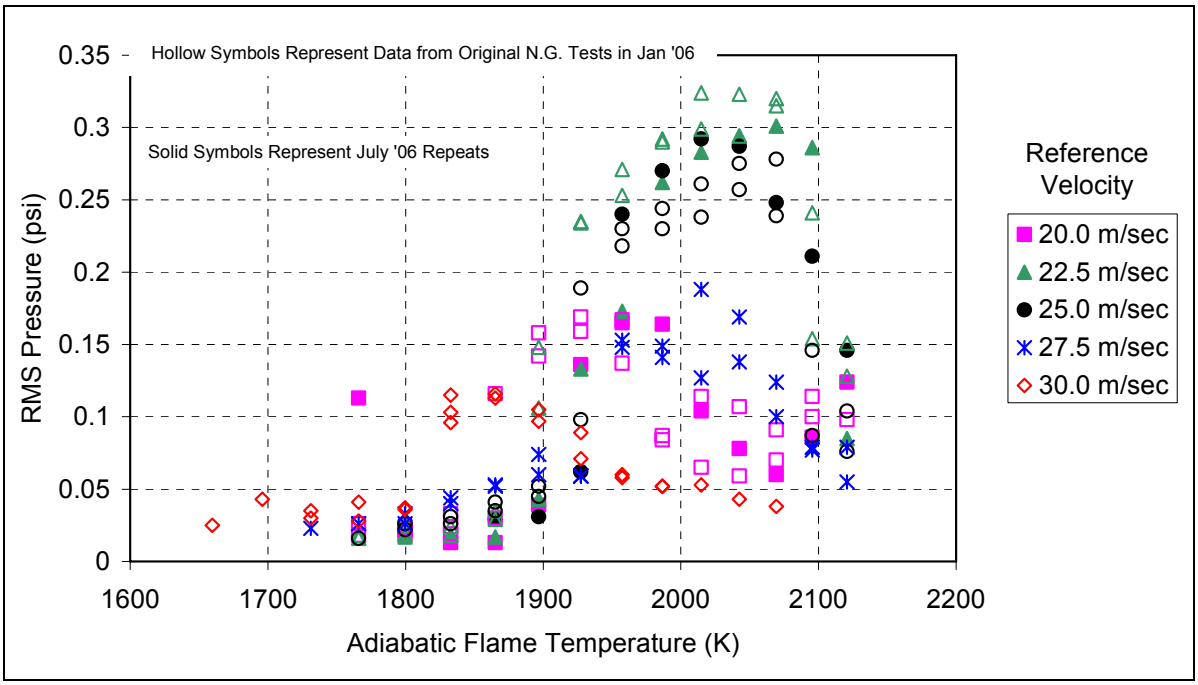

Figure 5-28: Amplitude of Pressure Oscillations for the Natural Gas Reference Case.

5.10.1 Dynamic Pressure Amplitudes versus Fuel Composition

The pressure amplitude results from the base case (i.e., natural gas, Wobbe = 51.5 MJ/m^3) fuel are shown in Figure 5-28. This combustor is typically steady at lean operating conditions (low flame temperatures) and makes a transition to unsteady combustion with large amplitude pressure oscillations as the flame temperature is increased by increasing the fuel/air ratio. The amplitude and frequency of these oscillations and the flame temperature at which the transition occurs varies from one reference velocity to another. At a reference velocity of 20 m/sec, the pressure amplitude was generally low (< 0.05 psi) until an adiabatic flame temperature of 1900 K was reached, where the pressure amplitude increased to 0.15 psi. These moderate pressure amplitudes continued until a temperature of approximately 2000 K was reached, where rms pressure decreased to the 0.05-0.10 psi range. At reference velocities of 22.5 and 25.0 m/sec, the location and amplitude of the combustion instabilities differed from those at 20.0 m/sec. At these velocities, pressure amplitudes were low until an adiabatic flame temperature of 1900-1950 K was reached, where there was a sudden transition to amplitudes of 0.22-0.33 psi, with the amplitudes beginning to decrease again when the flame temperature was increased to 2100 K. The unsteady behavior at a reference velocity of 27.5 m/sec was similar to that at 22.5 and 25.0 m/sec, except that the amplitudes were lower (approximately 0.17 psi) and the decrease in amplitude was less abrupt as the flame temperature was increased. The pattern changes again at 30 m/sec, where the peak amplitude reduced to 0.12 psi with a transition from steady to unsteady at 1830 K.

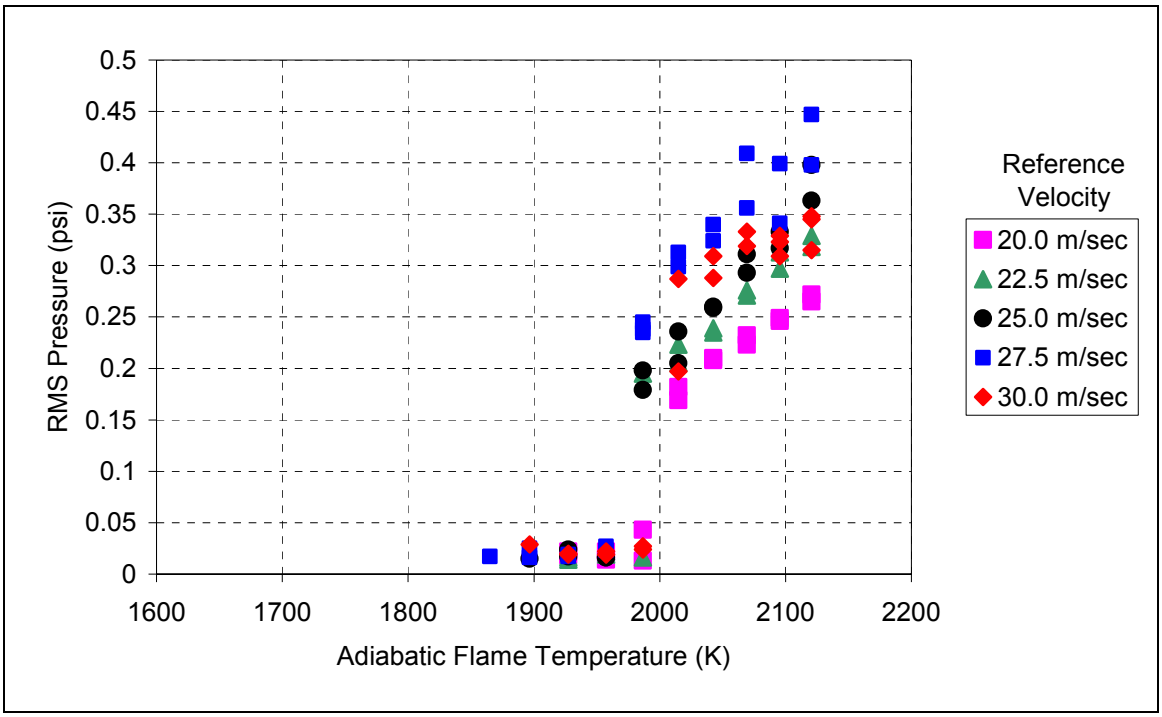

Figure 5-29: Amplitude of Pressure Oscillations for the 100% propane tests.

A similar figure for the commercial propane case (Wobbe = 76.0 MJ/m^3) is shown in Figure 5-29. This case represents the extreme of chemical composition and Wobbe Index. It is readily evident that the combustion instability patterns for this fuel are quite different from those of natural gas. At all reference velocities, there was a transition from steady to unsteady combustion at 1990-2015 K, with amplitudes increasing as the adiabatic flame temperature was further increased toward 2100 K. The various reference velocities had distinctive pressure amplitudes. Also note that compared to Figure 5-28, the amplitude of the oscillation is larger. This larger amplitude with propane is consistent with expectations from the theoretical model presented in Section 5.9, and also from observations of the dynamic flame response of a simple flame in Section 5.7.

A similar plot for a fuel consisting of 62% propane and 38% nitrogen (WI = 51.5 MJ/m^3) is shown in Figure 5-30. This blend has the same Wobbe Index as the natural gas used in generation of the Figure 5-28 data, but the pattern is clearly much more like that of the undiluted propane in Figure 5-29. There appears to be a transitional adiabatic flame temperature around 2030 K, above which oscillations begin. The five reference velocities less distinct in regards to their pressure amplitudes than in Figure 5-28 presumably due to the need to precisely meter dilution N_2 in this case compared to pure propane.

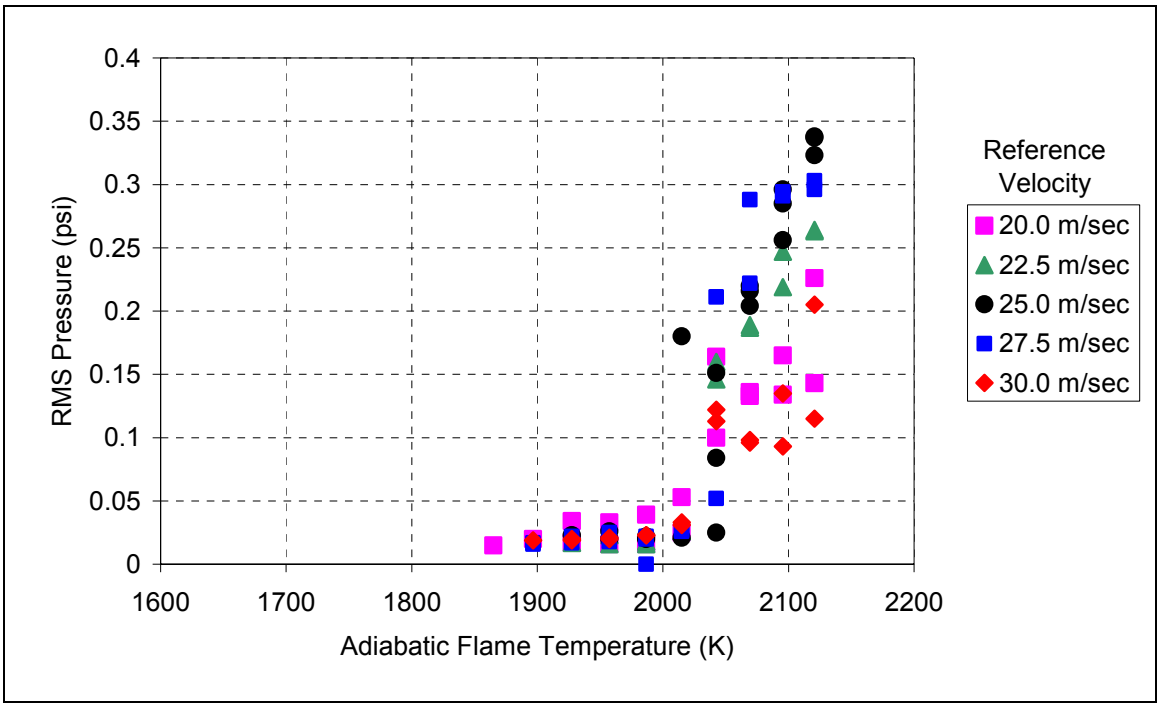

Figure 5-30: Amplitude of Pressure Oscillations for the Propane/Nitrogen Blend Tests.

Comparing Figure 5-28 and Figure 5-30, two fuels having the same Wobbe Index, but different composition demonstrate a significantly different dynamic response. This is consistent with the theoretical results presented in Section 5.9, and demonstrates that with fuel variability, methods to hold Wobbe Index constant will not produce constant dynamic response from premixed combustion systems. Based on the theoretical analysis, the changing fuel system impedance cannot be compensated by methods to maintain constant Wobbe, such as N_2 addition.

Experimental cases presented in Figure 5-31 through Figure 5-33 considered a dramatic change in fuel composition, but with significant nitrogen blending to hold a constant Wobbe Index. Such a large change in fuel composition is not representative of what is expected in practice. In Section 5.9, it was shown that more modest changes in fuel composition would not have as significant an effect. To affirm this expectation, tests were carried out using 90% natural gas and 10% propane (WI = 59.5 MJ/m^3). This is a unrealistically high propane level for natural gas supplies, but was used to show the impact of fuel composition. Pressure amplitude results are shown in Figure 5-31, with hollow symbols representing natural gas, and solid symbols representing the blend with propane. These data are very similar to those of the base natural gas case (Figure 5-28). The data for the natural gas/propane blend falls within the patterns described for natural gas in Figure 5-28, and the amplitude is similar. Not as many data points were collected for the blended fuel because the behavior was so similar to the natural gas.

The results presented in Figure 5-28 through Figure 5-30 do not support the hypothesis that the Wobbe Index alone can fully predict a combustor's dynamic behavior for a change in fuel from propane versus natural gas. However, the results do provide evidence that a combustor with adequate stability margin is relatively insensitive to a "realistic" change in natural gas composition even for changes significantly beyond the NGC+ box. This is consistent with the

analysis of Section 5.9. It is again emphasized that combustors operating right near their stability margin may shift from stable to unstable with changing fuel composition (but this is similar to the effect caused by changes in ambient temperature).

5.10.2 Dynamic Frequency and Flame Position versus Fuel Composition

The flames produced by the four fuel blends described in Table 5-5 can be characterized by quantities other than the RMS of the pressure oscillations. Features such as the frequency of the unsteady combustion oscillations and even measures extracted from photographic images of the flame, such as the center of "mass" (i.e., intensity) along the axis of the combustion chamber, can be used. The dominant frequencies extracted from spectral analysis of the pressure oscillations are plotted in Figure 5-32. As a general trend, frequencies tended to increase as the fuel/air ratio was increased and as the reference velocity was increased, both of which produced higher temperatures in the combustor. This general trend does not always hold, as the combustion oscillations can change suddenly to another frequency "mode" when conditions at the initial frequency become unfavorable. Note also that frequencies are more scattered or noisy in conditions where the pressure amplitude was low and there was no distinct dominant frequency. As with pressure oscillation amplitude, the frequency data also indicates that 90% natural gas plus 10% propane is similar to the baseline natural gas fuel. The 62% propane / 38% nitrogen is similar to 100% propane fuel, and the frequencies themselves are typically slightly lower than with the natural gas cases. Again, a frequency shift like this was suggested by the analysis shown from the open-loop response model presented in Figure 5-22 through Figure 5-25.

Digital color photographs of the flames, using manual mode to ensure consistent focus, f-stop, and "shutter" speed, were converted to gray-scale images and were integrated to compute the first moment along the axis of the combustor to find a center of "mass" or intensity, as an index of flame length and position. The results are shown in Figure 5-33. The high-temperature (richer) flames tended to be short and close to the premix injector outlet. Some of their intensity signature may have been due to glowing of the quartz combustion chamber walls. As the flame temperature was reduced (i.e., the equivalence ratio was reduced), the center of mass tended to decrease slightly – some of which may be attributed to reduction of the glowing walls and another to a reduction in flame in the "corners" of the combustion chamber. As the adiabatic flame temperature was reduced further, the center of "mass" began to increase rapidly as the flame length began to grow. The flame length in this combustor, not being confined by any restriction in diameter or any tail pipe per se, continued to lengthen until it exceeded the area of the viewing port. Eventually, as the equivalence ratio was further reduced, the flame form would change from an extended conical flame attached to the tip of the premix injector center body to a narrow vortex-shaped flame extending down the center of the combustion chamber. Experience with this combustor has shown that flame extinction occurs shortly after this change in form. When this change occurred, in order to prevent flame extinction, the equivalence ratio was increased and that particular test series was terminated. These features of the flame images (relative length and position; the temperature at which transition to longer flames occurred; the "rate" of flame lengthening, e.g., gradual vs. abrupt; and the low flame temperature or lean limit of operation) can be observed in Figure 5-33. As with the amplitude and frequency of pressure oscillations, the image behavior of the propane/nitrogen blend flames, even though they had the

same Wobbe Index as the natural gas base case, were more like those of 100% propane while the behavior of the 90% natural gas / 10% propane blend was similar to that of the baseline natural gas.

The change in the flame mean position has some practical implications. As described earlier, the flame dynamic response is the part of the combustion feedback loop (Figure 5-18) that is most difficult to predict accurately, and even the static position and shape of the flame are known to affect the overall feedback loop.[52] These data suggest that the flame shape effect is significant for changes from natural gas to propane, but not very large for the natural gas/propane blend. Again, nitrogen/propane at the same Wobbe as the natural gas appeared to behave much like propane itself.

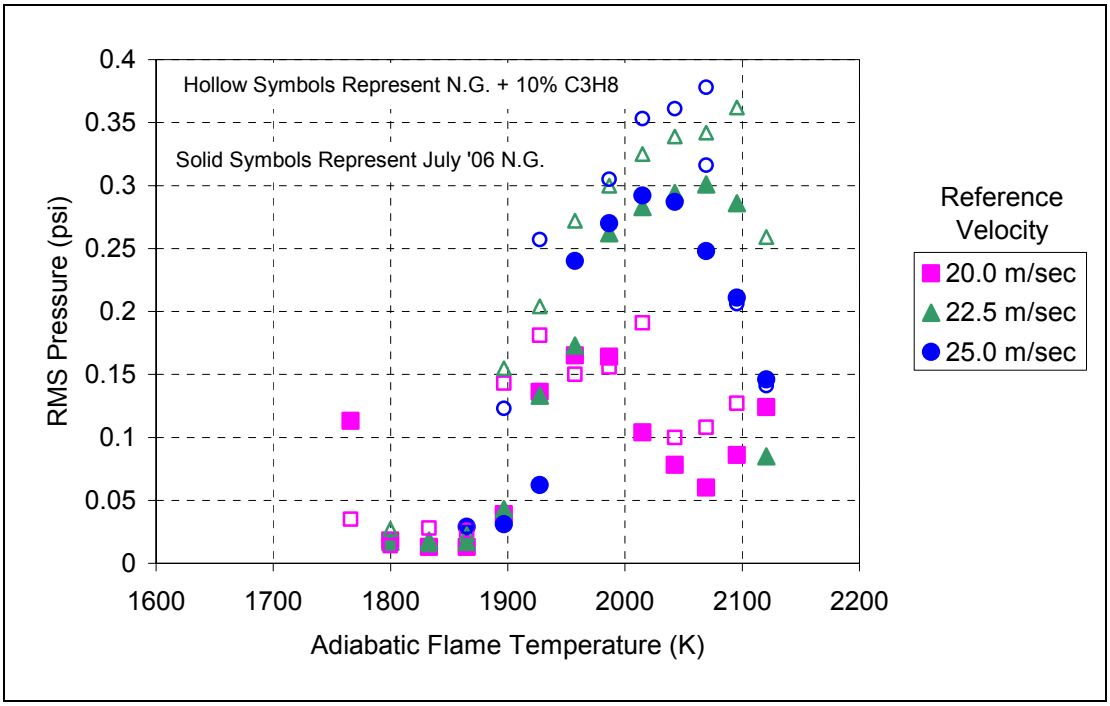

Figure 5-31: Amplitude of Pressure Oscillations for the 90% Natural Gas / 10% Propane Blend. The solid symbols are the base natural gas, and are comparable to Figure 5-28.

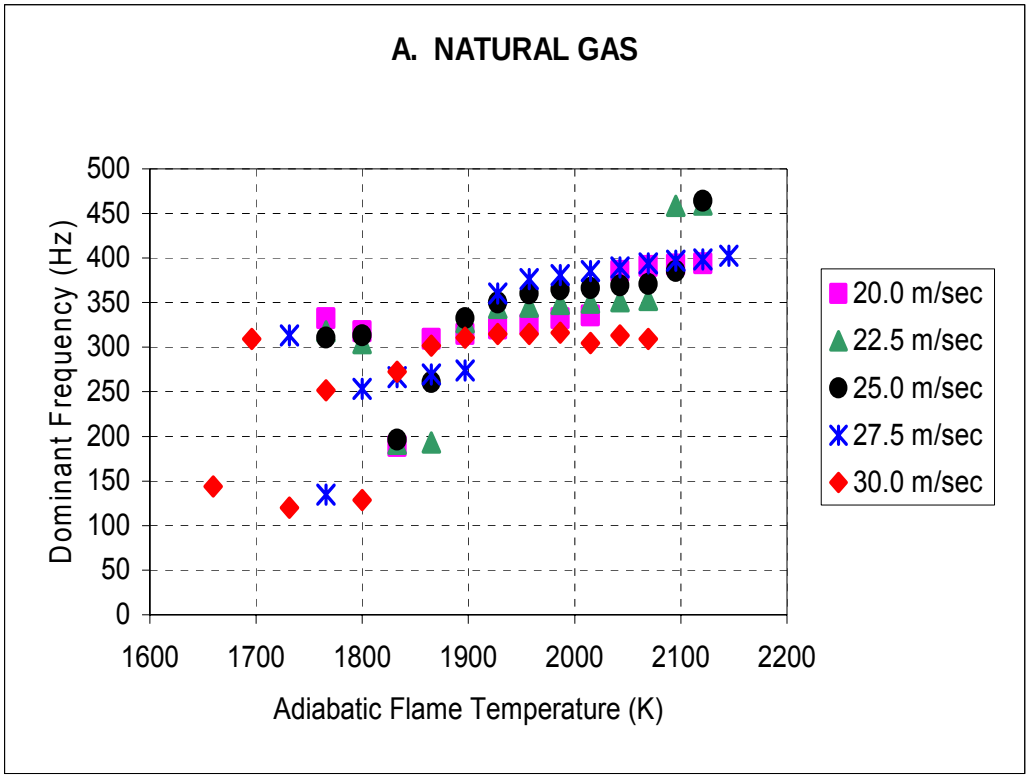
A. NATURAL GAS
Dominant Frequency (Hz)
500
450
400
350
300
250
200
150
100
50
0
1600
1700
1800
1900
2000
2100
2200
Adiabatic Flame Temperature (K)
20.0 m/sec
22.5 m/sec
25.0 m/sec
27.5 m/sec
30.0 m/sec

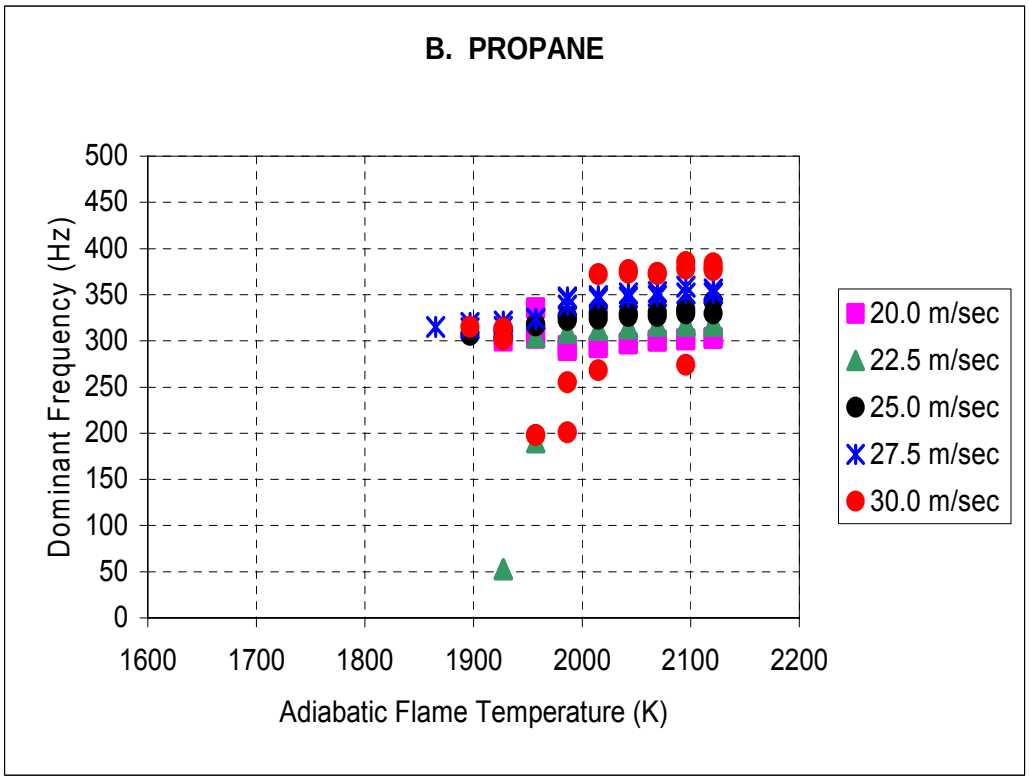
B. PROPANE
Dominant Frequency (Hz)
500
450
400
350
300
250
200
150
100
50
0
1600
1700
1800
1900
2000
2100
2200
Adiabatic Flame Temperature (K)
20.0 m/sec
22.5 m/sec
25.0 m/sec
27.5 m/sec
30.0 m/sec

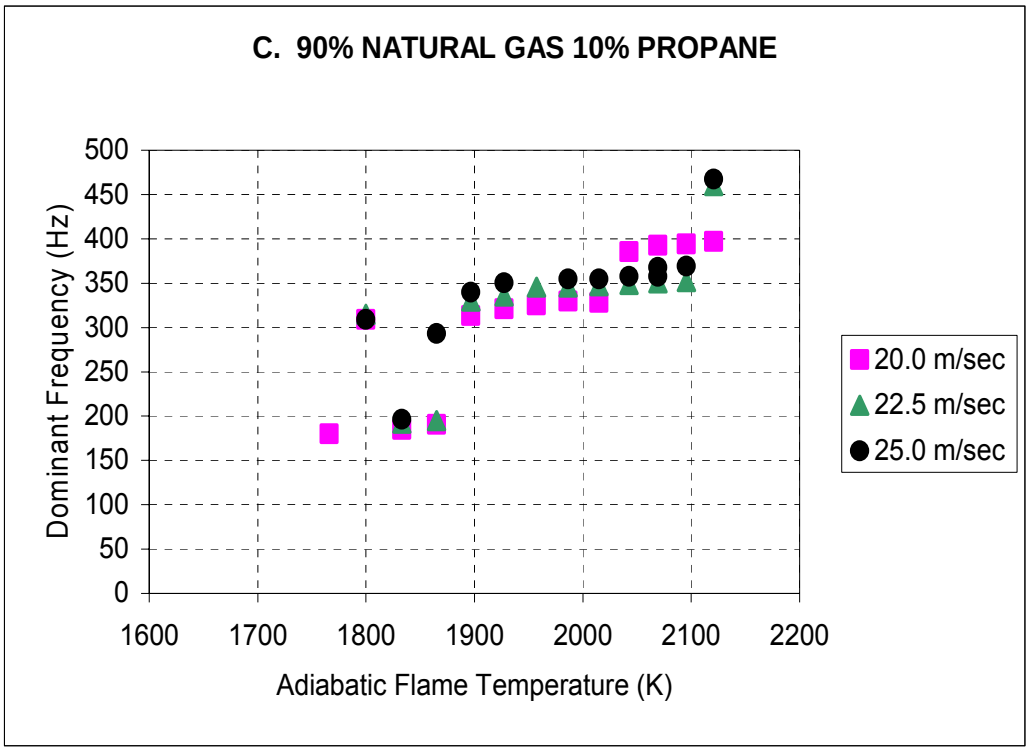

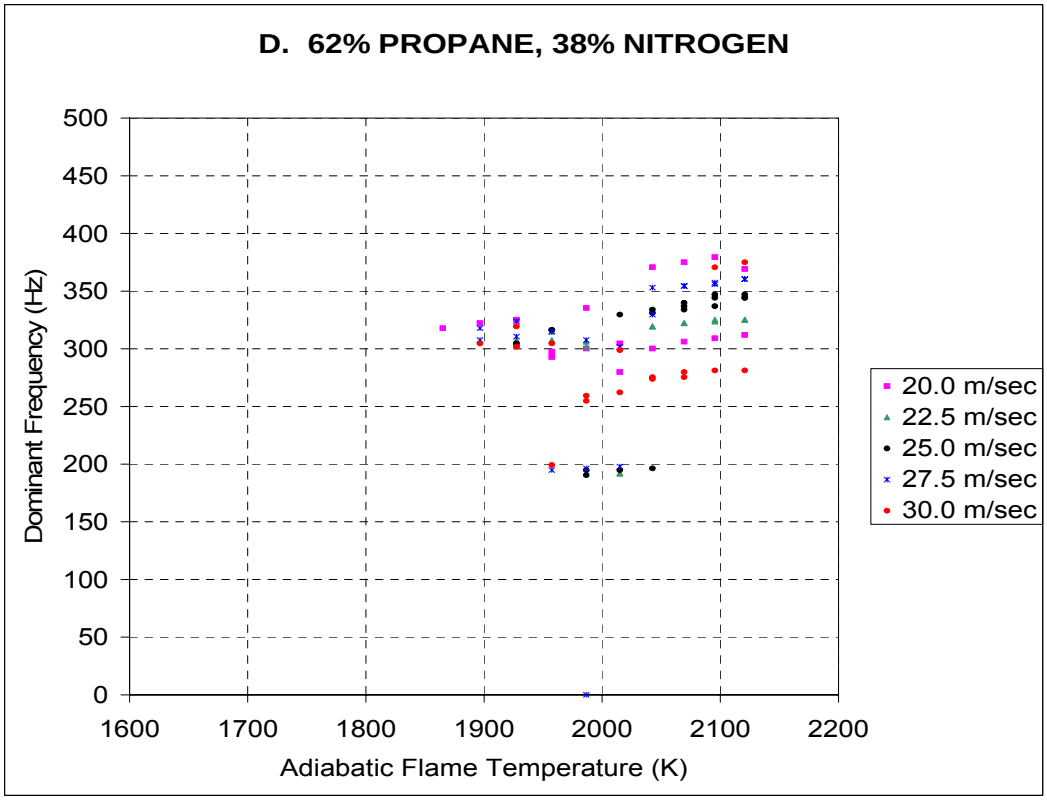

Figure 5-32(a-d): Dominant Pressure Oscillation Frequencies for each of the Four Test Fuels.

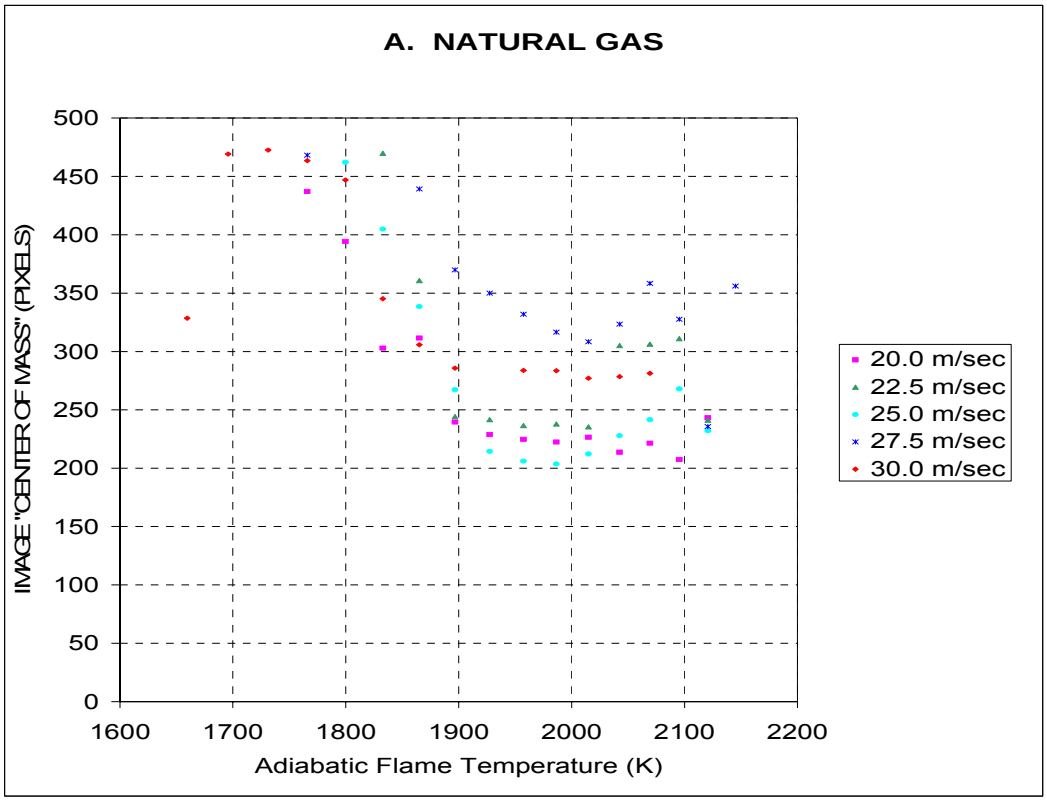
A. NATURAL GAS
IMAGE "CENTER OF MASS" (PIXELS)
500
450
400
350
300
250
200
150
100
50
0
1600
1700
1800
1900
2000
2100
2200
Adiabatic Flame Temperature (K)
20.0 m/sec
22.5 m/sec
25.0 m/sec
27.5 m/sec
30.0 m/sec

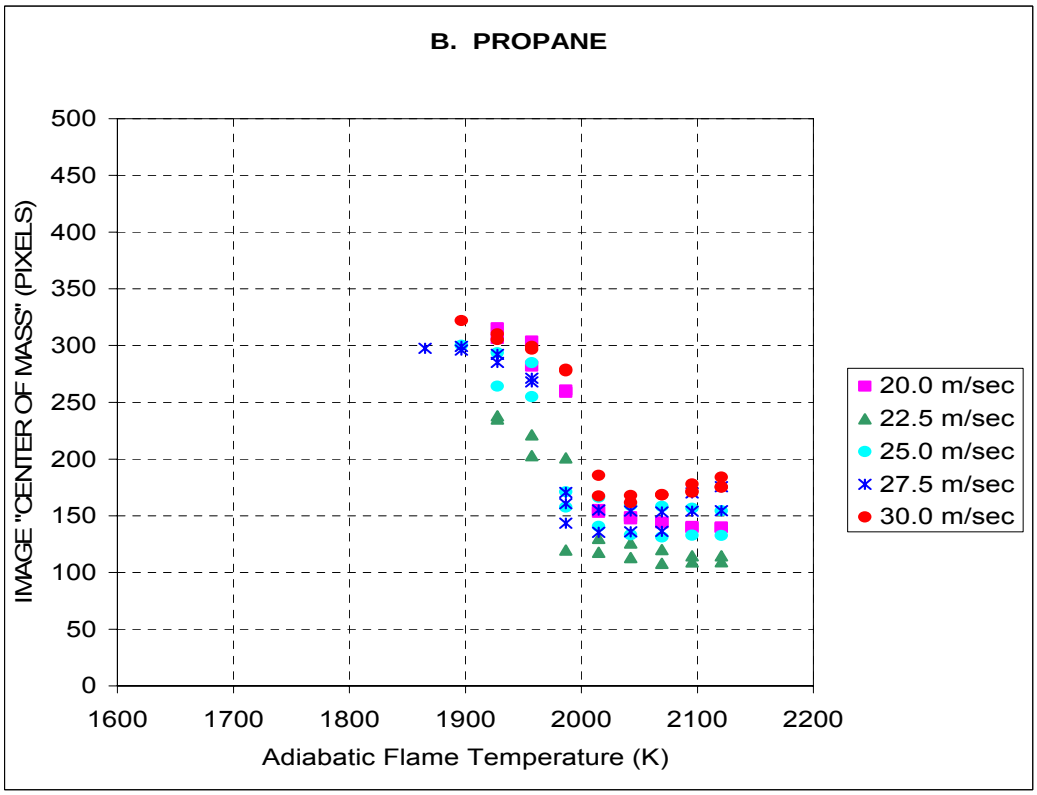
B. PROPANE
IMAGE "CENTER OF MASS" (PIXELS)
500
450
400
350
300
250
200
150
100
50
0
1600
1700
1800
1900
2000
2100
2200
Adiabatic Flame Temperature (K)
20.0 m/sec
22.5 m/sec
25.0 m/sec
27.5 m/sec
30.0 m/sec

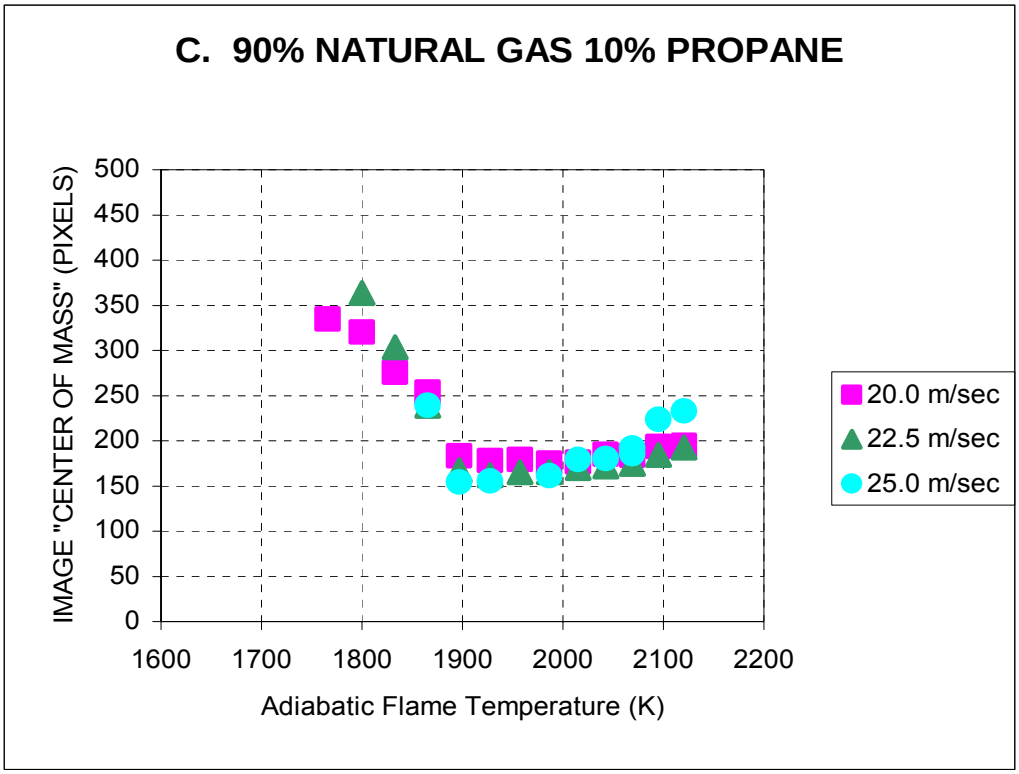

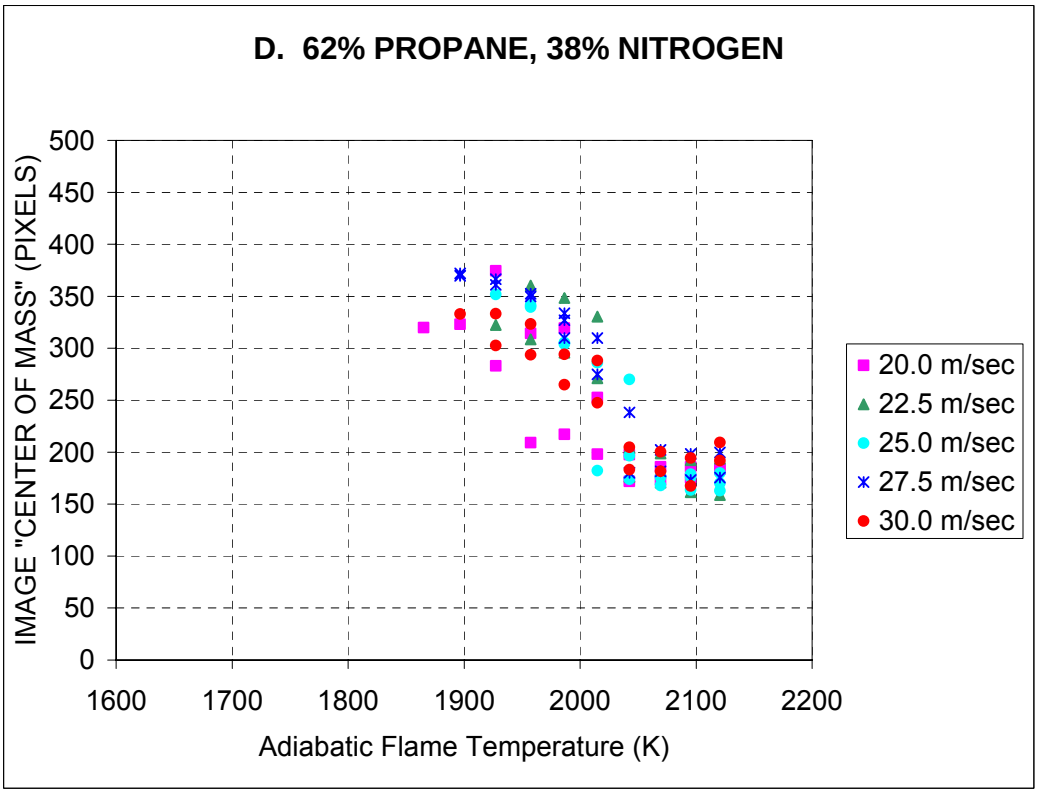

Figure 5-33(a-d): Flame Image Center of "Mass" for each of the Four Test Fuels.

5.10.3 Fuel Effect on Lean Blowout

The background on lean blowout was presented in Section 5.4. It was not expected that any appreciable change in lean blowout would occur when using different hydrocarbons. A different result was observed experimentally. Figure 5-34 shows the operating map for natural gas, propane, 90/10% NG/Propane blend, and the 62% propane/nitrogen blend.

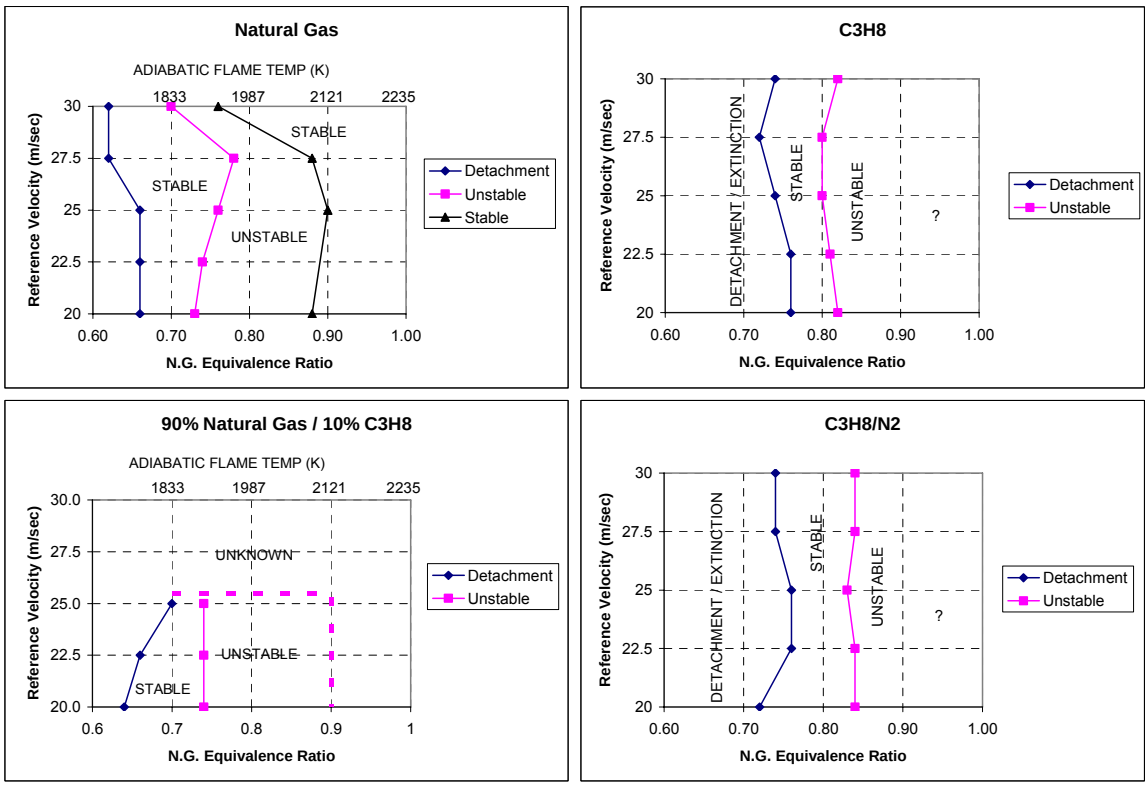

Figure 5-34: Operating Map of the Combustor with Various Fuels.

The surprising feature in this data is the dramatic shift in the lean extinction boundary when comparing propane to natural gas. As explained in Section 5.4, this result is not predicted from current understanding of lean extinction models, however, similar behavior has been observed by Flores et al.[63] These observations may be a result of how the flame is anchored. If, for example, the flame anchor is related to the *turbulent* flame speed, then the observed shift is consistent with the recent recognition that the turbulent flame speed of propane/methane is lower than methane alone, see Figure 5-3. Whatever the mechanism, this point needs further study from a fundamental viewpoint. However, from a practical standpoint, the blend with natural gas and propane was not dramatically changed compared to natural gas. Thus, again, modest gas composition changes associated with LNG are not expected to produce a major shift in lean blowout. Notice also that the propane/N_2 blend appeared very similar to the propane. Thus, in spite of the gigantic difference in Wobbe between propane versus propane/N_2, the blowout behavior is nearly the same. The implication is that Wobbe is not an adequate indicator of the blowoff behavior.

5.11 Single-Injector High Pressure Combustor Apparatus

The high-pressure test rig described in the following paragraphs was designed to study thermo-acoustic instabilities. This rig is capable of conducting experiments at a maximum pressure of 10 atmospheres and a maximum air-flow rate of 1.8 pounds-per-second. A photo of the test rig without the inlet air plenum is shown in Figure 5-35. A schematic cross-section of this test rig is shown in Figure 5-36.

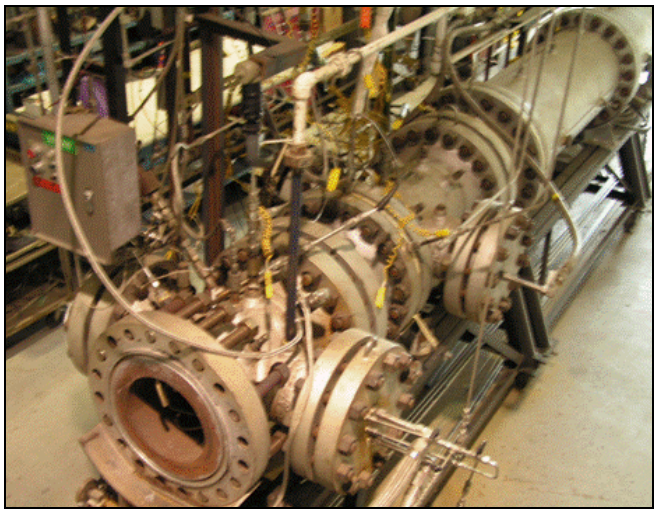

Figure 5-35: Photo of Pressurized Combustion Test Rig.

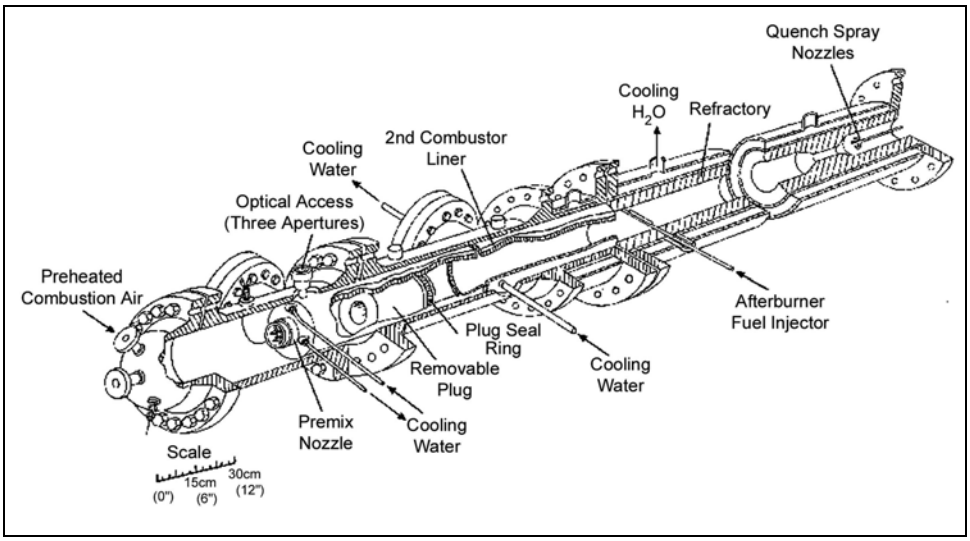

Figure 5-36: Cross-Section of Pressurized Combustion Test Rig.

A non-vitiated air preheater is used to control the inlet-air temperature. Although the preheater is capable of achieving an air preheat temperature of approximately 1000 °F, the maximum inlet-air temperature for the test rig is limited to 650 °F. Preheated air enters the test rig from two separate air flow loops. These air flow loops are described in more detail in the next section. The inlet-air plenum contains a series of three perforated plates to provide a uniform flow and turbulent intensity at the inlet of the fuel-air premixer.

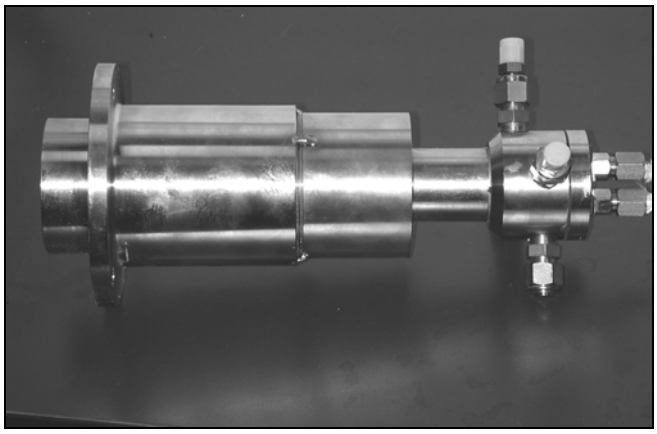

Figure 5-37: Photo of the Fuel-Air Premixer.

The premixer has been designed and fabricated by Woodward Industrial Controls (see Figure 5-37). The centerbody of the premixer is cooled using pilot fuel that is injected into the combustion region via 12 small jets (see Figure 5-38). This pilot fuel stabilizes the flame near lean-extinction, and for all of the cases described in this report, the pilot fuel flow split is maintained at 5 percent of the total fuel flow.

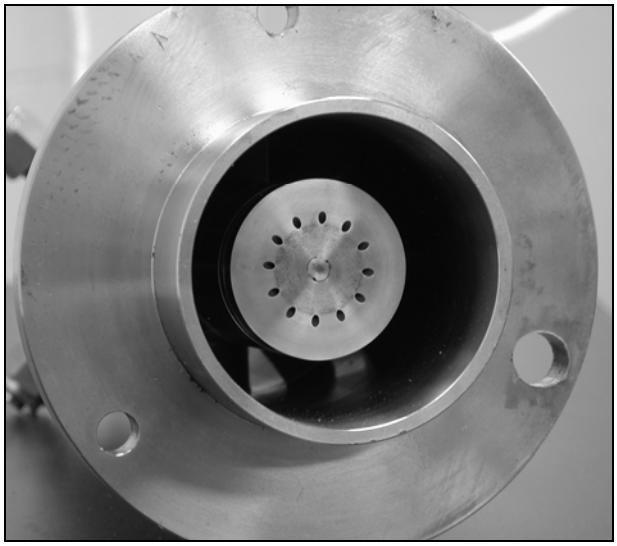

Figure 5-38: Photo of the Centerbody Tip and Pilot Fuel Injection.

The combustion liner is constructed from a water-cooled stainless-steel pipe with a 19.4 cm (7.6 in) inside diameter. The cooling water is re-circulated and does not mix with the products of combustion. A cylindrical refractory insert is installed 0.78 meters (31-inches) downstream of the combustor inlet. This refractory insert reduces the flow passage from a 19.4 cm (7.6-in) diameter to 8.9 cm (3.5-in) diameter. The length of this refractory insert is 15.2 cm (6-in) and immediately downstream of this flow restriction the flow area increases to the original 19.4 cm (7.6-in) diameter. This refractory plug is positioned to provide acoustic feedback in a frequency range of about 500 Hz. The high temperature exhaust gases are quenched to approximately 450 °F using a water spray that is located approximately 4 meters (13.25 ft) downstream of the

combustor inlet. A second flow restriction is located immediately upstream of this water quench to enhance mixing with the atomized water spray. A high-temperature back-pressure control valve is used at the outlet of the apparatus. The air preheater, flow control valves and back-pressure control valve allow independent control of the inlet-air temperature, combustion air flow, and test rig pressure, respectively.

A water-cooled stainless-steel sample probe is inserted into the exhaust stream approximately 2.16 meters (85-in) from the combustor inlet. This probe is located downstream of the refractory insert described in the previous paragraph, and extracts an area-weighted gas sample through five 1.24 mm (0.049-in) diameter holes. Since the test rig operates at elevated pressure, the gas sample flows through the holes in the probe to the sampling system.

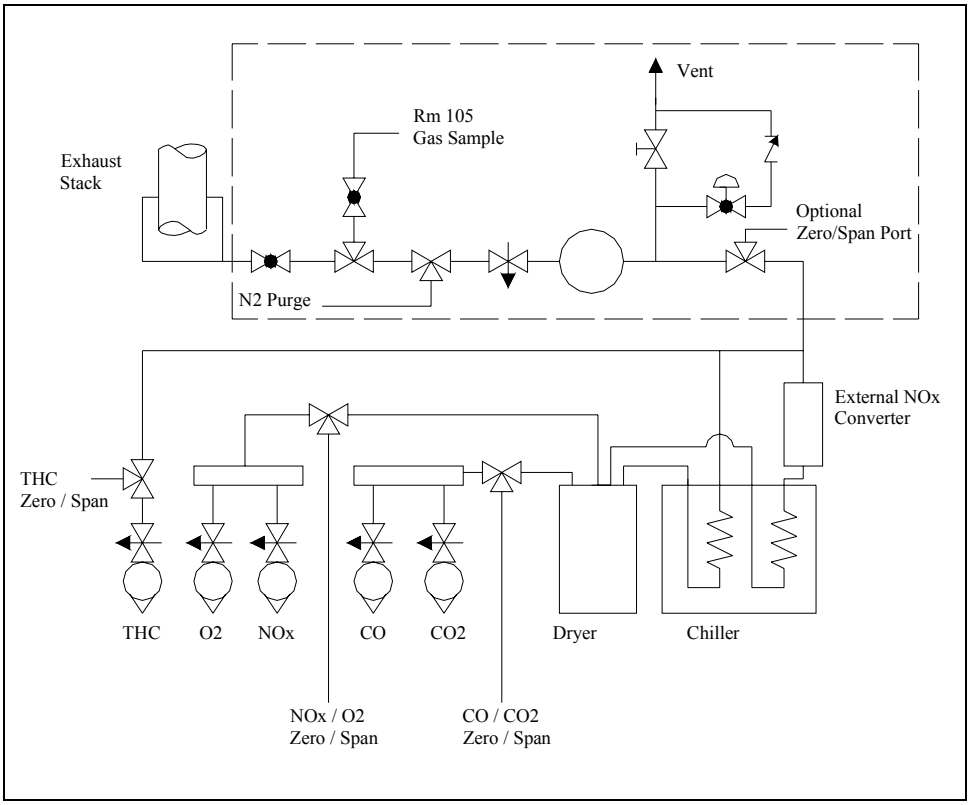

Figure 5-39: Flow Schematic of the Gas Sampling System.

Condensate is particularly important to avoid for single-digit NO_x measurement, due to the solubility of NO_2 in water which could bias the results. The gas sample is transported through a heated 6.4 mm (1/4-in) stainless-steel line to a pressure control and sample conditioning station. A schematic flow diagram for the gas sampling system is shown in Figure 5-39. A small pressure control valve is used to vent excess flow though the sampling system and maintain a constant pressure in the gas analyzer manifold. Some of the gas analyzers are very sensitive to changes in flow or pressure, so this pressure control is finely tuned and closely monitored during testing. There are also a series of block valves that allowed the chiller and gas analyzers to be isolated, while high pressure nitrogen can be used to back-flush the sampling system.

The exhaust sample is split so a portion of the heated sample passes through a NO_2-NO converter prior to entering a chiller/dryer to remove moisture that could later condense in the analyzers. Conversion of water soluble NO_2 to non-soluble NO ensures a more accurate NO_x measurement. This leg of the flow loop also supplies sample to the O_2 analyzer. A separate flow loop through the chiller/dryer that does not pass through the converter supplies the CO and CO_2 analyzers. The remaining exhaust sample bypasses the converter and chiller/dryer assemblies to provide sample for the total hydrocarbon measurement.

Table 5-6 shows the species that are measured, and the type of individual gas analyzers that are used in the test facility. Each of the gas analyzers are checked daily with a zero gas and a span gas. Although not shown in Figure 5-39, a Thermo ONIX (Model Prima delta-B) mass spectrometer is also used to measure certain key gas components (e.g., CO_2 and O_2). This redundancy allows a secondary check of the O_2 and CO_2 readings during operation.

Table 5-6: Gas Analyzers and Manufacturer Model Number.

Gas Component	Manufacturer	Model	Range	Manufacturer Specified Accuracy
CO2	Horiba	PIR-2000	0-20%	+/- 0.2 %
O2	M&C	PMA-12	0-21%	+/- 0.21 %
CO	California Analytical Instr.	Model 601CO	0-100 ppmv	+/- 1 ppmv
NOx	Horiba	CLA-510 SS	0 - 50 ppmv	+/- 0.5 ppmv

5.11.1 Data Analysis and Error Discussion

The air flowrate is metered using standard orifice plate flow meters, and the air flow is controlled using high temperature flow control valves. Two air flow loops (i.e., a low-flow and a high-flow) are used to meter and control the amount of combustion air flowing through the test rig. The main fuel (i.e., natural gas and propane) flows are metered using Rosemount 3095MFP Mass ProPlate meters that are accurate to less than two percent of reading. The pilot fuel (i.e., natural gas and propane) flows are metered using Siemens MassFlo Mass2100 DI 1.5 Coriolis sensors that have an accuracy of less than one percent of reading. All of the air and fuel flow meters are compared against secondary flow standards prior to testing (see Table 5-7). In the case of the fuel flow meters, nitrogen is used during this flow verification. All of the loops used in this experiment are accurate to within two percent full-scale reading after corrections for systematic biasing errors are employed.[64]

Table 5-7: Flow Loop Errors and (1-sigma) Uncertainties.

Flow loop	BIAS (SLOPE)	PRECISION (Y-INTERCEPT) (scfh)	STANDARD ERROR OF READINGS (scfh)	STANDARD ERROR OF MEASUREMENT (scfh)
Air (Low Flow)	0.9927	39.62	28.70	28.91
Air (High Flow)	1.007	-11.89	222.3	220.8
Nat. Gas Pilot	0.988	0.59	0.58	0.59
Nat. Gas Main	0.984	19.6	8.3	8.4
Propane Pilot	1.006	-0.07	0.023	0.023
Propane Main	1.002	3.3	1.2	1.2

The fuel composition is measured using an on-line gas chromatograph (Agilent Model 3000A micro-GC) and periodic gas grab samples are also collected and analyzed using an independent gas chromatograph. Table 5-8 is a list of chemical species that are measured in each of these instruments. Table 5-8 also lists the molecular weight, heating value, and standard density values for each of these components. These values have been taken from a chemical property database that is available on-line at the National Institute of Standards and Technology (NIST) Chemistry WebBook website.[65]

It is important to note that an analysis of the vapor exiting the propane tank is also measured at the beginning of each day. The as-delivered propane can contain a significant amount of ethane in the vapor phase (i.e., 10-15%); however, the higher volatility of ethane relative to propane will cause the ethane concentration in the vapor phase to drop significantly as vapor is removed from the storage tank. This produces a change in the composition of the liquefied petroleum gas (LPG) vapor as a function of the LPG tank level. The propane concentration in the blended fuel, β_p, can be determined based on the measured flows of propane and natural gas and the actual propane concentration of the vapor exiting the storage tank, X_p (see Equation 5-18). Equation 5-18 neglects the initial concentration of propane in the natural gas, which is typically on the order of 0.5-1.0 percent, however a formal uncertainty analysis of Equation 5-18 shows that if the propane concentration in the vapor exiting the propane storage tank varies by more than 0.5 percent, the error introduced by X_p will dominate the uncertainty in the propane concentration calculation, β_p. As a result, the fuel compositions will be reported based on the GC analysis of the blended fuel. If several GC measurements are available for a given test period, the average and standard deviations will be reported.

Table 5-8: Gas Components Measured In Gas Chromatographs and Component Properties.

Component name	On-line micro-GC	Laboratory gc	molecular weight	LHV (KJ/mol)	HHv (KJ/mol)	density (kg/m3)
Methane	X	X	16.04	890.7	802.7	0.678
Ethane	X	X	30.07	1560.7	1428.7	1.279
Propane	X	X	44.10	2219.2	2043.2	1.894
C4 (various)	X	X	58.12	2873.3	2653.2	2.532
C5 (various)	X	X	72.15	3531.9	3268.3	2.452
C6 (various)	X	X	86.18	4180.6	3878.6	3.043
C7+C8 (various)	NM†	X	100.20	4853.5	3886.7	4.227
N_2	X	X	28.01	0	0	1.182
H_2	NM	X	2.02	286.2	242.2	0.085
CO_2	NM	X	44.01	0	0	1.868

†NM = not measured

$$\beta_p = X_p \cdot \left[\frac{Q_{p_main} + Q_{p_pi;ot}}{Q_{p_main} + Q_{p_pi;ot} + Q_{NG_main} + Q_{NG_pi;ot}} \right] \tag{5-18}$$

The fuel component properties listed in Table 5-8 and the on-line micro-GC measured mole-fractions of each fuel component will be used to calculate the Wobbe Index using Equation 5-19. The specific gravity of the fuel is normalized by the density of air at standard conditions (i.e., 1.223 kg/m^3).

$$Wobbe = \frac{\sum_{i=1}^{N} X_i \cdot HHV_i}{\sqrt{\sum_{i=1}^{N} X_i \cdot \left(\frac{\rho_i}{\rho_{air}} \right)}} \tag{5-19}$$

The fuel-air ratio can be calculated independently by either utilizing the measured fuel and air flow rates entering the combustion test rig (see Equation 5-20), or based on the carbon-to-hydrogen ratio of the fuel and the measured species in the exhaust (i.e., CO_2, O_2, etc.). It should be noted that the concentrations of CO and unburned hydrocarbons are negligible for the test data described in this report. These two independent methods provide a means to check for mass closure, and based on the uncertainties in the fuel and air flows a nominal ± 3-sigma uncertainty for the FAR is ± 6E-04.

$$FAR_{flows} = \frac{Q_{p_main} + Q_{p_pilot} + Q_{NG_main} + Q_{NG_pilot}}{Q_{air_1} + Q_{air_2}} \tag{5-20}$$

Assuming complete combustion and omitting the CO_2 concentration in the fuel, Equation 5-21 can be used to determine the fuel-air ratio based on the measured gas composition of the

products of combustion. Absent from the equation is the concentrations of CO and unburned hydrocarbons which, as previously stated, were determined to be negligible.

$$FAR_{CO2} = \frac{[CO_2]_{POC,dry} - [CO_2]_{air}}{\left(n + \frac{m}{4} \cdot [CO_2]_{POC,dry}\right)} \tag{5-21}$$

Where,

$[CO_2]_{POC,dry}$ = Mole-fraction of CO_2 in the products of combustion (dry basis)
$[CO_2]_{air}$ = Mole-fraction of CO_2 in the incoming air (nominally 0.00034)
n = Moles of carbon atoms per mole of fuel
m = Moles of hydrogen atoms per mole of fuel

Similarly, it can be shown that the fuel-air ratio based on the measured oxygen concentration in the products of combustion can be determined based on Equation 5-22.

$$FAR_{O2} = \frac{[O_2]_{air} - [O_2]_{POC,dry}}{\left(n + \frac{m}{4} \cdot \left(1 - [O_2]_{POC,dry}\right)\right)} \tag{5-22}$$

Where,

$[O_2]_{POC,dry}$ = Mole-fraction of O_2 in the products of combustion (dry basis)
$[O_2]_{air}$ = Mole-fraction of O_2 in the incoming air (nominally 0.20948)

The stoichiometric fuel-air ratio based on the fuel gas composition can be calculated as shown in Equation 5-23. This stoichiometric fuel-air ratio is used in this report to normalize the actual fuel-air ratio calculations from Equations 5-20 – 5-22 to a fuel-air equivalence ratio.

$$FAR_{stoich} = \frac{[O_2]_{air}}{\left(n + \frac{m}{4}\right)} \tag{5-23}$$

5.11.2 Dynamic Stability

Thermo-acoustic combustion instabilities are an important consideration for lean premixed (LPM) gas turbine combustion systems. These instabilities are sensitive to many different factors. For example, small changes in ambient conditions or even the temperature history of the system can affect the dynamic stability. To illustrate this point, Figure 5-40 shows how the stability boundary can shift as a function of the initial conditions. This behavior is typical for the premixer investigated in this study. In other words, if the combustor is initially unstable (i.e., high RMS pressure level), then the transition to a stable condition occurs at a relatively lean operating condition. However, if the combustor is initially stable, then the transition to an

unstable condition occurs at an equivalence ratio of approximately 0.57 (see Figure 5-40). This type of behavior is characteristic of non-linear dynamic systems. These hysteresis effects can complicate the data analysis, but the knowledge that they exist is very helpful when developing an experimental test plan.

As a result of these hysteresis effects, test procedures were standardized on approaching the stability boundary from a stable, fuel-lean operating condition until the combustor becomes unstable. The nominal values for the premixer velocity, combustor pressure and inlet air temperature for the data presented in this section were 70 m/s, 760 kPa (110 psia), and 589 K (600 °F), respectively. The composition of the baseline fuel and the simulated LNG fuel is shown in Table 5-9. Cases 1 and 2 consist of baseline natural gas with typical composition fluctuations, while Cases 3 and 4 provide a simulated LNG by mixing approximately 4.6% propane to the baseline natural gas supply.

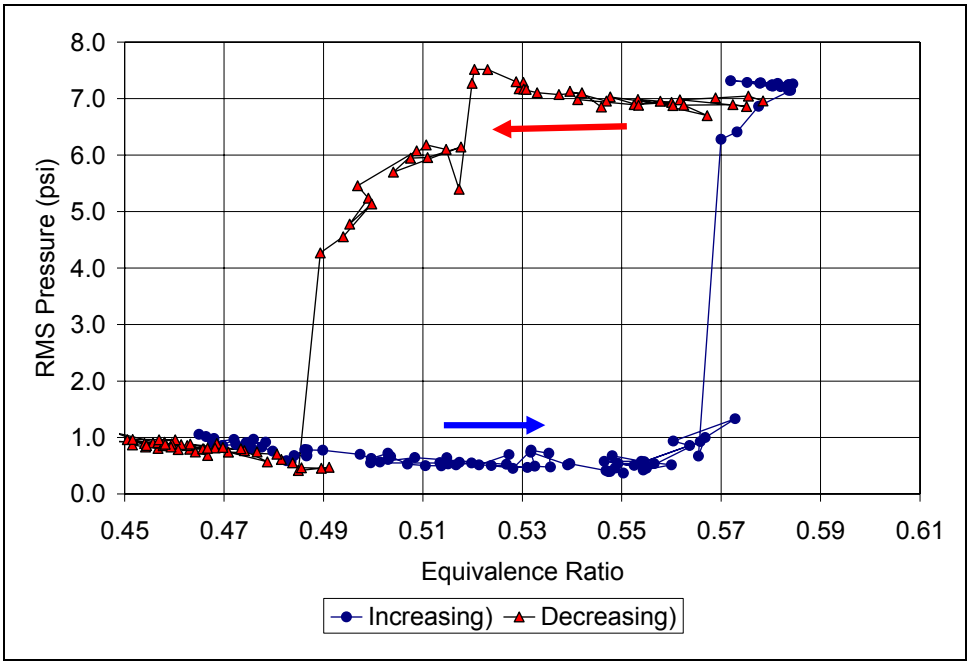

Figure 5-40: Hysteresis of Combustion Instabilities.

Figure 5-41 shows the calculated Wobbe Index and higher heating value (HHV) for the fuels described in this section. This figure also shows the seasonal variation in the site natural gas that was compiled from November 2004 to November 2005. The average Wobbe Index for the site natural gas for this period was 1370 BTU/scf and the average HHV was 1060 BTU/scf. However, during the testing described in this section, the average natural gas composition shifted to the nominal values shown as Case 1 and Case 2. Although some LNG sources can have Wobbe indices greater than 1400 and heating values of greater than 1120 BTU/scf, it was not possible to consistently achieve these fuel properties over the range of operating conditions investigated due to limitations in the propane flow loop configuration. This flow loop can be reconfigured if higher propane blends are considered relevant.

Table 5-9: Gas Composition for the Baseline Fuel (Case 1 and Case 2), and the Simulated LNG Fuel (Case 3 and Case 4).

	Case 1	Case 2	Case 3	Case 4
CH_4	0.9577	0.9635	0.9196	0.9191
C_2H_6	0.0268	0.0231	0.0254	0.0241
C_3H_8	0.0051	0.0034	0.0456	0.0462
C4 (various)	0.0016	0.0012	0.0012	0.0013
C5 (various)	0.0006	0.0005	0.0004	0.0005
C6 (various)	0.0004	0.0003	0.0002	0.0003
N_2	0.0063	0.0064	0.0059	0.0069
CO_2	0.0016	0.0017	0.0017	0.0016
Total	1.0000	1.0000	1.0000	1.0000

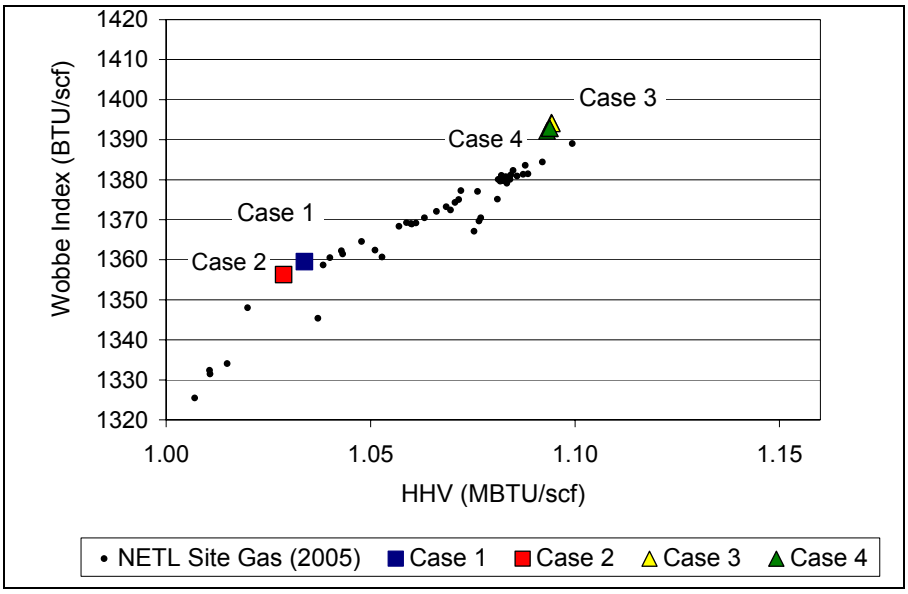

Figure 5-41: Range of Heating Value and Wobbe Index Investigated for Dynamic Stability Performance.

The stability boundary for this test rig is very distinct, as indicated by a small change in the equivalence ratio leading to significant changes in the observed RMS pressure levels. Figure 5-42 shows the variation in the dynamic stability boundary for the baseline natural gas fuel. Note that the stability boundary for the site natural gas fuel shifts somewhat from Case 1 to Case 2. This variation in the stability boundary represents the amount of variation in the experimental setup. This data was compiled from high-speed data that is sampled at 6000 samples per second. Each data point in Figure 5-42 represents an average of about 16,000 data points which corresponds to a time resolution of about 2.7 seconds. In any event, based on the data presented in Figure 5-42, the stability boundary for the baseline fuel is in the equivalence ratio range of 0.57 to 0.58.

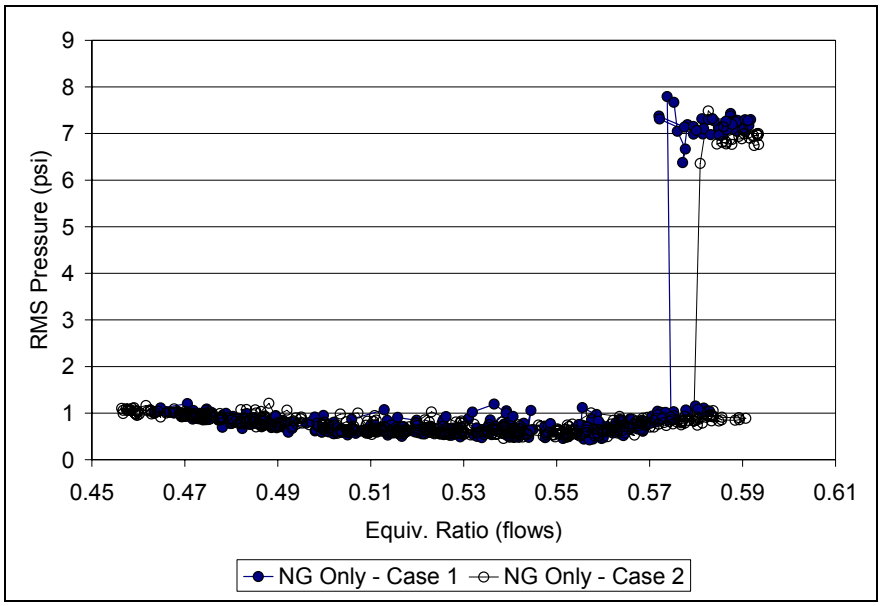

Figure 5-42: Variation in Dynamic Stability Boundary (Baseline Fuel).

In order to vary the fuel composition, propane vapor was blended with the baseline natural gas. For Case 3 and Case 4, the propane level in the fuel was around 4.6%, whereas, the propane level in the baseline fuel was on the order of 0.5%, or less. The Wobbe Index increased from about 1360 (BTU/scf) for the baseline fuel to about 1395 (BTU/scf) for the simulated LNG. These fuel properties are summarized in more detail in Table 5-10.

Table 5-10: Fuel Properties for Natural Gas (Case 1 and Case 2), and Simulated LNG (Case 3 and Case 4).

	Case 1	Case 2	Case 3	Case 4
Avg MW	16.81	16.68	17.89	17.91
Stoich. FAR	0.1023	0.1030	0.0968	0.0969
Moles Carbon per mole fuel	1.040	1.030	1.117	1.117
Moles H-atoms per mole fuel	4.061	4.042	4.216	4.213
HHV (kJ/mol)	914.4	908.1	965.9	965.4
HHV (mBTU/scf)	1.036	1.029	1.094	1.094
LHV (kJ/mol)	825.0	819.2	873.2	872.6
LHV (mBTU/scf)	0.935	0.928	0.989	0.989
Density @ 60 °F, 1atm (kg/m^3)	0.710	0.705	0.757	0.758
Specific Gravity	0.581	0.577	0.620	0.620
WOBBE kJ/m^3	50690	50534	51947	51889
WOBBE BTU/scf	1360	1356	1394	1393

Figure 5-43 shows the observed stability boundary for the simulated LNG fuel. For Case 4, the observed stability boundary occurs at a somewhat higher equivalence ratio than the baseline

natural gas, whereas Case 3 occurs at a somewhat lower fuel-air equivalence ratio than the baseline natural gas. It should be noted that the range of equivalence ratio conditions for which the stability boundary was observed in the baseline fuel falls within the range observed when propane is added to the fuel (see Figure 5-43). Although it appears that the simulated LNG fuel has a greater variability in the stability boundary, more data is required to validate this statement. Therefore, based on the data collected from this experimental setup, fuel composition does not seem to have a significant effect on the equivalence ratio at which combustion instabilities are encountered. However, the reader should be cautioned that the results from a different experimental setup may have a different outcome, depending on the acoustic coupling with the fuel system and other factors that have not been studied in great detail for this experiment.

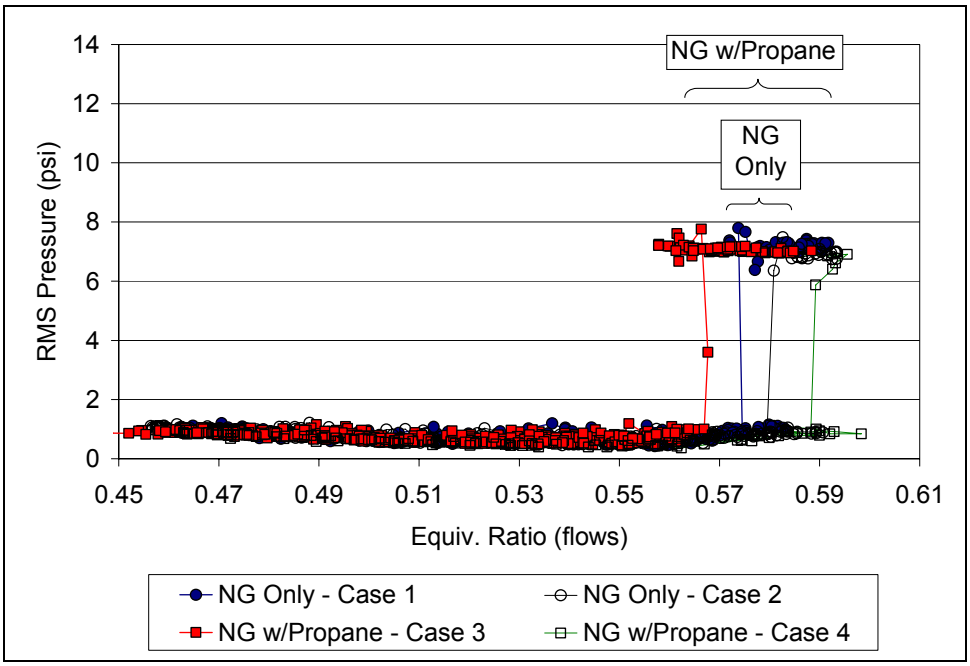

Figure 5-43: Dynamic Stability Boundary (NG and Simulated LNG).

5.11.3 Pollutant Emissions

The gas sampling system and the instruments for measuring emissions have been described in the experimental setup. Oxides of nitrogen, or NO_x, and carbon monoxide are two pollutants that must be carefully characterized. It is also important to note that the dynamic stability of the combustor can affect the measured NO_x emissions (see Figure 5-44). This figure shows that the NO_x emissions suddenly decrease as the RMS pressure levels increase. It is believed that the observed reduction in NO_x is due to improved mixing near the centerbody pilot during these oscillations.

Since the magnitude of these pressure oscillations cannot be controlled independently, it is important to account for the RMS pressure levels when conducting the emissions measurements. The RMS pressure level can actually confound the emission results, thus emissions measurements were made during dynamically stable operation, at very lean equivalence ratio conditions (i.e., less than 0.52 as determined by the measured flow rates). The lower boundary for the emissions study is fixed by the lean extinction limit.

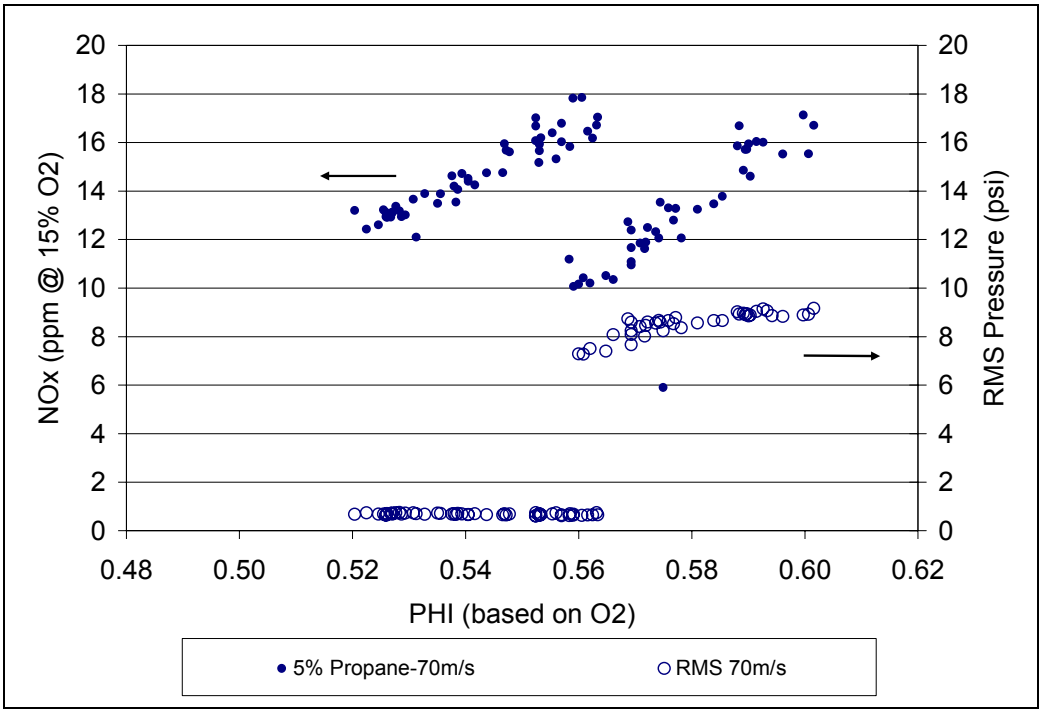

Figure 5-44: Confounding Effect of Combustion Instabilities on NO_x Emissions.

5.11.3.1 Test Plan

In order to investigate the effect of fuel composition on pollutant emissions, a simple two-level factorial experimental design is used (see Table 5-11). The two independent variables studied are the equivalence ratio and the fuel composition (i.e., level of propane blending). As previously mentioned, the equivalence ratio range is limited on the low end by the lean extinction limit and on the high end by the dynamic stability boundary. The upper limit for the amount of propane blending is set at 5 percent for this test plan. Each data point has been replicated once to provide some estimate of the variance in the measurements. The order in which the test points are investigated is randomized, so the propane blending system had to be cycled on-line and off-line during this test. The randomization is important from a statistical standpoint to account for variables that are not controlled (i.e., ambient conditions, uncontrolled variations in the fuel composition, etc.).

Table 5-11: Operational Conditions Performed During Testing.

Pressure (kPa)	Ref. Velocity (m/s)	Percent Pilot Fuel	Target Equiv. Ratio	Target Propane Level
760	70	5%	0.48	5.0%
760	70	5%	0.48	0.0%
760	70	5%	0.42	5.0%
760	70	5%	0.42	0.0%
760	70	5%	0.48	5.0%
760	70	5%	0.48	0.0%
760	70	5%	0.42	5.0%
760	70	5%	0.42	0.0%

The data collected from the on-line GC suggests that the propane level in the baseline natural gas is about 1.1 percent. The corresponding Wobbe Index is 1380 BTU/scf for the baseline natural gas and about 1425 BTU/scf for the fuel with propane addition. Figure 5-45 shows the Wobbe Index and higher heating value for all of the fuel compositions investigated in this test.

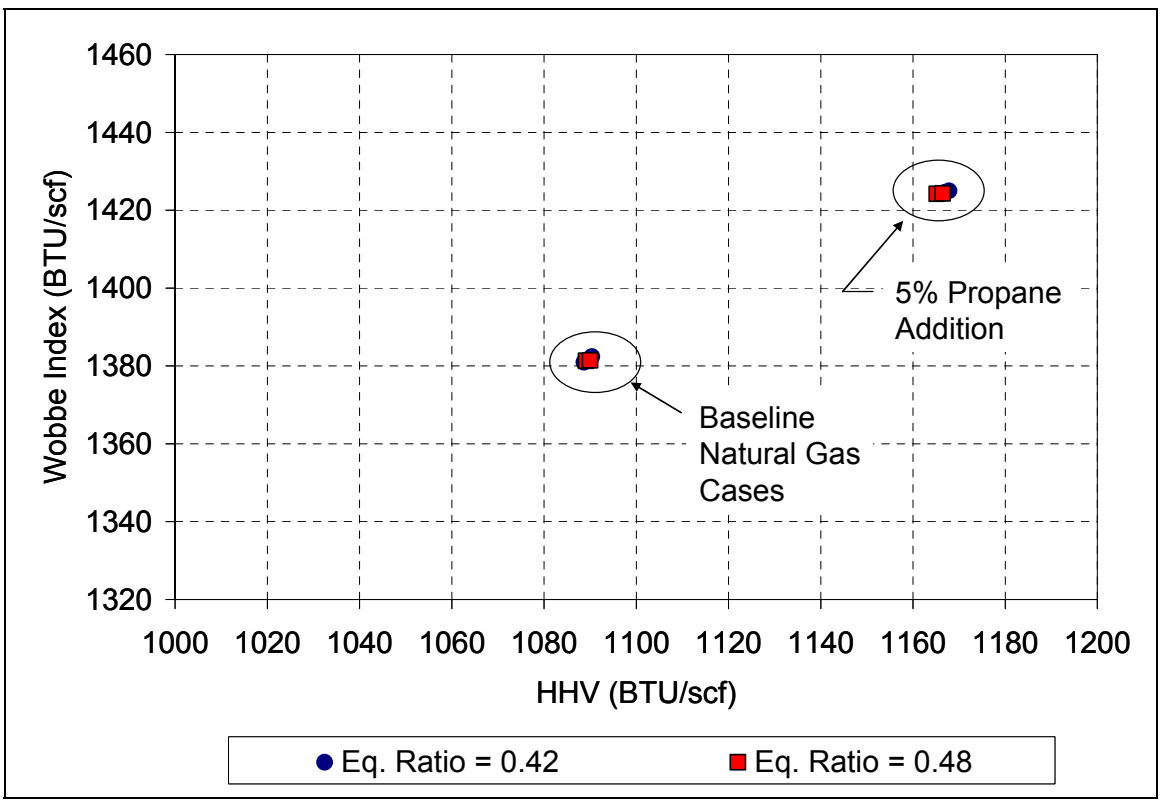

Figure 5-45: Wobbe versus HHV for Fuels used in Emission Testing.

It should be noted that this combustor is fueled by a piloted premixer. For these tests, five percent of the total fuel is injected through the centerbody pilot. When propane is added to the baseline natural gas, both the pilot fuel and the main fuel have the same level of propane addition on a percent volume basis. It is well-known that a diffusion pilot produces the largest percentage of the NO_x observed from this type of fuel injector. As a result, the observed NO_x emissions are

above 10 parts-per-million. Since this pilot fuel flow provides critical cooling for the centerbody, and also prevents blow-off, the pilot fuel has been maintained at a constant level, instead of trying to optimize the burner for lower emissions at one operating condition.

As described in the data and error analysis section, the fuel-air ratio that is measured directly from the fuel and air flows can be cross-checked with the fuel-air ratio calculated based on the concentration of oxygen or carbon dioxide in the sampling system. Figure 5-46 shows this comparison. Each of these data points represents an average over a 4 – 6 minute period of steady operation. The error bars represent ± 3 standard deviation uncertainties in the fuel-air measurements using the data from Table 5-7. If carbon-dioxide emissions are used as a basis for comparison with the flow measurements, a similar level of agreement is observed. In summary, the fuel-air ratio calculated based on the emissions measurements (i.e., oxygen and CO_2) are within the expected level of uncertainty for the experiment. This is true for all of the data points in the test matrix.

It should be noted that in our preliminary measurements (presented to reviewers of this report) this high level of agreement was not observed. Additional testing conducted since the review indicated that the exhaust composition was not homogeneous at the initial sample probe location. When the sample probe was re-located, the agreement between the calculations based on the exhaust measurements and the flow measurements were within an acceptable range. The sample probe was moved downstream of an internal flow restriction in order to improve the mixing and homogeneity of the combustion products at the sample probe location. Thus, the measurement accuracy presented here is better than in our early data. The conclusions about the effect of fuel composition on emissions are not changed, but supported by more accurate data.

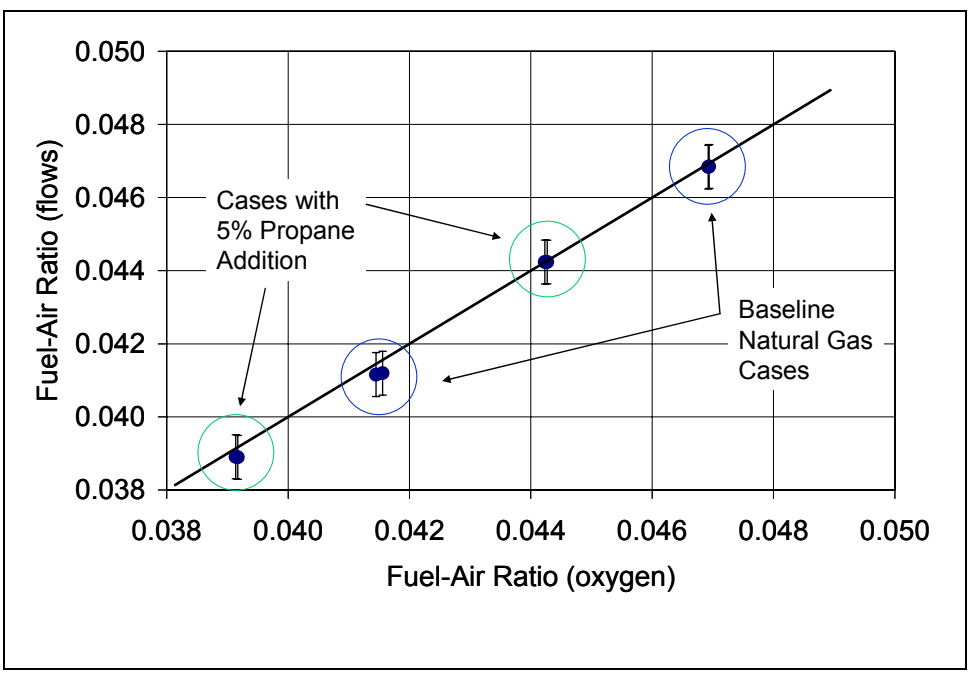

Figure 5-46: Discrepancy between Calculated and Measured Fuel-Air Ratio.

5.11.3.2 Emissions Results

Figure 5-47 shows the measured NO_x emissions as a function of the propane level in the gaseous fuel. The square symbols indicate the observed NO_x emissions for overall equivalence ratio conditions of 0.48 (as indicated by the flow measurements). The round symbols indicate the observed NO_x emissions at a significantly lower equivalence ratio. The error bars for the NO_x emissions (i.e., ± 0.7 ppm) are shown in Figure 5-47. These error bars represent 95% confidence intervals based on a Student (t-distribution) with four degrees of freedom. It should be noted that this level of uncertainty is somewhat higher than the instrument uncertainty listed in Table 5-6, but these error bars are based on the experimental replications and represent the variations in the entire process.

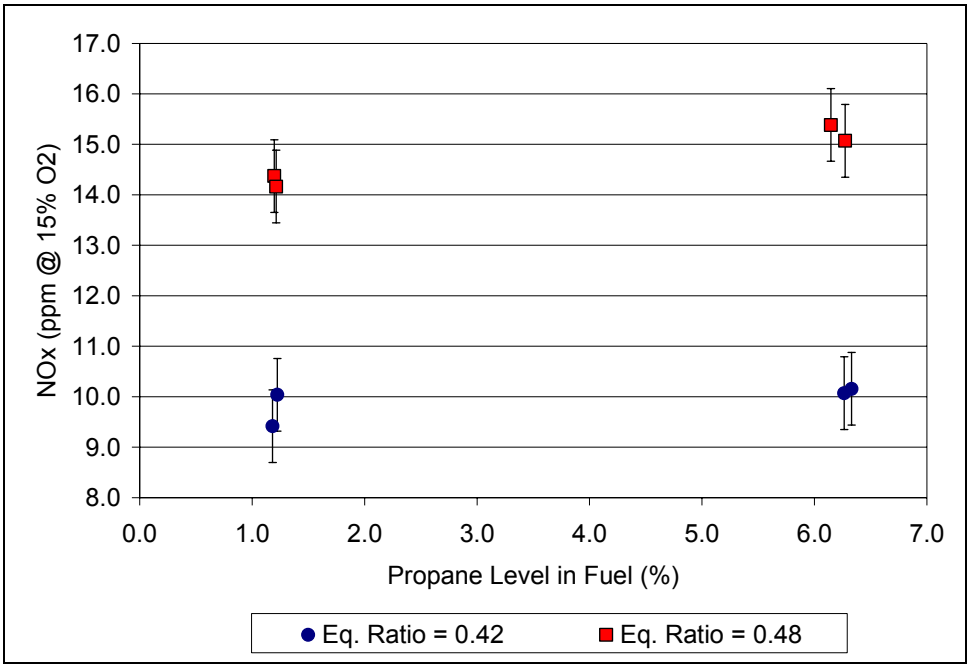

Figure 5-47: NO_x Emission as a Function of Propane Level.

The raw data is shown in Table 5-12. The flame temperature values listed in Table 5-12 are calculated based on the measured fuel composition and the fuel-to-air ratio based on the flow measurements. A Cantera software program utilized the chemical database from GRI-Mech 3.0 as a basis for these calculations. Since the GRI-Mech 3.0 does not include hydrocarbons heavier than propane, the fuel composition had to be normalized. The inert species in the fuel were included in these calculations, but the concentrations of argon and carbon dioxide in the air were neglected. It should be noted that localized temperatures in the flame region may be significantly higher than the values calculated, since the diffusion pilot fuel will burn closer to stoichiometric temperatures. However, for the purposes of this analysis, the pilot fuel has been combined with the premixed fuel and ideal mixing has been assumed.

Close examination of the data in Table 5-12 shows a nominal 10-15 K increase in the adiabatic flame temperature when propane is blended with the natural gas at a constant equivalence ratio. A small increase in flame temperature is expected based on existing flame temperature data for different fuels. Gulder[66] has developed an empirical curve fit of adiabatic flame temperature for

hydrocarbon fuels. In this relation, the dependence on the hydrogen-to-carbon ratio of the fuel can be clearly separated from the effects of the equivalence ratio. For the conditions encountered in this experiment, the flame temperature is inversely related to the hydrogen-to-carbon ratio of the fuel by a negative exponent. Therefore, as additional propane is added to the fuel, the hydrogen-to-carbon ratio decreases slightly, resulting in a slight increase in the adiabatic flame temperature.

For the operating conditions in this test, the largest difference between the Gulder flame temperature relation and the results from the GRI-Mech 3.0 was 2 K. Using the Gulder flame temperature relation, the hydrogen-carbon ratio effect can be isolated and the effect should only be on the order of 0.1 to 0.2 percent, or approximately 3 K. Figure 5-49 shows the calculated flame temperature as a function of the equivalence ratio based on the flow measurements. Note that the fuel compositions with propane blending exhibit a consistently higher adiabatic flame temperature and a slightly higher equivalence ratio. Based on the previous discussions, an approximate 3 K increase is due to the fuel composition and the remainder of this increase in flame temperature is due to variations in the equivalence ratio. Therefore, it is important to carefully consider the possibility of confounding the fuel composition effects and the effects due to flame temperature variations.

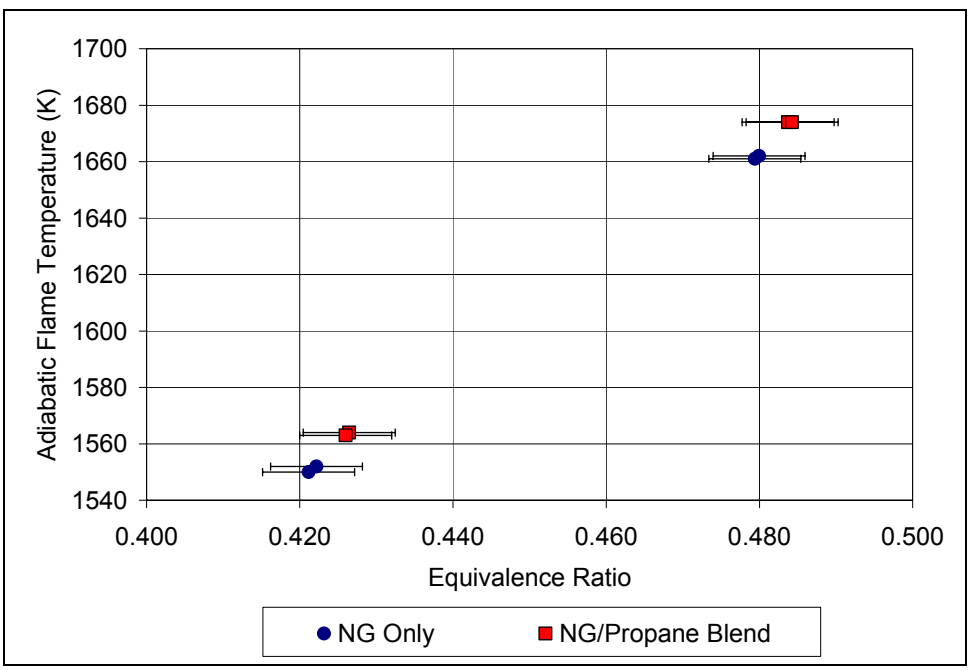

Figure 5-48: Adiabatic Flame Temperature as a Function of Equivalence Ratio and Fuel Composition.

At this point, it is instructive to plot the observed NO_x emissions as a function of the flame temperature. Theoretically, the relationship between NO_x emissions and adiabatic flame temperature should be exponential, however for the relatively small range of flame temperatures investigated in this study, the relationship is fairly linear (see Figure 5-49). The baseline natural gas data are shown as round symbols on this figure, and the operating conditions with approximately five percent propane are shown as square symbols. The effect of propane addition can be seen by comparing the symbols near the lower left and upper right of Figure

5-49. This figure suggests that the slight change in NO_x emissions observed in this study could be due to variations in the adiabatic flame temperature.

A simple regression analysis of the NO_x emissions data (listed in Table 5-12) has been performed. A confidence level of 95% is used as the criteria to determine the statistical significance. The independent parameters are the adiabatic flame temperature and the percentage of propane in the fuel (measured using the on-line GC). The results from this regression are summarized in Table 5-13. Note that the effect of propane addition on the observed NO_x emissions is not significant over the range of values investigated in this experimental setup.

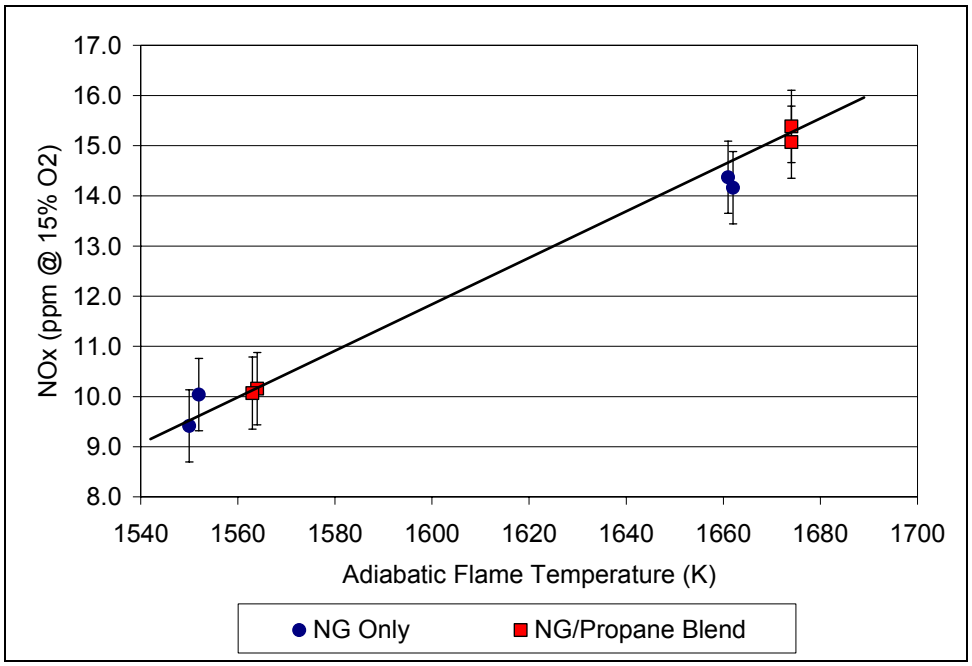

Figure 5-49: NO_x Emission as a Function of Adiabatic Flame Temperature.

Table 5-12: Comparison of Adiabatic Flame Temperature with Testplan Targets and Actual Operating Conditions.

Test Point†	Target Equiv. Ratio	Actual Equiv. Ratio (flows)	Target Propane Level	Actual Propane Level (%)	Wobbe Index (BTU/scf)	Adiabatic Flame Temp. (K)	Measured NO_x Emissions (ppm @ 15% O_2)
2	0.48	0.484 + 0.006	5.0%	6.15 + 0.13	1424	1674	15.4
3	0.48	0.479 + 0.006	0.0%	1.20 + 0.04	1381	1661	14.4
6	0.42	0.426 + 0.006	5.0%	6.33 + 0.05	1425	1564	10.2
1	0.42	0.422 + 0.006	0.0%	1.22 + 0.05	1382	1552	10.0
5	0.48	0.484 + 0.006	5.0%	6.27 + 0.04	1424	1674	15.1
7	0.48	0.480 + 0.006	0.0%	1.21 + 0.02	1381	1662	14.2
8	0.42	0.426 + 0.006	5.0%	6.26 + 0.02	1425	1563	10.1
4	0.42	0.421 + 0.006	0.0%	1.18 + 0.02	1381	1550	9.4

† The test points have been numbered in chronological order

Table 5-13: NO_x Emission Regression Analysis Summary Table.

N=8 (# of data points)	Regression Coefficient	Standard Error in Regress. Coeff.	t-Value (dof=5)	Probability of Significance (1-p)
Intercept	**-58.58**	**2.66**	**-22.05**	**>0.9999**
Propane Effect	0.029	0.036	0.80	0.542
Flame Temperature Effect	**0.044**	**0.0016**	**26.57**	**>0.99999**

5.11.4 High Pressure Test Summary

Single injector rig tests were conducted at 7.5 atmospheres with an air preheat of 588 K (600 °F). The fuels investigated included pipeline natural gas and a blend of pipeline natural gas with approximately five percent propane. The fuel injector was not optimized for lowest possible emissions. Approximately five percent of the total fuel flow was injected through the centerbody to provide a diffusion pilot. The primary response variables of interest were the dynamic pressure levels (i.e., combustion instabilities) and the pollutant emissions (i.e., NO_x and CO).

The dynamic stability boundaries are very sensitive to hysteresis effects, so the stability boundary was approached by ramping the fuel flows through the stability boundary over a period of 10-20 minutes. The stability boundary is very distinct for this experimental setup, and the boundary was always approached in the same direction. This stability boundary did not change dramatically as a function of the fuel composition.

The NO_x emissions were strongly affected by the presence of combustion-driven instabilities. Since the pressure oscillations could have a confounding effect on the emissions measurements,

the operating range for the emissions testing was restricted to fairly lean operating conditions (i.e., equivalence ratio conditions between 0.42 and 0.48).

The CO and unburned hydrocarbons were very small for all the test conditions reported in this section. The NO_x emissions ranged from 9 to 16 parts-per-million at 15% oxygen basis (see Table 5-12). The equivalence ratio and the level of propane addition were used as independent factors in a 2x2 level factorial designed experiment. A single-factor regression analysis shows a strong correlation with adiabatic flame temperature (see Table 5-13 and Figure 5-50).

The effect of blending approximately five percent propane with the natural gas did not produce a significant effect on the NO_x emissions over the range of conditions investigated in this experiment. Although these results differ from the 100 percent premixed results of Hack and McDonell,[16] they are consistent with Flores et al.[63] in which a swirl-stabilized atmospheric burner was operated with and without a pilot fuel circuit. Attempts to operate this test rig with lower levels of pilot fuel resulted in dynamic combustion instabilities which can confound the NO_x emissions measurements. Therefore, it was not possible to isolate the effects of the pilot from the effects of the combustion instabilities in this test rig.

5.12 Summary and Conclusions

In this section, fuel interchangeability effects on gas turbine combustor performance have been described in considerable detail. The results presented in this section have focused on the underlying fundamentals of gas turbine combustion. As a result, the conclusions represent generalizations that have some scientific foundation, but may not necessarily cover every engine specific condition. Actual performance on operating engines could vary depending on individual design factors such as dynamic stability margin, flashback margins, control system design, etc. The following points are important outcomes of this work:

- Since the mid-1990's, lean premixed gas turbine combustor designs have become increasingly popular. It is believed that fuel interchangeability issues will be most prevalent in these combustion approaches. Since lean premixed approaches are relatively new to the industry, and very little information is available in the public literature, this effort has been focused toward premixed systems.

- If there is adequate flashback margin designed into the combustion system, it is believed that flashback issues can be avoided for realistic changes in fuel composition. Evidence suggests that although the laminar flame speeds for higher hydrocarbon species are higher than domestic natural gas, other work has shown that the turbulent flame speeds actually decrease with the addition of heavier hydrocarbon species.[10] It is more likely that flashback events could be triggered by combustion instabilities which are discussed in more detail below.

- Hack and McDonell and others have operated a premixed combustors on relatively high heating value fuels without any autoignition problems, however, there is relatively little fundamental data on auto-ignition delay times for hydrocarbon fuels at conditions of

interest to all gas turbines. Thus, it is recommended that operational data and OEM experience be gathered.

- Modeling results show that fuel jet penetration into a cross-flow is inversely proportional to the Wobbe Index of the fuel. However, for "realistic" range of fuel compositions and typical premixer residence times, variations of fluid dynamic mixing as result of fuel variability is not expected to have a significant effect on NO_x production.

- Combustion instabilities are a significant concern for lean premixed systems, and a significant level of effort has been directed toward this issue. The stability boundary and the observed pressure amplitude are not significantly affected by "realistic" variations in the fuel composition. This statement is based on data collected from a lab-scale ring-stabilized burner, a one-atmosphere swirl-stabilized combustor, and a pressurized swirl-stabilized single-nozzle test rig. As was pointed out by a reviewer, for engines operating right at the stability limit, this may indeed change the operating margin, but the effect observed here is small.

- Dynamic system modeling results suggest a small shift in the phase and gain of the open-loop response are observed when using fuels comparable to those expected in typical CNG and LNG blends. For systems operating well inside their stability window this would suggest that changes in fuel composition may not pose a serious concern. However, systems that are marginally stable may experience difficulties in maintaining stability similar to those occurring as a result of typical variances in operating conditions (e.g., changing inlet air temperature).

- Both experimental and modeling results show that significant differences in the stability boundary and pressure amplitude are observed for pure propane and propane diluted with nitrogen to obtain the same Wobbe Index as the baseline natural gas. As already noted, for realistic natural gas composition ranges these changes are small.

- A review of the publicly available literature suggests that NO_x emissions will increase, if the concentration of higher hydrocarbon species (C2's and higher) in the fuel increases. For diffusion flame combustors, it is believed that the NO_x increase will be proportional to the natural logarithm of the flame temperature relative to some reference (i.e., methane) flame temperature (see Equation 5-1). For 100% premixed systems, it is believed that the NO_x emissions increase is some function of the higher hydrocarbon species (see Figure 5-5 and Equation 5-4). Results from NETL's high pressure test facility show no significant changes in NO_x emissions as a function of adding as much as 5% propane to the baseline natural gas (i.e., a nominal Wobbe increase from 1380 to 1425 BTU/scf).

5.13 Additional Information – Fuel Heating and Modified Wobbe Index

This section was added after completing the main body of work to determine how fuel heating may affect the dynamic response of the combustor, and how, or if, the "Modified" Wobbe Index may be used to characterize these effects.

Fuel interchangeability has often been characterized by the classical Wobbe Index. For a given fuel pressure drop, any fuel with the same Wobbe Index will produce the same heat input. This is very useful for evaluating fuel interchangeability in self-aspirated burners. In contrast, experimental results presented earlier have shown that the Wobbe Index may not be as useful at describing dynamic stability margins in premixed turbine combustors. Nevertheless, the Wobbe Index is still a widely referenced parameter, and will likely still be used to discuss interchangeability. A key question that emerged in the course of this work was whether or not fuel heating could serve as a means of compensating for changes in combustor performance with different fuel types. Elevating the fuel temperature reduces the density of the fuel; however as the specific gravity and heating value calculations in the Wobbe Index are based on standard conditions with the fuel and air at the same temperature, the index does not capture this effect. An alternative approach is to utilize the Modified Wobbe Index (MWI) which includes a fuel temperature parameter. MWI is defined by the following mathematical equation:

$$MWI = \frac{LHV}{\sqrt{SG_{fuel} x T_{fuel}}} \tag{5-24}$$

Where,

LHV = Lower heating value of the fuel gas (MJ/m^3).
SG_{fuel} = Specific gravity of the fuel relative to air. Equivalent to MW_{fuel}/MW_{air}.
MW_{fuel} = Molecular weight of the fuel gas.
MW_{air} = Molecular weight of dry air.
T_{fuel} = Absolute temperature of the fuel gas (K).

Maintaining a constant Modified Wobbe Index (MWI) will ensure that the required fuel nozzle pressure ratios are maintained during all modes of operation regardless of fuel composition. Constant pressure ratios could, for example, be useful to insure that premixer jet penetration is constant with different fuel types. It should be recognized that existing fuel systems often use fuel heating to avoid difficulties with liquid dropout. Does fuel heating offer a means of retuning the dynamics response of a combustor that is stable on some baseline fuel?

Utilizing the model developed in Section 5.9, it is possible to vary the fuel temperature in an attempt to understand its impact on the dynamic response of the fuel injector and combustor. This model considers only the physical parameters that occur in the combustor such as changes in the fluid temperature, density, speed of sound, etc. It does not consider how chemical changes, such as reaction times and flame speeds, may impact the occurrence of flashback, flame blow-off or combustion instabilities. However, the model has been shown to be quite useful as large changes in the fuel injector impedance predicted by this model as a result of changing fuel composition did correlate well with experimental data in which significant deviations in the dynamic response were observed.

Table 5-14 lists the fuel properties including fuel temperature, Wobbe Index and MWI that were evaluated. Tests conducted on these fuels were used to generate the gain and phase plots shown in Figure 5-50 (a & b). Five fueling options are given in Table 5-14 with two of the five having

the same composition but varied temperature in order to match the MWI of the baseline case given by Case "A' which was 100% methane.

Table 5-14: Fuel Properties of Test Fuels.

Fuel Blend	100% Methane	High Methane	High Methane	High Propane	High Propane
Label	A	B	C	D	E
Methane	100	92.19	92.19	82.76	82.76
Ethane	0	6.45	6.45	4.38	4.38
Propane	0	0.92	0.92	11.06	11.06
C_4+	0	0.43	0.43	0.37	0.37
CO_2	0	0	0	0.13	0.13
N_2	0	0	0	0.99	0.99
Tfuel (K)	288	288	307	288	333
Wobbe Index	1352	1392	1392	1443	1443
MWI	71.82	74.12	71.80	77.12	71.72
cfuel (m/sec)	442	423	441	391	447

Case B and C are described as a high methane content fuel and its temperature was increased by 19 K in order to match the MWI of Case A, while Cases D and E have a higher propane content which required an increase in fuel temperature of 45 K to obtain a similar MWI as Case A.

Figure 5-50 (a & b) are plots of the amplitude and phase of the acoustic impedance inside the fuel injector for Case A – E. Figure 5-50(a) shows that although increasing the temperature of the fuel to produce a similar MWI as Case A did move the respective responses closer to Case A's, it was never able to duplicate it. Additionally, in both Cases C and E there was only a small change in gain from Case B and D, respectively. This response was echoed in the phase plots shown in Figure 5-50(b) where a similar phase was shown in all Case A – E although at different frequencies. The observed change is most likely the result of a difference in the theoretical speed of sound caused by the temperature increase. Table 5-14 also lists the speed of sound in the fuel which indicates both C and E are approaching the value calculated for Case A.

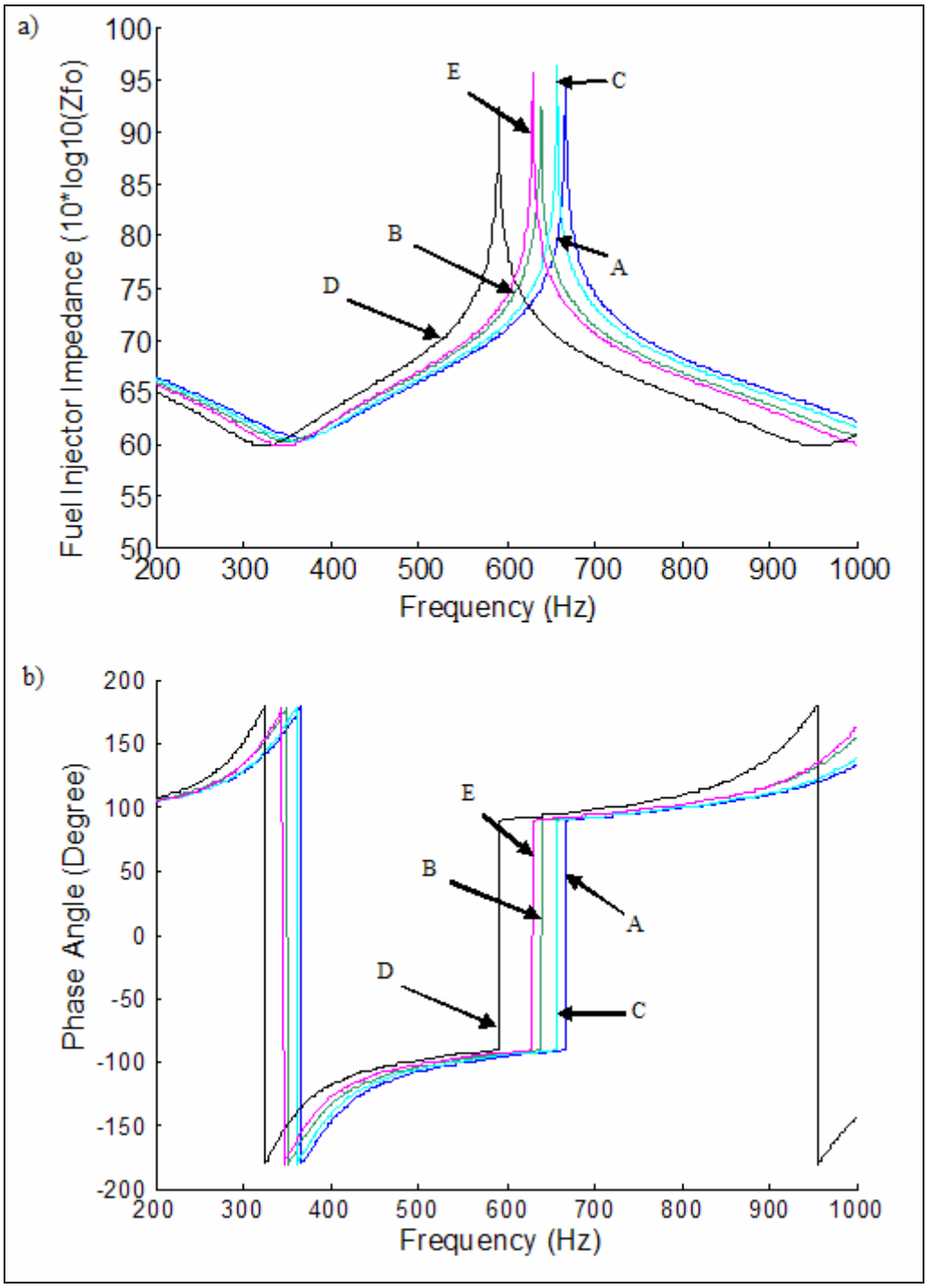

Figure 5-50: Gain and Phase of Injector Impedance for Fuel Cases in Table 5-14.

Additional fuels with higher propane content were also tested as shown in Table 5-15. Recall from earlier in this section, that nitrogen diluent was used to reduce the Wobbe Index of a pure propane fuel to something which was comparable to the baseline 100% methane case (Case A). The modeling results of the amplitude and phase from these fuels are reproduced in Figure 5-51 and Figure 5-52, respectively. As was previously concluded, matching Wobbe Index alone did not appear to be a viable method for reproducing the dynamic response of the fuel injector. As

with the results shown in Figure 5-50 (a & b), increasing the temperatures of the fuels containing higher concentrations of heavier hydrocarbons in order to match the MWI did improve the correspondence as shown with Case H compared to Cases A and G. However, the large quantity of propane in Case H still resulted in a gain and phase for the fuel injector impedance that was considerably different than Case A. The source of the discrepancy may be the result of a significantly different speed of sound that still exists irrespective of the matching MWI between Case A and H. However, if we further increase the temperature of this fuel blend in order to achieve a similar speed of sound, as shown in Case I, a response was obtained that is nearly identical to Case A. Thus, it would seem that matching the speed of sound was of greater importance in predicting the dynamic response of the fuel injector, than matching the Wobbe Index or even Modified Wobbe Index. It is recognized that a fuel preheat of 760 K may be impractical, but this calculation shows the significant role of the speed of sound, and lower fuel preheat may be used with less dramatic changes in fuel blends.

Table 5-15: Fuel Specifications with High Concentrations of Propane.

Fuel Blend	100% Methane	100% Propane	Propane / Nitrogen	Propane / Nitrogen	Propane / Nitrogen
Label	A	F	G	H	I
Methane	100	0	0	0	0
Ethane	0	0	0	0	0
Propane	0	100	62.3	62.3	62.3
C_4+	0	0	0.43	0.43	0.43
CO_2	0	0	0	0	0
N_2	0	0	37.7	37.7	37.7
Tfuel (K)	288	288	288	306	760
Wobbe Index	1352	2034	1364	1364	1364
MWI	71.82	110.35	74.03	71.82	45.57
cfuel (m/sec)	442	247	278	286	442

Although matching the speed of sound in the fuel blends to that of Case A does appear to provide a means of reproducing its dynamic response *of the fuel injector*, it can not be overlooked that the combustor model used here only considers physical parameters in the injector. The model does not account for changes in the dynamic response of the flame itself. In addition, the engine control system may compensate for a changing fuel preheat and may produce similar confounding effects. As the fuel preheat is raised, the thermal input needed from the fuel will drop, producing subtle changes in fuel/air ratio. For engines operating near their stability margin, this could lead to dynamic oscillations. Specific conclusions depend on the engine, but the calculations shown here suggest that dynamics may be affected by fuel preheat. The injector response is most directly described by the speed of sound in the fuel as a function of the fuel temperature, and not by the Modified Wobbe Index.

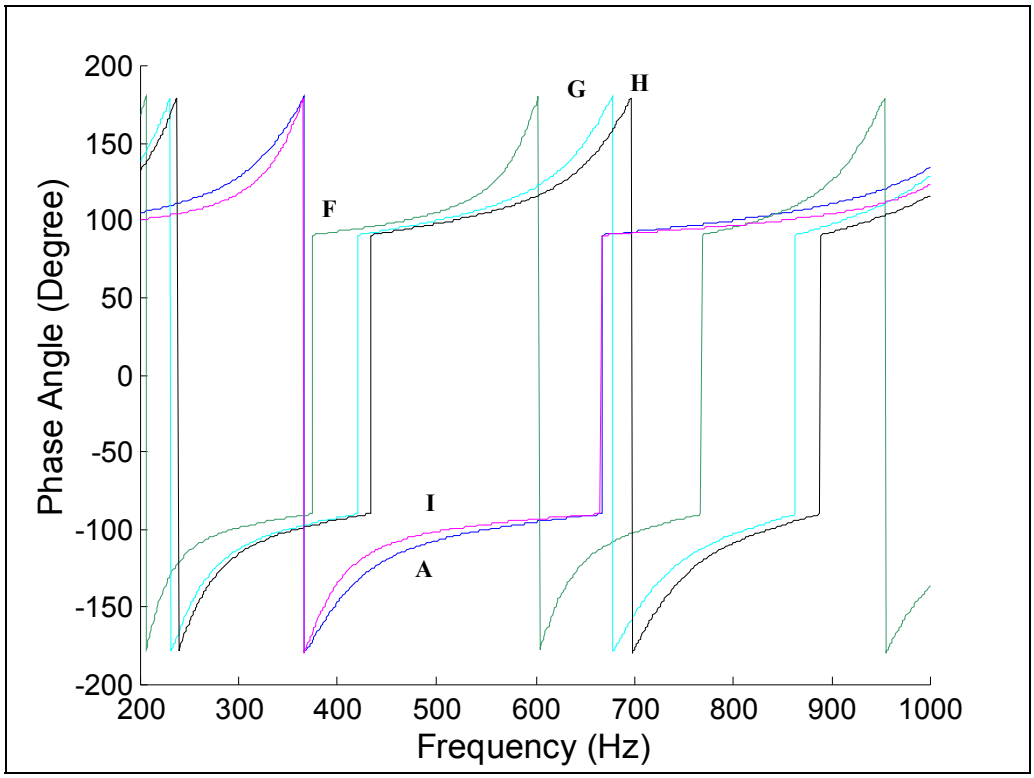

Figure 5-51: Phase Plot for Cases of Table 5-15.

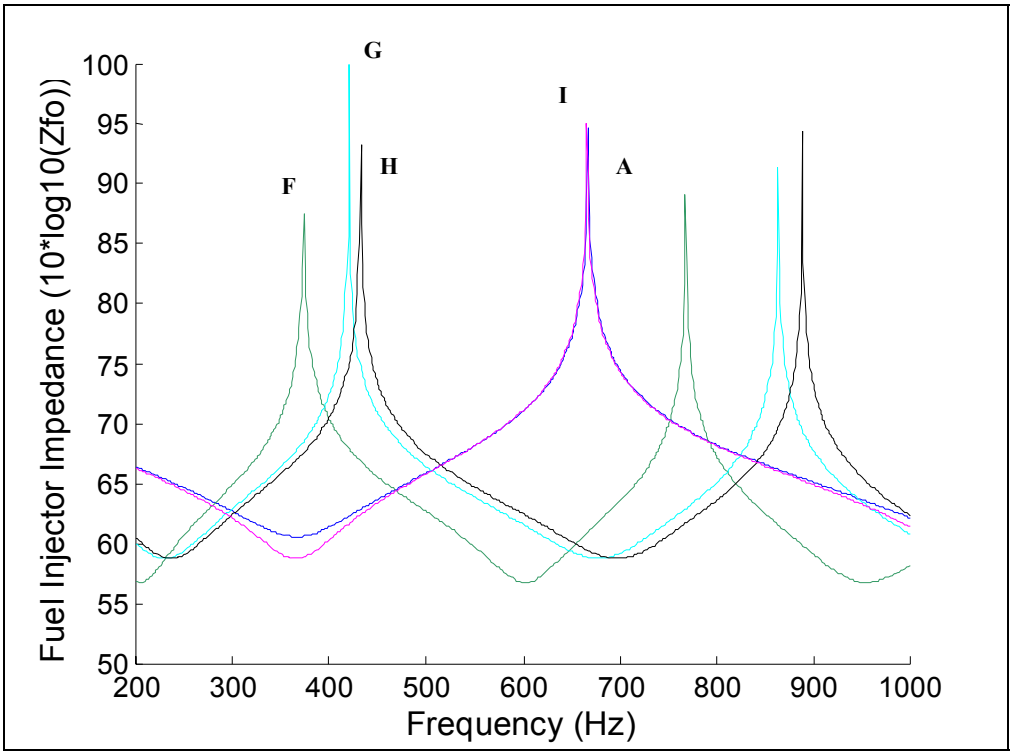

Figure 5-52: Gain Plot for Cases in Table 5-15.

[1] Sewell, J. B., Sobieski, P. A., (2005). Monitoring of Combustion Instabilities: Calpine's Experience, in Combustion Instabilities in Gas Turbine Engines, Lieuwen, T. C., Yang, V. [eds.], American Institute of Astronautics and Aeronautics, pp. 147 – 162.

[2] Kurz, R. (2004). Gas Turbine Fuel Considerations, Gas Machinery Conference, 2004.

[3] Personal communications Chuck Linderman ,Director, Energy Supply Policy, Alliance of Energy Suppliers A Division of the Edison Electric Institute, 202-508-5652.

[4] Maden, K. H. (1998) Fuel Flexibility in Industrial Gas Turbines, Solar Turbines Inc., Turbomachinery Technology Seminar TTS121/398/2M.

[5] Hung, W.S.Y. (1976). "A Diffusion Limited Model that Accurately Predicts the NOx Emissions From Gas Turbine Combustors Including the Use of Nitrogen Containing Fuels," Journal of Engineering for Power, ASME Series A, Vol. 98.

[6] Hung, W. S. Y. (1977). "The NO_x Emission Level of Unconventional Fuels for Gas Turbines," Journal of Engineering for Power, ASME Series A, Vol. 99.

[7] GasEQ (2005), http://www.gaseq.co.uk/

[8] Mongia, H.C., Held, T. J., Hsiao, G. C., Pandalai, R.P. (2003). Challenges and Progress in Controlling Combustion Dynamics in Gas Turbine Combustors, AIAA J. Prop. and Power, Vol.19, No. 5, pp. 821 – 829.

[9] D. L. Oostendoorp and H. B. Levinsky J. Inst of Energy, Vol 63 pp. 160-166.

[10] Kido, H., Nakahara, M., Hashimoto, J., Barat, D. (2002). Turbulent Burning Velocity of Two-Component Fuel Mixtures of Methane, Propane, and Hydrogen, Japanese Society of Mechanical Engineering International Journal, Series B, Vol. 45, No. 2, pp. 355 – 362.

[11] Noble, D., Zhang, Q., Shareef, A., Tootle, J., Meyeres, A., Lieuwen, T. (2006). Syngas Mixture Composition Effects upon Flashback and Blowout, ASME paper GT2006-90470.

[12] Angelo, L. and Castaldini, C (2004) Combustion Tuning Guidelines: Understanding and Mitigating Dynamic Instabilities in Modern Gas Turbine Combustors, ASME GT2004-54081.

[13] Cowell, L. H., Lefebvre, A.H., (1986). Influence Of Pressure On Autoignition Characteristics Of Gaseous Hydrocarbon-Air Mixtures, SAE paper 860068.

[14] Spadaccini, L. J., Colket, M. B. (1994). Ignition Delay Characteristics Of Methane Fuels, Progress in Energy and Combustion Science, Vol. 20, pp. 431-460.

[15] Naber, J. D., Siebers, D. L., DiJulio, S. S., Westbrook, C. K., (1994). Effects of Natural Gas Composition on Ignition Delay Under Diesel Conditions, Combustion and Flame, Vol. 99, pp. 192-200.

[16] Hack, R. L., McDonell, V. G. (2005). Impact of Ethane, Propane, and Diluent Content in Natural Gas on the Performance of a Commercial Microturbine Generator. ASME GT2005-68777.

[17] Mansour, A. Straub, D. L., Benjamin, M. A., Richards, G. A. (2001). Application of Macrolamination Technology to Lean Premix Combustion *ASME Journal of Engineering for Gas Turbines and Power*, Vol. 123, No. 4, pp. 796-802.

[18] Kalitan, D. M., Petersen, E. L., Mertens, J. D., Crofton, M. W., (2005). Ignition and Oxidation of Lean CO/H_2 Fuel Blends in Air, AIAA paper 20005-3767.

[19] Samuelsen, S., McDonell, V., Chen, J., Jermakian, V. (2003). Correlation Of Ignition Delay With Fuel Composition And State For Application To Gas Turbine Combustion, Final Report Contract No. 00-01-SR084CS,South Carolina Institute for Energy Sciences, sponsored by the National Energy Technology Laboratory, Contract Number DE-FC21-92MC29061.

[20] Lee, J. C. Y. (2000). Reduction of NOx Emissions for Lean Prevaporized-Premixed Combustors, Ph.D. Thesis, University of Washington, Seattle WA.

[21] Leonard, G., Stegmaier, J. (1994). Development of an Aeroderivative Gas Turbine Dry Low Emissions Combustion System, ASME J. Eng. For Gas Turbines and Power, Vol. 116, pp. 542 – 546.

[22] Klassen, M. (2005). White Paper on Natural Gas Interchangeability and Non-Combustion End Use, NGC+ Interchangeability Work Group., Section C.3, Power Generation, available American Gas Association, www.aga.org

[23] Flores, R. M., McDonell, V. G., Samuelsen, G. S. (2003). Impact of Ethane and Propane Variation in Natural Gas on the Performance of a Model Gas Turbine Combustor, *ASME J. Eng, Gas Turbines and Power, Vol. 125,* pp. 701 – 708.

[24] Consultant Report, Aspen Environmental Group, Natural Gas Quality: Power Turbine Performance During Heat Content Surges, California Energy Commission report CEC-700-2006-001, May 2006.
[25] Nord, L. O.. Andersen, H. G. (2003). Influence of Variations in the Natural Gas Properties on the Combustion Process in Terms of Emissions and Pulsations for a Heavy-Duty Gas Turbine, ASME Paper IJPGC2003-40188.
[26] Nord, L. O.. Andersen, H. G. (2004). A Study of Parameters Affecting the Combustion Stability and Emissions Behavior of Alstom Heavy-Duty Gas Turbines, ASME Paper GT2004-53228.
[27] Hunderup, J. W., Robey, R. J. (1996). An Experimental Investigation of the Conversion of No to NO2 at High Pressure, ASME J. Eng. Gas Turbines and Power, Vol 118, pp. 756- 764.
[28] Hori, M., Matsunaga, N., Marinov, N., Pitz, W., Westbrook, C. (1998). An Experimental and Kinetic Calculation of the Promotion Effect of Hydrocarbons on the NO-NO2 Conversion in a Flow Reactor, *The 27th (International) Symposium on Combustion,* pp. 389-396. The Combustion Institute, Pittsburgh PA.
[29] Hori, M., Koshiishi, Y., Matsunaga, N., Glaude, P., Marinov, N. (2002). Temperature Dependence of NO to NO2 Conversion by n-Butane and n-Pentane Oxidation, Proceedings of the Combustion Institute, Vol. 29, pp. 2219-2226. The Combustion Institute, Pittsburgh PA.
[30] Hori, M., Matsunaga, N., Malte, P., Marinov, N. (1992). The Effect of Low-Concentration Fuels on the Conversion of Nitric Oxide to Nitrogen Dioxide, *The 24th (International) Symposium on Combustion,* pp. 909-916. The Combustion Institute, Pittsburgh PA.
[31] Griebel, P, Boscheek, E., Jansohn, P. (2006). Lean Blowout Limits and NOx Emissions of Turbulent, Lean Premixed Hydrogen-Enriched Methane/Air Flames at High Pressure, ASME paper GT2006-90490.
[32] Noble, D. R., Zhang, Q., Shareef, A., Tootle, J., Meyers, A., Lieuwen, T. (2006). Syngas Mixture Composition Effects upon Flashback and Blowout, ASME paper GT2006-90470.
[33] P. Strakey, T. Sidwell and J. Ontko (2006). "Investigation of the Effects of Hydrogen Addition on Lean Extinction in a Swirl Stabilized Combustor", Presented at the 31st International Symposium on Combustion, Heidelberg, Germany, Aug 6-11, 2006.
[34] Mongia, H.C., Held, T. J., Hsiao, G. C., Pandalai, R.P. (2003). Challenges and Progress in Controlling Dynamics in Gas Turbine Combustors. *AIAA Journal of Propulsion and Power*, Vol. 19, No. 5, pp. 822-829.
[35] Muruganandam, T., Seitzman, J.M. (2003). Optical Sensing of Lean Blowout Precursors in a Premixed Swirl Stabilized Dump Combustor. ASME GT 2003-38104.
[36] Benson, K., Thornton, J. D., Straub, D. L., Huckaby, E. D., Richards, G. A. (2005). Flame Ionization Sensor Integrated Into a Gas Turbine Fuel Nozzle, ASME Journal of Engineering For Gas Turbines and Power, Vol. 127 pp. 42 - 48
[37] Sholz, M. H., Depietro, S.M., (1997). Field Experience on DLN Typhoon Industrial Gas Turbines, ASME 97-GT-61.
[38] Richards, G. A., Straub, D. L., Robey, E. H. (2005). Passive Control of Combustion Instabilities in Stationary Gas Turbines, in *Combustion Instabilities in Gas Turbine Engines,* Lieuwen, T. C., Yang, V. [eds.] AIAA Press, pp. 533-579.
[39] Chu, B. T. "On the Generation of Pressure Waves at a Plane Flame Front," *Proceedings of the Combustion Institute,* Vol. 4., 1953, pp.603 - 612.
[40] Mongia, H.C., Held, T. J., Hsiao, G. C., Pandalai, R.P. (2003). Challenges and Progress in Controlling Dynamics in Gas Turbine Combustors. *AIAA Journal of Propulsion and Power*, Vol. 19, No. 5, pp. 822-829.
[41] Cohen, J. H., Rey, N.M., Jacobson, C. A., Anderson, T.J. (1999). Active Control of Combustion Instabilities in a Liquid-Fueled Low-NOx Combustor. ASME Journal of Engineering for Gas Turbines and Power, Vol. 121, No. 2, pp. 281 - 284.
[42] Sattinger, S.S, Neumeier, Y., Nabi, A., Zinn, B. T., Amos, D. J., Darling, D. D. (1998). Subscale Demonstration of the Active Feedback Control of Gas Turbine Combustion Instabilities, ASME Paper 98-GT- 258.
[43] Seume, J. R., Vortmeyer, N., Krause, W., Hermann, J., Hantschk, C.-C., Zangl, P., Gleis, S., Vortmeyer, D., and Orthmann, A., (1998). Application of Active Combustion Instability Control to a Heavy Duty Gas Turbine. ASME Journal of Engineering for Gas Turbines and Power, Vol. 120, No. 4, pp. 721 -726.

[44] Kokanovic, S. Torchalla, S., Guidati, G., Shuermans, B. (2006). Active Combustion Control System for Reduction of NOx and Pulsation Levels in Gas Turbines, ASME GT2006-90895.
[45] Lipatnikov, A.N., Chomiak, J. (2005) Molecular Transport Effects on Turbulent Flame Propagation and Structure (2005). Progress in Energy and Combustion Science, Vol 31, pp. 1-73.
[46] Hautman, D. J., Haas, R. J., and Chiappetta, L. (1991) "Transverse Gaseous Injection Into Subsonic Air Flows" AIAA 91-0576
[47] Goldmeer, J., Sanderson, S., Myers, G., Stewart, J., D'Ercole, M. (2005). Passive Control of Dynamic Pressures in Dry Low-NOx Combustion System Using Fuel Gas Circuit Impedance Optimization, ASME GT2005-68605.
[48] Raun, R., Beckstead, M., Finlinson, J., Brooks, K., 1993, A Review of Rijke Tubes, Rijke Burners and Related Devices, Prog. Energy Combust. Sci., 19:313-364.
[49] Ferguson, D., Richards, G., and Woodruff, S., "Acoustic Velocity Measurements in a Naturally Oscillating Flame," 3rd Joint Meeting of the U.S. Sections of The Combustion Institute
March 16-19, 2003.
[50] Ferguson, D., Lee, D.H., Lieuwen, T., and Richards, G. A., "Velocity Field Measurements in an Oscillating Bunsen Flame, " 30th International Symposium on Combustion, Chicago, IL, July 26-30, 2004
[51] Ferguson, D., "Experimental Investigation of Oscillatory Heat Release Mechanisms and Stability Margin Analysis in Lean-Premixed Combustion", Ph.D. Dissertation, West Virginia University, https://eidr.wvu.edu/etd/documentdata.eTD?documentid=3854, 2005
[52] Lieuwen, T., "Modeling Premixed Combustion – Acoustic Wave Interactions: A Review," Journal of Propulsion and Power, V19, 5, 2003, pp. 765-781.
[53] Baukal, C., Schwartz, C. E., (2001). The John Zink Combustion Handbook, CRC Press, pp. 436.
[54] Hautman, D. J., Haas, R. J., and Chiappetta, L. (1991) Transverse Gaseous Injection Into Subsonic Air Flows, AIAA 91-0576
[55] Munjal, M. L., (1987). Acoustics of Ducts and Mufflers, J. Wiley Publishing, NY.
[56] Scheurmans, B. H., Polifke, W., Paschereit, C. O. (1999). Modeling Transfer Matrices of Premixed Flames and Comparison with Experimental Results. ASME 99-GT-132.
[57] Lee, J. G., Kim, K., Santavicca, D. A., "A Study of the Role of Equivalence Ratio Fluctuations During Unstable Combustion in a Lean Premixed Combustor," AIAA 2002-4015, 2002.
[58] Steele, R. C., Cowell, L. H., Cannon, S. M., and Smith, C. E., (2000). Passive Control of Combustion Instability in Lean Premixed Combustors, ASME Journal of Engineering for Gas Turbines and Power, Vol. 122, No. 3, pp. 412-419.
[59] Richards, G. A., Straub, D. L., and Robey, E. H., "Passive-Active Control of Combustion Oscillations," Presented at the Central States Section of the Combustion Institute, Knoxville TN, April 7 – 9, 2002.
[60] Richards, G. A., Straub, D. L., Robey, E. H. "Control of Combustion Dynamics Using Fuel System Impedance," ASME GT-2003-38521, 2003
[61] Richards, G. A., Straub, D. L., Robey, E. H., "Dynamic Response of A Premix Fuel Injector," ASME 2001-GT-036, 2001
[62] Munjal, M. L., Acoustics of Ducts and Mufflers, J. Wiley Publishing, NY, 1987
[63] Flores, R. M., Miyasato, M. M., McDonell, V. G., and Samuelson, G. S., "Response of a Model Gas Turbine Combustor to Variation in Gaseous Fuel Composition," ASME Journal of Engineering for Gas Turbines and Power, V 123, pp. 824 – 831.
[64] Doebelin, E. O., Measurement Systems - Application and Design, McGraw-Hill, 3rd Ed., 1983.
[65] http://webbook.nist.gov
[66] Gulder, O. L., "Flame Temperature Estimation of Conventional and Future Jet Fuels," ASME Journal of Engineering for Gas Turbines and Power, Vol. 108, pp. 376 - 380.

6 NATURAL GAS COMPOSITION: SENSOR REVIEW WITH APPLICABILITY FOR TURBINE CONTROL

6.1 Introduction

6.1.1 Objective

The conversion of energy via industrial gas turbines requires control systems which optimize efficiency, minimize pollutants, and protect hardware. With these criteria in mind, the objectives of this white paper are to review the state-of-the-art gas composition sensors as potential solutions to adequately determine gas composition for industrial gas turbine applications.

This review is motivated by both a projected widening in the diversity of the domestic natural gas supply as well as an increase in gas turbine performance requirements, which has elevated the perceived importance for utilizing fuel composition monitoring as a means for controlling turbine performance and emissions. Modern dry low emission (DLE) gas turbines use lean premix (LPM) combustion technology where the fuel and air are deliberately premixed at fuel lean (excess air) conditions before combustion. These combustion systems are susceptible to operational concerns such as dynamic pressure oscillations, lean flame blowout, and flashback. The stability margin for DLE turbines is significantly smaller than the margin for older diffusion-flame technology operating closer to stoichiometric conditions. Many DLE systems are operational worldwide, and gas supply stability issues can have a major economical and environmental impact for industrial applications (e.g., power generation). One obvious method for mitigating the effects of an unstable fuel supply is monitoring the fuel quality and controlling the combustion system accordingly. In fact, some engine OEMs are already applying gas composition sensors for engine control. In Riccius, et al.,[1] a novel infrared (IR) sensor is used to measure fuel composition for turbine control. In this example, the gas supply contains transient levels of C2+ that motivate the implementation of gas composition monitoring for maintaining turbine performance.

Low emission power-generating technologies, like DLE turbines, are important for achieving the Department of Energy's ultimate goal of zero-emissions advanced power systems. Recent changes in the department's gas turbine program have placed emphasis on turbines operating with coal-derived synthesis gas (syngas), and eventually pure hydrogen, as a fuel. Syngas composition is made up of mainly hydrogen, carbon monoxide, and carbon dioxide.[2] For syngas turbines, the challenges related to fuel composition will be similar to those for natural gas fired turbines. The syngas fuel will likely be generated locally by a coal-fired gasification system as part of a total power plant configuration such as an Integrated Gasification Combined Cycle (IGCC) plant. Although this less-diverse local-production of the syngas fuel will conceivably be more predictable, the possibility exists for transients in operations and subsequent fuel composition changes that can have a similar effect on gas turbine operations. However, the object of this report is related to the changing natural gas properties causing operational problems for low-emission combustion systems. Therefore, this report will focus on sensors capable of determining natural gas composition to mitigate the issues related to natural-gas-fired turbines.

6.1.2 Natural Gas

Processed natural gas is composed mainly of methane (~90%). For example, the natural gas composition shown in Table 6-1 is derived from weekly samples of the gas supplied to the National Energy Technology Laboratory (NETL) in Morgantown, West Virginia., from January to December 2005. The table shows the mean, standard deviation (STD), maximum, and minimum values computed from the gas chromatograph analysis results. The STD indicates long-term stability of the gas supply with approximately 2% variation in methane concentration. However, the minimum and maximum data indicate a wider variation. Although the specific reason for the composition swing is not known, and the composition changes were not monitored at sufficient frequency to provide a time scale for the supply transients, the data does show a change of approximately 8% methane replaced mainly by ethane.

Unprocessed natural gas, however, can contain hydrocarbons ranging from methane to noanes plus (C_1 - C_9+) and non-hydrocarbon species such as nitrogen (N_2), oxygen (O_2), carbon dioxide (CO_2), helium (He), hydrogen sulfide (H_2S), and water vapor (H_2O). Gas composition may vary widely from source to source and increases in the demand for natural gas as well as other economic factors are broadening the diversity of sources, and heightening the concern for a stable gas composition supplied to the end-user. Furthermore, the boost in imported liquefied natural gas (LNG) being introduced into the domestic supply are also contributing to these concerns due to the higher range of heavier hydrocarbons (C_2+) contained in LNG.

The Federal Energy Regulatory Commission (FERC) and other government agencies are teaming with industry and academia to review issues related to the domestic natural gas supply. Recent white papers from technical working groups, known as NGC+, provide detailed discussions of the issues for natural gas interchangeability,[3] and the issues surrounding natural gas liquids and liquid dropout.[4,5]

Table 6-1: Average NETL Natural Gas Composition and the Standard Deviation for 2005.

Natural Gas	Mean	STD	Maxium	Minimum
Species	Volume fraction			
CH_4	0.9174	0.0235	0.9681	0.8851
C_2H_6	0.0556	0.0196	0.0836	0.0186
C_3H_8	0.0084	0.0028	0.0135	0.0019
C_4 (various)	0.0031	0.0011	0.0052	0.0006
C_5 (various)	0.0013	0.0005	0.0021	0.0003
C_6 (various)	0.0006	0.0002	0.0011	0.0001
C_7+C_8 (various)	0.0004	0.0002	0.0008	0.0001
N_2	0.0111	0.0027	0.0192	0.0053
O_2+Ar	0.0009	0.0013	0.0096	0.0000
H_2	0.0000	0.0000	0.0000	0.0000
CO_2	0.0012	0.0004	0.0024	0.0005
AvgMolWt.	17.5166	0.4228	18.0251	16.5826
StoichRatio	10.0770	0.2222	10.3354	9.5222
Moles CO_2/Mole Fuel	1.0802	0.0305	1.1156	1.0067
Moles H_2O/Mole Fuel	2.0657	0.0314	2.1013	1.9821
HHV (mBTU/scf)	1.0651	0.0233	1.0920	1.0070
HHV (mBTU/LB)	23.0844	0.1339	23.4276	22.7763
HHV (cal/g)	12824.6086	74.3714	13015.2922	12653.4447
LHV (mBtu/Lb)	20.9637	0.1234	21.2759	20.6799
LHV (cal/g)	11646.4986	68.5649	11819.9327	11488.7865
C/H ratio	0.2611	0.0036	0.2653	0.2533

6.1.3 Thermodynamic Considerations in Burning Hydrocarbons

Various hydrocarbon mixtures will release different amounts of energy during combustion. However, if one knows the composition, then the amount of energy released during a complete burn can be predicted from the change in enthalpy (or enthalpy of combustion). The change in enthalpy is calculated by:

$$\Delta H_{Tot} = \sum_{m=1}^{i} \Delta H_{prod,m} - \sum_{n=1}^{j} \Delta H_{react,n}$$

The heat of combustion (or heating value) is a positive number equal to the magnitude of the enthalpy of combustion. The higher heating value (HHV) of the fuel is calculated by assuming all of the product water has condensed to a liquid, thus extracting the most amount of energy from the reaction. The lower heating value (LHV) assumes the water remains in a gas phase. For example, the following enthalpy data (Table 6-2) was acquired using FACT-Website[6] (Note: 1 joule = 0.0009478171 BTU).

$$CH_{4(g)} + 2O_{2(g)} \rightarrow CO_{2(g)} + 2H_2O_{(g)}$$

Table 6-2: Methane Thermodynamic Combustion Data as a Function of Temperature. A negative change of enthalpy indicates that the reaction is exothermic (gives off heat).

T(K)	Delta_H(kJ)	Delta_G(kJ)	Delta_Vol(l)	Delta_S(J/K)	Delta_Cp(J/K)	Keq
------ $CH_4(g) + 2O_2(g) \rightarrow CO_2(g) + 2H_2O(l)$ ------						
298.15	-890.3	-818.0	-4.8E+01	-242.5	93.5	2.0E+143
300	-890.1	-817.5	-4.9E+01	-241.9	93.4	2.2E+142
373.5	-883.2	-800.5	-6.1E+01	-221.5	93.8	8.9E+111
------ $CH_4(g) + 2O_2(g) \rightarrow CO_2(g) + 2H_2O(g)$ ------						
H_2O(1 mol): DH = 40.8 kJ DG = 0 ------ DS = 109.385 J/K						
373.50	-801.6	-800.5	0	-2.7	9.5	8.9E+111
400	-801.3	-800.4	0	-2.1	9.1	3.3E+104
500	-800.5	-800.3	0	-0.3	6.5	4.0E+83
600	-800.0	-800.3	0	0.6	3.6	4.7E+69
700	-799.8	-800.4	0	0.9	0.8	5.3E+59
800	-799.8	-800.5	0	0.9	-1.5	1.8E+52
900	-800.1	-800.6	0	0.6	-3.3	2.9E+46
1000	-800.5	-800.6	0	0.1	-4.7	6.6E+41

As shown in Table 6-3, one can consider the enthalpy of combustion (kJ/mol) of all major natural gas composition materials. Assuming the combustion temperature is 400 K, a slight change in the natural gas composition, e.g., 1 mol% of methane is replaced by 1 mol% of ethane, would result in a change in the energy produced by burning:

$$[(-1425.5) - (-801.3)] \text{ kJ/mol} * 0.01 = -6.241 \text{ kJ/mol}$$

Table 6-3: Enthalpy of Combustion (kJ/mol) for Methane (CH_4), Ethane (C_2H_6), Propane (C_3H_8), Butanes (C_4H_{10}), Hydrogen Sulfide (H_2S), and Carbon Monoxide (CO) at the Temperature between 298 K to 1000 K.

T(K)	Methane	Ethane	Propane	Butanes	H_2S	H_2	CO
$H_2O(l)$ ------							
298	-818.0	-1559.8	-2220.0	-2878.6	-562.2	-571.7	-566.0
300	-890.1	-1559.6	-2219.7	-2878.0	-562.1	-571.5	-566.0
373	-883.2	-1548.7	-2205.1	-2861.1	-559.3	-566.9	-566.0
$H_2O(g)$ ------							
373	-801.6	-1426.2	-2041.7	-2657	-518.5	-485.2	-566.0
400	-801.3	-1425.5	-2040.8	-2656.5	-518.6	-485.7	-567.0
500	-800.5	-1422.4	-2036.6	-2655.5	-518.8	-487.7	-567.3
600	-800.0	-1418.8	-2031.5	-2655.6	-519.0	-489.5	-567.3
700	-799.8	-1414.7	-2025.8	-2656.7	-519.2	-491.3	-567.1
800	-799.8	-1410.1	-2019.3	-2658.5	-519.3	-492.9	-566.6
900	-800.1	-1404.5	-2012.2	-2661.0	-519.6	-494.4	-566.0
1000	-800.5	-1399.5	-2004.5	-2663.8	-519.8	-495.7	-565.3

Similarly, the following table, Table 6-4, shows the relative heat change caused by the change of the natural gas composition between different gases. That is, the values in the table provide the change of heat after complete combustion when 1 mol% of the original gas on the left column is replaced by 1 mol% of the current gas, which is listed along the top row.

Table 6-4: Enthalpy Change (kJ/mol) After Burning when 1 mol% of the Gas in the Left Column is Replaced by 1 mol% of the Gas Listed in the Top Row.

	Methane	Ethane	Propane	Butanes	H_2S	CO_2	N_2	H_2	CO
Methane	0	-6.241	-12.395	-18.551	2.828	8.013	8.013	20.408	20.408
Ethane	6.241	0	-6.153	-12.310	9.069	14.255	14.255	26.565	26.565
Propane	12.395	6.153	0	-6.157	15.222	20.408	20.408	5.186	5.186
Butanes	18.551	12.310	6.157	0	21.379	26.565	26.565	0	0
H_2S	-2.828	-9.069	-15.222	-21.379	0	5.186	5.186	0	0
CO_2	-8.013	-14.255	-20.408	-26.565	-5.186	0	0	0	0
N_2	-8.013	-14.255	-20.408	-26.565	-5.186	0	0	0	0
H_2	-3.156	-9.397	-15.551	-21.707	-0.328	4.857	4.857	0	-0.812
CO	-2.343	-8.584	-14.738	-20.895	0.484	5.670	5.670	0.812	0

As an example, the values in the table indicate that a 1 mol% increase in butanes (and 1 mol% less in methane) will produce a change of heat energy by 18,551 J/mol. Assuming that the composition initially was purely methane and that it was being burned to completion, this change represents ~ 18,551/800,000 ~ 2.3% change in the energy content. The energy content of the fuel will effect the combustion temperature depending on the operating equivalence ratio of the

system. Small increases in the heavier gas content (propane and butanes) relative to the lighter gases (methane) will produce much more heat and so increase the burn temperature. The opposite will occur if the combustible gas composition is diluted by non-combustible materials such carbon dioxide.

For many applications, the gas composition changes are transparent unless a problem arises due to changes in the burning characteristics of the fuel. The Wobbe Index is widely used for defining domestic gas quality to the end-user,

$$WI = \frac{HHV}{\sqrt{SGgas}}$$

where HHV is the calorific (higher heating value) value of the fuel (BTU/scf), and SGgas is the specific gravity of the fuel with respect to air. The Wobbe Index is proportional to the heat flux of a given gas mixture through an orifice. The Wobbe Index for the average data in Table 6-1 is 1370, with less than 1% standard deviation indicative of a stable supply.

Traditionally, a variety of parameters are used to characterize gas quality for the end user. In industrial and power generation applications, a different index known as the modified Wobbe Index is used to define natural gas quality,

$$MWI = \frac{LHV}{\sqrt{SGgas \cdot Tgas}}$$

where LHV is the lower heating value of the fuel and Tgas is the temperature of the fuel. The MWI is used to account for heating of the fuel, and the unrecovered heat from water vapor formed during combustion.

Strict emission regulations require industrial and power applications to employ low-emission combustion technology which entail expensive treatments after exhaust to control emissions. In state-of-the-art natural-gas-fired turbines, like those used for power generation, lean premixed (LPM) combustion technology is used to minimize nitrogen oxides (NO_x) and carbon monoxide (CO) pollutants and to eliminate the need for treatments after exhaust. In LPM systems, the fuel and air are premixed to fuel-lean (excess air) conditions before combustion. The combustion flame is aerodynamically stabilized where the burning velocity matches the flow velocity of the fuel-air mixture. To achieve low emissions, the system must operate near the lean flammability limit, where the combustor is most susceptible to operational concerns such as combustion dynamics, flashback, and lean blowout.[5] Hence, changes in gas composition can be very problematic for stable and safe equipment operation in state-of-the-art industrial gas turbines.

This paper will explore the available sensor technology to measure gas composition. Sensors and controls can be applied in many end-user applications to reduce the impact of gas composition variations and facilitate more reasonable regulations. Naturally, depending upon the technology, the economics of applying sensors for many low-cost residential applications

may be prohibitive. For industrial and power applications, however, this is not the case. A more detailed discussion of industrial gas turbines and the potential benefit follows.

6.1.4 Summary of Gas Composition Effects on Gas Turbine Performance

Low-emission gas turbines are designed to operate on a nominal fuel quality (i.e., MWI), and the system is capable of handling limited MWI variations due to the temperature limits of the hardware components, permitted emissions performance, and the lean flammability limit of the system. For owners and operators of gas turbines, achieving low exhaust emissions is secondary to the reliability, availability, and maintainability (RAM) of the engine. Sophisticated control strategies and design changes have been implemented with the goal of maintaining low exhaust emissions while providing robust operability to protect the hot gas path components both upstream and downstream of the combustor. Even with elaborate control schemes, state-of-the-art natural-gas-fired turbines maintain a wide operating margin, away from the lean blowout limit, compromising emission performance for operability.[7] With adequate stability margins, however, robust operability is achieved over a wide MWI range. In advanced combustor testing,[8] premixed operability was maintained over a 20% variation in MWI, however the affects on emissions or potential turbine hardware damage for operations outside the designed limits were not discussed. The reluctance of original equipment manufacturers (OEMs) to minimize the stability margin stems from a lack of durable-responsive in situ combustion monitoring, and the many factors that can change the lean blowout limit during operations including component wear, environmental changes, and variations in fuel composition.

Perhaps the most important operating parameter for LPM combustors is equivalence ratio. The equivalence ratio is defined as the operating fuel-to-air ratio divided by the stoichiometric fuel to air ratio.

$$\Phi = \frac{(Fuel/Air)}{(Fuel/Air)_{stoichiometric}}$$

When values for equivalence ratio are less than one, it is described as a fuel-lean, or lean equivalence ratio, and when greater than one it is a rich equivalence ratio condition. Low NO_x emissions are achieved at lean equivalence ratios, where turbines are tuned for the regional gas composition to maintain premixed operability at a relatively constant combustion temperature. Changes in fuel composition can change the equivalence ratio and burning velocity (flame speed) of the fuel, even at constant MWI, resulting in operational concerns such as dynamic pressure oscillations, flashback, and lean blowout.

Combustion dynamics are a result of thermoacoustic coupling between the combustion heat release and the acoustics of the hardware. Changes in equivalence ratio and therefore combustion temperature can trigger the thermoacoustic coupling and potentially cause expensive hardware damage if mitigation strategies are not used to minimize the magnitude of the pressure pulsations.

At lean equivalence ratios, the flame speed of heavier hydrocarbons is greater than the flame speed for methane. Changes in concentration of heavier hydrocarbons (C_2 and above) can

change the burning velocity and increase the propensity of flashback or lean blowout in LPM combustors. Flashback is when the flame moves back into the premixing fuel injector, where hardware damage can occur quickly. Flashback can be triggered by increases in the flame speed and/or decreases in flow velocity. Lean blowout, on the other hand, is when the flame is extinguished due to a decrease in flame speed and/or increase in flow velocity. With rapid fuel composition changes, the possibility for flashback or lean blowout can also change rapidly, thus reducing the feasibility of using in situ or post-combustion measurements for control, and providing motivation to use fuel composition monitoring for controlling gas turbine combustion. Some engine OEMs are already applying more responsive fuel gas composition sensors for engine control, based on the concern of changing concentrations of higher hydrocarbons (C_2+) in the fuel. In Riccius, et al.,[1] a novel infrared (IR) sensor is used to measure fuel composition for turbine control. A review of IR sensor techniques is discussed later in this document.

6.2 Gas Turbine Control

The energy output of a power-generating gas turbine is controlled based on the electric load requirements. The gas turbine handbook is a good resource for understanding the different gas turbine technologies and configurations.[9] A common configuration for power applications is a single-shaft combined-cycle configuration, where the gas turbine, steam turbine, and generator are connected by a single shaft.[7] For single shaft power systems, the turbine is directly coupled with the generator, and the shaft speed (i.e., turbine speed) is maintained to provide the proper frequency over a wide range of load demands. The mass flow of fuel and air to the turbine combustor is controlled to maintain the turbine speed. The ratio of fuel and air, or equivalence ratio, to the combustor determines the combustion temperature and is controlled with the goal of achieving constant turbine inlet temperature (TIT) over the load range. The flow control for both air and fuel differ based on the original equipment manufacturer (OEM) configuration. A recent evaluation of control strategies for gas turbine plants[10] indicates the importance of maintaining a constant TIT for both thermodynamic and economic benefits.

The air flow to each local combustion zone is controlled by the pressure drop across the individual premixers. For large turbines, several premixers comprise a combustion can, and several cans around the annulus of the turbine form the turbine combustion system.[7] Fuel flow is supplied to the premixer through a pressurized fuel manifold. The manifold pressure and the pressure drop through the fuel path of the premixer regulate the fuel flow. Fuel flow control is achieved by changing the manifold pressure. State-of-the-art systems use a more complex fuel delivery system where the fuel is supplied by multiple manifolds.[7] When more power is needed, an appropriate increase in both the fuel and air must be made simultaneously to maintain a consistent TIT. At the same power, however, a change in gas composition will require adjustments of only one, either the fuel or air, to maintain the TIT.

6.2.1 Potential Control Solutions

A possible solution to maintaining flame stability without compromising emissions is to employ the necessary in situ combustion monitoring and fuel-control hardware for local combustion control. A case-in-point is the automotive and natural gas internal combustion (IC) engine industries, where direct fuel injection and exhaust-mounted oxygen sensors are being used for

local fuel/air ratio control, resulting in robust operability and low emissions. However, this is a potential solution for gas turbine combustors only if precursors to critical events (e.g., flashback, lean blowout) are detected in sufficient time to prevent them from occurring. Unlike the IC engine, turbines are continuously fired. To prevent the onset of instabilities, flashbacks, or flameout conditions, significant changes in the gas composition must be detected and compensated for before combustion. In other words, it may be too late to apply corrective action once the flame is anchored inside the premixer (flashback), or the flame is extinguished (lean blowout).

For changes in gas composition, several control options are feasible. For example, the temperature of the fuel could be increased to maintain a constant MWI. The time required for this is based on the capabilities of the fuel heating system. Generally, the heating time required for large volume flows will limit this control option to slow transients. Another option is to change the fuel flow to maintain a constant equivalence ratio. Turbine fuel control valves are very responsive, some capable of full-range actuation in less than one second. The volume of the manifold will impact the total response time, but fuel-flow control is certainly feasible and potentially the best option for transients in gas composition. The third option is to control very fast momentary shifts in gas composition by engineering design changes to the fuel delivery system which will provide the necessary volume and mixing capability to slow the transient (by mixing) to the capabilities of the fuel control system. It is noted that rather than measure the fuel composition, some combustion behavior like dynamics can be measured directly, and fuel split adjustments between pilot and main can be used to accommodate changing fuel composition, or ambient effects. This approach is practiced in some existing applications, but the (empirical) retuning of flow splits may be different with widely different fuel composition. This emphasizes the value of future, real-time composition monitoring and control.

To achieve robust control of the combustor in the wake of transient gas-composition changes requires a responsive gas-composition sensor for continuous monitoring. The remaining issues for sensors include lifetime, physical size, costs and, most importantly, the capability to accurately determine composition during changing fuel properties. To match the capabilities of the fuel control systems, the sensor should provide an accurate measure of fuel composition within one second. The sensor should be capable of individual species measurements for accurately determining the MWI and equivalence ratio changes, and the rate of change of these, due to changing gas composition. Ideally, the proposed sensor should be capable of measuring hydrocarbons ranging from C_1–C9+ as well as additional species, such as N_2, O_2, CO_2, He, H_2S, and H_2O. Obviously, other measurements are necessary to accurately determine MWI and equivalence ratio, but it is reasonable to expect measurements such as flow rates, pressure, and temperature measurements to exist as part of the industrial system.

Below, we review the state-of-the-art sensors for natural gas composition monitoring. Emphasis is placed on species currently found in the natural gas supply, a 0.1% volume fraction accuracy, and a minimum sample rate of one second for complete composition determination.

6.3 Gas Composition Sensors

6.3.1 General Comments Regarding Chemical-Sensing Technologies

Discerning one chemical species from another plus the quantitative concentration of each requires multiple pieces of information and hence multiple measurements. This can be accomplished in various manners only with certain physical measurement mechanisms. For example, simply measuring the specific heat of a sample containing a mixture of elements yields a single data point, the integrated specific heat. One has information, but it is not clear how many different materials are present, or at what concentrations. The same could be said of measuring the electrical resistance, thermal conductivity, viscosity, mass, or optical absorption at a single wavelength. However, if any of these physical attributes varies uniquely over some parameter that can be varied in time, then multiple measurements can be taken as the parameter is varied. If there is not too much overlap between the response function of any two of the material species, then it may be possible to separate the responses and thus discern how much of each of the species exists. The parameter that is varied must be controlled during the measurement. Typically, this might be done in time but in some cases could also be done in physical space or with multiple sensor detectors. Most commonly, the response function to a given species has breadth with respect to the measurement parameter. This breadth, especially for high species concentrations, can also result in response overlap.

Many chemical species measurement applications are concerned with contamination measurements, or very small amounts of one material in a large amount of a background material. Hence, the properties of the background material must be invariant or sufficiently non-interacting with the measured so that its signal does not interfere. However, the natural gas composition application is considerably different from this more common contamination measurement application. This means that many of the sensors to be discussed have not been studied in these high concentration regimes.

6.3.2 Traditional Laboratory Sensor Technologies

Natural gas is a mixture of multiple combustible hydrocarbon gases and non-combustible gases. Although it consists primarily of methane, it can also include ethane, propane, butane and pentane as well as high quantities of non-combustibles, such as carbon dioxide, nitrogen, and water. The composition can vary significantly[11] as shown in Table 6-5.

Table 6-5: Typical Composition of Natural Gas.[11]
(Used With Permission)

Component	Formula	Range (vol. %)
Methane	CH_4	70-90%
Ethane	C_2H_6	0-20%
Propane	C_3H_8	
Butane	C_4H_{10}	
Carbon Dioxide	CO_2	0-8%
Oxygen	O_2	0-0.2%
Nitrogen	N_2	0-5%
Hydrogen sulfide	H_2S	0-5%
Rare gases	Ar, He, Ne, Xe	trace

The most commonly employed laboratory instruments for gas-composition determination utilize either gas chromatography or mass spectroscopy. These two techniques are closely related in that they are based upon the separation of the gas species followed by detection or by direct separation and detection. The separation process can be performed by various methods, as can the detection. The strongest distinction between these two techniques is the introduction of a column in the chromatography technique, through which the gas must pass. The column provides a pathway, which tends to separate the species based upon molecular size, charge, polarizability, and other physical parameters which limit interactions between the gas species and the column materials. Hence, the species exit the column temporally. The traditional mass spectrometer utilizes other methods of species separation based primarily upon the mass and the charge of the ionized species. These separations are thought of as being part of the detector or detection process. Obviously, the separation technique of gas chromatography can be combined with the further separation techniques of mass spectroscopy resulting in a blurred distinction between the instruments.

6.3.2.1 Gas Chromatographs

6.3.2.1.1 Introduction and General Comments

A Gas Chromatograph (GC) separates the various components of a complex gas mixture by using an appropriate column for sorption and desorption events, which results in the transport of the various species of the gas mixture at different rates to the detector. An inert carrier gas (e.g., nitrogen, helium, etc.) is used to transport the gas sample through the columns.

The GC is widely used in laboratory and industrial applications for monitoring gas composition. The time required for transport of the various species through packed columns prevents continuous monitoring and limits the response time of the instrument.

6.3.2.1.2 Gas Chromatography Instrumental Components

The basic components for a typical GC instrument are (1) a carrier gas system, (2) a sampling system, (3) a column system, and (4) a detector system.

Carrier Gas
The carrier gas system contains the chemically inert carrier gas, and the necessary flow control hardware for controlling and metering the flow of the carrier gas to the required level for transporting the sample through the column. The type of inert carrier gas used will depend on the desired transport efficiency and the type of detector used in the GC.

Sample Inlets
The sampling system is designed to vaporize the sample and will vary depending on the intended sampling of gas, liquid, or solids. The sample system has a heater to maintain the appropriate temperature for introducing a vaporized sample at the head of the column.

Columns
The GC column is used to separate the main species of the sample and is typically either a packed or capillary design. The packed column contains layers of coated solid inert support material which are designed to promote the sorption and desorption of the sample for effective separation. The capillary column is designed to use the coated wall of the capillary itself for separation, and as a result, has much smaller diameter.

Detectors
The detector, which is located at the end of the column, produces a response that is proportional to the amount (mass or concentration) of the component that is separated by the column.

6.3.2.2 Mass Spectrometers

6.3.2.2.1 Introduction and General Comments

Several types of Mass Spectrometers (MS) have been developed, as described below. All types measure the mass-to-charge ratio of ionized gaseous atoms, molecules and molecule fragments. This creates a signal composed of peaks versus atomic mass number and is referred to as the mass spectrum of the sample.

The mass spectrum is generated by first ionizing all species and then accelerating them with an electric field. The ions are separated by their momentum distribution. The ions are monitored via charge detection as they impact, or approach, one or more detectors. The signal results are then used to calculate volume concentrations. Special precaution in the instrument design or signal interpretation must be used to avoid creating multiple ionization from the initial electron impact.

Each mass peak can be uniquely assigned to an element when singly charged, monomolecular gaseous atoms are present in a sample. However, other species and anomalies can make identification between mass spectrum peak and elemental form more difficult. For example,

different molecules with the same mass number will all appear as a single species. Likewise, double charging of a molecule can occur in the ionization process. Overlap between peaks, due to non-zero peak width, can make it difficult to distinguish species. The effect of rare stable isotopes of the principal constituent elements of gas streams (H_2, C_{13}, N_{15}, O_{17}, O_{18}, S_{33}, S_{34}, and S_{36}) may contribute signals. For molecules, one peak is produced with the same mass as the parent molecule. This is known as the "parent ion". In addition, peaks from multiple charged molecular ions and molecular fragments are created. For a single compound, the collection of peaks is referred to as the fragmentation pattern. Interpreting the fragmentation pattern is useful to distinguish species with (nearly) the same mass, e.g., CO and N_2 at mass 28.

Sample time may be a consideration in applying mass spectrometry to natural gas analysis. Mass spectrometers operate in a data cycle that progresses through the various masses. A time delay is required to allow parameters to stabilize before data acquisition for the next mass can begin. If the sampled gas composition changes during the mass spectrum acquisition, this can lead to errors in signal interpretation. Where significant, this problem can be solved if all the monitored ions are created at the same time. This can be accomplished by using arrays of detectors for simultaneous measurement or with time-of-flight mass spectrometers.

Thus, there are multiple factors which affect the accuracy of mass spectrometer measurement and signal interpretation. For this reason, different types of mass spectrometers have been developed. Common mass spectrometer designs with varying capabilities are listed in Table 6-6.

Table 6-6: Common Mass Spectrometer Types.

Sensor	Price ($k)	Size	Species	Gas Composition Update Rate (Data Sets/Second)
Scanning Magnetic Sector	40 - 100	60" H x 30" x 30" (Typical)	H_2, He, CH_4, H_2O, N_2, CO, C_2H_6, O_2, H_2S, Ar, CO_2, C_3H_8, SO_2, COS, CS_2, and hydrocarbons > C4	< 0.1
Scanning Quadrupole	10 - 100	Benchtop	" "	> 1
Time-of-Flight	> 10	Benchtop	" "	> 10
Detector Array Magnetic Sector	> 10	Benchtop	" "	1000

Other types of mass spectrometers include cyclotron resonance, Fourier transform, and ion trap instruments. Some of these are less accurate and more prone to various data artifacts,[12] but have other advantages. More details on some types of mass spectrometers are given below.

6.3.2.2.2 Mass Spectrometer Instrumental Components

A mass spectrometer produces the mass spectrum for determination of a sample's composition. The three main components of a mass spectrometer are (1) the ion source, (2) the mass analyzer, and (3) the detector.

Ion Source

Electron Ionization (EI) and Chemical Ionization (CI) techniques are employed to ionize the gases and vapors of the sample. Electron Ionization sources use a collimated beam of electrons that impact the sample molecules and force the release of an electron. Chemical ionization is achieved by using a chemical to promote ionization during collisions in the source. Both ion sources can cause fragmentation of the molecule into smaller ions and neutral fragments, and generate both negative and positive ions. However, only the positive ions are transported to the mass analyzer and detector.

Mass Analyzers and Detectors

The mass analyzer is used to separate the positively charged molecules based on the mass to charge ratio. Several types of mass analyzers exist: magnetic sector, quadrupole, ion traps, time-of-flight, Fourier transform, and ion cyclotron resonance. The more common analyzers are the magnetic sector, quadrupole, and ion trap types. Brief descriptions of the various types are given below.

Scanning Magnetic Sector Mass Spectrometers

A scanning magnetic sector mass spectrometers are based upon the use of the Lorentz force on a charged particle, $F = q(E+vxB)$, where q is the charge of the ion, E is the electric field vector, v is the velocity vector of the ion and B is the magnetic field vector. The ions are first accelerated with the electrical field and then deflected with a perpendicular magnetic field toward a detector.

The radius of curvature of the ion trajectories is inversely proportional to the square root of the mass, producing well-defined ion beams for each mass, deflecting to a greater degree the more charged and faster-moving, lighter ions. One ion is detected at a time by switching, or scanning, the magnetic field strength or static electric field strength to route the selected beam through a slit to a single detector. The analyzer can be used with fixed field values to select a narrow range or a single mass (mass to charge ratio) value, or it can be used to scan through a range of expected masses.

The accuracy and stability of the scanning magnetic sector mass spectrometers are the best available among commercial mass spectrometers.[12] Magnetic sector instruments can run for weeks on multi-component mixtures without recalibration. More complex gas mixes, though, will require more frequent recalibrations due to the sensitivity of calculated gas concentrations to small changes in the fragmentation patterns.

Some drawbacks include the time required to monitor all the required masses, the range being from seconds to tens of seconds depending on how many masses are monitored. The varying of large magnetic fields is usually slow. And the mass spectrometer is large.

Only a subset of the mass range of 1 to 100 or 1 to 200 amu (Atomic Mass Unit) is typically monitored due to time constraints, because sampling the entire mass range would decrease the throughput by an order of magnitude. Selecting which masses to monitor involves assumptions about the gas composition. Unexpected components can produce errors in calculated

compositions of expected components. The cost is around $100,000. With some compact units (cycloidal mass spectrometers) available for $40,000.

Scanning Quadrupole Mass Spectrometer

An electric quadrupole is a four-fold symmetric gradient field arrangement originating from four charge sources. By constructing this with cylindrical metal rods or wires, the field geometry is cylindrical and does not vary along the z-axis. A quadrupole mass analyzer uses four parallel metal rods connected together electrically. When a charged particle travels along the z-axis through these gradient fields, it is deflected. However, if the fields are properly varied in time, the charged particle deflection direction can be reversed back and forth temporally. If the deflection rate and the velocity are chosen appropriately, the charge particle propagates along the z-axis without colliding with the rods or escaping from the quadrupole field region. At this point the particle motion is said to be in resonance. This scanning of the mass-to-charge ratio, by varying the voltages, allows selection of a particular ion. Mass analysis is performed sequentially in time.

Quadrupoles are more compact than magnetic sectors and can switch between masses faster. A set of masses can be sampled several times a second with some designs. Sensitivity is higher than the case with a magnetic sector because some quadrupoles can operate at a higher pressure within the vacuum chamber (e.g., more ions are available).

Quadrupole mass spectrometers tend to be less stable than magnetic sector instruments and require frequent calibration (much more frequently than magnetic sectors, based on past experience). Maintenance is expected to be more frequent than with magnetic sectors due to the accumulation of static charges on contaminated areas of the quadrupole rods. Resolution is dependent upon the length of the mass analyzer, which is difficult to make into a compact device. Only a subset of the mass range is monitored due to time constraints, leading to errors if unexpected components are present. The cost runs from less than $20,000 for the least expensive units (known as residual gas analyzers), to $100,000.

Ion Trap Mass Spectrometer

An ion trap uses two foci-facing hyperbolic metal electrodes and a third hyperbolic ring electrode halfway between them, and AC ~ 1 MHz and DC electric fields to trap ions in space. The AC field oscillates in phase between the two facing hyperbolic electrodes and out of phase with the center hyperbolic electrode to trap the ions. The subsequent ion cloud that forms will vary with the AC field, resulting in long thin or short wide ion clouds. When the ion trap is used in conjunction with a quadrupole separation technique (described in a previous section) improved signal to noise and reduced size of the mass spectrometer are achieved.

Time-Of-Flight Mass Spectrometer (TOFMS)

In time-of-flight (TOF) mass spectrometer, physical drift is used to separate particles by mass.[12] The measurement process is initiated by a rapid ionization of all species at a single location, typically by pulsed electrical current or pulse laser excitation, so that a cluster of ions (plasma) originates from one physical spot at the same time. After ionization, each particle's charge is quantized and ideally will have only one charge per particle. Provided there are no significant ion-ion interactions, all ions are then accelerated, via a uniform electric field, to the same

constant kinetic energy per charge, $E = (mv^2)/2$. Hence, the ions exit the electric field region with a velocity which is proportional to the square root of the mass. Because of the differing velocities, after passing through a given distance (drift region) the ions are separated in time as they arrive at the detector. This means that the transit time for lighter mass ions is shorter than for heavier mass ions. The mass separation (resolution) is proportional to the drift region distance, so the resolution in time is largely determined by the length of the device. This distance must be very large compared to the physical size of the initial plasma geometry to provide adequate mass separation. For this reason, long distances are required. This is commonly achieved via folded designs.

A reflectron composed of a series of electrically excited rings or grids acting as an ion mirror is employed to reverse the direction of the ions. This mirror provides the added benefit that it decreases the differences in flight times of ions that leave the ionization chamber with identical mass-to-charge ratios, but different kinetic energies, this improving the instrument's resolution.

A TOFMS provides a snapshot of a gas stream quickly enough so that changing gas compositions are not significant. The duty cycle (the fraction of time the signals are being monitored) ranges from 5% to 30%, but may approach 100% for some designs.[13]

TOF mass spectrometers are the only type of single-detector mass spectrometers that can sample rapidly enough to avoid mathematical errors from changing gas compositions. Several gas compositions per second should be easily available. Many TOF instruments can sample much faster.

All of the masses within a given mass range (1 to 100 or 1 to 200 amu for gas turbine applications) are sampled, allowing observation of unexpected components in the gas stream. However, the analogue/digital (A/D) converter that digitizes the time-domain signals must be fast and in some cases has a limited dynamic range.[12] The cost is tens of thousands of dollars.

Fourier Transform Mass Spectrometer (FTMS)

A Fourier transform ion cyclotron resonance mass spectrometer, sometimes referred to as just a Fourier transform mass spectrometer (FTMS), consists of an ion source, ion optics to guide the ions to a magnetic field and a Ion Cyclotron Resonance (ICR) cell or Penning trap (a static electric/magnetic ion trap) to hold the ions. Once the ions are trapped in the ICR cell they are excited by an oscillating RF electric field applied to the transmitter plates of the resonance cell. This field, along with the magnetic field of the trap causes ions with the proper mass-to-charge ratio to travel in a cyclotron orbit within the cell. The moving charges induce potentials in the receiver plates as they pass by them, producing an oscillating signal. Applying a Fourier transform to this signal gives the resonant frequency of the ions which is determined by ion's mass-to-charge ratio. FTMS provides improved sensitivity and resolution since each ion is essentially counted many times, however there are concerns about the overall accuracy of their measurements because of signal harmonics.[12]

Ion Cyclotron Resonance Mass Spectrometer

Ion cyclotron resonance mass spectroscopy (without Fourier transform signal processing) is similar to FTMS. An RF field is used to excited ions in a Penning trap, forcing the ions to move

in a spiral path until they make contact with the wall. Different masses are determined by the time it takes ions to reach the detector, located at the trap wall.

Detectors sense ions by measuring current flow when an ion impacts the detector, or by measuring induced current from passing ions. Because the ion concentrations leaving the mass analyzer at a particular instant are usually quite low (either intrinsically or in order to achieve resolution) some type of electron multiplier is typically employed in the detector, although other detectors (such as Faraday cups) have also been used. Significant amplification at the early detection process step is often necessary to get the signal above the electronic noise. The common cathode geometry of a photo multiplier tube can be used to understand electron multiplication, but Microchannel Plate Detectors are commonly used in modern commercial instruments. This same device is employed in modern night vision goggles to amplify the small amount of IR photons available. The microchannel plate is a porous plate with microchannels etched through its thickness. A field applied across the plate thickness causes electrons, which are created by the ions that arrive at the surface or enter the channels, to accelerate down the channels to be avalanched (multiplied) as they collide with the channel walls. Hence, for each ion that bombards at the plate surface, hundreds of electrons emerge from the microchannel plate to be detected.

6.3.2.3 Hybrid Techniques

6.3.2.3.1 Gas Chromatography/Mass Spectrometry

To achieve a higher performance analysis, mass spectrometry can be preceded by the separation process of gas chromatography (GC/MS). Each of the techniques has its own limitations in identifying compositions. For example, some different species in a mass spectrometer can produce the same signal because their ion fragments have the similar charge to mass ratios. Likewise, some different species in a gas chromatograph analysis will produce the same signals when the species travel through the column in the same time. Using both techniques together can serve to differentiate these species because it uncommon that both techniques are unable to distinguish property differences.

6.3.2.3.2 Ion Mobility Spectrometry (IMS)/Mass Spectrometry

The principle of the ion mobility spectrometer (IMS) is a time-of-flight measurement in the presence of a medium. A gaseous sample is injected into the spectrometer and ionized by a radioactive source. Charged ions are accelerated by an electric field and sent to a detector. Time-of-flight is measured. Due to atomic collisions with a neutral gas at atmospheric pressure, the transient time is determined by the ion radius relative to the charge of the ion. In contrast with a mass spectrometer, vacuum pumps are not required since the IMS operates under atmospheric conditions. As such, an IMS unit can be made physically smaller.

It is also possible to combine mobility spectrometry and mass spectrometry (IMS/MS). Ions are separated by their transit times as in conventional IMS, and then sent to a conventional mass spectrometer. This approach provides information from both the IMS separation and the mass-to-charge ratio of the ions.

6.3.2.4 Example Commercial Devices

6.3.2.4.1 Quadrupole Mass Spectrometer (QMS) Products

Moorfield Associates has produced a portable QMS system: the ecoSys-P device.[14] The following information was taken from the vendor website:

The ecoSys-P can be easily carried by an individual (26kg) and can operate in a full remote mode, via a phone line or mobile phone. The standard system can detect to a single part per billion (ppb) level at very high speeds (100 millisecond (ms) per mass) and has a sample transfer time between process event and M/S detection of less than 100 ms for capillary versions and less than 1 second (s) for membrane inlets. It can detect up to 64 species in real time. The addition of an automatic thermal absorber allows detection to parts per thousand (ppt) levels, but increases the point analysis time to 90 seconds. It can even identify the unknown species.

This instrument has fast real-time measurement (less than 1 second), good discrimination capabilities, and a wide detection range of chemicals in real time. It is sensitive to ppb~ppt level and is portable. However, it is quite expensive (more than $40,000) and fairly large (26 kg). No information is given on hydrocarbon selectivity.

6.3.2.4.2 Natural Gas Analyzer (NGA) – Agilent

The Agilent 3000 Natural Gas Analyzer (NGA)[15] is a gas chromatography system designed for natural gas. The following information was obtained from the vendor website:

A reliable modular design that enables fast instrument repair, and results that can be obtained in under 2 minutes (which might take over 20 minutes otherwise). The NGA is accurate, with extended dynamic range, digital pneumatics, and a multi-channel design that supports data integrity by performing repeat measurements with confirming peak identification in less time than a single measurement would take using a conventional GC. It is accessible for operators at various skill levels, with Cerity Networked Data System for Chemical QA/QC, and is claimed to be a superior alternative to most conventional lab GCs. For routine measurement of fixed gases, this instrument measures C_1 to C_5 hydrocarbons from parts per million (ppm) to high percent, and C_6 to C_{12} from ppm to low percent (optional sample conditioners allow analysis of LPG, high-calorific-content natural gas, and liquefied natural gas).

6.3.2.4.3 Heated Hydrocarbon Analyzer – CAI

California Analytical Instruments, Inc. (CAI Inc.) has produced a heated hydrocarbon analyzer (Model 300 HFID),[16] as advertised:

"It is designed to continuously measure the total concentration of hydrocarbons within a gaseous sample. The Model 300 HFID uses the Flame Ionization Detection (FID) method to determine the total hydrocarbon concentration within a gaseous sample. The analyzer has an adjustable heated oven (60 to 200 °C) which contains a heated pump and a burner in which a

small flame is elevated and sustained by regulated flows of air and either pure hydrogen or a 40/60 mixture of hydrogen and nitrogen."

The methane-only option provides the capability for measuring methane only or total hydrocarbons. The sensitivity is 0.1 ppm carbon. The response time is less than 1.5 seconds for 90% of full scale. There is, however, no selectivity.

6.3.3 Exploratory Sensor Technologies

Most chemical-sensing technologies strive to detect very small amounts of species in a background of air or other constant environment. The gas composition sensing application is essentially the inverse of this, for here the materials to be determined are in high concentrations. Hence, many of the chemical sensor technologies are not appropriate. For example, the use of organic based sensors, which are quite promising for detection in the ppm range, might very well dissolve in the high concentration of certain gas species.

6.3.3.1 Infrared Optical Spectroscopy

6.3.3.1.1 Introduction

The interactions between materials and electromagnetic waves can be used to determine the molecular structure of a material. The electromagnetic wave with a frequency range from 10 to 13,000 cm^{-1} (wavenumbers) is categorized as infrared radiation, and its application to organic chemistry is known as IR spectroscopy. Photon energies in this part of the spectra can excite vibarational bonds, and absorption lines connected with specific bonds can be used to identify molecules.

The IR spectrometer is one of most common analytical instruments used to identify all types of organic and many inorganic compounds, and to determine the functional groups in organic materials. The technique involves collecting and plotting the IR absorption intensity, or percent transmittance, as the y-axis versus the x-axis wavelength, or wavenumber. A nondestructive and non-contact measurement method, IR spectroscopy has minimal sensitivity to working environments. This quality makes it a good method for various operation conditions.

Since natural gas is composed primarily of organic materials, IR spectroscopy can be a very powerful tool to determine the composition of a natural gas sample. Figure 6-1, shows the typical mid-IR (400 to 4000 cm^{-1}) absorption spectrum of some of the more common materials in natural gas.

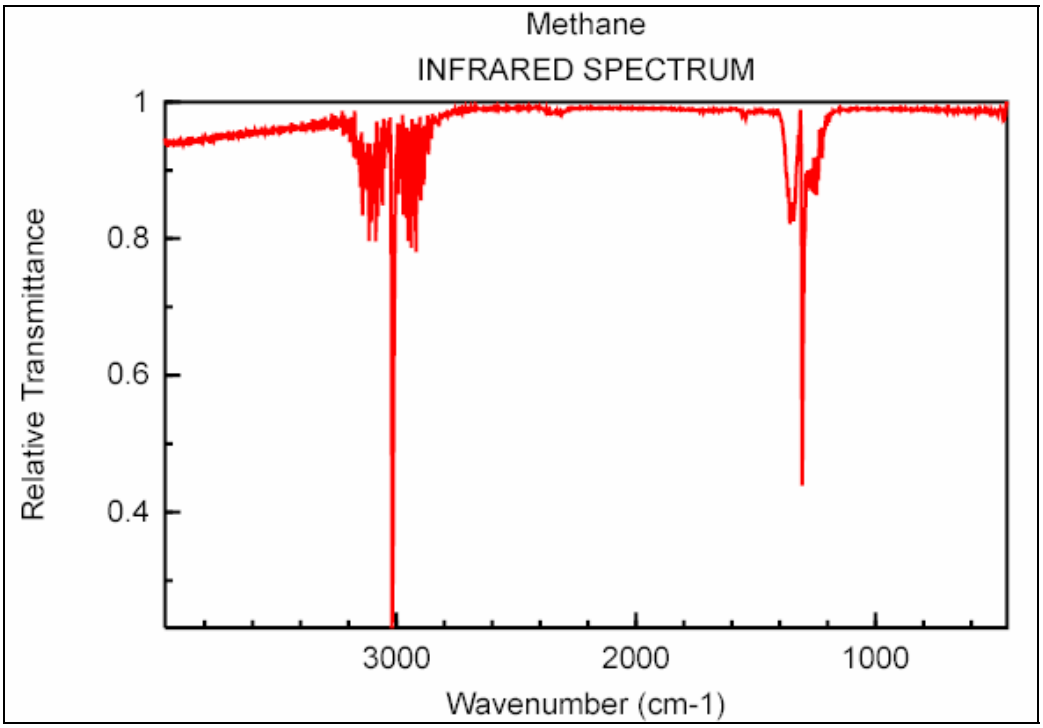

Figure 6-1a: Infrared Absorption Spectrum of Methane (from lab measurements of one author of this report).

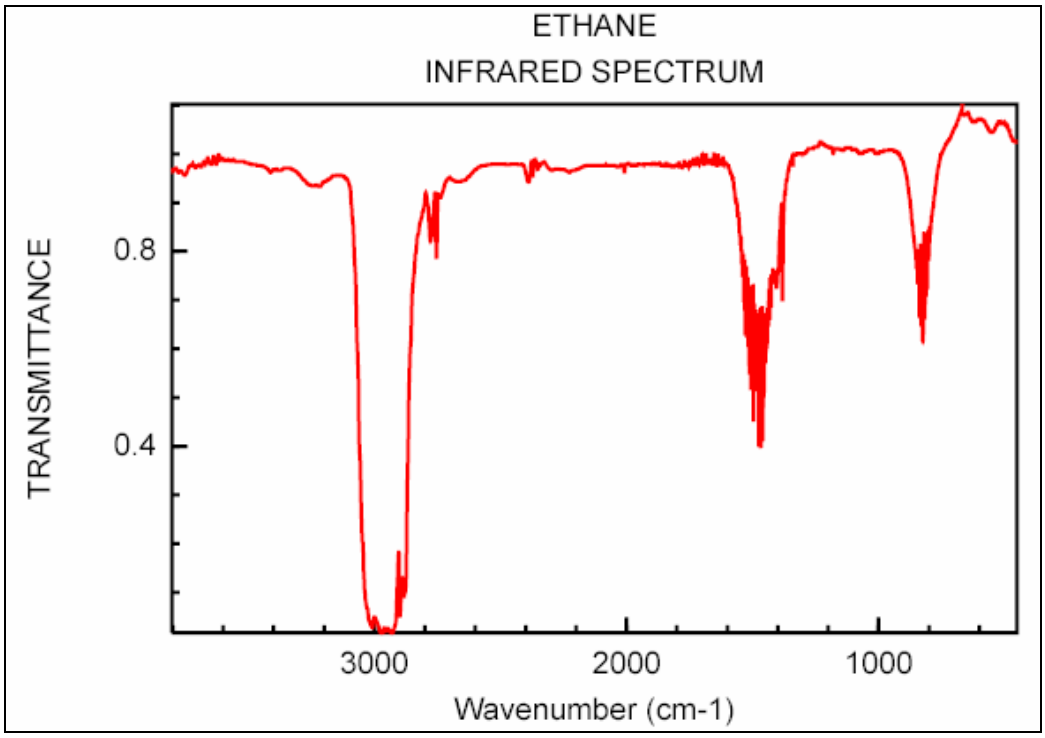

Figure 6-1b: Infrared Absorption Spectrum of Ethane.

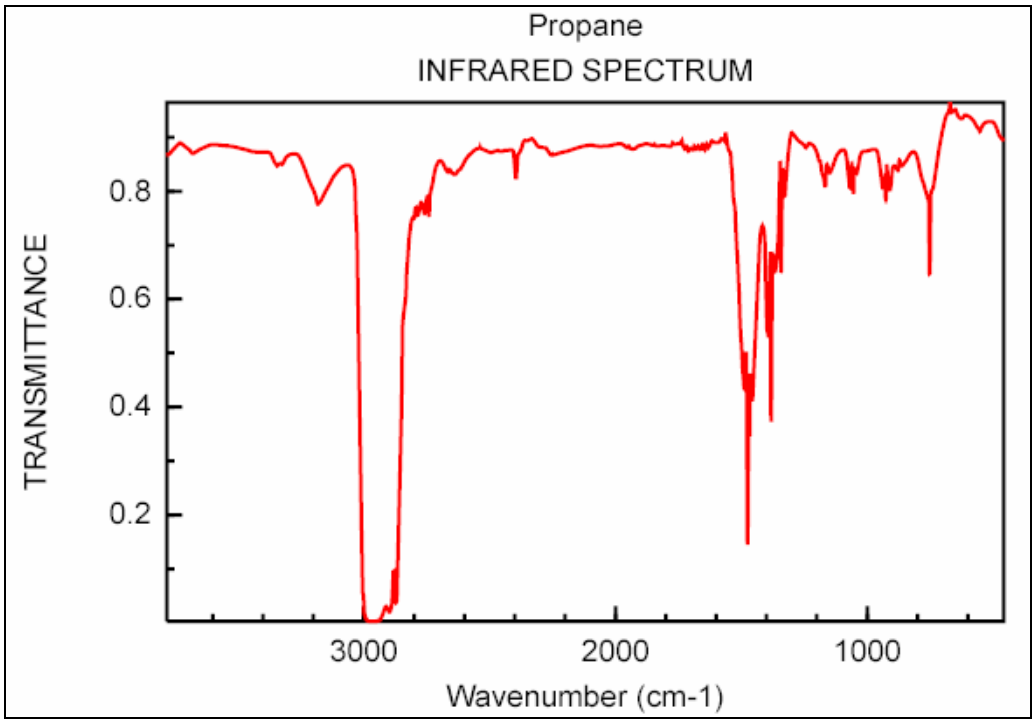

Figure 6-1c: Infrared Absorption Spectrum of Propane.

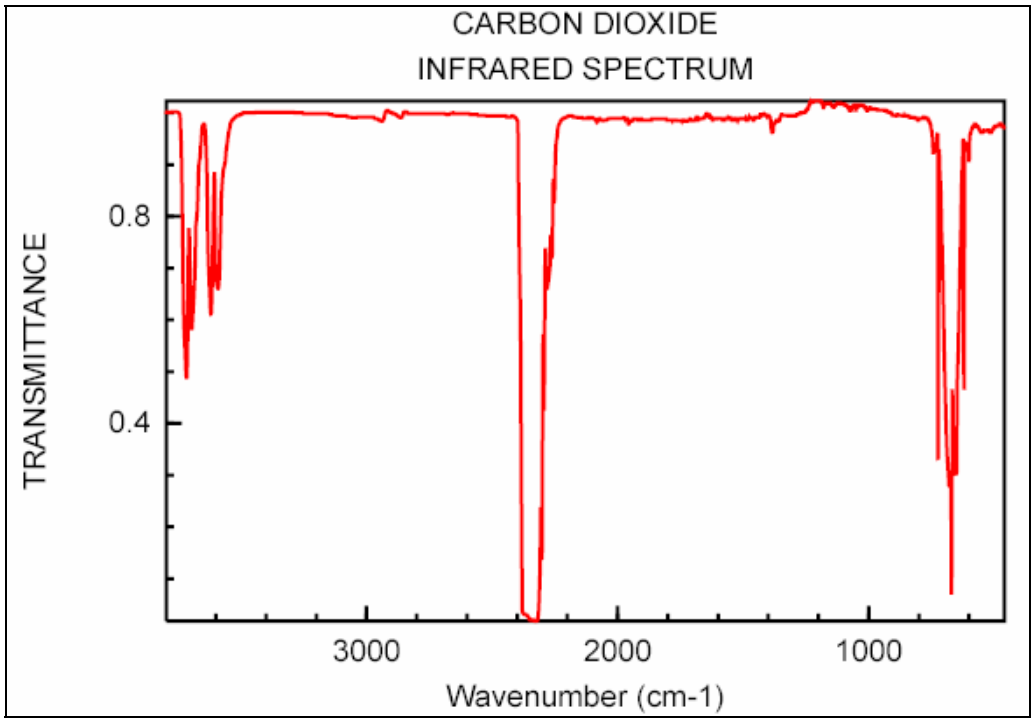

Figure 6-1d: Infrared Absorption Spectrum of Carbon Dioxide.

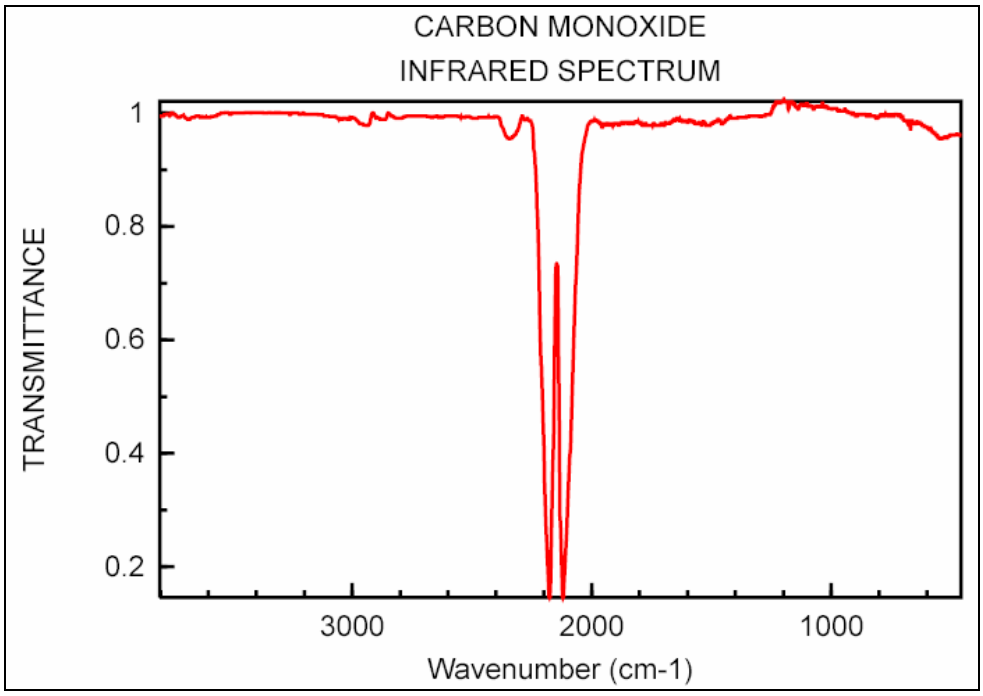

Figure 6-1e: Infrared Absorption Spectrum of Carbon Monoxide.

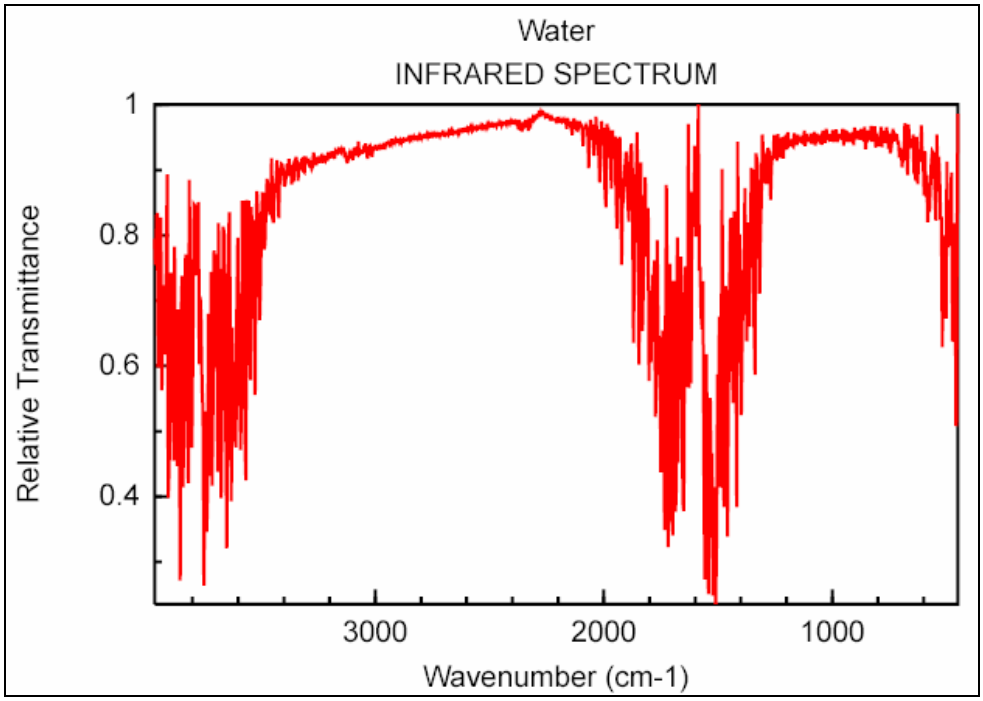

Figure 6-1f: Infrared Absorption Spectrum of Water.

6.3.3.1.2 <u>IR Spectrometer Instrumentation</u>

The dispersive IR spectrometer and Fourier transform spectrometer are the two most common IR spectrometers commercially available.[17]

Dispersive IR, another widely used IR technique, was first introduced in the mid-1940. The major components of an IR spectrometer include: (1) radiation (light) source; (2) monochromator; and (3) a detector. The radiation source is usually a blackbody formed by electrically heating a cavity or surface between 1000 to 1800 °C. Due to the spectral range, the detector technology is non-trivial. Semiconductor optical detector technology is limited in this spectrum and only recently have new devices started to emerge which can respond over the necessary range of wavelengths. The traditional detector over this range of wavelengths is the thermal bolometer, which is composed of a thermal pile made up of a series-connected group of thermal couples. Recent advances in MEMS technology have resulted in thermal piles being constructed with fast response times. Hence, while it has limited sensitivity without cooling, it is universal in its responsivity.

The monochromator divides the light into wavelength ranges of interest, similar to a prism. The sample and reference cell signals, at the wavelength of interest, are sent to the detector for comparison.

Recently, Fourier transform IR spectrometers have become very popular because they can produce an analysis faster, and have better sensitivity than conventional IR systems. Instead of a monochromator, the FTIR uses an interferometer with two beams to generate an optical path difference. This can be used to study IR spectra by modulating the path difference (in time, from a translating mirror) to create the signal. When combined, these beams generate an interference signal which is converted from the time domain to the frequency domain a using Fourier transform.

6.3.3.1.3 Response Time, Sensitivity, and Selectivity

Depending upon the type of a spectrometer, the response time of an IR spectrometer can vary from seconds to tens of minutes. However, the FTIR spectrometer has the distinct advantage of a faster response time than the dispersive IR spectrometer. An FTIR instrument can achieve the same signal-to-noise (S/N) ratio as a dispersive spectrometer in 1 second or less versus 10 to 15 minutes. For situations where detection speed is important, such as in-line gas monitoring, the response time of the FTIR system is definitely an advantage.

IR spectrometers have very high selectivity with organic materials due to their operation principle. We can clearly see the difference in the IR spectrums of the gases shown in Figure 6-1. The distinctive characteristic arrives from the knowledge of the shape of the entire absorption of a given species. That is, considerable information is contained in a measurement.

6.3.3.1.4 Application to Natural Gases Analysis

Due to the advantages of fast response and high selectivity, infrared spectroscopy has gathered considerable interest for in situ and online gas monitoring applications.[18,19,20,21,22] Since the measurement can be made at a distance from the mechanical components, the IR spectrometer has no fundamental limitation on operation temperature or gas pressure. This makes it an ideal technique for combustion control of turbines and burners.

Natural gas is a combination of several gases, thus the IR spectrum of natural gas is a convolution of the IR spectrum from all the gas species in the sample. Therefore, it is impossible to tell the composition of a natural gas from its IR spectrum directly. However, a calculation algorithm can be applied to obtain the composition information. To do this, Mullins et al.[18] applied principal component analysis to data points taken from a four-wavelength channel in the near-infrared spectrum of tested gas mixtures achieving reasonable agreement between estimated concentration and real concentration. Clearly, this opens the possibility of not actually requiring a dispersive element if the detector could be constructed to have a minimal optical selectivity.

Kastner[22] combined optical techniques with a thermal conductivity measurement of the gas and analyzed the correlation between the two sets of information to determine the natural gas composition. An in situ measurement device has been developed with potentially a fairly low cost. Natural gas runs through the inlet to the outlet, and system measures the pressure, temperature, total thermal conductivity, and IR optical absorption of hydrocarbons and carbon dioxide. From the IR absorption spectrum, the mole fraction of hydrocarbons and carbon dioxide can be determined since their absorption peaks are well separated. Thermal conductivity of the total gas can provide the concentrations of hydrocarbons and nitrogen. The system has about 20 to 25-second response time, but it is conceivable that this can be reduced. The accuracy of the system is satisfactory with a ± 0.25% deviation from a reference chromatography.

6.3.3.1.5 Commercial Availability

- IR spectrometers are available at several vendors. PerkinElmer, Inc. (www.perkinelmer.com) provides complete series of FTIR and FTNIR spectrometers.
- Newport, Inc. (www.newport.com) provides benchtop IR spectrometers and minispectrometers.
- Ion Optics developed a miniature IR sensor system, named SensorChip. It is a wavelength-tuned, MEMS-based micro-bridge element. Even though it cannot provide the very good resolution of traditional analytic IR instruments, MEMS technology based IR systems potentially could have a much smaller size with much lower cost and power consumption compared to state-of-the-art IR technology. This would be very attractive for portable applications, or as an in situ device.
- Currently there are no commercially available in-line monitoring IR spectrometer systems on the market.

6.3.3.1.6 Infrared Semiconductor Light Sources and Detectors

Light Sources

Until recently, infrared light sources in the spectral region stretching from 2 to 12 μm were dominated by incandescent lamps or black body sources. Selection of a particular wavelength or spectral region for a specific application such as spectroscopy was accomplished by using a monochromator or a filter. While this approach works quite well, the intensity of the light selected is attenuated by the narrowed bandwidth. In some cases, this can complicate the application or the interaction of the infrared light with the sample medium. In absorption or fluorescence spectroscopy, for example, this makes the detection of the resultant or residual light

difficult because of the low signal-to-noise ratios. The advent of infrared laser sources in the infrared spectral region has helped simplify some of the spectroscopic applications of infrared light. The first generation of these lasers was based on the Pb-salt semiconductors of PbTe and PbSe. For optimal operation, they are usually cooled to low temperatures during operation, depending on the wavelength. For the spectral region between 2 to 4 µm, they can generally be cooled by thermoelectric coolers to about -50 °C; for the spectral range from about 4 to 12 µm, they are cooled to cryogenic temperatures (~200 °C).

The PbSe lasers are commercially available from several companies in this country and abroad, such as Ekip Tech, Inc, Norman, OK, USA (www.breathmeter.com). The nominal cost of these lasers is about $5,000. Another type of laser that covers the mid-infrared range (1.8 to 3.8 µm) of the spectrum is fabricated from gallium-antimony (GaSb)-based semiconductors. Lasers of this type are commercially available from companies such as the Sarnoff Corporation in Princeton, NJ (http://www.sarnoff.com/products_services/optoelectronics/mid_ir.asp). These lasers can be operated at room temperature.

In general, compared to lasers in the near-infrared (0.85 to 1.55 µm), mid-infrared lasers tend to be expensive, costing anywhere from about $2,000 to $30,000. The upper end of the price range represents sophisticated, tunable lasers with programmable control electronics. The higher-cost lasers are generally used in very specialized and critical applications. The price difference between the near-infrared lasers and mid- to far-infrared lasers is in part due to technical reasons, but mostly due to market size. In the near-infrared, there are many consumer applications for near-infrared lasers. The other market driver for these lasers is data communications; in the 1.3 to 1.5 µm range, lasers are used in telecommunications. Over the years, the large demand for products in this range of the spectrum has steadily driven their price down to the point where near-infrared lasers can be acquired at the rather inexpensive price of $1 or less in large quantities.

The latest and most advanced infrared lasers available today are the quantum cascade lasers available from manufacturers such as Alpes Lasers, Switzerland (http://www.alpeslasers.ch). These sophisticated lasers can cover the spectral range from 4 to 20 µm. The quantum mechanical concept of cascade tunneling has recently been extended to making Terahertz (THz) lasers. The THz laser sources are only available in small quantities for research and are not yet commercially available.

Detectors

Detectors in the infrared region of the optical spectrum come in two varieties: thermal, or bolometric, detectors and photon detectors. Bolometeric detectors are spectrally flat and are generally used in applications where one is not concerned with spectral resolution or precision. Photon detectors, on the other hand, are spectrally sensitive, have finite bandwidths, and exhibit a spectral threshold for detection.

The most common infrared photon detector is silicon, however for near-infrared spectroscopic applications germanium (Ge) is standard because it can cover the range from 0.6 to 1.6 µm. In the mid-infrared (1.6 to 4.5 µm) range, the detectors of choice are Indium-Arsenic (InAs) and lead-sulfur (PbS). These are usually cooled to low temperatures (<-30 °C) for optimal operation.

When the need is for detection of radiation beyond 5 μm, the photon detector commonly utilized is a cryogenically cooled mercury-cadmium-telluride (HgCdTe or MCT). MCT detectors can be made to span the spectral range from 3 to 18 μm. These detectors are commercially available at reasonable cost ($300 to $2,000) from a number of companies. The least expensive of these detectors can be obtained for less than $200[23] from Judson Technologies, Montgomeryville, PA.

6.3.3.2 Raman Spectroscopy

Just as mass spectroscopy is commonly used to determine composition of gases, Raman spectroscopy has become a popular technique for the determination of the composition of biological or organic (hydrocarbon) solids and liquids. However, unlike optical-absorption spectra-peaks where the incident light energy is selected to match the spectra peak and the optical transition energy, the Raman effect is an indirect optical scattering process related to the polarization of an entity by energetic electromagnetic radiation. In the same way that a change in the polarization represents a separation of charge, the excitation represents a vibration mode or rotational mode among molecular bonds, or possibly even a direct-absorptive, electronic-energy transition. These vibration and rotation-mode energies are dependent upon the molecule bond structure as well as on the neighboring bonded atoms or environment. Because the probability of Raman scattering is only about 1 in 10^7 of the other photon-molecule interactions (non-wavelength-altered Rayleigh scattering), the resulting signals are weak unless the optical power and the molecule concentration, or both, are high. This is the reason the Raman spectroscopy is traditionally applied to solids or liquids and is less effective with the dilute species concentrations in gases. Also, since highly ionized bonds such as the oxygen-hydrogen (O-H) bonds are already highly polarized, the electrical field of the incident radiation is usually ineffective at altering the polarization and so show little Raman effect. On the other hand, bonds that are covalent or that distribute electron clouds (such as the pi-electronic structure of a double-carbon bond) can effectively be polarized by the electric field of the radiation.

Reasonably useful tutorials and references on the Raman effect can be found on a number of web sites, such as Kaiser Optical Systems Inc.,[24] McPherson Inc.,[25] and HORIBA Jobin Yvon.[26]

The Raman process irradiates the sample with a photon of energy higher than the vibration transition energy. The molecule is excited to a virtual state and immediately (in 10^{-14} second) reradiates a second scattered photon. The difference in the energy of these two photons is equal to that of the Raman transition energy (the vibration or rotational-mode energy). Hence, the Raman photon frequency is equal to the difference between the excitation and the scattered photon frequency. If the species in the ground state is excited, the resulting scattered photon is of less energy than the exciting photon (Stokes Raman scattering). On the other hand, if the species is initially at an elevated temperature and the vibration or rotational mode is already excited, the Raman signal will be due to a scattered photon energy which is greater than the exciting photon because the process leaves the species in the ground state (Anti-Stokes Raman scattering). In either case, the Raman difference wavelength is the same, but the signal intensity can differ considerably. At low or normal temperatures, the Anti-Stokes scattering yield is low due to the initially low density of excited species. As the sample temperature is raised, the Anti-Stokes scattering intensity grows rapidly, and an intensity measurement can provide a measure of the sample temperature. The choice of the use of the Stokes versus Anti-Stokes scattering

measurement depends on the choice of the excitation frequency ($\nu_e = c/\lambda_e$) versus the measured scattered frequency ($\nu_s = c/\lambda_s$).

The Raman effect can be produced via ultraviolet, visible or very near IR radiation. The Raman scattering wavelength, λ_R, is determined by finding the difference between the excitation frequency and the scattered photon frequency: $\nu_R = 1/\lambda_R = c|\ 1/\lambda_e - 1/\lambda_s\ |$. Since the vibration- and rotation-mode frequencies are usually in the IR spectrum (a few microns to tens of microns), the spacing between the excitation and scattered wavelength is typically small and is quoted in units of cm^{-1}. Since two large numbers are to be subtracted to obtain a small number, calibration is very important. This also implies that very good dispersive optical systems (monochrometers) are needed to separate the two wavelengths to determine the wavelength differences. When the wavelengths are farther into the visible where strong optical sources (lasers) and good optical detectors are available, the issue of discerning the scattered signal from the source is exacerbated. An optical interference filter with a narrow bandwidth is commonly employed to prevent the source wavelength peak from overlapping with the measured wavelength peak. Sources and detectors in the near IR are preferable to allow smaller optical dispersive systems, such as simple diffraction gratings in combination with Si photo detector arrays.

As might be expected, the Raman effect intensity can increase by 2 to 4 orders of magnitude as the excitation energy approaches the absorption wavelength of the molecule. This is referred to as the resonance-enhanced Raman effect and can be very useful if the optical sources and detectors are available. However, if the excitation wavelength is of sufficient energy to cause fluorescence, as in many biological entities, interfering signals can overwhelm the Raman signal. Also, if there is considerable difference in the excitation frequencies of different species to be detected, then multiple sources and detectors are recommended. Likewise, when the species interacts closely with certain metallic surfaces or particles, surface-enhanced resonance Raman spectroscopy (SERS or SERRS) is observed. SERS is not fully understood, but can result in considerably enhanced signal strengths.

For lower performance requirements, there are now portable imaging systems and even microscope imaging systems. However, high performance Raman spectrometers are sophisticated bench instruments that are usually composed of high power sources, detector arrays such as CCDs or CMOS imagers, a 0.5 meter or larger monochrometer, computer software, and wavelength reference library. As with most bench-type scientific instruments, typical prices run in the several tens of thousands. However, provided the signals are strong the measurement time can be quite fast.

Examples of commercially available systems can be viewed at the web sites of McPherson Inc.,[27] Kaiser Optical Systems Inc.,[28] and HORIBA Jobin Yvon.[29]

6.3.3.3 Chemical Sensors Based on Organic Materials

While solid-state chemical sensors are based upon materials such as semiconducting metal oxides and silicon carbide, another class of chemical sensors utilize organic materials. With the development of new synthesis techniques, more and more organic materials are being found to hold interesting chemical-sensing properties. Organic materials can be designed with a large

number of different chemical structures, and these may be designed to interact more or less uniquely with the different chemical structures of the various analytes. Consequently, organic hydrocarbon-based chemical sensors are attracting intensive research attention, as noted by the rapidly increasing number of publications.

The most commonly mentioned organic materials for chemical sensing applications include conductive polymers, metal-substituted phthalocyanines, carbon black/polymer composites, and recently carbon nanotubes. The sensor device structures most often used for organic materials are: (1) Conductometric sensors, in which a change in the conductivity of the sensing material due to analyte exposure is measured; (2) Mass-sensitive sensors, in which the mass change due to the adsorption of analytes onto the sensing membrane is detected, such as surface acoustic wave (SAW) sensors, quartz crystal microbalance (QCM), and micro cantilever sensors. The detected changes in these sensors are from their vibration mode and frequency; and (3) Optical sensors, in which the optical properties of the sensing materials change when exposed to analytes such as colorimetric sensors and fluorescence spectrum sensors. In the following, an introduction to each of these three sensor techniques is given as well as a comparison of the performance of different organic materials.

6.3.3.3.1 Conductometric Sensors

Probably due to their very small size and simple construction conductometric sensors, also known as chemiresistive sensors, are the most common of the organic sensing devices. They function via the measurement of the resistance or conductance change during, or due to, the exposure to analyte. The typical device consists of an insulating substrate and a pair of electrodes that form electrical contact to the conductive materials. A serpentine, or interdigitated, electrode structure is commonly used both to enable construction of a compact device and to increase the area of measurement. Depending on the sensing material, the contact electrodes are usually made from precious metals like gold (Au) and platinum (Pt) in an attempt to make an ohmic contact to the sensing organic material while maintaining inertness and corrosion resistance. The substrate is electrically insulating. Because of their availability and high-temperature properties, the more commonly used insulators are glass, quartz, ceramics, or single-crystal silicon with a thermally grown, insulating silicon dioxide. However, because of the low temperature operation, even low-cost insulating plastic is a conceivable substrate. The sensing material is usually deposited after the electrode structure is made via the use of metal evaporation through a shadow mask, but the deposition order is sometimes reversed to achieve better electrical contact between the metal and the hydrocarbon.

Depending upon the sensing material and the analyte, the conductance measured between the two contact electrodes can either increase or decrease upon exposure to the analyte. The mechanism of the conductance change can have many possible origins. For example, for semi-conductive materials such as polymers, the most basic electrical properties of the polymer chain can be altered by the analyte interaction chemistry. Likewise, electrical interactions can be modulated at the interfaces between the material grains, the molecules, or even between the hydrocarbon and the metal electrode. This can be thought of as modulation of an interface potential barrier height. In some cases this can be thought of as a Schottky barrier.[30]

Summary

Compared to other sensor techniques, organic sensors can have several advantages:

- Ease of Construction: It is relatively easy to design and fabricate a conductivity measurement sensor when compared to other types of sensors. The structure is essentially a single layer, which has the potential of being easily integrated into today's microelectronics technology so that on-chip interface circuitry is available. This circuitry can enable an entire sensor system while potentially holding costs to only pennies.

- Optimum performance at ambient temperature: Generally, not only can chemical sensors using organic materials be operated at room temperature, but they prefer it. This is in contrast to most of the solid state sensors which require elevated temperatures. Of course, this can be a disadvantage should the sensing have a need to take place at extreme temperatures. Almost all sensor technologies are temperature-dependent. Hence, the temperature needs to either be controlled or measured and accounted for.

- Good linearity and selectivity: Substitution of various functional groups on organic materials, or the substitution of an entirely different hydrocarbon family, can alter the selectivity of the sensing device to a large degree, especially when compared to solid-state sensor selectivity. Because the sensing mechanism is distributed over the material and the material has a certain dispersion to the strength of interactions, these materials commonly have a large linear operation range.

- Sensitivity to more than one small molecule: Due to their ubiquitous characteristics, small molecules are hard to distinguish. Because there are so many possible variations in the chemistry that is useable for organic sensors, a matrix of sensors can be used to gather multiple responses. This is essentially how the mammalian nose and the taste systems work to distinguish different smells and tastes. Hence, the electronic version of this matrix of sensors has become known as an "electronic nose." Of course, this also implies that when high concentrations of one analyte are present, it is very difficult to discern small concentrations of others. For example, in some sensing materials the presence of water vapor overwhelms the response.

6.3.3.3.1.1 Conductometric Sensor Based On Conductive Polymers

Conjugated polymers are one of most important types of conductive polymers. They come with alternating single and double carbon-carbon bonds in their molecular structure. This special chemical structure forms continuous overlapping of π-orbitals along the polymer backbone, allowing the charge carrier (polaron, bipolaron) to transport through the polymer chains. Commonly reported conjugated polymers include polypyrroles, polyacethlenes, polythiophenes, polyindoles and polyanilines.

Conductive sensors based on conductive polymers are most often studied for their sensing properties for volatile organic compounds, a special group of hydrocarbons. These vapors are a concern for public health, environmental monitoring, medical products, diary products, and homeland security. The desired detection concentration of these gases is at the very low end of

the detection range, a few ppm or less. Typical analytes seen in literature are mostly organic solvents, like alcohols, toluene, benzene, chloroform, acetone, etc. Figure 6-2 shows a response example of dedecylebenzenesulfonate acid-doped polypyrrole, spin-cast on a gold interdigitated electrode, to toluene vapor.[31] As can be seen, about 5% change in resistance was observed for a high concentration of toluene in nitrogen. Figure 6-3 shows a response map of various organic semiconductors including both conductive polymers and oligomers to 16 saturated organic vapors.[32] The response difference is clearly shown in the map, which provides evidence to the feasibility of using multiple organic sensing materials to develop an electronic "nose" for hydrocarbons. Polythiophene polymers, which are more relevant to this report, have also been studied for their sensing properties for methane. A poly (3-n-dodecylthiophene) thin film was tested in air for its sensitivity to 300 ppm of ammonia, chloroform, methane, iso-butane and ethanol, with an operating temperature of 25, 40, and 60 °C.[33] It was seen that at 25 to 40 °C, the polymer has no response to methane; however, at 60 °C the polymer has shown a resistance increase of about 10%.

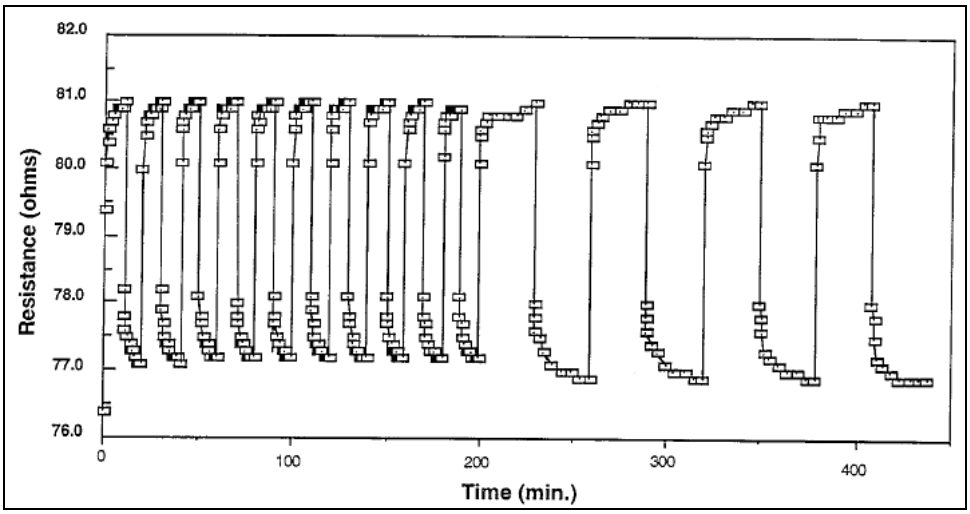

Figure 6-2: Response of a Conducting Polypyrrole Based Sensor to a Stream of N_2 Saturated with Toluene Vapor Passing Over Sensor for 10 minutes, Followed by Pure N_2 for 10 minutes. The results are given for first 10 complete 20-minute cycles and subsequent cycles with a cycle time of 60 minutes.[31]
(Used With Permission)

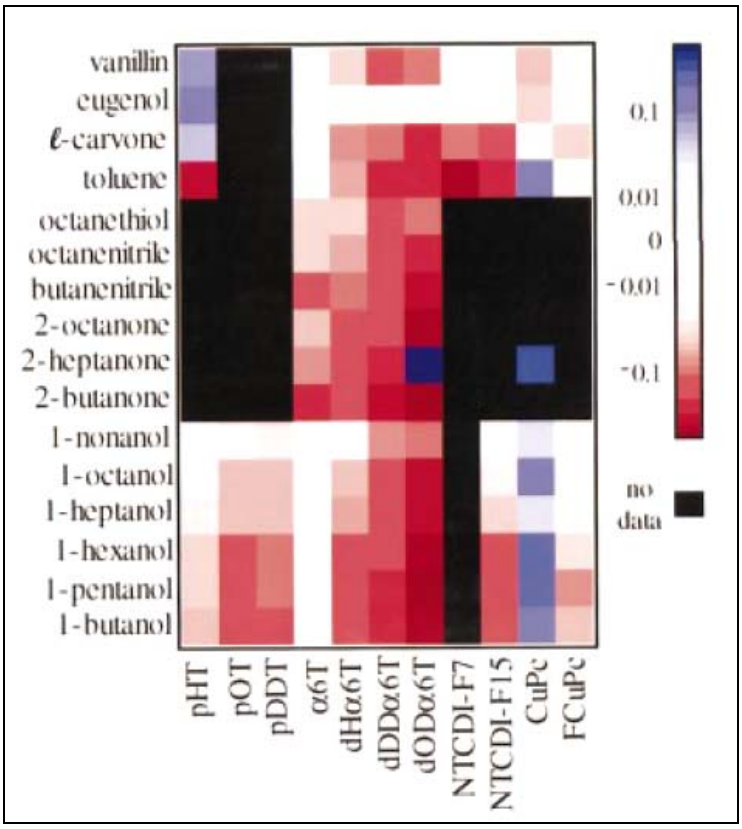

Figure 6-3: Effect of 16 Analytes on 11 Sensor Materials.
Black - data are not available, white - negligible response,
blue - increases in sensor current, red – decreases in sensor current.[32]
(Used With Permission)

The response time of conductive-polymer sensors range from seconds to minutes depending upon the polymer structure, film thickness, film morphology, sensor device structure, and analyte transport to the sensor. Micro-sensors generally have better response time because of thinner film thickness and less exposed area, resulting in less time needed for the sensor to reach an equilibrium state when exposed. The response of a polymer sensor is commonly reversible and repeatable; however, if the reaction between polymer and analyte is highly energy-releasing (exothermic) then reversibility is questionable. Responses are usually quite linear over a large range of analyte concentrations. With regard to the lowest detection limit, it is not uncommon to achieve a reasonable signal-to-noise ratio down to a few ppm of analyte concentration.

Another advantage of polymer chemical sensors is that the easy modification of the polymer chemical structure could functionalize a polymer[34] to have specific selectivity to certain analytes. A study of chemical-sensing properties of various polythiophene polymers with differing molecular structures was recently reported by Bo Li et al.[35] As they reported, polythiophenes with different structures have very different responses to 200 ppm organic vapors. By applying the appropriate pattern recognition algorithm, the response pattern can be used to identify a mixture of gases.

The sensing mechanism of conductive polymers is still an active research topic. Very little is known about sensing mechanism details for many of the conductive polymers, perhaps due to some physical interaction between the polymer material and the tested analytes through electrostatic forces. These interactions correspondingly induce conformational changes inside the polymer structure, resulting in a conductivity change.

6.3.3.3.1.2 Conductometric Sensors Based On Carbon Black-Polymer Composites

Conductive chemical sensors use thin films of carbon black particles dispersed into insulating organic polymers.[36] The carbon black particles provide electrical conductivity to the thin films, whereas different organic polymers provide specificity to different chemicals to be detected. The conduction mechanism can be explained in the framework of percolation theory.[37] Swelling of the organic polymers when exposed to chemicals can increase the distance between conductive particles, resulting in an increase of resistance of the films. On a sensor array, different composites can be used for each sensor element to make an electronic nose system.[38,39,40] Dickson et al.[38] developed an 18 x 18 sensor array based on carbon black-polymer composites. The sensor's response is linear with concentration, but the response time is several minutes. A portable electronic nose system called E-Nose was also developed by Y. T. Kim et al.[39] The sensor had 16 sensing elements on a single silicon substrate. The sensor was installed in a handset device, and a laptop or a PDA could be used to interface to the handset device to implement the pattern recognition calculation.

6.3.3.3.1.3 Conductometric Sensors Based On Carbon Nanotubes

Carbon nanotubes are molecular-scale wires formed by carbon atoms. They are generally structured as a nanometer diameter cylinder consisting of a single or multiple graphene sheet layers rolled up to form a tube.[41] Since their discovery in 1991,[42] carbon nanotubes have been intensely studied for their electrical properties and their potential applications in electronics. The techniques for making them are now quite well developed, and their potential to be used as chemical vapor sensors has also been investigated by different groups.[43,44,45,46] The simplest form of using carbon nanotubes as a chemical sensor is to build a conductometric sensor that measures the conductivity change of carbon nanotubes upon exposure to chemical species. Depending on the structure of the carbon nanotubes, they can be either metallic or semiconducting. The semiconducting nanotubes seem to show better sensor response than metallic ones.[43] This type of nanotube chemical sensor was studied for sensing properties to NO_2 and NH_3 by Hongjie Dai's group.[43] A single-walled carbon nanotube (SWNT) was deposited between two metal contacts on a SiO_2/Si substrate. The SWNT in their study showed p-type transistor characteristics at room temperature.

The sensing mechanism is believed to be a doping and de-doping process. When exposed to NO_2, charge transfer is likely to occur from a SWNT to NO_2 because of the electron-withdrawing power of NO_2 molecules. Thus, the conductivity of SWNT increases. NH_3, on the other hand, is likely to donate electrons to the SWNT, resulting in a decrease in conductivity. The response time of the SWNT sensor ranges from several seconds to several minutes depending on the analyte concentration. The response can be very strong with several orders of magnitude changes in conductance. However, while response time is determined by the arrival

of the analyte onto the nanotube, at room temperature, they commonly require several hours to release the analyte.

6.3.3.3.2 Mass Sensitive Sensors

Mass-sensitive sensors are devices that measure the mass of species accumulated in a sensing layer. Any analytes that can be adsorbed on the sensing layer should be detectable. Mass changes can be observed via several device structures, such as a surface acoustic wave (SAW) device, a quartz microbalance (QMB), and by micro cantilever.

6.3.3.3.2.1 Surface Acoustic Wave Devices (SAW)

SAW devices yield a signal representing the interaction of an acoustic wave propagating along the surface of the device with adsorbed chemicals on or near the surface. An organic receiver layer is deposited on top the surface of the piezoelectric material so that the surface acoustic wave in the piezoelectric substrate carries the organic layer as a mass load. An AC voltage is applied to the input transducer electrodes generating an electrical field, and this results in a temporally and spatially modulated strain in the surface of the piezoelectric substrate. This surface acoustic wave travels away from the excitation electrodes and arrives at the output transducer electrodes after passing through a sensing region. When the surface acoustic wave arrives at the output electrodes, it generates an electrical AC signal via the inverse piezoelectric effect. The signal can be monitored via the shift in the amplitude, frequency, and phase.[47] As the mass loading of the receiver layer changes due to absorption of analyte, the output signal of the SAW device will change. The typical operational frequency of SAW sensors is in the 50 to 1000 MHz range. This high frequency and high Q of the piezoelectric material enables SAW devices to sensor very small mass changes.

6.3.3.3.2.2 Quartz Crystal Microbalance (QMB) Mass Sensor

The Quartz Crystal Microbalance, QMB or QCM, is also called a Bulk Acoustic Wave (BAW) sensor. The resonance frequency of the QMB depends on the crystal orientation, thickness, mass of the crystal, and temperature. Because of their superior mechanical and piezoelectric properties,[48] the AT-cut quartz crystals are the most commonly used QMB sensor material.[49]

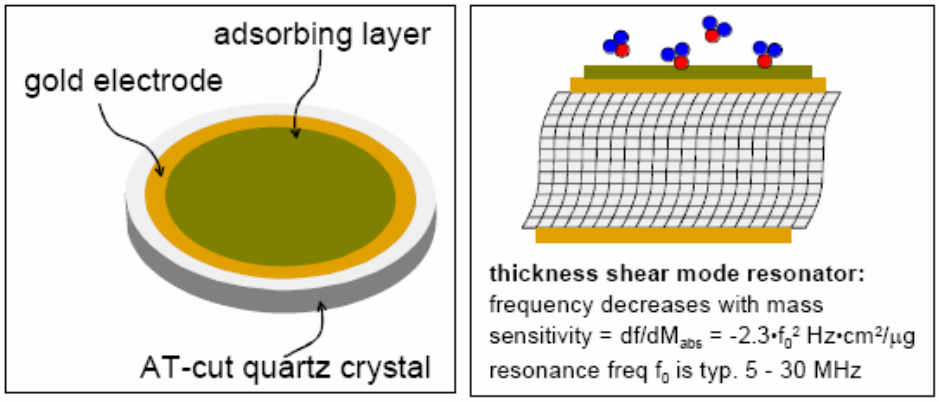

Figure 6-4: Sketch of a QMB Sensor and the Operation Principle.[49]
(Used With Permission)

The AT-cut quartz crystals can yield nearly zero-temperature coefficients at room temperature. The fundamental frequency and nominal oscillation frequency of all standard QMB sensors is 5 MHz. The frequency accuracy is within ± 1000 ppm for an unperturbed crystal. Figure 6-4 shows a schematic of a QMB sensor and its operation principle. Voltage-excitation Au electrodes are deposited on both side of an AT-cut quartz crystal that is used as a resonating element. The device is placed in a feedback-based oscillator circuit and forms the energy storage element. For sensing, a thin film layer, usually organic, is deposited on top of the device to provide an adsorbing layer for the substances to be detected. As the analyte arrives and sticks to the adsorbing layer, the parasitic mass on the device changes, resulting in a change in the resonance frequency of the element and oscillator. Monitoring the oscillator frequency yields the mass accumulation. Selectivity of the detected material is determined by the choice of the adsorbing thin-film layer material.

The QMB is an extremely sensitive sensor capable of measuring mass changes in the ng/cm^2 range with a dynamic range extending into 100 µg/cm^2 range.[48] The minimum detection level is typically a few ng/cm^2, and it is limited by the noise specifications of the crystal oscillator and the resolution of the frequency counter.

<u>Commercial Availability</u>
International Crystal Manufacturing Company, Inc. (ICM) (www.icmfg.com) provides a series of quartz crystal microbalance devices with different frequency ranges and sensor sizes for mass sensoring. Stanford Research Systems, Inc. (www.thinksrs.com) provides OCM measurement systems with both OCM sensors and frequency counters in their product QCM100 and QCM200.

6.3.3.3.2.3 Micro Cantilever Based Mass Sensor

The bending cantilever is another type of commonly studied mass sensitive device. Because of the well developed silicon microelectronic-fabrication technology, the device is usually fabricated from silicon. The device structure is composed of a bending cantilever, supporting substrate, and organic receiving layer deposited on the cantilever.

As analyte arrives at the beam, the mass increases resulting in a signal change. The deflection of the cantilever is dependent upon the entire mass of the cantilever, receiver polymer, and the absorbed analyte, but the sensor performance depends upon discerning the deflection due only to the change in the analyte mass. Hence, it is desirable to minimize the parasitic mass of the beam and receiving polymer. Therefore, micro-cantilevers such as those available via MEMS (Micro-Electro-Mechanical-Systems) processes are preferred. Generally, a cantilever sensor can be operated in two ways.[50] 1) Static mode: The cantilever changes its shape due to mass loading. This may be in response to the weight of the accumulated analyte or bending resulting from a change in stress due to expansion or contraction of the receiver material relative to the ridged cantilever. Measurement of the shape changes is usually done by optical methods such as detecting the laser light-reflection angle changes that occur as the reflecting cantilever beam bends.[51] 2) Dynamic mode: The cantilever is driven into resonance and the resonance frequency will shift as the additional mass of the analyte is deposited on the cantilever. The resonance frequency of a spring-mass system is proportional to the square root of the ratio of the spring constant to the mass. Hence, the resonance-frequency shift is proportional the change in the mass (mass loading). The resonance frequency is monitored by electrical signals from built-in secondary sensors such as piezoresistors that are placed at the bending portion of the beam or by changes in capacitance between electrodes placed on the cantilever and electrodes placed on the stationary substrate.[52,53] The beam can be excited by the electric fields associated with capacitor electrodes or by localized temporal heating of a small portion of the beam to cause a modulated strain. The static mode allows sensor size to be very small, which gives it superior sensitivity. However, because of the need for optical components, the system size is large and cost is high. For the dynamic mode cantilever sensor, the frequency detection and cantilever can be integrated together on a single electronic chip, resulting in reasonable sensitivity. This piggy-backing onto the Si microelectronics technology can result in a low cost system. MEMS sensors are now manufactured in mass for a number of applications. One of the better advertised applications is accelerometers for automobile airbag-deployment. The selectivity of this sensor is provided by different receiver materials.

6.3.3.4 Calorimetric or Specific Heat Determination

Mass flow controllers are based upon the concept of calorimetric measurement and are commonplace in the gas-handling technologies. There are a number of manufactures of these devices. For example, MKS Instruments (http://www.mksinst.com) or the McMillan Company (http://www.mcmflow.com) each have a large selection of models. However, as a chemical sensor these devices are of limited value due to the lack of selectivity.

Mass flow controllers operate by measuring the energy absorbed in a unit of gas as it passes a heater. The principle of operation in a mass flow controller is to control the gas flow rate by measuring the inlet-outlet temperature difference as a known energy (heat) is input to the gas. Likewise, one can measure the amount of energy transfer to or from the gas at the heat sources. Since the gas species and the specific heat are known, the instrument is calibrated to allow a fixed mass to traverse based upon maintaining a constant temperature difference or constant energy transfer.

This concept of operation can be inverted to determine the calorimetric properties of the gas. That is, for a constant gas flow one could measure the inlet-outlet gas temperature difference for a constant energy input. The temperature difference will be proportional to the calorimetric-specific heat parameter of the gas mixture. These devices, at a few hundred dollars, are relatively inexpensive and simple to install.

6.3.3.5 Solid State Sensors for Hydrocarbon Detection

There are a large variety of solid state sensors for hydrocarbon detection. In general they are based upon the concept that a surface catalyst promotes the dissociation of the hydrocarbon. In so doing the hydrocarbon transfers charge changing the carrier properties or some interface boundary properties. Hence, the electrical properties of the semiconductor material changes according to the chemical interaction between the hydrocarbon and the semiconductor catalyst. To promote this process these devices are commonly operated at elevated temperatures. Because of the large number of possible catalyst these devices are prime candidates for use in the electronic nose concept.

6.3.3.5.1 Metal Oxide Chemical Sensor

Materials

There are three basic criteria for material selection of a metal oxide chemical sensor for detection of hydrocarbon gases: (1) oxygen physisorption onto the polycrystalline sensor surface and the grain boundaries at high temperatures; (2) subsequent chemisorption of the physisorbed oxygen as stable ions; (3) electronic properties such that bound carriers are released into the conduction band of the sensor (causing an increase in conductivity/decrease in resistivity) when chemisorbed oxygen reacts with a combustible reducing gas. Employment at high temperatures is necessary to ensure a high rate of reaction between the combustible gases and the chemisorbed oxygen. The material of choice and industry standard for metal oxide sensors is tin dioxide (SnO_2).[54]

Sensing Mechanism

The sensing mechanism of the metal oxide chemical sensor is the increase in conductivity (decrease in resistivity) upon exposure to a combustible reducing gas. When a polycrystalline metal oxide such as SnO_2 is initially heated to between 200 and 400 °C in air, oxygen is chemisorbed onto the surface and the exposed grain boundaries as O_2^-, O^-, and O^{-2} via transfer of electrons from the oxide. This lowers the total number of negative charge carriers within the conduction band of sensor. The transfer of electrons leave positive charges in space charge layers[54] located primarily at the grain boundaries. As shown in Figure 6-5, interface potentials with a magnitude E_s are thus formed at the boundaries, each of which serves as a potential barrier against electron flow (carrier movement) in an applied field. The electrical resistance of the sensor is attributed to these potential barriers.

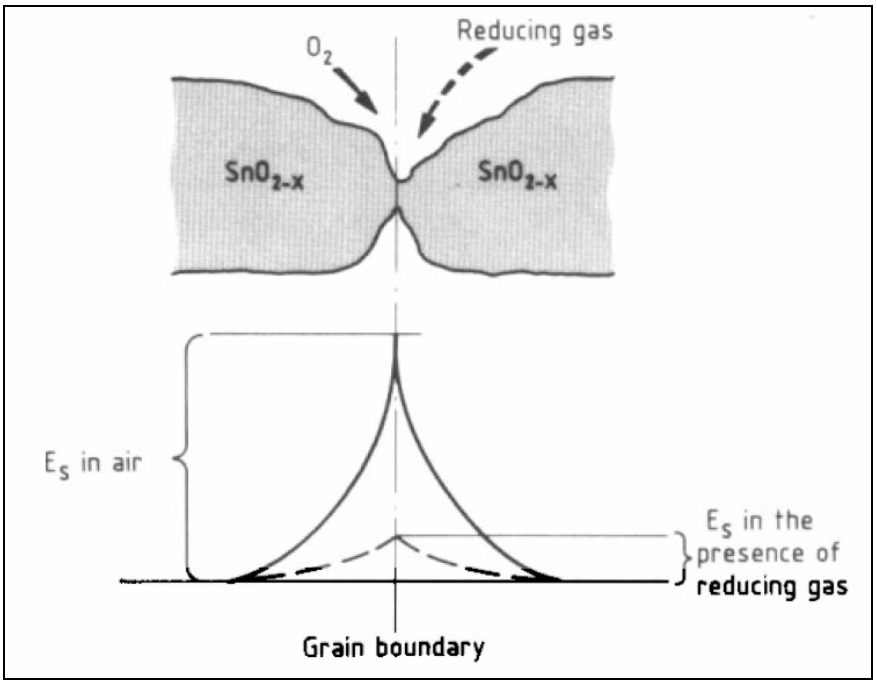

Figure 6-5: Schematic for Potential Barrier at Crystallite Boundary.[54]
(Used With Permission)

Subsequent exposure to a mixture of reducing gas and oxygen results in a reaction involving the reducing gas and chemisorbed oxygen, forming CO_2 and H_2O. Removal of chemisorbed oxygen from the surface releases electrons into the conduction band and removes the space charge layers within each grain and grain boundary. The addition of once-bound charge carriers to the conduction band increases the total number of carriers. The removal of the space charge layers causes a decrease in the height of the barrier at the grain boundary (as seen in Figure 6-5). Both cause an increase in conductivity (decrease in resistivity) of the sensor.[54]

The oxygen contained in the reducing gas acts as a source to replenish the chemisorbed oxygen being depleted on the sensor surface and in the grain boundary. The two competing reactions (oxygen chemisorption, and depletion) indicate an equilibrium chemisorbed oxygen density, and thus an equilibrium conductivity. Both are inversely proportional to the partial pressure of the reducing gas.[54]

The relationship between the electrical resistance of the metal oxide sensor and the concentration of reducing gas is given by the following formula:[55]

$$R_S = A[C]^{-\alpha}$$

Where

R_S = electrical resistance of the sensor

A = constant that is specific for a given sensor

C = concentration of reducing gas

α = slope of the R_S vs. C curve for the sensor material and reducing gas

Sensor Response, Sensitivity, and Selectivity

Figaro USA Inc.,[55] produces a sensor that responds to all reducing gases. The sensitivity to certain gases will change depending upon the operating temperature. The data in Figure 6-6 indicates that the maximum sensitivity of a very stable gas such as methane will occur at high temperatures, while gases that are less stable such as CO will have maximum sensitivity at lower temperatures.[54]

At low temperatures, there is not enough energy to decompose the more stable molecules and enable surface reaction. Therefore only the less stable molecules are detected. At high temperatures, the reaction rates for the less stable molecules are significantly faster than for the more stable ones. Thus it is possible to distinguish among the drops in resistance caused by each individual reducing gas based upon the operating temperature.[54] However, there is considerable overlap below the maxima in the curves for most reducing gases, as shown in Figure 6-6 for CO and methane. In a mixture of gases, it is difficult to determine how each gas is contributing to the change in the conductivity/resistivity at a certain temperature. Thus, temperature is not a particularly effective means for controlling selectivity.[54]

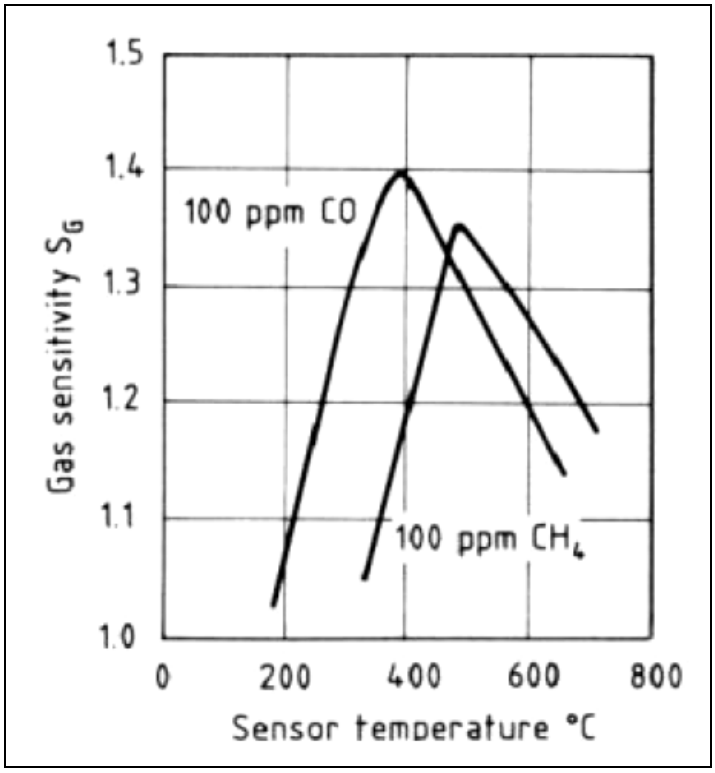

Figure 6-6: Effect of Operating Temperature on Gas Sensitivity.[54]
The gas sensitivity is a ratio of the resistance in air and the resistance in reducing gas.
(Used With Permission)

An additional technique to engineer selectivity is doping the active (metal oxide) part of the sensor. For example, a 0.2% inclusion of palladium will enhance the sensitivity towards CO. Adding 1.0% will cause the sensor to be more sensitive to methane at high temperatures. Examples of other additives are Au, Rh, Ru, In, and several metal oxides.[54]

Selectivity from one gas to another in separate exposures can be achieved through the techniques described above. However, the discrimination of compositions and concentrations of various reducing gases contained in a mixture is difficult to impossible, even when using a metal oxide sensor array.[54]

Commercial Availability

Figaro USA, Inc. (www.figarosensor.com) has developed tin dioxide sensors for detection of C- and H-containing gases. The TGS 2610 is sensitive to propane and butane. The TGS 813 is sensitive to CO, ethanol, hydrogen, methane, propane and isobutane. The detection limit for both is between 500 to 1000 parts per million. The TGS 2620 is sensitive to methane, isobutane, hydrogen, ethanol, and CO. The detection limit is 50 to 5000 parts per million. Gas differentiation in all three sensors is difficult.

6.3.3.5.2 Metal Oxide Semiconductor Capacitors

Structure and Materials

The basic structure of a metal-oxide semiconductor (MOS) capacitor sensor consists of a metal, an insulator and a semiconductor, as shown in Figure 6-7. The semiconductor of choice for high temperature, corrosive and reducing atmospheres is SiC.[56,57] The metals, used to catalyze the decomposition of the combustible gas and for the gate electrode of the device have been Pt,[56,57,58] or Pd,[58] or Ir.[58] The insulator is SiO_x,[59] Si_3N_4,[59] or SiO_2.[57,58] Thermal oxidation occurs easily on the surface of SiC (forming SiO_2), thus SiO_2 is commonly employed.[57]

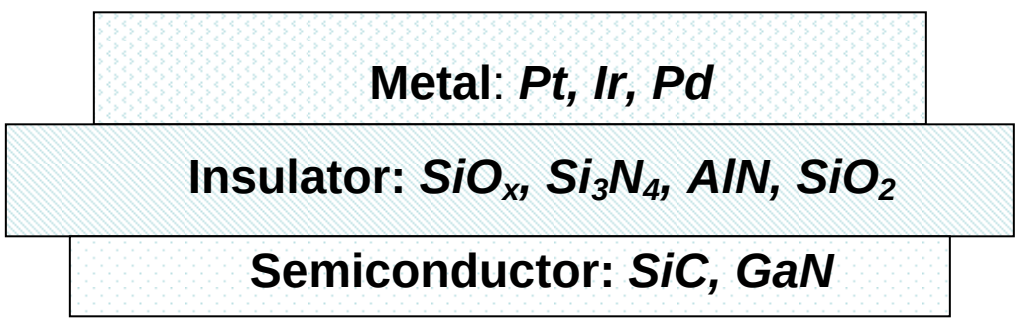

Figure 6-7: Basic Structure for a MOS Parallel Capacitor Sensor. The metal (gate) and semiconductor are the electrodes.

Sensing Mechanism

In general, as the gate voltage is swept from positive to negative bias in a stepwise manner, the SiC near the SiC/insulator interface is depleted of majority carriers. As the device goes from accumulation (positive bias) to depletion (negative bias), the capacitance decreases due to the increased thickness of the depletion region. Tobias et al.[60] have determined that the capacitance – voltage curves for a SiC-based MOS capacitor sensor are different in oxygen and hydrogen atmospheres

Traditionally, it has been believed that this shift in the capacitance - voltage curve is caused by a three-fold process of hydrogen adsorption and decomposition on the surface of the metal catalyst/gate, diffusion of atomic hydrogen through the metal layer, and the formation of a dipole

layer at the metal- oxide interface. If this dipole layer is the sole cause of the shift in the C-V curve, the shape of the curve should not be affected. However, the experimental results reveal that a change in shape is observed at high temperatures.[60]

The experimental results may be explained by the formation of interface states in the presence of oxygen. The nomenclature below is used in the following text,

E_F = SiC Fermi Energy (reference energy for electrons in device)

V_{FB} = Applied voltage, Difference between reference energy and Fermi Level in Pt divided by q

E = Difference between Fermi Level in Pt and conduction band in insulator

F = Difference between Fermi Level in SiC and conduction band in insulator (independent of gas exposure)

Interface states are states at the SiO_2/SiC interface wherein charge carriers can reside. They are not observed during hydrogen exposure. Interface states are accessible to charge carriers if the energy level of the interface state is below the reference energy for electrons (the Fermi level, $E_{F,\,SiC}$), or are within thermal excitation (kT of $E_{F,\,SiC}$).[60]

Compensating states of opposite polarity are also formed at the oxide/metal interface. The compensating states cause an electric field in the oxide. This causes a voltage drop, qU, across the oxide, which is dependent upon the density of interface states, n.

$$qU = \frac{nqt}{\varepsilon}$$

t = insulator thickness

ε = dielectric constant of insulator

q = charge of electron

A perusal of the band diagram shows that:

$$-qV_{FB} = F + (-qU) - E$$

Using the previous equation, an equation for the change in applied voltage when switching atmospheres can be derived:

$$\Delta V_{FB} = \Delta\frac{nqt}{\varepsilon} + \Delta\frac{E}{q}$$

Regardless of the applied voltage, the change in E is positive and constant, hence the parallel shift. The change in E can be attributed to the initial mechanism, which is the removal of the hydrogen dipole layer.[60]

The number of accessible interface states, n, is a direct function of the applied voltage. An increase in the voltage results in an increase in the energy of the electrons in the device. This, by definition, causes an increase in the reference energy (the Fermi level of the semiconductor). As the reference energy increases, more interface states are made accessible. As one loses carriers to these interface states, it will take a larger voltage to reach higher capacitances.[60]

This explains the change in shape of the C-V curve observed when switching from hydrogen to oxygen. The real shift is a combination of a parallel shift (caused by the loss of a hydrogen dipole layer), and a shift which requires larger voltages to reach higher capacitances (caused by the interface states).

Sensor Response, Sensitivity, and Selectivity

A typical test is run at constant capacitance and the voltage required to keep that capacitance in different atmospheres is reported as the sensor response. Hence, the response time of a metal – insulator – silicon carbide sensor is variable depending upon the capacitance at which the sensor is held constant. Set at 80 pF, the sensor response time is on the order of 5 minutes.[61] The extended response time can be due to the complex associated circuitry needed to perform the measurements. Additional research is needed to fully characterize and understand the response time for MOS capacitor sensors.

The operation of this type of sensor depends on the chemisorption of hydrocarbons and diffusion of hydrogen derived from the decomposition of the hydrocarbon by the metal gate. Thus, this type of sensor, in its present form, cannot discriminate among the different hydrocarbons. Arrays of MOS capacitor sensors have not yet been explored. An array of MOS capacitor sensors, each with a different metal catalyst and operating temperature, may offer the desired selectivity. More research is needed to explore this possibility.

A secondary concern is the maximum hydrocarbon concentration to which these sensors can be subjected before saturation. Reported tests[57,61] have exposed these sensors to 0.05 to 0.1% volume hydrocarbon in nitrogen. Gases exiting a flue or contained in a pipeline have markedly higher percentages of hydrocarbon gases. Research is needed to determine if this type of sensor can detect these gases when they are in high concentration.

In summary, the present embodiment of MOS capacitor sensors seems to lack selectivity among different hydrocarbon gases. However, an array of MOS capacitors may offer the desired selectivity. Further research is needed to fully characterize the response time, understand the detection capabilities at high hydrocarbon concentrations, enhance the selectivity of the sensor, and explore the possibility of an array of sensors.

Commercial Availability

Research regarding these devices as sensors at major universities, e.g., the University of Michigan in the United States (Dr. R. Ghosh), Linkoping University in Sweden (Dr. A. Spetz) and corporations, e.g., Applied Sensors (Linkoping, Sweden) has been conducted, however these devices are not yet commercially available.

6.3.3.5.3 Metal Oxide Semiconductor Schottky Diode

Structure and Materials

Capacitor sensors require complex surrounding circuitry to detect the gas response. The diode sensor is attractive in the simplicity of its associated circuitry.[57] The structure of the MOS Schottky diode is a metal – semiconductor junction, as shown in Figure 6-8. A thin (~nm) interfacial layer is added to increase the stability of the sensor and the reproducibility of the response.[57] The semiconductor is either Si,[62] or SiC[57,63,64] or GaN.[57,65,66,67] The metal (acting as a contact and a catalyst for hydrocarbon breakdown) is either Pt,[57,63,64] or Pd.[57,62] Mixed ion conductors ($BaSnO_3$[57,67]) have also been tested as a catalytic contact layer. The thin (~nm) interfacial layer is typically a combination of Ta,[57,59,68] $TaSi_x$,[57,59,68] SiO_2,[57,59,62] and AlN.[57,59,63] The stability of the interfacial layer is a problem. Degradation occurs at high temperatures and long operating times.[57,59] Improved stability and selectivity has been reported by using SnO_2.[69]

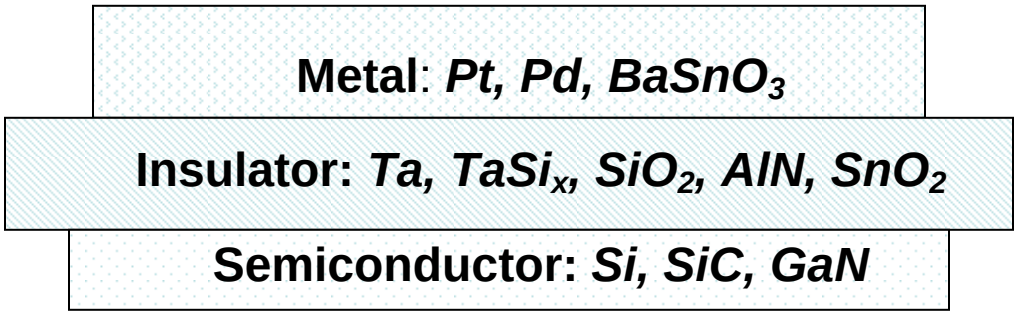

Figure 6-8: Basic Structure of MOS Schottky Diode.

Sensing Mechanism

Additional research is needed to determine the sensing mechanism. Research is also needed to determine the effect of using different interfacial layers and any associated change in the mechanism of sensing. The similarity of the sensor response to hydrocarbons compared to that of MOS capacitors is attributed to similarities in device structure (metal/insulator/ semiconductor). Some Schottky diode sensors can be used as capacitor sensors in reverse bias.[63]

Current starts to flow within the device when a voltage large enough to excite the electrons over the potential barrier (thermionic model of diode operation) or to cause tunneling[67] through the barrier is applied. Upon exposure to hydrocarbons, dehydrogenation occurs at the metal surface and a dipole layer of adsorbed hydrogen forms at the metal – insulator interface. This lowers the potential barrier, thus lowering the turn-on voltage of the diode.

Sensor Response, Sensitivity, and Selectivity

Typical experiments are conducted under constant current with the applied voltage shifted to maintain the current. In different atmospheres, the voltage needed to maintain the current changes and the change in voltage is recorded as the sensor response.

The sensor is very responsive, and the response time is on the order of milliseconds. It should be noted that the sensor response would vary depending on the current at which the sensor is being operated.[64]

At high temperatures (above 600 °C), the metal surface undergoes a rapid transition from being covered with adsorbed oxygen to hydrogen/hydrocarbon species. The signal response is dependent upon the amount of reducing gas and, at these high temperatures, is more or less independent of the gas composition.[70]

At lower temperatures (below 600 °C) some gas molecules are only partly combusted on the metal surface. Different hydrocarbons could give different responses at a certain temperature. This shows promise for use in sensor arrays to give detailed information about a gas mixture.[70]

Hunter et al.[69] reported that diodes having the material structure of $Pd/SnO_2/SiC$ give different sensor responses depending upon the reducing gas. They maintained the sensor at a constant voltage and measured the effect of the reducing gas on current as a sensor response. Additional research is needed to test the extent of selectivity, as well as to better characterize the effect of using SnO_2 as an interfacial layer.

Selectivity data of GaN-based Schottky devices have been reported.[71] Different responses were reported for Ga-face and N-face GaN. GaN-based Schottky devices show promise in being able to distinguish between various hydrocarbons, however more research is needed to explore the sensing mechanism and the extent of selectivity achievable.

An array of MOS diode sensors, each with a different metal catalyst and operating temperature, may be sufficient to give the needed information. More research is needed to explore this possibility.

Reported tests[62,69,71] have exposed the sensor to hydrocarbons in the concentration range of a few ppm to a few volume percentages. The concentration of hydrocarbons in a gas from a flue line or contained in a pipeline is significantly higher. Research is also needed for these devices to determine their detection capabilities of MOS diode sensors at high concentrations of these types of gases.

In summary, MOS diodes show promise in being selective but are currently unable to give detailed information on flue gas mixtures. An array of MOS diode sensors may have the selectivity to give the information needed. Additional research is needed in certain areas: (1) determination of the sensing mechanism for different interfacial layers; (2) engineering the detection capabilities at higher hydrocarbon concentrations; (3) determination of the extent of selectivity to different hydrocarbons and the ability to give detailed information about a mixture of hydrocarbons; and (4) exploring the possibility of an MOS diode sensor array, each sensor having a different metal catalyst and operating temperature.

Commercial Availability

Research regarding these devices as sensors is being conducted at major universities, e.g., the University of Michigan in the United States (Dr. R. Ghosh) and Linkoping University in Sweden (Dr. A. Spetz) as well as at corporations, e.g., Applied Sensors (Linkoping, Sweden); however, these devices are not yet commercially available.

6.3.3.5.4 Metal Oxide Semiconductor Field Effect Transistor Sensors

Structure and Materials

Metal-oxide field-effect transistor sensors (MOSFET) have been explored[57] due to the disadvantages of capacitors (complex associated circuitry) and Schottky diodes (degradation of the thin interfacial layer at high operating temperatures and times). While some field-effect transistors are very complex, the basic structure, shown in Figure 6-9, consists of a semiconductor substrate, source (S), drain (D), insulator, and catalytic metal gate.[72] As in the previous MOS devices, the catalytic metal gate is either Pt,[57,59,73] or Ir.[57,59] The insulator is typically SiO_2[73] and the semiconductor is typically SiC.[57,59,73]

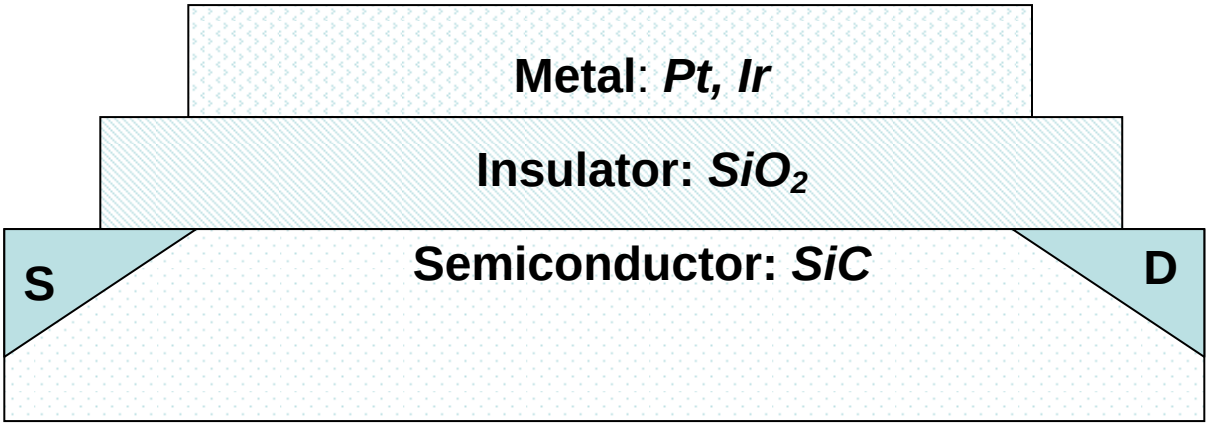

Figure 6-9: Structure of Basic MOS Field Effect Transistor.

Sensing Mechanism

The sensing mechanism for MOSFET gas sensors has not been studied as extensively as that for MOS capacitors and more research is needed to better characterize the sensing mechanism. The similarities in gas response to the MOS capacitor and diode can be attributed to the similar structure (metal/insulator/semiconductor) of the active sensing part.

In standard MOSFET operation, the source and drain are disconnected (cut-off mode) until the voltage applied to the gate metal exceeds a threshold voltage. The gate/insulator/semiconductor structure between the source and drain can be viewed as a capacitor. When the voltage applied to the gate exceeds the threshold voltage, an inversion channel is formed between and connects the source and drain.[74]

If the metal/insulator/semiconductor is considered as a capacitor, the response and mechanism for the MOS capacitor apply. Higher capacitances can be reached at lower voltages when the sensor is exposed to hydrogen as opposed to oxygen. This means that the inversion channel forms at lower applied voltages, effectively lowering the apparent gate threshold voltage. Thus under hydrogen exposure, a higher drain current can be reached at lower drain voltages.

Sensor Response, Sensitivity, and Selectivity

The device is held at a constant current and the response is the change in drain voltage required such that the constant current is maintained. The response depends upon the operating current of

the device. Sensor response as reported by Savage et al.[75] indicated approximately 2 seconds for the sensor signal to reach saturation.

Like the MOS capacitor and diode, hydrocarbon breakdown on the metal surface is required for sensing. Due to this, the selectivity of this type of sensor should be comparable to that of the MOS capacitor and Schottky diode. Operating the sensor at high temperatures should result in very little selectivity due to the rapid rate of the surface reaction. At lower temperatures, partial hydrocarbon breakdown occurs, which can lead to different responses to different hydrocarbons at specific temperatures. Additional research is needed to characterize the selectivity of this type of sensor.

An array of MOSFET sensors may provide the sensitivity and selectivity needed. The array would consist of multiple sensors, each with a different catalyst metal and operating temperature.

The results of tests that have exposed the sensor to hydrocarbons in the concentration range of a few ppm to a few volume percentages have been reported.[73,75] Additional study is needed to understand how these devices will respond to the high hydrocarbon concentrations typical of flue and pipeline gases.

In summary, a single MOSFET shows promise in being selective but is currently incapable of analyzing gases with high concentrations of hydrocarbons with great detail. Additional research is needed in certain areas, including the determination of (1) the sensing mechanism, (2) the detection capabilities at higher hydrocarbon concentrations, (3) the selectivity to different hydrocarbons and the ability to give detailed information about a mixture of hydrocarbons, and (4) the possibility of using a MOSFET sensor array.

Commercial Availability

Research regarding these devices as sensors has been conducted at major universities, e.g., the University of Michigan in the United States (Dr. R. Ghosh) and Linkoping University in Sweden (Dr. A. Spetz), and at corporations, e.g., Applied Sensors in Linkoping, Sweden.

Applied Sensors of Linkoping, Sweden (www.appliedsensor.com) has developed two SiC-based MOSFET hydrogen sensors (AS-FHH-400 and AS-FHH-450). The response time for both is approximately 5 seconds. The detection limit of the AS-FHH-400 is between 10 and 2000 ppm in air. The detection limit of the AS-FHH-450 is between 500 ppm and 5% in air. Both sensors are more sensitive to hydrogen than hydrocarbons. Neither is selective between different hydrocarbons.

6.3.3.5.5 High Electron Mobility Transistor

Structure and Materials

The operation of a high electron mobility transistor (HEMT) is based on the formation of a two-dimensional electron gas (2DEG). The basic structure consists of a thin AlN layer (buffer layer, ~20 nm), thicker GaN layer (~1 nm), thin AlGaN layer (~30 nm), source (e.g., a Ti/Al bilayer), drain (e.g., a Ti/Al bilayer), and catalytic metal contact (Pt). The GaN layer can be either Ga-

polar or N-polar, the difference being the principle atom on the surface. The Al content in AlGaN is typically 15%.

Sensing Mechanism

The 2DEG is formed at the interface between GaN and aluminum gallium nitride (AlGaN), due to the differences in both the piezoelectric polarization and the spontaneous polarization in these two materials. The piezoelectric polarization is caused by the mechanical distortion of the lattice. Ambacher et al.[76] has shown that when AlGaN is grown on top of GaN, the distortion is always a tensile stress in the AlGaN. This causes a piezoelectric polarization that is parallel to the spontaneous polarization. Spontaneous polarization is due to permanent dipoles caused by ionic bonding among the constituent atoms of the lattice, as shown in Figure 6-10. The arrows in Figure 6-10 symbolize permanent dipoles, pointing from negative nitrogen ions to positive Ga or Al ions. The lengths of the arrows indicate the relative magnitudes of the dipoles. The spontaneous polarization in AlGaN is larger than that of in GaN.[77,76]

As noted above, the discontinuity in the polarization gives rise to a positive, fixed polarization charge, $+\sigma$, at the interface, as shown in Figure 6-10. The termination of the crystal causes a negative polarization charge, $-\sigma$, that can interact with ions with which it comes into contact.[71,77]

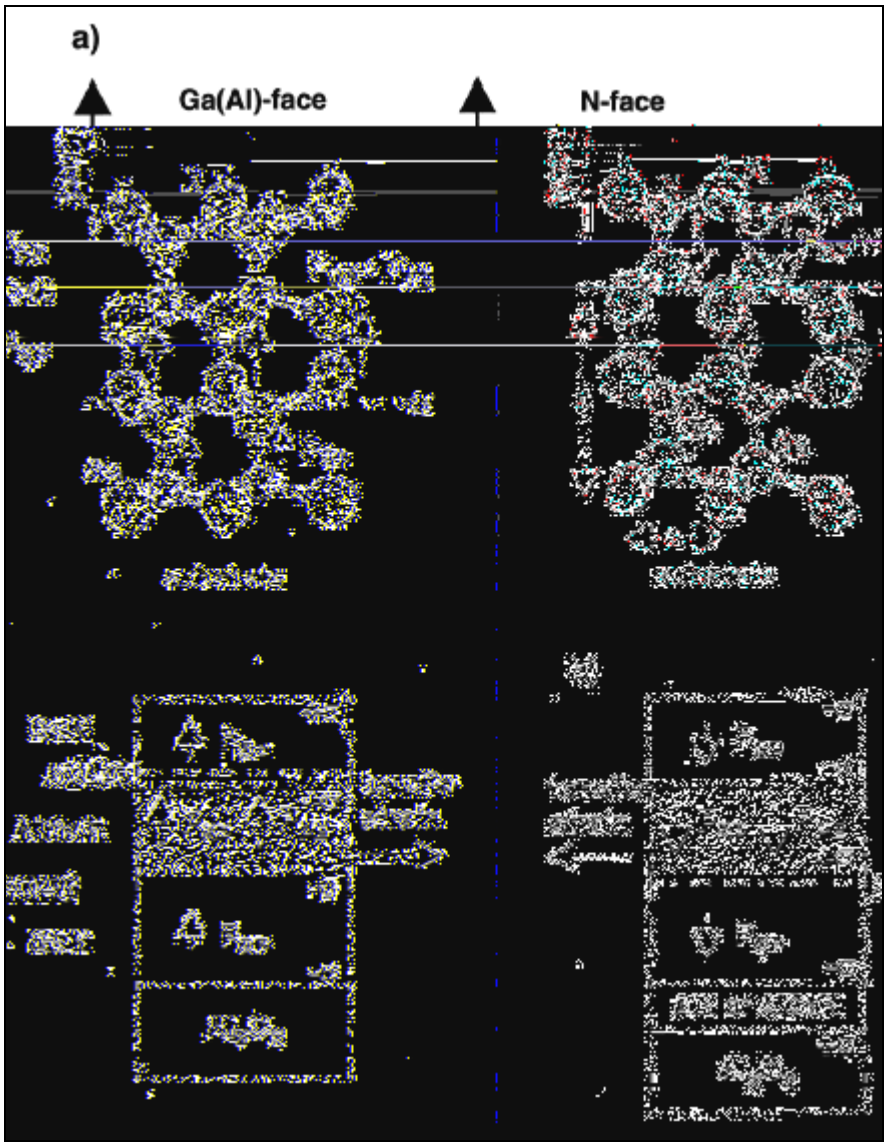

Figure 6-10: (a) Atomistic Representation of the GaN (Both Ga-polar and N-polar)/AlGaN Interface and Near-interface Regions. The large arrows represent the direction and magnitude of the dipole. (b) Epitaxial representation of the 2DEG (Both Ga-face and N-face). Note that the 2DEG for Ga-face and N-face are on opposite sides of the AlGaN layer. This is due to the opposite direction of the spontaneous polarization, and the tensile strain.[76]

The polarization charge gives rise to a pronounced downward band bending, causing electrons to accumulate at the interface, forming a 2DEG that is typically confined within 2 nanometers (nm). The carrier density of the accumulated electrons can be as high as 10^{13} cm^{-2} (mobility is approximately 1000 cm^2/Vs @ 300 K).[76,77]

The Pt gate catalyzes the breakdown of the hydrocarbons. The hydrogen ions diffuse through the metal, adsorbing onto the AlGaN/Pt interface. These ions act as compensating charges to the polarization charge present at the terminating end of the AlGaN, and will alter the charge density

in the 2DEG, and thus the conductivity. More research is needed to better understand the 2DEG and to characterize the detection mechanism of this type of sensor.[77]

Without the Pt gate, it has been shown by Stutzman et al.[77] that there is still a response to a combustible environment. This is due to free ions and dipole moments present in the gas, however additional study is needed to characterize in greater detail this type of response.

Sensor Response, Sensitivity and Selectivity

Sensor response for the GaN HEMT structure has been reported. In an experiment conducted, a fixed forward bias was placed upon the transistor. The current was recorded with respect to time and environment (switching from pure N_2 to 10% H_2/90% N_2). The response time was very fast, on the order of and perhaps shorter than 10 seconds.[78] However, in this experiment, the feed gas was stopped before allowing the sensor response to saturate.

Reported selectivity data is limited. Data examining the selectivity of the HEMT structure towards various hydrocarbons are not available at this writing. The low gas concentrations at which the sensor saturates at are of great concern.[71]

An array of GaN HEMT sensors may yield the selectivity needed to analyze flue gas lines in great detail. The array would consist of many GaN HEMT sensors, each with a different catalyst metal and operating temperature.

Summary

The HEMT structure shows considerable promise of selectivity towards various hydrocarbons, however the ability to effectively operate under high hydrocarbon concentrations is of great concern. Additional research is needed in (1) sensing mechanism (2DEG formation, effect of gas on conductivity); (2) sensor selectivity (ability to distinguish between various hydrocarbons); and (3) sensor response (ability to be sensitive at higher concentrations).

Commercial Availability

Research regarding these devices as sensors has recently been conducted at major universities, e.g., the University of Florida in the United States (Dr. S. J. Pearton), and institutes, e.g., Walter Schottky Institute in Germany (Dr. M. Stutzmann); however, these devices are not yet commercially available.

6.3.3.5.6 Electrochemical Cell

Structure and Materials

An electrochemical cell typically consists of a solid electrolyte, active electrode (catalyzes hydrocarbon breakdown), and reference electrode. The solid electrolyte is typically yttria-stabilized zirconia (YSZ). Yttria is added for better mechanical properties, and to create oxygen vacancies. Other stabilizing compounds include CaO and MgO.[79] The inert electrode is reported as Au.[80,81] The active electrode is reported as Pt,[82] Pd,[80] Au, or MnO_2,[82] with various additives (e.g., InO_2, proton conductors.[79])

Sensing Mechanism

More research is needed to fully understand the sensing mechanism and the mechanism changes associated with changing electrode metals. The electrochemical cell gas sensor is based upon an electromotive force (EMF) being produced as the degradation of hydrocarbons occurs at the active electrode. It is assumed that there is no hydrocarbon breakdown at the inert electrode.[79]

Upon exposure to a mixture of hydrocarbons and oxygen, oxygen physisorbs onto the solid electrolyte surface. The physisorbed oxygen then moves across the solid electrolyte surface until it reaches the metal-solid electrolyte interface. The oxygen then chemisorbs onto the metal as one of a few stable ions (e.g., O^-, O^{2-}). The stable oxygen ion reacts with the hydrocarbons, forming either CO_2 and H_2O, or CO and H_2 (depending upon the amount of oxygen available).[83]

Since no reactions involving the hydrocarbon occurs at the inert electrode, the potential of the inert electrode is solely dependent upon the extent of oxygen chemisorption, and thus the partial pressure of oxygen. The difference in potential between the inert and active electrodes will give rise to a voltage drop across the solid electrolyte. This voltage drop from the inert to the active electrode can be calculated by:[81]

$$\Delta V = \frac{RT}{4F} \ln\left(\frac{P_{O_2}^{Inert}}{P_{O_2}^{Active}} \right)$$

$$\mathrm{R} = \text{Gas Constant}$$

$$\mathrm{F} = \text{Faraday's Constant}$$

$$\mathrm{T} = \text{Temperature}$$

Hence, the larger the voltage difference, the lower the oxygen partial pressure at the active electrode. This indicates that more oxygen is used up in reactions with the hydrocarbon. Thus, the voltage drop is related to the hydrocarbon concentration.[81]

A dual electrochemical cell gas sensor has been reported.[80,81] The active electrodes of the two electrochemical cells (i.e., Cell I and II) are facing each other. One electrochemical cell (Cell I) is connected to a voltmeter measuring the voltage drop caused by the depletion of oxygen over the active electrodes. The second cell (Cell II) is connected to a DC source which supplies current to Cell II. The EMF generated in Cell I is compensated by supplying a direct current to Cell II. The current applied turns Cell II into an oxygen pump. Thus, the oxygen depleted by hydrocarbon breakdown is replenished by that pumped through the solid electrolyte. The amount of current applied is thus an indicator for how much hydrocarbon is in the atmosphere.

Sensor Response, Sensitivity, and Selectivity

A single-celled electrochemical gas sensor was placed in an atmosphere containing oxygen and ethane. The EMF generated was measured and used as the sensor response. The sensor response is a result of the breakdown of hydrocarbons on the active electrode surface. More hydrocarbons in the atmosphere would require a longer time for the hydrocarbons to decompose, hence the sensor response time is based upon the amount of hydrocarbons in the atmosphere. The response times are on the order of a few hundred seconds.[84]

The electrochemical cell seems to have the ability to differentiate between different hydrocarbons. However, more research is needed to understand the extent of selectivity and the potential to fabricate a sensor array to analyze a mixture of hydrocarbons in great detail. An issue of great concern is the concentration of hydrocarbon that the sensor can be exposed to before saturation. Reported tests have exposed the sensor to only low hydrocarbon concentrations (lower than 1000 ppm).[80] Research is needed to determine the detection capabilities of this type of sensor at high concentrations.

In conclusion, the electrochemical cell gas sensor shows potential in being able to distinguish between various hydrocarbons. However, the sensor response time and low saturation concentrations are of concern. More research is needed to further investigate ways to engineer shorter sensor response times and higher saturation concentrations.

Commercial Availability

Research regarding these devices as sensors has recently been conducted at Nagoya University in Japan (Dr. Takashi Hibino); however, these devices for the detection of hydrocarbons are not yet commercially available. Electrochemical cell gas sensors have been used in other applications (e.g., oxygen sensors in cars and Nitrox analysis in the self-contained underwater breathing apparatus [SCUBA] diving industry) to detect other gases. A large number of companies (e.g., Drager Safety) market electrochemical cell gas sensors for detection of gases such as oxygen, hydrogen, hydrogen sulfide, etc. The sensors that are marketed possess a wide range of detection capabilities (~ ppm to high concentrations), and target a wide range of applications.

6.3.3.6 Hybrid Sensor Technology Concept

It appears that any given sensor family may have performance deficiencies or failures under some conditions. Analogously to the concept of the electronic nose, or the combination of gas chromatography with the mass spectroscopy detection technologies, it is often desirable to utilize the information from a variety of sensing technologies to reach a final detection conclusion. The combined sensor approach can often provide better accuracy for both qualitative and quantitative analysis. The term “spectroscopy” or “spectrometer” implies that the technology has multiple sensor “channels” and so does detection over a variable range. Many of the sensor technologies can be so employed if the costs can be tolerated. Also, it is sometimes viable to use not only multiple but diverse technologies to produce a complete sensor data set. For example, many of the calorimetric types of sensors provide very little detailed information about the specificity of the chemical species. This is especially the case when the sample is a mixture of gases. However, the information obtained can be quite valuable as it provides an integrated picture of the sample attribute. The same can also be envisioned for a total mass detector such as a gravimetric MEMS device where the analyte receptor, such as a high surface-area activated-carbon powder, is specifically designed to capture all materials. Hence, should a sensor, even one with multiple channels, be blind to a given chemical or confused by the presence of multiple chemical species, then it may be possible to utilize the multiple channel sensor information along with that from other sensors, either integrating type or multiple channel type, to extract a more precise picture of complete sample composition. In many cases, this approach can be advantageous as to cost, size, or response time. Kastner’s natural gas sensor system[22] illustrates

this very technique while utilizing a minimalistic set of sensor technologies: two-channel I.R. absorption spectroscopy, conductivity, and total pressure.

6.4 Summary of Sensor Technologies for Gas Turbine Control

A summary of capabilities of the sensor technologies discussed is shown in Table 6-7.

Table 6-7: Summary of Detection Technologies.
It is noteworthy that the costs estimates for several technologies largely represent engineering development and not production costs.
(Used With Permission)

Sensor	Estimated Unit Cost ($k)	Size	Species	Gas Composition Update Rate (Data Sets/Second)
GC/Mass Spectrometer	> 10	Benchtop	Detector Dependent	< 0.1
Scanning Magnetic Sector Mass Spectrometer	40 -100	60" H x 30" x 30" (Typical)	H_2, He, CH_4, H_2O, N_2, CO, C_2H_6, O_2, H_2S, Ar, CO_2, C_3H_8, SO_2, COS, CS_2, and hydrocarbons > C4	< 0.1
Scanning Quadrupole Mass Spectrometer	10 - 100	Benchtop	Same as above	> 1
Time-of-Flight Mass Spectrometer	> 10	Benchtop	Same as above	> 10
Detector Array Magnetic Sector Mass Spectrometer	> 10	Benchtop	Same as above	1000
Dispersive IR	< 10	Benchtop to Compact	Requires IR absorption	< 1, SNR dependent
FTIR	> 10	Benchtop	Requires IR absorption	> 10
Raman	> 10	Benchtop	Requires IR absorption	~ 1
Conductometric Sensors	< 5	Compact	Chemical alterability dependent	~ 1
Mass-Sensitive Sensors	< 5	Compact	All	~ 1
Calorimetric of Specific Heat Determination	< 10	Compact	All	~ 1
Solid-State Sensors	< 5	Compact	Oxidizable materials	~ 1

For gas turbine control, the emphasis is placed on composition measurements within 1 second and with a 1% volume fraction accuracy. This table represents only an estimate of the sensor technology attributes for the application, and since some of these technologies could be designed more specifically for the application these estimates could change. For example, cost is highly dependent upon product volume as well as upon the configuration for the application. In high volume, one might anticipate integrated sensor technology such as MEMS-based or Solid State

devices to be very inexpensive. High production volume accelerometers, as employed for automobile airbag systems, cost only a few dollars. While the manufacturing cost for such a device or other solid state devices could be quiet low, one would expect the system cost to be dominated by system engineering issues and service. Likewise, for example, Raman spectroscopy is usually applied to solids, but due to the anticipated high gas pressure and concentrations it may very well be suitable for this application as a benchtop tool. As such, its cost and response time would very well be dominated by the laser system employed to achieve a satisfactory signal-to-noise ratio.

Depending upon how the information for such a sensor system might be employed, a more or less complex computer analysis and control system may be needed. Hence, once again the cost may be more accurately reflected by consideration of the system issues. If one simply desired a fixed embedded control system based upon a few channels of sensor information, then one could expect the unit cost to be low. However, if the device has to be so versatile as to be used on a large variety of customized turbines, then engineering costs will again dominate. It may be more appropriate to focus on the attributes of size, detection accuracy, and response time.

6.4.1 Gas Chromatography

Gas Chromatography is considered accurate and reasonably reliable and can be constructed for the analysis of a large variety of materials. However, it is usually slow, somewhat bulky, and the columns require considerable maintenance. By itself, it is not considered practical for this continuous on-line application.

6.4.2 Mass Spectrometers

Mass spectrometers can be used to measure principal components and many minor components with varying accuracy, depending on the mass spectrometer design and the complexity of the gas mix. A stand-alone unit is usually rather large, and much of the cost is associated with the high engineering content. Its system complexity allows it to be used to obtain more information than may be needed for the control system. Most mass spectrometers have software that determines gas concentrations from peak intensities and allows the user to set up real-time calculations for the Wobbe Index, mass balances, and other items. A spectrometer appropriate for fuel gases should be capable of observing masses 1 through at least 100, and preferably 200 if there are C_8 or heavier hydrocarbons present. Expected components in fuel gas are H_2, He, CH_4, H_2O, N_2, CO, C_2H_6, O_2, H_2S, Ar, CO_2, C_3H_8, SO_2, COS, CS_2, and hydrocarbons C_4 and heavier, including straight-chain and branched hydrocarbons. Alkenes, alkynes, cycloalkanes, and hydrocarbons with heteroatom substituents (N, O, S) are assumed to be negligible. (The accuracy of this assumption is uncertain for coal-derived synfuels.)

A mix in which all of the expected species are present produces a complex spectrum with overlapping fragmentation patterns that require deconvolution. This necessitates the complexity of the computer software in most laboratory analysis applications, but a somewhat reduced amount of analysis should be allowed for the turbine control application. Lighter hydrocarbons (CH_4, C_2H_6, and C_3H_8) have only one isomer and one fragmentation pattern. Heavier hydrocarbons have more than one isomer, each one having its own unique fragmentation pattern.

Butane, pentane, and hexane, for example, have 2, 3, and 5 isomers respectively. A mixture of the above components up to and including C_6 (as may occur in coal-derived synfuels) requires sampling a minimum of 25 different mass numbers (one for each component) to deconvolute the individual fragmentation patterns. The sensitivity of calculated concentrations to slight variations in fragmentation patterns can produce significant errors, whether from calibration errors or from changes in gas composition during a sampling cycle. Accurate analysis requires a mass spectrometer that is both fast and accurate. Sampling 25 masses several times a second is beyond the reach of most commercially available scanning mass spectrometers but may be possible with TOF and detector array mass spectrometers.

6.4.2.1 Detector Array Mass Spectrometers

Detector array mass spectrometers are in an early stage of development. Existing models can sample the entire mass range, including signals from unexpected species, several times a second or faster. Long-term stability data is scarce with prototypes and is invalid after improvements are made. An inexpensive way to test the stability of a particular unit is to run it for extended periods (e.g., 24 hours or longer) on room air. If the instrument performs satisfactorily, a long-term test using a complex hydrocarbon mix of C_1-C_6 would indicate the stability of the fragmentation patterns. The composition of this gas does not need to be known or specified very accurately; only changes in the ratios of different peaks are important for such a test.

Detector array mass spectrometers are expected to become more compact and portable as the technology develops. One prototype weighs 395 grams and is small enough to fit into the palm of a hand.[85] This miniaturization means detector array mass spectrometers will become more versatile and competitive with bulkier and more expensive machines.

6.4.2.2 Time-of-Flight Mass Spectrometers

TOF mass spectrometers can provide a snapshot of the gas stream several times a second and observe all the masses, including those from unexpected species. Long-term stability data is not readily available, but can be evaluated in the same way as detector array mass spectrometers, e.g., with extended runs on room air and hydrocarbon mixes.

Compact TOF mass spectrometers are being developed for use in spacecraft.[86] TOF spectrometers potentially may be miniaturized to the size of a soda can, and will become more versatile and portable than the present state-of-the-art technology.[87]

6.4.3 Optical Spectroscopy (Dispersive IR, FTIR, Raman)

Benchtop dispersive IR optical spectroscopy, FTIR spectroscopy and Raman spectroscopy normally employ physical displacement of an optical element to perform the sensor channel (wavelength) scan. In order to achieve high resolution scanning over a large bandwidth, a long optical path and a bright source are required. Hence, they are rather bulky for the application and can be rather expensive. Their response to particular species is totally dependent upon the vibrational absorption bands of the species. Since the IR absorption bands are formed via the atomic bonding and because the bonding is similar for several natural gas species, they are not

independent from each other. However, the spectra are perturbed by the secondary atomic bonding and so has a considerable degree of uniqueness. In this regard, after the spectra are taken, a mass-spectroscopy analogous software-based deconvolution is required. However, unlike the mass spectroscopy there are some species which are transparent in the IR and so produce no optical signal. Hence, all optical spectroscopy techniques are blind to some materials and the optical sensor channels must be supplemented with some complimentary sensor technology.

With a finite number of natural gas species to be detected, it is quite feasible to measure via only a finite number of a pre-selected measurement channels (wavelengths). Doing so could be accomplished with optical filters as the wavelength selection mechanism. This would significantly reduce the physical size, cost and measurement time. In the IR, black-body thermal detectors (thermal piles) have been traditionally utilized. These can easily be constructed via MEMS technology and be fully integrated with signal-conditioning electronics. More recently, MEMS technology, combined with new quantum well emitter/detector structures, is enabling the development of vertical-cavity surface-emitting laser (VCSEL) technology with a built-in voltage-tunable, wavelength-selectable etalon (Fabry-Perot interferometer) for precision wavelength selection.[88] This technology could also be applied to the IR for detectors.[89] Using MEMS technology, reflective parallel-plate etalons can be constructed with controllable spacing between the plates. These can therefore be tuned to the desired wavelength. This technology could enable individual, wavelength-specific, matched emitter-detector sensor pairs at the integrated circuit device size.

6.4.4 Electronic and Physical (Solid-State, Mass, Calorimetric)

While calorimetric sensor technology has been actively used for many years in flow controllers, it is an integrating technology with virtually no specificity. It is reasonably inexpensive and can be utilized with other technology as a complementary channel. Furthermore, calorimeters could be constructed via MEMS technology to further reduce size and cost. Likewise, gravimetric, or mass sensing, technology via QMB and SAW devices are available technology. MEMS-based devices, which should be integratable into multi-channel systems, are still largely in the research phase but the technology appears to be viable. All of these rely upon receptor chemistry coatings which are largely hydrocarbon-based. As such, they are limited in their operating temperature range. They may also be limited in the concentration range by the solubility of the receptor chemistry.

Electronic conductometric- and solid-state devices, which are being actively studied, fall into two very broad classes, which can be further bifurcated. Some are based upon organic receptor chemistries, which may have specificity via the chemical make up of the receptor. They would suffer from the same limitations associated with the hydrocarbon-based gravimetric sensors; however, they can be extremely simple to construct, are potentially very small, and lend themselves well to the multi-channel electronic-nose concept. As such, they are potentially inexpensive. They are also, integratable with on-board signal-processing technology and other sensor techniques that are compatible with MEMS.

A number of purely solid state technologies were discussed at length. They can be constructed as either passive (variable resistance) or active (transistor with internal gain) devices. They all appear to rely upon chemical reactions via surface catalytic activity to decompose the gas and inject carriers into the solid state materials. The decomposition rate is dependent upon the analyte, the catalysis, and the temperature. Hence, they too may lend themselves well to the electronic-nose concept. Even if a single catalytic material was used for several sensors, the temperature might be swept to generate analysis channels. If device response time is critical, an array of MEMS based devices might be constructed with individual heaters and temperature controllers. The response time of an individual channel device is anticipated to be very fast and primarily limited by the surface diffusion time of the gas to be broken down. Assuming the signal in such a sensor is limited by the analytic concentration or the response time, an active device, with gain, would be appropriate.

---

[1] Riccius, O., R. Smith, F. Guthe, and P. Flohr. 2005. The GT24/26 combustion technology and high hydrocarbon ("C2+") fuels, *Proceedings of ASME Turbo Expo 2005, Reno-Tahoe, Nevada*. ASME Paper # GT2005-68799.

[2] http://www.netl.doe.gov, Seventh edition fuel cell handbook, Chapter 8," pp. 21.

[3] N. I. W. Group, "White Paper on Natural Gas Interchangeability and Non-combustion End Use," 2/28/2005 2005.

[4] N. I. W. Group, "White Paper on Liquid Hydrocarbon Dropout in Natural Gas Infrastructure," 2/28/2005 2005.

[5] G. A. Richards, M. M. McMillian, R. S. Gemmen, W. A. Rogers, and S. R. Cully, "Issues for Low-Emission, Fuel-flexible Power Systems," *Progress in Energy and Combustion Science*, vol. 27, pp. 141-169, 2001.

[6] http://www.crct.polymtl.ca/factweb.php?lang=en.

[7] M. Feigl, F. Setzer, R. Feigl-Varela, G. Meyers, and B. Sweet, "Field Test Validation of the DLN2.5H Combustion System on the 9H Gas Turbine at Baglan Bay Power Station," *ASME Paper #GT2005-68843*, 2005.

[8] G. Myers, D. Tegel, M. Feigl, F. Setzer, W. Bechtel, D. Fitts, B. Couture, and R. Tuthill, "Dry Low Emissions for the 'H' Heavy-Duty Industrial Gas Turbines: Full-Scale Combustion System Rig Test Results," presented at Proceedings of ASME Turbo Expo 2003, Atlanta, Georgia, 2003.

[9] M. Boyce, "Gas Turbine Engineering Handbook Second Edition," *Gulf Professional Publishing*, 2001.

[10] V. Vittorio and R. Borchiellini, "Exergetic and economic evaluation of control strategies for a gas turbine plant," *Energy*, vol. 29, pp. 2253-2271, 2004.

[11] http://www.naturalgas.org/overview/background.asp.

[12] http://www.ivv.fhg.de/ms/ms-analyzers.html.

[13] I. V. Chernushevich, A. V. Loboda, and B. A. Thomson, "An Introduction to Quadrupole-Time-of-Flight Mass Spectrometry," *J. Mass Spectrom*, vol. 36, pp. 849-865, 2001.

[14] http://www.moorfield.co.uk/ecoSys.html.

[15] http://www.chem.agilent.com/scripts/pds.asp?lpage=1917.

[16] http://www.gasanalyzers.com/index.php?option=content&task=view&id=60&Itemid=77.

[17] F. A. Settle, *Handbook of Instrumental Techniques for Analytical Chemistry*: Prentice Hall, 1997.

[18] Maria A. van Agthoven, Go Fujisawa, Philip Rabbito, and O. C. Mullins, "Near-Infrared Spectral Analysis of Gas Mixtures," *Applied Spectroscopy*, vol. 56, pp. 593-598, 2002.

[19] C. W. Brown and S.-C. Lo, "Feasibility of On-line Monitoring of the BTU Content of Natural Gas with a Near-Infrared Fiber Optic System," *Applied Spectroscopy*, vol. 47, pp. 812-815, 1993.

[20] G. E. Fodor, "Analysis of Natural Gas by FTIR; Calibrations & Validations," Southwest Research Institute, San Antonio, Texas 1997.

[21] N. Goldstein, M. Gersh, F. Bien, S. Richtsmeier, J. Gruninger, and S. Adler-Golden, "Real-Time Optical BTU Measurement of Natural Gas at Line Pressure," presented at 4th International Symposium on Fluid Flow Measurement, Denver, Colorado USA, 1999.
[22] J. F. Kastner, "Online Gas Quality Measurement Technique Based on Optical and Thermal Gas Properties," 2005.
[23] http://www.judsontechnologies.com/prod.htm.
[24] http://www.kosi.com/raman/resources/tutorial/index.html, "Kaiser Optical Systems Inc."
[25] http://www.mcphersoninc.com/whatisraman.htm, "McPherson Inc."
[26] http://www.jobinyvon.com/usadivisions/Raman/tutorial1.htm, "HORIBA Jobin Yvon."
[27] http://www.mcphersoninc.com/ramanspectroscopy/ramanspectroscopy.htm.
[28] http://www.kosi.com/raman/index.html.
[29] http://www.jobinyvon.com/usadivisions/Raman/research_raman.htm.
[30] Jiri Janata and M. Josowicz, "Conducting polymers in electronic chemical sensors," *Nature Materials*, vol. 2, pp. 19-23, 2003.
[31] A. G. MacDiarmid, "Polyaniline and polypyrrole: where are we headed?," *Synthetic Metals*, vol. 84, pp. 27-34, 1997.
[32] B. Crone, A. Dodabalapur, A. Gelperin, L. Torsi, H. E. Katz, and A. J. Lovinger, "Electronic sensing of vapors with organic transistors," *Applied Physics Letters*, vol. 78, pp. 2229-2231, 2001.
[33] H.-S. J. Yoshiaki Sakurai, Toshinori Shimanouchi, Takao Inoguchi, Seiichi Morita, Ryoich Kuboi, Kazuki Natsukawa, "Novel array-type gas sensors using conducting polymers, and their performance for gas identification," *Sensors and Actuators B*, vol. 83, pp. 270-275, 2002.
[34] Richard D. McCullough, Genevieve Sauvé, Bo Li, Malika Jeffries-EL, Suresh Santhanam, Lawrence Schultz, Rui Zhang, Mihaela C. Iovu, Jessica Cooper, Prathapan Sreedharan, Joseph C. Revelli, Aaron G. Kusner, Tomasz Kowalewski, Jay L. Snyder, Lee E. Weiss, David N. Lambeth, and G. K. Fedder, "Regioregular polythiophene nanowires and sensors," presented at the Proceeding of SPIE, 2005.
[35] Bo Li, S. Santhanam, L. Schultz, M. Jeffries-EL, M. C. Iovu, G. Sauvé, J. Cooper, R. Zhang, J. C. Revelli, A. G. Kusne, J. L. Snyder, T. Kowalewski, L. E. Weiss, R. D. McCullough, G. K. Fedder, and D. N. Lambeth, "Volatile Organic Compound Discrimination Using Nanostructured Polythiophene Sensors," presented at IEEE Sensors 2005, Irvine, USA. , 2005.
[36] Mark C. Lonergan, Erik J. Severin, Brett J. Doleman, Sara A. Beaber, Robert H. Grubbs, and N. S. Lewis, "Array-based vapor sensing using chemically sensitive, carbon black-polymer resistors," *Chemical Materials*, vol. 8, pp. 2298-2312, 1996.
[37] K.-M. Jäger, D. H. McQueen, I. A. Tchmutin, N. G. Ryvkina, and M. Klüppel, "Electron transport and ac electrical properties of carbon black polymer composites," *Journal of Physics D: Applied Physics*, vol. 34, pp. 2699-2707, 2001.
[38] J. A. Dickson and R. M. Goodman, "Integrated chemical sensors based on carbon black and polymer films using a standard CMOS process and post-processing," presented at Proceedings of the IEEE International Symposium on Circuits and Systems, Geneva, Switzerland, 2000.
[39] Y. S. Kim, S.-C. Ha, Y. Yang, Y. J. Kim, S. M. Cho, Haesik Yang, and Y. T. Kim, "Portable electronic nose system based on the carbon black-polymer composite sensor array," *Sensors and Actuators B*, vol. 108, pp. 285-291, 2005.
[40] Y. S. K. Seung-Chul Ha, Yoonseok Yang, Young Jun Kim, Seong-Mok Cho, Haesik Yang, Youn Tae Kim, "Integrated and microheater embedded gas sensor array based on the polymer composites dispensed in micromachined wells," *Sensors and Actuators B*, vol. 105, pp. 549-555, 2005.
[41] P. L. McEuen, M. S. Fuhrer, and H. Park, "Single-walled carbon nanotube electronics," *IEEE Transactions on Nanotechnology*, vol. 1, pp. 78-85, 2002.
[42] S. Iijima, "Helical microtubules of graphitic carbon," *Nature*, vol. 354, pp. 56-58, 1991.
[43] Jing Kong, Nathan R. Franklin, Chongwu Zhou, Michael G. Ghapline, Shu Peng, Kyeongjae Cho, and H. Dai, "Nanotube molecular wires as chemical sensors," *Science*, vol. 287, pp. 622-625, 2000.
[44] Jing Kong, Michael G. Chapline, and H. Dai, "Functionalized carbon nanotubes for molecular hydrogen sensors," *Advanced Materials*, vol. 13, pp. 1384-1386, 2001.

[45] Liming Dai, Prabhu Soundarrajan, and T. Kim, "Sensors and sensor arrays based on conjugated polymers and carbon nanotubes," *Pure Applied Chemistry*, vol. 74, pp. 1753-1772, 2002.
[46] Yi Cui, Qingqiao Wei, Hongkun Park, and C. M. Liever, "Nanowire nanosensors for highly sensitive and selective detection of biological and chemical species," *Science*, vol. 293, pp. 1289-1292, 2001.
[47] D. Diamond, *Principles of Chemical and Biological Sensors*, 1998.
[48] S. R. Systems, *QCM200 Quartz Crystal Microbalance Digital Controller and QCM25 5 MHz Crystal Oscillator*, 2005.
[49] A. L. Spetz, "Chemical Sensors Technologies, Tutorial 2006," 2006.
[50] A. Hierlemann and H. Baltes, "CMOS-based chemical microsensors," *Analyst*, vol. 128, pp. 15-28, 2003.
[51] J. Fritz, M. K. Baller, H. P. Lang, H. Rothuizen, P. Vettiger, E. Meyer, H. J. Güntherodt, C. Gerber, and J. K. Gimzewski, "Translating biomolecular recognition into nanomechanics," *Science*, vol. 288, pp. 316-318, 2000.
[52] A. Hierlemann, D. Lange, C. Hagleitner, N. Kerness, A. Koll, O. Brand, and H. Baltes, "Application-specific sensor systems based on CMOS chemical microsensors," *Sensors and Actuators B*, pp. 2-11, 2000.
[53] H. Jensenius, J. Thaysen, A. A. Rasmussen, L. H. Veje, O. Hansen, and A. Boisen, "A microcantilever-based alcohol vapor sensor-application and response model," *Applied Physics Letters*, vol. 76, pp. 2615-2617, 2000.
[54] J. Watson, K. Ihokura, and G. S. Coles, "The Tin Dioxide Gas Sensor," *Measurement Science and Technology*, vol. 4, pp. 711-719, 1993.
[55] "Technical Information on Usage of TGS Sensors for Toxic and Explosive Gas Leak Detects," vol. 2005: Figaro Sensors, 2004.
[56] A. Samman, S. Gebremariam, L. Rimai, X. Zhang, J. Hangas, and G. W. Auner, "Silicon-carbide MOS capacitors with laser-ablated Pt gate as combustible gas sensors," *Sensors and Actuators B*, vol. 63, pp. 91-102, 2000.
[57] A. L. Spetz and S. Savage, "Advances in SiC field effect gas sensors," in *Recent Major Advances in SiC*, J. Choyke, H. Matsunami, and G. Pensl, Eds. Berlin: Springer, 2004.
[58] R. N. Ghosh, P. Tobias, S. G. Ejakov, and B. Golding, "Interface States in High Temperature SiC Gas Sensing," presented at IEEE Sensors, 2002.
[59] A. L. Spetz, S. Nakagomi, and S. Savage, "High-Temperature SiC-FET Chemical Gas Sensors," in *Advances in Silicon Carbide Processing and Applications*, S. E. Saddow and A. Agarwal, Eds. Boston: Artech House, 2004.
[60] P. Tobias, B. Golding, and R. N. Ghosh, "Sensing Mechanism of High Temperature Silicon Carbide Field-Effect Devices," in *Transducers*, 2003.
[61] P. Tobias, B. Golding, and R. N. Ghosh, "Sensing Mechanism of High Temperature Silicon Carbide Devices for Exhaust Gas Applications," presented at IEEE Sensors, 2003.
[62] L. L. Tongson, B. E. Knox, T. E. Sullivan, and S. J. Fonash, "Comparative study of chemical and polarization characteristics of Pd/Si and Pd/SiO_x/Si Schottky-barrier-type devices," *Journal of Applied Physics*, vol. 50, pp. 1535-1537, 1979.
[63] A. Samman, S. Gebremariam, L. Rimai, X. Zhang, J. Hangas, and G. W. Auner, "Platinum-aluminum nitride-silicon carbide diodes as combustible gas sensors," *Journal of Applied Physics*, vol. 87, pp. 3101-3107, 2000.
[64] P. Tobias, A. Baranzahi, A. L. Spetz, O. Kordina, E. Janzen, and I. Lundstrom, "Fast Chemical Sensing with Metal-Insulator Silicon Carbide Structures," *IEEE Electron Device Letters*, vol. 18, pp. 287-289, 1997.
[65] B. P. Luther, S. D. Wolter, and S. E. Mohney, "High Temperature Pt Schottky diode gas sensors on n-type GaN," *Sensors and Actuators B*, vol. 56, pp. 164-168, 1999.
[66] J. Schalwig, G. Muller, U. Karrer, M. Eickhoff, O. Ambacher, M. Stutzmann, L. Gorgens, and G. Dolinger, "Hydrogen Response Mechanisms of Pt-GaN Schottky Diodes," *Applied Physics Letters*, vol. 80, pp. 1222-1224, 2002.
[67] J. Cerda, J. R. Morante, and A. L. Spetz, "New Tunnel Schottky SiC Devices Using Mixed Conduction Ceramics," *Materials Science Forum*, vol. 433-436, pp. 949-952, 2003.
[68] P. Tobias, S. Nakagomi, A. Baranzhai, R. Zhu, I. Lundstrom, P. Martensson, and A. L. Spetz, "Electrical Characterization of Chemical Sensors Based on Catalytic Metal Gate - Silicon Carbide Schottky Diodes," *Materials Science Forum*, vol. 264-268, pp. 1097-1100, 1998.

[69] G. W. Hunter, P. G. Neudeck, L. Y. Chen, C. C. Liu, Q. H. Wu, M. S. Sawayda, Z. Jin, J. Hammond, D. Makel, M. Liu, W. A. Rauch, and G. Hall, "Chemical Gas Sensors for Aeronautics and Space Applications III," in *Sensors Exposition*, 1999.
[70] A. L. Spetz, P. Tobias, A. Baranzahi, P. Martensson, and I. Lundstrom, "Current Status of Silicon Carbide Based High-Temperature Gas Sensors," *IEEE Transactions on Electron Devices*, vol. 46, pp. 561-566, 1999.
[71] J. Schalwig, G. Muller, O. Ambacher, and M. Stutzmann, "Group III-Nitride based Gas Sensors for Exhaust Gas Monitoring," in *Transducers '01: Eurosensors XV*, 2001.
[72] A. L. Spetz, in *Bio and Chemical Sensors Conference*. Uppsala, Sweden, 2004.
[73] H. Svenningstorp, L. Uneus, P. Tobias, I. Lundstrom, L. G. Ekedahl, and A. L. Spetz, "High Temperature Gas Sensors Based on Catalytic Metal Field Effect Transistors," *Materials Science Forum*, vol. 338-342, pp. 1435-1438, 2000.
[74] R. S. Mueller and T. I. Kamans, *Device Electronics for Integrated Circuits*. New York: Wiley, 2003.
[75] S. Savage, A. Konstantinov, A. M. Saroukhan, and C. I. Harris, "High Temperature 4H-SiC FET for Gas Sensing Applications," *Materials Science Forum*, vol. 338-342, pp. 1431-1434, 2000.
[76] O. Ambacher, B. Foutz, J. Smart, J. R. Shealy, N. G. Weimann, K. Chu, M. Murphy, A. J. Sierakowski, W. J. Schaff, L. F. Eastman, R. Dimitrov, A. Mitchell, and M. Stutzmann, "Two dimensional electron gases induced by spontaneous and piezoelectric polarization in undoped and doped AlGaN/GaN heterostructures," *Journal of Applied Physics*, vol. 87, pp. 334-344, 2004.
[77] M. Stutzmann, G. Steinhoff, M. Eickhoff, O. Ambacher, C. E. Nebel, J. Schalwig, R. Neuberger, and G. Muller, "GaN-based heterostructures of sensor applications," *Diamond and Related Materials*, vol. 11, pp. 886-891, 2002.
[78] J. Pearton, B. S. Kang, S. Kim, F. Ren, B. P. Gila, C. R. Abernathy, J. Lin, and S. N. G. Chu, "GaN-based diodes and transistors for chemical, gas, biological and pressure sensing," *Journal of Physics: Condensed Matter*, vol. 16, pp. R961-R994, 2004.
[79] N. Docquier and S. Candel, "Combustion control and sensors: a review," *Progress in Energy and Combustion Science*, vol. 28, pp. 107-150, 2002.
[80] T. Hibino, Y. Kuwahara, Y. Kuroki, T. Oshima, R. Inoue, S. Kitanoya, and T. Fuma, "Solid electrolyte HC sensor on gasoline engines," *Solid State Ionics*, vol. 104, pp. 163-166, 1997.
[81] T. Hibino and S. Wang, "A novel sensor for C1-C8 hydrocarbons using two zirconia-based electrochemical cells," *Sensors and Actuators B*, vol. 61, pp. 12-18, 1999.
[82] A. Hashimoto, T. Hibino, K. Mori, and M. Sano, "High-temperature hydrocarbon sensors based on a stabilized zirconia electrolyte and proton conductor-containing platinum electrode," *Sensors and Actuators B*, vol. 81, pp. 55-63, 2001.
[83] N. Guillet, R. Lalauze, and C. Pijolat, "Oxygen and carbon monoxide role on the electrical response of a non-Nernstian potentiometric gas sensor; proposition of a model," *Sensors and Actuators B*, vol. 98, pp. 130-139, 2004.
[84] R. S. Glass and A. Q. Pham, "Challenges in the Development of Sensors for Monitoring Automobile Emissions," in *International Symposium of Automotive Technology and Automation*. Italy, 1997.
[85] M. P. Sinha and M. Wadsworth, "Miniature focal plane mass spectrometer with 1000-pixel modified-CCD detector array for direct ion measurement," *Review of Scientific Instruments*, vol. 76, pp. 025103, 2005.
[86] W. B. Brinkerhoff, A. F. Chang, R. W. McEntire, and G. G. Mamagadze, "Miniature Laser Ablation Time-of-Flight Mass Spectrometer," presented at Lunar and Planetary Science XXIX, 1998.
[87] W. B. Brinkerhoff, T. J. Cornish, R. W. McEntire, A. F. Cheng, and R. C. Benson, "Toward an In Situ Organic and Atomic Microprobe with Laser TOF-MS," presented at Lunar and Planetary Science XXXI, 2000.
[88] F. Sugihwo, C.-C. Lin, L. A. Eyre, M. M. Fejer, and J. J. S. Harris, "Broadly-Tunable Narrow-Linewidth Micromachined Laser Photodetector and Phototransistor," *IEEE IDEM*, pp. 665, 1998.
[89] F. Sugihwo, C.-C. Lin, J.-C. Bouteiller, M. Larson, and J. J. S. Harris, "Micromachined Tunable Vertical Cavity Lasers as Wavelength Selective Tunable Photodetectors," *IEEE IDEM*, pp. 561-564, 1998.

7 ASSESSMENT OF HYDROCARBON DEW POINT, HYDROCARBON DROPOUT AND EQUATIONS OF STATE FOR NATURAL GAS CONTAINING LONG CHAIN HYDROCARBONS SUPPORT

This status report outlines the progress that has been made to date on the ongoing project to address growing interest in improved prediction of hydrocarbon dewpoints. An accurate method for predicting the vapor-liquid equilibrium for various natural gas mixtures is being assessed and developed to predict liquid dropout conditions in hydrocarbon mixtures.

7.1 TASK 1.0 – Identification of Gas Compositions for Assessment

Informational postings with compositional data for heavy hydrocarbons (C6+) were tracked and averages for a selected set are found in Table 7-1. The determination of the actual compositions selected for equation of state evaluation was largely determined by the availability of experimental data on the dewpoint for natural gas mixtures. Often, informational postings include the Cricondentherm Hydrocarbon Dew Point (CHDP); however, in *all* cases this value is predicted using an equation of state.

Table 7-1: Average Compositions of Pipeline Gas from Selected Informational Posting Data.

Component	Average Mole %	Std. Dev
CO_2	1.59	0.45
N_2	0.27	0.27
CH_4	90.86	0.21
C_2H_6	5.28	5.28
C_3H_8	1.47	2.30
i-C_4H_{10}	0.21	0.21
C_4H_{10}	0.19	1.50
i-C_5H_{12}	0.05	0.05
C_5H_{12}	0.04	0.59
C6+	0.05	0.05

a) East Louisiana Trunkline 4/24/06 – 8/2/06,
Trans-Colorado 5/2/06 – 8/2/06,
Duke Energy 11/23/05 – 7/23/06

7.2 TASK 2.0 – Literature Assessment

Subtask 2.1

It is absolutely imperative in the evaluation of equation of state performance that one has access to experimental dewpoints for natural gas mixtures. Therefore, a comprehensive literature assessment of hydrocarbon dew point and liquid dropout in natural gas has been conducted. As a result of an extensive review of informational postings, academic literature, and any other available public data, sixteen different natural gas mixtures for which there has been an

experimental dewpoint curve determined have been found an examined. The compositions of the gases can be found in Table 7-5. Experimental details regarding the measurement of the dewpoint curves can be found in the corresponding references in Table 7-5.

Subtask 2.2

A comprehensive literature assessment of the commonly used equations of state (e.g., Peng-Robinson and Soave-Redlich-Kwong, etc.) used to describe pipeline quality natural gas was conducted. To date seven common equations of state have been investigated to determine their predictive ability for the behavior of natural gas vapor-liquid equilibriums. The investigated equations of state were Peng-Robinson[1] (PR), Soave-Redlich-Kwong[2,3] (SRK), Predictive Soave-Redlich-Kwong[4,5,6,7] (PSRK), Statistical Associating Fluid Theory[8,9,10] (SAFT), American Petroleum Institute[11,12] (API)-SRK, Benedict-Webb-Ruben-Starling[13,14] (BWRS), and Grayson Streed[15] (GS). These seven equations were chosen based on perceived accuracy for hydrocarbon mixtures.

7.3 TASK 3.0 – Identification of Hydrocarbon Dropout Conditions

Based on the gas compositions selected in Task 1 and the literature assessments conducted in Task 2, conditions conducive for hydrocarbon dropout were identified and experimental dewpoint envelopes are shown in Figure 7-1. As can be seen from Figure 7-1, the included mixtures are representative of varying concentrations of higher hydrocarbons (C6+), and thus spans a wide range of CHDPs (–60→+10 °C, –76→+50 °F). The dependence of the experimental CHDP on the gas composition was determined. As one might expect, higher hydrocarbons (C6+) affect the CHDP much more strongly than the lower hydrocarbons. The increase in CHDP per increase in mole fraction [$\Delta T(K)/\Delta mol\%$] is given in Table 7-2.

These values were determined by performing a multiple linear regression analysis on the relationship between the composition of the 16 gas mixtures and their experimental CHDPs. While a rigorous determination of these relationships would require independently varying the composition of individual components, this would be experimentally challenging and nearly intractable with the shear number of experiments necessary to find the experimental CHDP for many varying mixtures. Given the variability in the 16 gas mixtures studied here, statistically significant (i.e., P-value < 0.05 corresponding to a 95% confidence interval) values for $\Delta T(K)/\Delta mol\%$ have been determined for many of the gas components. The negative value of $\Delta T(K)/\Delta mol\%$ for ethane seems to contradict conventional wisdom on the subject of dewpoint curves for hydrocarbons and warrants further study. One would anticipate that the cricontentherm for a binary mixture of methane and ethane would increase with increasing ethane concentration; however, this is not the case in the mixtures studied. One possible explanation could be that mixtures of hydrocarbon gases may exhibit characteristics similar to that of a eutectic, where under the right conditions the dewpoint temperature is suppressed with increasing ethane concentration.

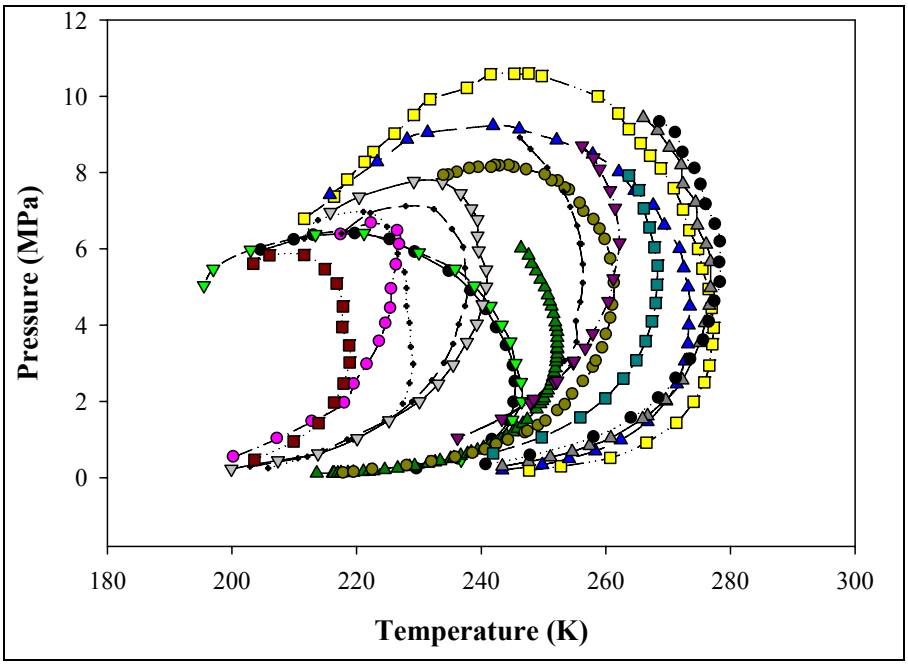

Figure 7-1: Experimental Dewpoint Envelopes for the 16 Natural Gas Mixtures. Symbols represent data points and the lines are simply curve fits to help illustrate the phase envelope.

Table 7-2: Dependence of Experimental Cricondentherm Dewpoint Temperature on Composition.

Component	Coefficient (ΔT(K)/$\Delta mol\%$)	P-value test for significance
N2	2.26	0.331
CO2	0.09	0.844
C2	-2.12	0.051
C3	9.38	0.009
C4	7.42	0.004
C5	36.89	5.0e-5
C6+	108.56	0.334

7.4 TASK 4.0 – Equation of State Modeling

Subtask 4.1

Equations of state identified in Task 2 were evaluated using the 16 experimental mixtures based on their ability to accurately predict hydrocarbon dropout conditions. While the assessment of the ability of the various equations of state in predicting liquid dropout amounts would be useful, this study is limited to the prediction of the dewpoint curve. However, these two predictive abilities are directly linked and the evaluation of the prediction of the dewpoint curve should provide insight into the liquid dropout amount predictive capabilities of the various equations of state. The first step in predicting the amount of liquid dropout under pipeline conditions is to predict the conditions that correspond to the dewpoint. Therefore, phase envelopes were calculated with each equation of state for every gas to determine how well the predicted values for hydrocarbon dewpoint match the reported experimental data. The Mean Absolute Deviation

(*MAD*) was calculated by determining the difference in temperature at a given pressure, to quantify how well each of the equations predicted the vapor-liquid equilibriums. The *MAD* equation is shown as Equation 7-1, where T_M is the experimentally measured temperature, T_P is the temperature predicted by the equations of state, and n is the number of data points.

$$MAD = \frac{\sum |T_M - T_P|}{n} \tag{7-1}$$

All of the equations of states were tested for the first three gases; however, for gases 4-16 the BWRS equation of state was eliminated due to the poor prediction of the first three vapor-liquid equilibriums. Generally, the SAFT, SRK, API-SRK, and the GS equations of state were all very comparable and usually agreed best with the experimental data. There were three major exceptions, in gases 14 and 16 PSRK out-performed the other equations of state and in Gas 10 PSRK and PR closely modeled the data, whereas the others greatly overpredicted the phase envelope. The *MAD* for the 16 gases and 7 equations of state can be found in Table 7-3. The overall *MAD* for the seven EOSs are listed in Table 7-4.

Table 7-3: Mean Absolute Deviation (*MAD*) for 16 Gas Mixtures.

	PR	SRK	PSRK	SAFT	API-SRK	BWRS	GS
Gas 1	3.15	0.41	0.25	0.37	0.43	3.89	0.41
Gas 2	2.86	1.36	1.95	1.36	1.32	2.22	1.36
Gas 3	3.2	0.43	0.33	0.43	0.46	4.03	0.43
Gas 4	3.26	1.02	1.06	1.02	1	-----	1.02
Gas 5	3.48	0.85	1.08	0.85	0.8	-----	0.85
Gas 6	1.78	1.13	1.52	1.13	1.13	-----	1.13
Gas 7	2.59	0.8	1.3	0.8	0.73	-----	0.8
Gas 8	1.95	0.81	1.35	0.81	0.72	-----	0.81
Gas 9	2.31	0.82	1.06	0.83	0.78	0.83	-----
Gas 10	0.88	4.67	0.2	4.67	4.71	4.66	-----
Gas 11	2.48	0.31	0.98	0.31	0.26	0.31	-----
Gas 12	3.51	2.23	2.41	2.23	2.14	2.23	-----
Gas 13	2.45	1.27	1.79	1.27	1.18	1.27	-----
Gas 14	3.39	2.2	1.54	2.2	2.13	2.2	-----
Gas 15	4.2	2.17	2.91	2.17	2.1	2.17	-----
Gas 16	4.08	2.46	1.72	2.46	2.35	2.46	-----

Table 7-4: Overall Mean Absolute Deviation (*MAD*).

PR	**2.95**
SRK	**1.48**
PSRK	**1.41**
SAFT	**1.43**
API-SRK	**1.48**
BWRS	**3.36**
GS	**1.48**

Subtask 4.2

Appropriate numerical models and modifications to the existing database of interaction parameters will be used to improve existing equations of state for varying natural gas compositions in order to enhance predictive ability over all ranges of composition and thermodynamic conditions that are identified in Task 3. Currently, molecular dynamics simulations are being designed and developed that will assist in determining the interactions between heavy hydrocarbons and the light hydrocarbons that determine the hydrocarbon dewpoint curve for these mixtures. The solvent effect of the methane phase on the confirmation of the large hydrocarbons will be determined, along with the change in free energy of the mixture due to introduction of large hydrocarbon molecules. These free energy changes will assist in the improvements over the existing equations of state.

Table 7-5: Synthetic Natural Gas Compositions.

Mole %	Gas 1	Gas 2	Gas 3	Gas 4	Gas 5	Gas 6	Gas 7	Gas 8	Gas 9	Gas 10	Gas 11	Gas 12	Gas 13	Gas 14	Gas 15	Gas 16
Reference	Avila 2002a[19]	Avila 2002a	Avila 2002a	Avila 2002a	Avila 2002a	Avila 2002b[18]	Avila 2002b	Avila 2002b	Avila 2002b	Jarne 2004[17]	Jarne 2004	Morch 2006[16]	Morch 2006	Morch 2006	Morch 2006	Morch 2006
Nitrogen																
(N2)	0.618	0.313	2.8	6.9	5.651	0.67	0.48	0.862	0.41	1.559	0.772	0	0	0	0	0
Carbon Dioxide																
(CO2)	0.187	0.202	0.2	0.51	0.284	0	0	0	0	25.908	1.7	0	0	0	0	0
Methane																
(CH4)	98.943	90.4183	96.6159	88.1882	93.3482	89.9584	88.7634	86.4838	96.4654	69.114	84.446	93.505	84.28	96.611	94.085	93.6
Ethane																
(C2H6)	0.082	8.038	0.18	2.72	7.526	8.22	8.54	9.832	2.51	2.62	8.683	2.972	10.067	0	4.468	2.63
Propane																
(C3H8)	0.065	0.801	0.1029	0.85	2.009	0.9	1.68	2.388	0.213	0.423	3.297	1.008	4.028	0	0	0
Isobutane (C4H10)	0.05	0.081	0.0499	0.17	0.305	0.11	0.22	0.183	0.184	0.105	0.293	1.05	0.597	1.527	0	1.49
Butane																
(C4H10)	0	0.123	0.0095	0.32	0.52	0.13	0.29	0.231	0.197	0.104	0.589	1.465	1.028	1.475	0	1.49
Isopentane (C5H12)	0.017	0.01	0.0166	0.085	0.12	0.0084	0.0182	0.0139	0.0096	0.034	0.084	0	0	0.385	1.447	0.795
Pentane																
(C5H12)	0	0.0079	0	0.094	0.144	0.0032	0.0084	0.0063	0.01	0.023	0.086	0	0	0	0	0
Hexane																
(C6H14)	0.032	0.0047	0.016	0.119	0.068	0	0	0	0.001	0.11	0.05	0	0	0	0	0
Heptane																
(C7H16)	0.0027	0.0011	0.0054	0.0258	0.0138	0	0	0	0	0	0	0	0	0	0	0
Octane																
(C8H18)	0.0033	0	0.0038	0.018	0.011	0	0	0	0	0	0	0	0	0	0	0

[1] Peng, D. Y. and D. B. Robinson, *Ind. Eng. Chem. Fundam.*, 15, 59 (1976).
[2] Soave, G., *Chem. Eng. Sci.*, 27, 1197 (1972).
[3] Gundersen, T., *Computer and Chem. Eng.*, 3, 245 (1982).
[4] Th. Holderbaum, J. Gmehling, "PSRK: A Group Contribution Equation of State Based on UNIFAC," Fluid Phase Equilibria 70, 251-265 (1991).
[5] K. Fischer, J. Gmehling; "Further Development, Status and Results of the PSRK- Method for the Prediction of Vapor-Liquid Equilibria and Gas Solubilities," Fluid Phase Equilibria 121, 185 (1996).
[6] K. Fischer, J. Gmehling; "Further Development, Status and Results of the PSRK- Method for the Prediction of Vapor-Liquid Equilibria and Gas Solubilities II," Fluid Phase Equilibria 141, 113-127 (1997).
[7] S. Horstmann, K. Fischer, J. Gmehling; "PSRK group contribution equation of state: Revision and Extension III," Fluid Phase Equilibria 167, 173-186 (2000).
[8] Chapman, et al. "SAFT: Equation-of-State Solution Model for Associating Fluids." *Fluid Phase Equilibria.* 52. (1989). pp. 31-38
[9] Huang, Stanley H.; Radosz, Maciej. "Equation of State for Small, Large, Polydisperse, and Associating Molecules." *Industrial and Engineering Chemistry Research.* (1990). 29(11), pp. 2284-94.
[10] Huang, Stanley H.; Radosz, Maciej. "Equation of State for Small, Large, Polydisperse, and Associating Molecules: Extension to Fluid Mixtures." *Industrial and Engineering Chemistry Research.* (1991). 30(8), pp. 1994-2005.
[11] API Technical Data Book, Volume 1.
[12] Gundersen, T., Computer and Chem. Eng., 3, 245 (1982).
[13] Starling, K. E., Fluid Thermodynamics Properties of Light Petroleum Systems, Gulf Publishing Company, 1973.
[14] Benedict, M., Webb, R. B., Rubin, L. C., J. Chem. Phys. 8, 1940.
[15] Chao, K. C. and Seader, J. D., A General Correlation of Vapor-Liquid Equilibria in Hydrocarbon Mixtures, *AIChE Journal*, 7, No. 4 (December 1961).
[16] Morch, Ø., et al. "Measurement and Modeling of Hydrocarbon Dew Points of Five Synthetic Natural Gas Mixtures." *Fluid Phase Equilibria* 239 (2006), pp.138-145.
[17] Jarne, C., et al. "Thermodynamics Properties of Synthetic Natural Gases. 5. Dew Point Curves of Synthetic Natural Gases and Their Mixtures with Water and with Water and Methanol: Measurement and Correlation." *Ind. Eng. Chem. Res.* **43** (2004), pp. 209–217.
[18] Avila, S., et al. "Thermodynamic Properties of Synthetic Natural Gases. 2. Dew Point Curves of Synthetic Natural Gases and Their Mixtures with Water and Methanol. Measurement and Correlation." *Ind. Eng. Chem. Res.* 41 (2002), pp. 928-934.
[19] Avila, S., et al. "Thermodynamic Properties of Synthetic Natural Gases. 1. Dew-Point Curves of Synthetic Natural Gases and Their Mixtures with Water and Methanol. Measurement and Correlation." *Ind. Eng. Chem. Res.* 41 (2002), pp. 3714–3721.